NASA CONTRACTOR REPORT

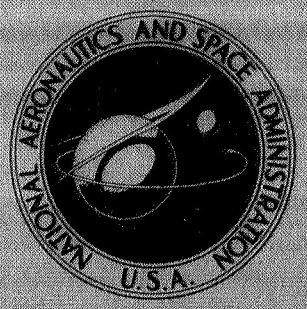

NASA CR-2336

NASA CR-2336

STUDY OF CRITICAL DEFECTS IN ABLATIVE HEAT SHIELD SYSTEMS FOR THE SPACE SHUTTLE

by C. C. Miller and W. D. Rummel

Prepared by
MARTIN MARIETTA AEROSPACE
DENVER DIVISION
Denver, Colo. 80201
for Langley Research Center

NATIONAL AERONAUTICS AND SPACE ADMINISTRATION • WASHINGTON, D. C. • FEBRUARY 1974

FOREWORD

This report was prepared by Martin Marietta Aerospace, Denver, Colorado, under National Aeronautics and Space Administration Contract NAS1-10289, "Study of Critical Defects in Ablative Heat Shield Systems for the Space Shuttle." Langley Research Center, Hampton, Virginia, directed administration of the contract.

The program was conducted by the Research and Development Division of Martin Marietta at its Denver facility from April 1970, to April 1973. The effort consisted of five tasks. The first three tasks were conducted and reported by R. L. Thompson, W. D. Rummel and W. E. Driver. NASA issued this report in April 1972, as NASA CR-2010. Tasks IV and V, reported herein, were conducted by C. C. Miller and W. D. Rummel.

Invaluable assistance and guidance were received from the following:

Martin Marietta Aerospace

D. V. Sallis	Program Manager - Tasks I, II, III
R. W. Seiferth	Program Manager - Tasks IV, V
R. L. Thompson	Original Principal Investigator
D. L. Carlson	Interim Principal Investigator
J. W. Maccalous	Chief, Plastics Laboratory
R. V. Kromery	Ablator Fabrication Leader
G. J. Schmidt	Chief, MMA Plasma Arc Facility
W. K. Johnson	Chief, Thermal Vacuum Facility
C. H. Estes	Acoustics Facility
R. H. Gibb	Mechanical Properties Laboratory
P. H. Todd	Non-Destructive Test Laboratory
W. K. Etchison	Image Processing
T. L. Tedrow	X-Ray Facility
C. Cancalosi	Schedule Expeditor
W. L. Brown	Technical Presentation

Lockheed - Georgia

W. K. Hopkin — In-Motion Radiography

G C Optronics

L. Kersch — Holography

STUDY OF CRITICAL DEFECTS IN ABLATIVE HEAT SHIELD SYSTEMS FOR THE SPACE SHUTTLE (TASKS IV AND V FINAL REPORT)

By Christopher C. Miller and Ward D. Rummel

SUMMARY

An experimental program was conducted to evaluate the effects of manufacturing defects on ablator performance. Correspondingly, a study to provide adequate detection methods for critical defects was also accomplished.

The use of ablators as the thermal protection system of a space shuttle orbiter depends on low fabrication costs. Two major means of achieving low cost are through the acceptance of units which have noncritical defects and through a minimum of rapid but meaningful inspections.

Objectives of this effort were, therefore:

- Determination of the effects of defects on performance;
- Designation of those defects which are critical;
- Evaluation of the ramifications of accepting noncritical defects;
- Establishment of inspection techniques.

The effort concentrated on ablators applicable for protecting the bottom of a Space Shuttle Orbiter. The baselines used were the NASA-Langley honeycomb-reinforced ablator MG-36 and a modification, SS-41, mounted on carrier sheets and honeycomb subpanels respectively.

Evidence of critical defects was found from poor processing of the ablator's honeycomb core with respect to undercutting, crushing, etc and the wet coat treatment prior to ablator filling. Improper curing was also cited, along with ablators which were deliberately made on the low density side. Inspection methods for these defects were established along with recommendations for future fabrication techniques and process controls.

CONTENTS

TABLES

FIGURES

INTRODUCTION

Both public and private sectors of aerospace development are concentrating on a reusable space orbiter. Proponents of every system that could be associated with this vehicle should critically examine the status of their disciplines.

This examination should be along the lines of: What's been our previous part in the emergence of this concept? How well does our potential contribution fit into the proposed missions and, What can we do to provide the necessary services, hardware, etc, at an economic rate without sacrificing safety and reliability?

This philosophy has strongly influenced the field of thermal protection systems (TPS). The concentration has its justification, because the design of a TPS for the Shuttle Orbiter is believed by many to be the most challenging aspect of the entire Shuttle design. E. S. Love, in his *Tenth Von Karman Lecture* (ref 1), attributes 8 out of 29 concerns in aerothermodynamics/configurations to thermal protection problems.

Potential Shuttle Orbiter Heat Shields

Considering the range of heat loads and multitude of missions anticipated for a workhorse Shuttle Orbiter, two categories of passive TPS emerge as workable candidates for Orbiter use. These are: (1) high temperature metals, and (2) nonmetallics, such as carbon/carbon (C/C), reusable surface insulations (RSI), and ablator composites. Presently baselined for the Orbiter at the initiation of the Phase C/D work are C/C for the nose cap and leading edges, and RSI for the main area of the vehicle.

As Love points out, "Ablators, [however], offer a confident fall-back solution [temporary] for both leading edges and large surface areas should development of the baseline approaches lag." Historically, ablative systems have proven successful and reliable in efforts from Mercury through Gemini and Apollo; enhancing the final flights of the X-15; and providing protection for the PRIME vehicle. During this period, the unit weight of the ablative systems dropped significantly while improving in thermal efficiency.

Ablative Systems

The drawbacks most often referred to by opponents of ablative systems for Shuttle use are the cost incurred by refurbishment after each mission, and the previous history of meticulous fabrication and installation of ablator TPS, i.e., successful reentry was essentially guaranteed through a perfect product, obtained by frequent rework cycles.

With respect to the first argument, ablator advocates have felt that large portions of the Orbiter vehicle (top of wing, body, etc) may not experience sufficient heat to warrant pyrolysis-induced replacement. However, fabrication and installation of large areas of new ablator panels is necessary after each flight. This process can and must be implemented at much less than currently-quoted unit costs.

In our program, we started the cost improvement by conceding that the second argument was true--designs such as Gemini and PRIME had been established based on ideal performance. System reliability was assured through elaborate manufacturing and quality control procedures that would produce a nearly defect-free TPS. That approach produced costly heat shields and, in reviewing the flight performance of programs such as Apollo, PRIME, etc, the question was raised concerning the necessity of a "defect-free" design. The possible cost savings from liberalizing (and/or simplifying) fabrication, inspection and application of ablators to vehicles the size of the proposed Space Shuttle Orbiter made it very desirable to further investigate the significant effects of these material variations on performance.

The basic objectives of our effort were to determine, through a comprehensive test program, considering all phases of the Space Shuttle flight environments: (1) effects of the commonly occurring fabrication from flaws on ablative panel performance, (2) inspection and certification methods of ablative heat shields, and (3) effects of accepting noncritical defects on heat shield panel fabrication and inspection.

Procedure of Work Effort

The study attempted to determine these effects before fabrication processes were firmly established. Thus the processes could be directed toward low-cost methods, and the need for process control and quality inspection minimized. Previous investigations

considered fabrication defects only during the hardware verification phases and very little experimental data were available concerning the defect sensitivity properties of critical material. The entire study, extending for three years, was subdivided into five work tasks:

- Task I - Identify and characterize potentially-critical defects, survey inspection techniques, evaluate those techniques most suitable for locating and identifying defects in the heat shield, and develop methods for inducing the appropriate defects into test specimens of the baseline heat shield system;

- Task II - Plan Tasks III, IV and V. Conduct nondestructive test inspections on GFP ablative panels (manufactured on previous contracts), using techniques found applicable in Task I;

- Task III - Investigate the effects of various fabrication-induced defects on the ablator performance in the simulated Shuttle reentry environment only;

- Task IV - Determine those fabrication-induced defects which are developed to a critical status during environments preceding Orbiter reentry. Verify through entry heating and acoustics simulation;

- Task V - Investigate updating of current state-of-the-art and the applicability of advanced methods for nondestructive inspection and certification of ablative heat shield systems.

Task Summaries

Considerable effort was expended during Task I in categorizing potentially-critical defects, and establishing the vehicle/mission concept to be used as a baseline for the study. A complete matrix of NDT techniques were reviewed for applicability.

The work accomplished in Task II, Part 1, is self-explanatory. Reasonable success was achieved in the quality control inspections of the GFP panels.

Task III initiated experimental investigations in conducting and correlating cause-and-effect testing. The NDT examinations were nearly established.

Task IV continued the experimental studies by including non-entry environments experienced by the Shuttle Orbiter as viable time periods for the formation of critical defects from manufacturing-induced variances. A mixture of state-of-the-art and advanced methods of quality inspection served this task.

Accomplishments in Task V included determining low-cost inspection methods amenable to automatic acceptance of basic ablator panels, and experiments with potential methods for acceptance of ablator-to-subpanel bonding.

A comprehensive report convering Tasks I, II, and III was issued by NASA as CR-2010 (ref 2). Pertinent condensations of the high points of that report are noted in this report.

Significance of Study

The program has demonstrated several important aspects concerning the rapid, mass production of ablative TPS panels.

1) Unusual appearances are often misleading and do not necessarily represent critical defects in a panel;

2) Lot process records must be monitored with respect to the lot histories on the ablator cure cycle and final net density;

3) Poor processing of the primer coating applied to the ablator's honeycomb reinforcement cell walls must be avoided;

4) Spallation is inevitable when the ablator honeycomb core does not extend the full thickness of the ablator, i.e., foreshortened due to undercutting, local crushing, etc;

5) Simplification and automation of fabrication processes should lead to lower rejection rates;

6) The results of this study substantiates ablator's proven reputation of "forgiving," despite the presence of defects;

7) A new approach to the fabrication/quality assurance cycle is postulated--one which concentrates on key, critical variances; is liberal toward non-sensitive flaws (consequently reducing inspections); and suggests that the path to automation is in sight.

RUDIMENTS OF A DEFECT STUDY (TASK I)

In establishing the basis for a study involving the effects of intentional defects, it was necessary to select a baseline approach from the many aspects of environments, possible defects, and ablator configurations which could be adequately investigated within the scope of this program. In addition, proper definition of the performance expected was vital in that it created guidelines against which the reactions could be measured.

Development of quality control techniques which would adequately identify the presence of such defects had to be conducted concurrently with the experimental investigations.

Definition of a Critical Defect

A critical defect is defined as an anomaly in the ablative system that affects critical properties to the extent that the system does not meet basic performance requirements. The concept of a critical defect is further exemplified in fig 1, which shows the sequence of events for the life of the ablative panels. Defects introduced at one point in the material's history could theoretically develop to a critical stage later in the sequence of mission environment and eventually manifest itself in a phase such as reentry. In contrast, defects could be initiated during the orbiting portion of the flight, etc, and prove to be critical in reentry; these were not studied.

Performance Criteria

An ablative thermal protection system for the Space Shuttle Orbiter must be designed to meet the following performance requirements.

1) A thermal insulation capability to protect the structure to a given temperature;

2) A structural capability to insure retention of the ablative layer;

3) Retention of the char layer;

4) Compatibility with other onboard systems and with the payload and/or space stations.

These requirements define a set of critical properties for the ablative system. These properties must be established, together with the selected material and design, so that performance requirements are met. For the materials and the designs considered in this program, the basic critical properties have been identified as:

Thermal properties;

Ablative layer mechanical properties;

Char layer integrity;

Surface erosion resistance;

Chemical composition and stability;

Ablative layer bond to subpanel, e.g., face sheet, support panel, basic structure;

Panel dimensions;

Subpanel mechanical properties.

Thermal Criteria.- The critical thermal properties of the ablative panels necessary to ensure that the design structure temperatures are not exceeded are:

Thermal conductivity;

Specific heat;

Density;

Emissivity;

Degradation kinetics;

Degradation products;

Heat of reactions;

Surface recession kinetics.

Structural Criteria.- The requirements for structural performance of the material are established to assure that ablator panels with passable defects possess adequate strength to perform the following functions:

Transmit flight loads to the primary structure;

Accommodate thermal and pressure-induced loads without excessive cracking;

Provide adequate overall panel stiffness to limit load-induced strain in the char layer to acceptable levels;

Maintain adequate strength between the filler and cell walls to prevent loss of filler;

Prohibit attachment point failures that would jeopardize panel retention;

Withstand the launch and entry acoustics environments;

Possess sufficient mechanical properties (E, α, ε_{ult}) to preclude cracking at temperatures of -150°F (173°K) during orbit.

Char Layer Integrity.- Efficient performance of the ablative thermal protection system depends on the char layer, which in turn depends on a variety of factors. For this reason, its integrity is included as a system performance requirement. Char layer integrity is defined as retention of the char layer by maintaining its attachment to the virgin ablative material layer, the restriction of spallation of large particles of char, and chemical stability of the char constituents during the heated periods to preclude sudden melting or collapsing of the char layer. Char integrity must be maintained for the following conditions:

Heat rate, 13 to 55 Btu/ft^2-sec (0.147 to 0.625 MW/m^2);

Local pressure, 0.005 atm (507 N/m^2);

Heat transfer coefficient, 0.005 to 0.006 lb/ft^2-sec (0.0098 to 0.0294 kg/m^2-sec);

Enthalpy, 3000 to 12 000 Btu/lb (6.98 to 27.9 MJ/kg);

Viscous shear, $\sim$ 2 psf (95.8 N/m^2);

Local pressure gradients;

Substructure-induced strain (1.0%);

Prior environment exposures.

Cause And Effects

Defects that have been identified as potentially critical are shown in table 1, which also relates these defects in terms of their effects on critical properties. One of the most obvious conclusions drawn from this figure is that not only the thermal properties but also the mechanical and char integrity properties are important in assuring successful heat shield performance. The basis for this compilation was a literature search and review of the fabrication process.

Detailed discussions on the cause-and-effect possibilities are reproduced from reference 2 and presented in Appendix A. Specific defects were selected for investigation for Tasks I, II, and III and then for Tasks IV and V.

Ground Rules of Study

Assembly Configuration.- The selection of a particular structural design concept was required in order that the effect of various critical ablative defects on the Orbiter could be examined. For example, in a typical shuttle heat shield panel design, whether the ablator is load carrying or not many influence the criticality of some types of defects. A crack or delamination in a load-carrying ablator may be propagated and cause the loss of materials, while in a non-load-carrying ablator, the same crack may have no detrimental effects at all.

Composite used in Tasks I, II, and III: The heat shield assembly construction selected for the early tasks of this effort consisted of a full-depth, phenolic-glass honeycomb filled with an elastomeric ablator (MG-36) and bonded to a fiberglass backface sheet. The details are presented in figure 2. Complete data on the fabrication details are contained in Appendix B of reference 2.

Composite used in Tasks IV and V: A honeycomb subpanel-supported TPS design was selected for the Tasks IV and V studies because of its favorable refurbishment and maintenance turnaround costs. The components used are presented in figure 3. The MG-36 ablator composite was altered to provide a more uniform standard material and is identified as SS-41.

For this study, the subpanel was designed assuming it must carry all loads. Under the Low Cost Ablator Program, NAS1-10793 (ref. 3), a subpanel analysis was conducted which resulted in a high-strength, low-weight subpanel of HTS-Gemon L (Graphite Polyimide) facings and E-glass phenolic core. This system was designed to ±2.8 psi (±1.93 N/cm^2) air load and a maximum bondline temperature of 500°F (533°K). The analysis conducted under the above program was the basis for the subpanel design used in the later tasks.

In the interest of economy, a lower-cost face sheet material substitute, E-glass phenolic ($3/lb) ($6.60/kg) was used in place of the more expensive ($80/lb) ($176/kg) HTS Gemon L material. Analyses were conducted to determine an equivalent E-glass phenolic face sheet design, assuming a design moment of 126 in.-lb (14.24 m-N) and equivalent acoustic strength. The limits which constrained the design curves were: 1) no panel face wrinkling; 2) no intracell buckling; and 3) 1% strain in the ablator outer surface. The ablator panel stiffness was included in computing the 1% strain allowable. The results of the analyses are summarized in figure 4, showing a comparison of the panel unit weights, core thickness, and facing thickness for both the HTS Gemon L and the E-glass phenolic designs. The two circled points on the figure show the designs which have equal acoustic strength. The geometry defined by the circled point on the E-glass phenolic unit weight curve determined the subpanel dimensions.

Investigation point.- A considerable variety of missions are seen for a Space Shuttle Orbiter, each having its own particular set of environments. In every use, this system must integrate the basic characteristics of four vehicles--launch stage, orbiter, reentry body, and subsonic aircraft. Thermal protection requirements for the bottom centerline area of the orbiter were the basis of this study. The mission profile presented in figure 5 represents a logistics resupply of a space station; the insertion orbit is 50 x 100 n mi (92.6 x 185 km), while the referernce orbit is 270 n mi (500.0 km) and circular at 55° inclination. Additional details are presented in reference 2, which also lists other potential missions of interest.

Origin of investigation defects.- Except for those introduced by mishandling, all defects were assumed introduced before completion of the panel assembly. Furthermore, assuming the raw materials meet specific acceptance criteria, the majority of defects were introduced during the subcomponent fabrication (ablative material mixing, face sheet bonding) or during panel fabrication (filling, curing, and machining). Since the basic defects are created and should be detected and controlled in the subcomponent and panel fabrication phase, this phase was the focal point of this program.

Defect Detection Investigation

Defect detection investigations were carried out to identify and characterize potentially critical defects in elastomeric heat shields, inspection sensitivities of applicable state-of-the-art techniques, and to investigate advanced inspection methods for "low-cost," minimum-risk space shuttle heat shield production. Characterization of state-of-the-art inspection techniques were performed first to establish capabilities for analysis and measurement of engineering test models.

Selected inspection techniques were then applied to representative GFP production samples to establish production inspection applicability and identify potential scaleup problems. Selected techniques were then improved and supplemented by advanced techniques to determine methods for reducing inspection costs in terms of the criticality for inspection as identified by the engineering test program. This iterative approach enabled (1) quantitative characterization of all engineering test samples, (2) an opportunity to design for inspectability at minimum cost and highest reliability, and (3) a quantitative basis for establishing a production inspection program.

EFFECTS OF DEFECTS ON ENTRY PERFORMANCE (TASK III)

The following in a recapitulation of the effort reported in reference 2. It reviews the previously published accomplishments in order to maintain continuity of the entire study.

Customer-defined design ablator, MG-36, mounted on a carrier sheet substructure, served as the baseline material. The principal objective involved the determination of the reactions of defects in a reentry heating environment immediately after fabrication. An ancillary phase of the Task III effort investigated the tensile strengths of coupons of the defective material at temperatures other than ambient. Simultaneous studies involving the role of quality inspections in the defect study were also conducted.

Finally, an initial investigation in the effects of environments other than entry was undertaken in order to establish the groundwork for Task IV.

Reactions to Entry Heating Only

Cylinders of ablator material with intentional defects were fabricated and exposed (end heat splash tests) in the Martin Marietta Plasma Arc Facility.

Defects considered.- The following defects were selected for investigation during the reentry phase of the Space Shuttle mission from the compilation of potentially critical defects identified in the previous section, and Appendix A.

Density: Density variations seemed to have a definite effect on filler bond strength in the first fabrications. This effect was especially noticeable when the honeycomb core was pretreated with the DC-1200 silicone primer. Adhesion between the filler and the honeycomb was related to the density variation from the outer surface to the supporting facesheet.

The density variation models were made using an impact filling method and included models with a bulk density of 16 lb/ft^3 (256 kg/m^3) plus overpacked and underpacked models with bulk densities of 16 to 18 lb/ft^3 (272 to 288 kg/m^3) and 14 to 15 lb/ft^3 (224 to 250 kg/m^3). Anticipated results involved the possible

effects of: (1) bulk density variations and density gradients through the material on thermal efficiency, char depth, and char integrity, and (2) bulk density variations on char-to-core bond strength.

Filler bond to honeycomb: During initial fabrication it was discovered that a resin bond coating of the core was necessary before packing to obtain a good bond of filler-to-core. However, it was found that "excess" resin was carried down the cell by the wiping action of the filler. This excess resin was concentrated near the facesheet and was considered undesirable because of (1) its effect on material properties and homogeneity, and (2) increasing the difficulty in interpreting NDT inspection results. The test models were intended to provide data on the effects of bond coating on thermal performance, char retention strength, and filler bond strength.

Voids: Voids are common defects in honeycomb ablators if packing is improperly performed. Although the most common occurrences are near the facesheet, voids can occur in depth throughout the thickness. Thus, a large voids (25% of cell volume) in all cells were located at various depths within the specimen, as shown in figure 6, to evaluate their effect on char stability and thermal efficiency.

Formulation: In several of the models, the fibers were omitted as a constituent to determine the effect of fibers on the filler-to-honeycomb bond strength.

State-of-cure: The cure cycle is known to affect mechanical properties and may affect both the degree of core bonding and thermal properties. As an alternate, a lower temperature-longer time cure was investigated to determine the effect of cure cycle variations on char strength and thermal performance.

Specimen description.- The MG-36 ablative material entry heating specimens were machined from large billets in the form of 5.0-in. (12.7 cm)-diameter, 2.0-in. (5.08 cm)-thick flat-faced cylinders. The 23 specimens were instrumented with four thermocouples each to monitor the internal temperature. Thermocouple wire was 30-gage (0.25 mm) chromel-alumel and was covered with double-hole alumina tubing to electrically insulate the thermocouple leads from the ablative material char layer. A mounting ring of asbestos phenolic was bonded to the back surface of each specimen. An aluminum holder was mechanically fastened to the mounting ring for positioning the specimen on the inserter arm (see fig. 7). Forty-five non-instrumented specimens were also tested for char layer and bonding.

Testing.- Testing was conducted in a 1-MW plasma arc facility test chamber using an F-5000 thermal dynamic arc heater and a 6-in. (15.25 cm)-diameter supersonic nozzle. This test facility simulates hypervelocity heating during reentry by flowing a compressed gas mixture, simulating air, through an electric discharge. The gas undergoes a large thermal energy increase and is then expanded through a supersonic nozzle to approximately Mach three. All ablation performance tests during these investigations were performed by exposing material specimens to this thermal environment.

The selection of plasma arc test conditions for these studies was based on a high cross-range, 1500-n mi (2778 km) delta wing orbiter. The reference total integrated heat for a 1-ft (30.5 cm) nose radius for this trajectory was approximately 95 000 Btu/ft^2 (1078 MJ/m^2) for a nominal entry angle of 22.5 deg. Two test conditions were selected that were representative of heating along the bottom forward centerline and shoulder areas of the Space Shuttle Orbiter. Nominal facility conditions are summarized in table 2.

Results.- A comprehensive discussion of the results and trends observed during the heated entry exposures of splash specimens is presented in reference 2 and summarized here in table 3: (1) low density is not critical with respect to excessive backface temperature until it drops off to about 80% of the nominal density; (2) an excess amount of the ablator core wet coat resin creates a temperature violation because of an increase in net thermal conductance through the material; and (3) voids initiated in the ablator at fabrication are not critical until they reduce the net density of the medium to the above indicated value.

Omission of silica fibers were not found to be critical, and future formulation omitting them were envisioned and accepted in Task IV. Large variations in cure temperature, pressure and time did not affect thermal efficiency.

Mechanical Properties Evaluation

Tensile tests of representative coupons of control and defective ablator billets were conducted at temperatures ranging from -150°F (172°K) to 300°F (422°K) to establish any noticeable changes in physical properties which could affect the performance of the material.

Defects considered.- The potential defects included in this strength experiment involved wet coat variations, density variations, altered cures, and material omissions (fibers, core).

Specimen description.- A total of 95 tensile coupons were tested during this investigation. The majority of the test specimens (those having honeycomb core) were fabricated in accordance with figure 8 while the rest were made in the shape described in figure 9.

Testing.- The tension testing was conducted on an Instron Universal Testing Machine at a rate of 0.1 in./min (0.25 cm/min). A Custom Scientific environmental chamber, enclosing the specimen, provided the full temperature range by means of electric heaters and liquid N_2 cooling. Temperatures were monitored by thermocouple; load-optical extension readings were recorded mechanically.

Results.- Tensile tests were run with the honeycomb ribbon direction transverse to the direction of loading and five specimens were tested at each condition. This type of material is subject to more variations than a homogeneous material. Thus, the strength of each specimen is subject not only to normal variations such as machining, minute voids, etc., but also to honeycomb node bond, honeycomb filler bond, and filler strength. This resulted in more panel-to-panel and specimen-to-specimen scatter than with a homogeneous material.

The trends observed in this Task III study are shown in figures 10 to 12. Ultimate tensile strengths decreased for wet coat variations, off-densities (high and low), and altered cures. The same was true for ultimate elongation percentage. The data also indicated an absence of any increase in tensile modulus. Cold soak temperatures increased tensile strengths and moduli considerably at about equivalent % elongations. The elevated temperature tests lowered each parameter less drastically when compared to the ambient values.

Initial Investigation of Nonentry Environments

Two large ablative panels (numbers 1 and 2) were tested to evaluate the overall TPS response to a sequence of Space Shuttle environments. The objective at the end of Task III was to perform exploratory environmental exposure tests to obtain a basis

for the execution of Task IV work, during which nonentry environments were to be considered. With this objective in mind, panels were fabricated and exposed to simulated pre-reentry environments prior to a reentry thermal pulse and an acoustic spectrum.

Defects considered.- Panel 1 was made without defects while Panel 2 contained the following defects: (See fig. 13)

Metal particles

Underpacked material

Overpacked material

Fiber bundles (inhomogeneity)

Undercut core

No core bond coating

Crushed core near surface

Surface voids

Undercured

Delaminated facesheet

Core unbond from sheet.

Panel description.- Dimensions of the two test panels were 8 x 16 x 2 in. (20.3 x 40.6 x 5.1 cm). The defects outlined above were highly localized in specific areas of the defect-designated panel. See figure 13.

Testing.- Those nonentry environments which were most likely to precipitate critical defects from manufacturing defects during their influence period were selected and simulated as follows.

Ascent acoustics: Both panels were simultaneously exposed to the acoustic spectrum presented in figure 14. Tests were performed using a siren powered by two Allison jet engines. Four different impeller speeds were used to simulate the spectrum that would be encountered at booster liftoff.

Hot vacuum: The purpose of the 72-hr hot vacuum exposure was to obtain a precursory evaluation of material offgassing characteristics and aging effects during orbit conditions and to thermally strain the ablator-to-face sheet bondline. The maximum surface temperature was 300°F (422°K).

A 4-ft (1.2 m) diameter by 8-ft (2.4 m) vacuum chamber was used. Vacuum was maintained by a combination of pumps. A mechanical roughing pump with a rotor lobe blower was used to the 20- to 50-ft m range. Cryopumping reduced this vacuum to 1×10^{-4} torr (1.3×10^{-2} N/m^2) where an ion pump could be turned on. Operating pressure was attained using the ion pump, with an additional pumping capacity from a titanium filament sublimator. Pressure was measured with a hot cathode ionization tube. A quartz lamp was employed to heat the panels on the front face in order to induce thermal strains in the ablator and at the attachments.

Cold vacuum: The purpose of the 48-hr cold vacuum test was to strain the ablative filler bond to the honeycomb core and the ablative layer bond to the face sheet. This was accomplished using the same test setup as the hot vacuum testing.

A shroud inside the vacuum chamber was cooled with liquid nitrogen to a temperature of -320°F (78°K). Infrared heaters were used on both sides of the samples to maintain the sample temperature at -150°F (172°K).

Entry heating: Reentry heating was simulated in the Martin Marietta Plasma Arc Facility using a 10.0-in.-(25.4 cm) diameter nozzle with the panel positioned at a 20-deg angle to the test stream. The panel was rigidly attached to the model holder at the four attachment points. This holder was designed with a water-cooled leading edge machined to a 1.25-in.-(3.18 cm) radius. The blunting of the leading edge was found to enhance flow uniformity and improve heating distribution as shown in figure 15. This test condition was calibrated using a thin calorimeter body made of 0.063-in. (0.16 cm) Inconel X-750 sheet. Heating rates were calculated from the response of thermocouples that were spotwelded to the Inconel skin using the basic calorimeter equation. Both panels were exposed for 1000 seconds.

Descent acoustics: Following the heat pulse, the TPS panel containing the defects was exposed in the descent transonic acoustic environment to evaluate the behavior of charred material. After an exposure to the test environment of 150 dB for 120 sec,

initial char loss occurred where the honeycomb core had been crushed. The decision was then made to test at higher dB levels (up to 154) for additional test time.

Chronologically, these acoustic tests were conducted months after this entry heating exposure; improved acoustic facilities were then available (see the following section).

Results.- These environmental exposures provided a basic overall evaluation of the MG-36 ablator's ability to survive the hostile environments of launch noise, orbit temperatures and vacuum, and reentry heating. In addition, the tests provided a relative comparison of the effect of defects on ablative performance.

Ascent acoustics: Post-test visual examination showed no degradation of face sheet bond, attachments, or ablator panel integrity.

Hot vacuum: Some outgassing was evident during initial heating as the vacuum increased from 5×10^{-6} torr (6.6×10^{-4} N/m^2) to 7×10^{-5} torr (9.3×10^{-3} N/m^2) while heating the ablative surface. The vacuum stabilized at 6 to 7×10^{-6} torr (8 to 9.3×10^{-4} N/m^2) after two days at temperature.

Visual observation through the chamber window did not show any problems during the test. The chamber temperature was then decreased for the cold test without breaking the vacuum. The increase in hardness during the hot vacuum exposure was from 5 to 10 points on the Shore A scale.

Cold vacuum: In the cold conditions, the ablative filler was dished in the honeycomb core due to differential thermal contraction. The filler-to-honeycomb bond, however, did not show any sign of failure. Post-test visual examination failed to show any degradation of bonds, face sheet, attachments, or change in face sheet defects.

Entry heating: Panel 2 performed extremely well, with a strong, smooth char surface formed over 85% of the specimen. Surface-connected anomalies had no apparent effect on the critical strength properties of the char or on the ablator-to-face sheet attachment. Surface temperatures were very nearly uniform across the width of the panel, ±20°F (±11°K), and varied along the length from 2100°F (1420K) to 1900°F (1310°K).

Variations in internal and backface temperatures were attributed to the variation in heating rate and were not noticeably altered by the presence of small surface voids (1 to 3 cells), varying in depth from 0.125- to 0.375-in. (0.318 to 0.952 cm), or by small holes up to 0.189-in. (0.48 cm) in diameter through the ablator. The 8 $in.^2$ (51.5 cm^2) of unsupported char cracked into a random pattern, with little difference noted between the area of crushed core and undercut core. Char retention elsewhere was not noticeably affected by these localized core defects or by the surface discontinuties created by ablative material removal. The two upstream ablative plugs (used for panel attachment) formed integral char with the adjacent material and were securely fastened. The two downstream ablative plugs did not form an integral char and were loose in their holes, probably the result of cooldown shrinkage. The areas containing face sheet delamination and core unbonding from the face sheet were not affected by this test.

The comparative data desired from Panel 1 were invalidated because of the loss of a copper water plug on the specimen holder. This failure occurred at the beginning of the test and resulted in water being leaked into the test chamber. This resulted in an increase in chamber pressure and produced an unbalanced test stream with a corresponding strong shock cone emanating from the nozzle exit. A shock impingement with the specimen surface resulted from the interaction between this shock and the bow shock and created a "hot" spot on the forward 8 in.(20.3 cm) of the specimen. The increased heating and turbulent flow that resulted produced significant char removal and a grooving of the receded surface. A contributing factor in producing these grooves may have been the fact that the core ribbon direction was parallel to the flow. The groove width was approximately one-half the cell width since the honeycomb nodes were left standing to a height of approximately 0.125 in. (0.318 cm) above the surface. The char "skin," which seems to be formed at heating rates of 10 to 30 Btu/ft^2-s (0.113 to 0.341 MW/m^2), exhibited good attachment strength during this test. Pressure gradients and shear forces did not remove this char from the many open cells around the perimeter of the surface burnthrough region. Surface temperatures of 2500°F (1600°K) were measured in the receded area with a rapid falloff to 2000°F (1370°K) near the trailing in the receded area with a rapid falloff to 2000°F (1370°K) near the trailing edge.

Entry acoustics: This final test in Task III (table 4) was conducted on defect-filled Panel 2 which had experienced considerable char buildup in entry heating. After the initial char loss in the area of crushed core in the first exposure, the defects

were insensitive to two more exposures of 2 min each. The fourth exposure, lasting 4 min, created additional char losses in the areas of crushed core and new failures in the regions of undercut core and undercured material.

Quality Assurance Inspections

In Task I investigations, defects potentially critical to Space Shuttle heat shields were identified by fabrication process analysis and by analysis of mission performance requirements. Test samples were fabricated containing each of the defects identified. A survey was conducted to identify potential inspection methods and the most feasible methods were selected for evaluation on defect test samples. Visual, X-radiography, neutron radiography, sonic, thermal, microwave, holography and indentation hardness were selected for evaluation of potential defects. Visual, x-radiography, thermal and hardness techniques were selected for production evaluation.

Task II involved nondestructive evaluation of simulated production heat shields which were fabricated by four different organizations using four different fabrication processes. Applicability and difficulties of using the nondestructive inspection techniques were evaluated. Process dependent defects resulting from the various processes were identified. Most significant variations were noted in the uniformity and density of ablator packing and in the nature and effects of honeycomb core wet coat. As a result of Tasks I and II results, a change in wet coat material from silicone to phenolic resin was incorporated into the Task III efforts. Basis for the change were an improvement in panel sensitivity to inspections.

Task III defect investigation efforts were supported by inspection of all ablator billets using in-test model fabrication to assure material uniformity. In addition, all test models were x-radiographed to verify placement and location of instrumentation thermocouples.

On the basis of Task I, II and III efforts, a plan was generated for investigation of advanced inspection methods for critical defect location and identification at minimum cost.

EFFECTS OF TOTAL MISSION ENVIRONMENTS (TASK IV)

This task was established to determine the criticality of manufacturing defects in ablative thermal protection systems relative to environments other than hypersonic reentry. It would have been desirable that all conceivable manufacturing defects be tested in all possible environments throughout the service life of a Space Shuttle ablative heat shield subsystem. However, a program of such magnitude was not considered justified at this stage of the Space Shuttle Thermal Protection System (TPS) development. Rather, the defects and environments had to be evaluated and the matrix of potential environment-defect combinations reduced to a practical program which evaluated only the most critical.

As explained previously, the basic ablator fill material was changed from MG-36 to SS-41 (figs. 2 and 3) in the anticipation of obtaining a more uniform baseline material. An attempt was made to manufacture a version without honey comb reinforcement (SS-41F). This was discontinued when high density and delaminations appeared. Furthermore, in keeping with contemporary designs under consideration in the industry, the substrate configuration was changed from the single sheet approach to a faced honeycomb subpanel.

Subsequent investigations of defect-free panels of the above configuration were then conducted, followed by a detailed experimental study of the reaction of manufacturing defects in sequenced mission environments.

Intermediate Investigations of Other Environments

The first effort of Task IV concentrated on exposing ablative TPS panels, free of any known critical defects, to various combinations of environments in order to establish a sequence for final testing. The objectives were to characterize the defect-free ablative material in postulated environments and to select one or more sequences of environments which could interact with particular manufacturing defects to possibly precipitate failures in a typical Space Shuttle ablative heat shield system.

Specimen Description. - Ablative panels with total dimensions of 18-1/2 by 18-1/2 by 2 in. (47x47x5.08 cm) was selected for this task. These 16 panels (No. 3 to 18) furnished sufficient stock for the required test specimens and were large enough to

represent full-scale hardware. Each panel had a volume of 0.4 cu/ft (11 cm^3) and weighed approximately 6-1/2 lb (2.95 kg). Exact measurements and density are summarized in table 5. As a fabrication alternative, several of the ablative panels were made as a molding compound (see Appendix B).

Honeycomb sandwich subpanels were used to support the SS-41 ablative panels during the environmental exposures. The subpanels were made larger than the supported ablative panel to provide a 1/4-in. (0.6 cm) margin at the sides and 3/8-in. (0.9 cm) at the ends. The margins were used to hold the panels during test and to provide a vacuum seal surface.

Thermocouples were installed in the panels to be exposed to the thermal vacuum cycle. Three thermocouples were placed in each panel, two at 1/4-in. (0.6 cm) from the ablative surface, and the third at the subpanel/ablative panel interface. Ceramic insulation was used to position the junction at the proper depth and to protect the wires at their exit from the subpanel. Dow Corning 92-018 silicone adhesive was applied to the wires and the subpanel to prevent movement during handling.

After environmental testing, the panel assemblies were returned for preparation of flexural test specimens. Each ablative panel was separated from its subpanel and cut into eight specimens, 4 by 8-1/2 by 1-1/4 in. (10.2x47.0x3.2 cm). Four of the specimens were made with the honeycomb ribbon running in the direction of the long axis. The ribbon in the other four was at 90 deg to the long axis. All surfaces were ground by a diamond saw and by a surface grinder to assure a smooth, uniform texture.

Environments Investigated. - Exposures were selected as representative of the values anticipated on the bottom region of the Space Shuttle Orbiter based on reviews of references 4 and 5, and Space Shuttle preproposal effort.

Humidity: The humidity environment defined in figure 16 was used for most of the TPS panel tests. The environment is an accelerated test for 10 cycles of 24 hrs each for a total period of 240 hrs. Panels 4, 5, 6 and 7 were exposed to the reference environment, and, at the end of 10 days, Panels 4, 5 and 6 were removed for dehydration, while Panel 7 continued in the environment until 16 cycles. Due to the large fraction of weight gain in the SS-41, additional tests of several materials were initiated, using the environment shown in figure 17, which had a lower water-vapor pressure.

Dehydration: After removing the ablative panels from the humidity chamber, each was dehydrated. For dehydration, Panels 4, 5 and 6 were exposed to the following cycle:

- 24 hrs at 160°F (344°K) and 22 in. (560 mm) of Hg vacuum;
- 16 hrs at room temperature and 22 in. (560 mm) of Hg vacuum;
- 20 hrs at 160°F (344°K) and 22 in. (560 mm) of Hg vacuum.

Panel 7 was exposed to the following dehydration cycle:

- 48 hrs at 160°F (344°K) and 22 in. (560 mm) of Hg vacuum.

Acoustic excitation: A survey of the various acoustic environments indicated that the transonic acoustic environments, both during ascent and during descent, would be the design limiting environments. Typical required acoustic spectrums for these cases are shown in figure 18. Engine generated lift-off noise was found to be several dB higher in overall level than transonic acoustics, but it was eliminated as a test environment because it was confined to the aft end of the vehicle, was very short in duration, and most of the energy was at low frequencies, where the ablator panels are predicted not to respond.

Thermal vacuum: In selecting a realistic orbital temperature condition, it was assumed that orientation controls would not be used to actively control local temperatures and thus impose constraints on the mission. The minimum realistic fuselage temperature predicted was -167°F (162°K) and occurred near the engine pad mounted to the side of the tail structure. This temperature occurs at the outer surface of the TPS, and is based on a polar orbit. A colder temperature of -210°F (139°K) predicted on the engine pad is considered unrealistic, since heat addition within the engine pad would be required to prevent fuel freezing.

Studies have shown the maximum temperature during orbit, assuming an α_s/ε of 1.0, could be 260°F (400°K) and will occur for any orbit with $\beta \geq 75$ deg. Thermal control coatings should reduce the extreme temperatures. To be conservative, however, the thermal vacuum and cold soak test cycles shown in figure 19, which cover the environment extremes, were used in this task.

It was intended that only one thermal vacuum test cycle be used in these tests. However, failure of the heating system for one set of test panels resulted in the second test cycle (fig. 20) which included only vacuum exposure at ambient and cold soak temperatures.

Strain: A review made to determine the loading environment on the orbiter during the ascent flight phase revealed that a general consensus did not exist on the static design load, [± 3 psi (± 2 N/cm^2) load was being used at Martin Marietta]. Consequently, the decision was made to test to a design strain (1%) rather than a design load. A check made to determine if temperature was important during ascent found that temperatures below 15 to 30°F (263 to 272°K) were not expected at any point on the orbiter due to NASA's decision to go external with the LO_2 and LN_2 tankage. However, because it was realistic to assume some loading before reentry heating, straining cold [at -150°F (173°K)] to a proof load of 5 psi (3.5 N/cm^2) was chosen as a test condition.

Biaxial flexure of panels: The type loading chosen was to simply support the subpanel edges and apply a uniform pressure on the bottom of the subpanel, putting the ablator surface in biaxial tension. Pretest analysis predicted that a pressure of 9.08 psi (6.26 N/cm^2) would produce a 1% strain in the ablator surface at room temperature.

Four point flexure of beams: In order to further evaluate the possible changes which could occur in the ablator strength as functions of the environment (and eventually as functions of installed defects), four-point flexure beams, as previously described, were made from investigation panel ablator and tested at room temperature.

Material performance in environmental exposure. - Once the environmental exposure tests were begun, obvious changes occurred in the specimens. In the following sections, the available data on each specimen is summarized, including physical measurements, visual observations, and any other pertinent data taken during the environmental exposure. The specific sequence of environmental exposure for each test model is summarized in table 6.

Humidity effects: The SS-41 panels exhibited significant weight gain in a high-humidity, cyclic-temperature environment, with an average of 14% TPS panel weight gain at the end of 10 days in the specified environment. The weight gain versus time for these panels is shown in figure 21 and includes the subpanel weight. After exposure, the ablative filler in each panel was swollen and very soft, and the panels were noticeably warped with the ablator surface being convex. Due to the large percent weight gain of the TPS panels, additional humidity exposure tests were conducted at a lower peak temperature, to determine if lower water vapor pressure reduces the weight gain, to revaluate the ablative constituents, and to compare the SS-41 weight gain with that of a Martin Marietta ablator SLA-561 sample. The results of these tests are also shown in figure 21. To summarize, the phenolic microballoons were the apparent cause of the large weight gain, and apparently were capable of absorbing approximately 57% moisture by weight. In comparison, an SLA-561 ablative billet gained only approximately 5% moisture by weight. Lowering the water vapor pressure reduced the rate of weight gain.

Dehydration effects: Dehydration of the TPS panels brought their weights back to near their original weights and Shore "A" hardness and removed most of the warpage. Unfortunately, in all of the TPS panels, the ablative filler also separated from the honeycomb wall in many cells. It is believed that swelling during the humidity exposure may have crushed some of the microballoons, causing the filler to pull away from the cell wall during dehydration.

Transonic acoustics effects: Exposure of the ablative panels produced no observable adverse effects in either the ascent or descent spectrums. This was somewhat expected in that the ablator was in the unpyrolized state for both conditions. The spectrums experienced are presented in figure 22.

Thermal vacuum effects: The exposure of Panels 4, 6, 11 and 12 to the thermal vacuum cycle which included the hot [300°F (422°K)] cycle consistently caused darkening of the ablator and some warpage, indicative of considerable post curing and shrinkage of the ablator. The only other observable effect was the opening of cracks in Panel 4. The exposure of Panels 9, 10 and 14, which were exposed only to vacuum at ambient and cold soak temperatures, caused no observable change in the samples.

Strain effects (effects of biaxial flexure to 1% strain): In the biaxial flexure tests, the weakness of the bond which was initially used between the ablator billet and the subpanel compromised the test results, with disbonds occurring at loads and strains well below the desired levels. In addition to ablator/subpanel disbonds, obvious cracks occurred in the ablator surface in two specimens, Panels 5 and 9. Details of the test results are summarized in table 7 and figures 23 and 24. In all of the tests, measurements of the ablator surface strain showed inelastic behavior (both yielding and strain relief) due to TPS system failure at pressure levels and ablator strain levels well below anticipated values.

Biaxial flexure load to 5.0 psi (3.5 N/cm^2) during cold soak: The loading of Panels 8, 10, 12, 13 and 14 during cold soak caused no observable change in the samples. At the cold soak temperatures, the TPS panels were so stiff that very little strain occurred, even at the peak load 5.0 psi (3.5 N/cm^2). The deflection of the center of the panel was only on the order of .01 in. (0.025 cm).

Four point flexure of beams: The results of beam testing are presented in figure 25. Based on this data, the following observations were made: a) humidity and/or dehydration exposure obviously reduces the SS-41 material ultimate strain capability and stiffness; b) the ultimate strain of the SS-41F material is well below the ultimate strain capability of regular SS-41; c) the stiffness of the SS-41F was greater than that of the SS-41, however; d) minor variances appear to be the result of data scatter.

Conclusions. - Based on the test results of Part 1 of Task IV, the following environments were considered too severe for SS-41, at the test levels used:

- Excess humidity (and subsequent forced dehydration);
- 1% ultimate biaxial strain;
- Hot vacuum exposure.

Although the above are considered "critical" environments for defect-free SS-41 material, it was believed that future improvements to the thermal protection system could be eventually implemented to satisfactorily accommodate the actual environments

represented by the above tests. The weight gain and swelling on the SS-41 in the humidity environment, for example, can be reduced by changing formulation (e.g., cork filler as in SLA-561) or by possibly using a protective coating over the ablator panel. The 1% ultimate biaxial strain may be possibly achieved by either formulation change (e.g., increase the adhesive strength of the resin by filling with reinforcing particles much smaller than the bulk fillers), or process change (e.g., priming the fillers). The 300°F (422°K) temperature during the thermal vacuum exposure was considered unrealistically high, since it exceeded the predicted value of 260°F (400°K) for $\sigma_s/\varepsilon = 1.0$; use of thermal control coatings should significantly reduce the peak surface temperatures.

The investigations did verify the applicability of some degree of humidity, strain, hot/cold vacuum exposure, and the use of the four point beam flexure test as an index to strength changes. In addition, it was established that the SS-41 composite is a viable baseline for the remainder of this task and was suitable for the evaluation of manufacturing induced defects. A progress report was issued establishing the recommended approach to be used in the remainder of this task.

Final Investigations

Various manufacturing defects were exposed to a sequence of Space Shuttle-type environments to determine which defects later proved to be critical to mission performance. The applicability of conclusions from a study such as this is directly proportional to the ability to simulate the defects and environments in test specimens and the consistent performance of control models. Meaningful results were obtained and defects flagged despite some breakdown in optimum performance by the control specimens.

Selections. - The spectrum of environments was selected on the basis of the results of Tasks I, II and III (Ref. 2) and the investigation conducted during the early part of Task IV. Only those pre-entry environments which were believed able to develop manufacturing deviations into critical defects were chosen.

- High humidity (about a 5% weight gain);
- Ascent transonic acoustics (162 dB);
- Uniaxial flexure (∿1/2% strain in ablator);
- Thermal vacuum cycling (200 to -150°F-366 to 173°K).

Subsequent environments imposed on most of the test specimens, in order to display the ultimate sensitivity of the defects, were:

- Reentry heating [Q = 14 000 Btu/ft^2 (158.3 MJ/m^2)];
- Descent transonic acoustics (150 dB).

Although not specifically classified as an environment, four-point flexural testing to failure was conducted on beams extraced from many of the panels completing the vacuum exposure in order to obtain strength change trends.

Since mechanical performance is of major consideration in ablative heat shield design, particularly in nonentry environments, the flexural modulus and ultimate strain capability are two significant measures of material behavior. Variances in these measurements are believed to be strongly indicative of the effects of environmental exposure (and eventually, the effects of fabrication defects). Therefore, reliance was placed on the trends reported for the four-point flexure tests.

The selection of manufacturing deviations to be investigated in the above sequence of environments was based on a wide variety of probable defects classifications, considering our findings to date. Another guideline in the selection was the potential development of these variations to a critical condition during pre-entry exposures. Details fo the installed defects and panel number assignments are presented in figures 26 and 27.

Ablative Material Defects

- Delaminations;
- Unbonds to honeycomb;
- Density;
- State of cure;
- Filler moisture content;
- Inhomogeneities.

Honeycomb Core Defects

- Broken ribbons;
- Broken node bond;
- Undercut.

Disbond to Subpanel

The as-fabricated test panels are illustrated in figure 28, with the construction details presented in Appendices B and C. The subpanels were made larger than the ablative panel to hold the panel during tests and to provide a vacuum seal surface. In both the ablative billets and the subpanels, the honeycomb ribbon ran in the shorter direction. There was a total of 27 panels in this final phase of environmental investigation. The specific defects named were studied with variances of each defect considered. Seven panels were defect-free, control panels.

Also shown in figure 28 is the subsequent subdivision of the ablator billets for exposures in the later environments and beam flexure testing. Due to facility space limitations, the 27 investigation panels were grouped into three waves (8 each) and a control, nonenvironment group.

WAVE	PANELS							
I	19	23	25	27	28	29	31	33
II	21	22	24	26	30	34	35	36
III	37	38	39	40	41	42	43	44
By-Pass	20	32	45					

Wave III panel environments ended after the thermal vacuum exposure. All panels in Waves I and II went through all the tests, including reentry heating, descent acoustics and four-point beam flexure. The by-pass panels were introduced to the environment sequence at the reentry heating point.

The sequence of environmental exposures and interstitial quality control inspections on the waves of panels is graphically illustrated in figure 29, which represents a mission profile.

Those panels in Wave III, containing ablator honeycomb core defects and disbonds to the substructure, were not tested in four-point flexure or for descent acoustics effects on char. This was justified because the particular investigation objective for these panels was to determine whether or not the combination of these defects and environments (up to and including thermal vacuum exposure) would initiate or propagate a crack or a disbond in the total system in the unablated condition.

The numerous examinations dispersed through the exposure sequence displayed in figure 29 served as useful indices of periodic physical changes which could be symptomatic of defects developments and/or reaction to specific environments.

Environment Exposure Details

Humidity. - All three waves of panels were exposed to a single 24-hr cycle in our humidity chamber similar to those experienced in Part 1 of Task IV. This soaking was anticipated to produce an approximate weight gain of 5% moisture in the ablator material.

Ascent and descent acoustics. - Acoustic vibration tests were conducted to simulate liftoff and reentry transonic phenomena. It was expected that during the transonic period of the descent, the acoustic effects on the char could be significant since the char will have cooled considerably by that time and will be much more brittle than during the hypersonic heating phase. The tests were performed using a closed environment acoustic generator (Wiley Laboratory Model WAS-3000). Spectrum control was achieved using a modulator filtering system (General Radio Model 1925). Plywood dummy test panels were used for spectrum shaping with a B&K 1/4-in. (0.6 cm) microphone placed a short distance from the panel center. Test models were installed in rigid wooden frameworks with the subpanel extremities framed with plywood to facilitate adequate clamping. The required spectrum for ascent and descent was shown in figure 18.

Uniaxial flexure. - This test was designed to simulate the possible difference in pressure between the region under the subpanel vs the approaching vacuum on the ablator surface during ascent. Uniaxial flexure in the weak direction of the panels (constant moment perpendicular to the ablator honeycomb ribbons) was imposed on all three waves over a 400-in. (10.16 m)-radius mandrel calculated to produce a 1/2% strain in the surface of the ablator. This test was established as a result of measured strain data previously obtained in biaxial flexure tests. The bending load was applied by a vacuum bagging technique using electric monitors to verify contacts at numerous points on the subpanel and floating, nonstraining lengths of metal strips to indicate surface elongation on the ablator surface.

Thermal vacuum exposure. - The purpose of the hot/cold vacuum cycling of all three waves was to simulate the variations in conditions which can occur during the orbiting stage. These were extended exposures, lasting up to two weeks, and involved pumpdown, a heat soak for 40 hrs at 200°F (366°K), and five drops from ambient temperature to -150°F (173°K) and back to ambient temperature. The nominal vacuum level was to be 1×10^{-5} torr (1.3×10^{-3} N/m^2).

A chamber-within-a-chamber arrangement was used. Two rectangular temperature control boxes each supported four of the test panels. These boxes were lined with heater tapes and liquid nitrogen piping which varied the temperature histories as required in accordance with panel-installed thermocouple readings.

The boxes were centrally located in a 4-ft (1.2 m) diameter by 8-ft (2.4m) vacuum chamber with manipulator arms and viewing ports (Torr Vacuum Corp.). Vacuum was achieved using diffusion pumps, once a mechanical roughing pump with a rotor lobe blower reached the 20 to 50 μm range, and then maintained using an ion pump. Vacuum was monitored with a hot cathode ionization tube.

Each wave of panels had 24 iron-constant thermocouples installed at the surfaces and in the subpanels; details of the panel arrangements and thermocouple locations are presented in figure 30.

Reentry heating. - Reentry heating was simulated in the 1 mW Martin Marietta Plasma Arc Facility using a 10.0-in.-(25.4 cm) diameter nozzle with the panel positioned at a 20 deg angle to the test stream. The panel was rigidly attached to the model holder at the four attachment points. This holder was designed with a water-cooled leading edge machined to a 1.25-in.-(3.18 cm) radius. The blunting of the leading edge was found to enhance flow uniformity and improve heating distribution, as shown in figure 31. This test condition was calibrated using a dummy metal plate installed in the specimen location and equipped with five small calorimeter bodies.

The specimens consisted of just the ablator billets [8 by 12 by 1 1/2-in. (20.3 x 30.5 x 3.8 cm)], resting on an aluminum support plate's protruding rails. They were held in place with four coarse-thread screws installed from beneath and penetrating approximately 1 in. (2.54 cm) into the back surface of the ablator billet. Three chromel-alumel thermocouples were centrally located in each panel, with alumina tubing perpendicular to the back surface. The locations of the junctions were (nominally); outer surface, mid thickness and back surface.

The purpose of these exposures was to: display any critical aspects of the defects, compound any already developing disturbance, evaluate defect influence on thermal response, and create char formation for the subsequent acoustics exposure.

Four point flexure. - Beams made from parts of the panels in Waves I and II and three control panels (all virgin material) were tested in four-point flexure to determine changes in yield strength, ultimate strength and flexural modulus as a result of defects and/or the exposure environments. A sketch of the test beams and their dimensions was shown in figure 28. The load was applied at two centrally located points [2 in. (20.3 cm)] apart. A deflectometer was installed at the beam center, touching the bottom of the beam ("inner side" of the ablator) through a small, thin, metal pad. Data consisted of load vs deflection plots. The tests were conducted on a BLH PT100 Testing Machine using a speed of 0.25 in./min (0.64 cm/min).

Test data. - Data obtained from the exposure of 24 ablator panels (plus 3 by-pass panels), subsequently subdivided into 19 plasma arc/acoustic specimens and 133 flexural beams, are presented. This section summarizes the primary results while referring to the inner-sequence non-destructive examinations presented later. Discussions of the ramifications of the defect environment performance patterns emerging in the following summaries of test data and specimen appearance are covered at the end of this section.

Pretest appearance: The honeycomb subpanels were checked for flatness prior to ablator bonding while the ablator billets themselves were machined in a flat condition. Following the bonding of these two components at 200°F (366°K), the completed assembly took a slight curvature at room temperature due to differential thermal contraction in the materials involved. This appearance was not of sufficient magnitude to cause concern, however, since h_A in figure 32 was approximated at 0.025-in. (0.064 cm). Ablator surface hardness, which had an average value of 85.6 on the Shore D scale, is discussed later.

Humidity exposure: The investigation panels picked up an average of 7.53% moisture in a 24-hr humidity chamber exposure (see table 8). Correspondingly, a curvature opposite of that described above occurred due to material swelling, with an average resulting h_s of .087 in. (0.22 cm) in figure 32. Hardness values dropped to an average of 67.9 due to this environment.

A typical trace of relative humidity and chamber temperature vs time for a single 24-hour humidity exposure is presented in figure 33. These results differ from those presented in figures 16 and 17 because of a difference in venting procedure on the down side of the cycle and because the percentages reported in figure 21 included the weight of those subpanels [approximately 2.61 lb (1.18 kg)].

Ascent acoustics: Twenty-four test panels experienced an ascent acoustic environment typified by the spectrum presented in figure 34. The minimum overall dB range was 161.5 (Panel 24) and the maximum (Panel 37), 164.0, with an average of 162.9 dB (see table 8). No discernible damage was noted, even after an ultrasonic inspection of the bond system. Little change in panel curvatures was noted.

Uniaxial flexure: The initial investigations of this test were conducted with a 200-in. (5.08 m)-radius mandrel. Control Panels 31 and 44 were flexed in the longitudinal direction (perpendicular to ribbon direction) over this original mandrel, producing approximately 1% strain on the surface of the ablator in both experiments. A crack appeared in the ribbon direction for Panel 44 while none was observed in Panel 31. Since this pointed out the marginal aspect of this composite in the neighborhood of 1% strain, the mandrel was changed to a radius of 400 in. (10.16 m) in anticipation of 0.5% ablator surface strains.

All three waves of test panels were flexed over the 400-in. (10.16 m) radius mandrel in an attempt to produce 0.5% strain in the outer face of the ablator. The previous exposure in the humidity chamber, however, had already put a curvature into the composite assemblies due to ablator swelling from moisture absorption. Since the strain in existence on the ablator surface prior to flexing was identified as a moisture-induced swelling, the new strain measured during the uniaxial flexure represented just the incremental amount needed to achieve the planned 0.5% value (see table 8). This was further demonstrated by flexing a panel which had not been humidified (Panel 32). Measurements indicated 0.6% surface strain in uniaxial bending over the 400-in. (10.16 m)-radius mandrel.

The Wave III panels, following the vacuum chamber exposure (discussed later), were flexed again over the 400-in. (10.16 m) mandrel previously used for newly-made panels. The difference this time was that the ablator material was "dry", as compared with the former condition (humidity affected) of these and other panels. A comparison of the measured strains is also presented in table 8. No failures were noted.

Thermal vacuum cycling: The investigation panels were exposed to hot and cold cycling in the Martin Marietta thermal vacuum chamber in the three waves previously discussed. Results of these exposures, including the specific details of the temperature cycling, typical temperature histories, typical temperature extremes at each thermocouple location, and a vacuum history are presented in figures 35 to 41, and table 9.

Wave I experienced difficulties at one end of the thermal control boxes due to insufficient cooldown and heatup piping and tapes, respectively. Although this produced severe, unplanned-for, thermal gradients along the lengths of Panels 2, 3, 27, 29 and 33, no aspects of damage, cracking, delamination, etc. were noted in post-exposure examinations.

Wave II, in redesigned boxes, experienced much more uniformity in the temperature distributions, although the single hot cycle was somewhat in excess of the desired level.

Wave III was also tested in uniform environment cycles. Several areas of the temperature control boxes tended to overshoot during the cryogenic cooldown cycles, with no apparent damage to the specimens. The vacuum chamber pressure history for the Wave III exposure presented in figure 41 is typical of that experienced in the other two waves.

Post-test examinations indicated considerable weight losses due to the vacuum (density below the as-fabricated values), concave curvature on the ablator surface (with one exception), the highest average level of ablator hardness (88.1), and a minimum amount of surface discoloration (post curing). No ablator disbonding from the subpanel was noted. An upward bowing [h_A 0.05 in. (0.13 cm)] was noted in all panels except for Panel 30, which was essentially flat at the end of its vacuum exposure.

Test panel disassembly: All 27 test panels had their ablator billets removed with a band saw cut in the ablator material, just above the bondline. The immediate observation in each case was that the two separated components sprang back to an essentially zero curvature. This further substantiated the previous belief that a stress pattern with corresponding panel curvature had been established during the cooldown from the original bonding process. Only one separated billet presented an unusual appearance, Panel 30. The ablative filler columns in each honeycomb cell were completely separated from the cell walls and could be manually moved with ease in the Z direction.

Following the final X-ray, the billets for Waves I and II and the three by-pass control panels were subdivided into specimens for plasma arc exposure and beam flexure testing.

Entry heating exposure: The condition established for the wedge-type exposure of the 12 x 8 x 1.5 in. (20.3 x 30.5 x 3.8 cm) specimens in the Martin Marietta 1mW Plasma Arc Facility were as follows (center of panel conditions):

$\dot{q}_{cw}$ = 13 Btu/ft^2-sec (0.147 MW/m^2)

$H_{s(avg)}$ = 8545 Btu/lb (19.86 MJ/kg)

Rectangular heat pulse

1100 second duration

Q_{cw} = 14 300 Btu/ft^2 (162.6 MJ/m^2)

Wedge angle = 20°

Mass flow = 0.05 lb/sec (0.023 kg/sec)

p_s = 15 torr (2000 N/m^2)

$\sim$3 test panels per facility light-off.

A summary of the results is presented in table 10. The average surface temperature for all exposures was 1640°F (1713°K) while the back surfaces achieved a mean value of 250°F (394°K). The condition appeared ideal in that a copius amount of char was developed (of interest in the subsequent test) while the backface of the billets was essentially unpyrolyzed.

The test time on two of the specimens was foreshortened. Panel 26 had been in the environment 712 sec when a flame-out of the facility occurred. In consideration of the cooldown experienced during the repair of the facility, it was not considered advisable to reheat this specimen. A representative amount of char had been established in the exposure to a Q of 9250 Btu/ft^2 (105 MJ/m^2). Panel 30, with its loose core fill, lifted a fraction of an inch above the water-cooled copper leading edge at 900 seconds, completely voiding the surface heating rate distribution, as evidenced by the sudden loss of its high temperature glow. Similarly, the Q of 11 950 Btu/ft^2 (135.8 MJ/m^2) was sufficient.

Most panel surfaces appeared hardened into a tightly-knit cap skin characteristic of this type of ablator. In addition to numerous cell-fill displacements in Panel 30, the most spectacular surface failures occurred in Panels 35 and 36. Here, large pieces [10 sq. in. (64.5)] of the outer surface [0.1 to 0.2 in. (0.25 to 0.50 cm) thick] buckled off the main body of the ablator. Typical photographs of test specimens are shown in figures 42 and 43.

Plots of the maximum thermocouple readings through the thickness of the panel center are presented in figure 44. They appear to fall into the two groups indicated.

Entry transonic acoustics: Immediately after the entry heating exposure, the same investigation panels were arranged in pairs on their regular honeycomb subpanels, bonding carefully with a slight vacuum. The panels were butted side by side with a wooden form around the entire periphery to simulate a continuous TPS application. A typical recording of the descent acoustic spectrum imposed on the test assemblies is shown in figure 45, while table 11 summarizes the tests and their results. Figures 46 and 47 illustrate the range of surface reactions achieved.

About 1/3 of the panels went through the exposures without significant cell-fill losses. The most critical reaction was encountered in Panel 21. The average cell loss for the panels in the right-hand group of figure 44 was about 1 1/2 cells per panel while those in its left group averaged about 10. Those panels already damaged in the entry heating exposure (Panels 30, 35 and 36) lost considerable cells and apparently deteriorated their surface to a greater degree.

Four-point beam flexure: Summaries of the test results and data reduction on beams in four point flexure are presented in tables 12 to 15. One error in specimen fabrication (Panel 30) left us without proper D and E beams and essentially extra A and B beams. Extrapolation was applied based on the trends in the values on the other beams of Panel 30, however. In addition, all beams for Panels 20, 32 and 45 were fabricated 1 1/4 in. (3.18 cm)-thick and tested to failure prior to the plan of using two heights of beams.

Two beam heights were used in the major portion of this task because a recent study (see Appendix D) found that a low shear modulus contributes significantly to the flexural deformation of materials such as this ablator. Calculation procedures are presented in Appendix D. A comparison of the small increase in modulus (E) is apparent in examining table 14 against table 15.

Observations and Inspection Summary

Materials assurance. - All material used in test sample preparation was X-radiographed and the hardness verified to assure uniformity of test samples.

Panel evaluation. - The environmental exposure panels were characterized in the pretest condition and incrementally after each exposure sequence to provide bench marks for (1) monitoring the influence of environment on nondestructive evaluation methods, and (2) for monitoring programmed defects for growth induced by environmental exposure. All panels were visually inspected, X-rayed, sonically inspected and measured for hardness. No changes were noted during any exposure cycle by X-ray or sonic techniques. The hardness varied considerably with environmental exposure as shown in table 16.

Post-test examinations. - Charred specimens were examined by making cross-section cuts down the centerline of the ablator billets which had experienced the descent acoustics exposure in the charred state. Typical photographs of six of these views are shown in figures 48 and 49. In each of the samples examined, the cells in the immediate vicinity of the centerline diamond saw cut were carefully removed in order to cull out any crack patterns in the char which may have been introduced by the sawing.

Table 17 and the photographs indicate that greater ablator pyrolysis penetration occurred in the forward half of the models due to the high level of heat in the distribution shown in figure 31. The char depth values reported are measurements extending from the original surface to the approximate plane within the ablator representing full or near fully developed char. One third of the models had a large void zone in each cell in the char just below the cell's hardened outer cap. Unfortunately, panels containing these were standard, non-defect models.

The distribution of horizontal fissures (other than the outermost) indicates an even balance between those classified "few" and "many". Control specimens fared well in this respect (except Panel 45) along with Panels 25, 26, 30, 33, 35 and 36. A greater number of cracks per cell occurred in the areas of deeper ablation penetration. In all the specimens, the honeycomb node bondings opened up in the char regions. Char fissures such as these are typical in silicone ablators and usually occur during the cooldown portion of a heated exposure due to char shrinkage, reacted by sintered attachment of the material to the cell walls. In many of our cross-sections, continuous lines can be seen from cell to cell.

The variations in ablator density noted from time of fabrication to the time of separation from the subpanel, before entry heating are shown in table 18. Interim densities are noted for the period after a humidity exposure and the time immediately following a hot vacuum/cold vacuum sequence and were estimated based on an assumption that the subpanel part of the panel assemblies experienced no changes.

Task IV evaluation. - Several defects have proven to be critical when exposed to environments other than reentry. The first objective of this evaluation was to establish a norm for defect-free construction. Although the control specimens did not perform in a totally consistent or perfect manner, they still represent the norm against which the effects of intentional defects on performance must be assayed.

The second objective was to compare the reactions of the altered material against an established set of criteria, violation of which would be considered critical.

Control material standards: What are the characteristics of the control material in the sequence of environments? Recalling the observations reported, the baseline performed as follows, using average values in most instances.

The control panels gained about 7.2% moisture (by weight) in the humidity environment. Although uniaxial flexure strain data in the humidified state proved inconclusive, similar data in the as-fabricated and post-vacuum states indicated marginal elongation capability of the ablator in the 1% region and no failure at the 0.60% strain level. Physical appearance after the ascent acoustics and thermal vacuum cycling were good, with intact bonding to the subpanel.

The backface temperature in the entry heating pulse peaked at 315°F (430°K) [260°F to 400°F (400 to 477°K) range] while the surface experienced 1585°F (1136°K) [1515°F to 1665°F (1097 to 1180°K)]. All surfaces emerged with firm, hardened cell caps.

Descent acoustics spalled an average of six cells per control panel (0 to 14, range) with two panels developing fragile caps and three panels retaining a firm surface. Subsequent sectioning revealed a predominance of cells with a single, large void just beneath the outer caps and a relatively low number of internal char cracks, (exception: Panel 45). The average char thickness formed by control models was 0.75 in. (1.91 cm) (overall) for those fully exposed and 0.78 in. (1.98 cm) for the bypass group.

Four point flexural summaries for the control material are presented in table 19. It would appear that the exposure to the sequence of environments has had little effect on the average strength value of the ablator when comparing control specimens with and without environment histories in the virgin state.

Evaluation criteria: Evaluation of the basic material behavior, as well as the determination of the criticality of a given combination of defect and environment, required a definite design and performance criteria. For this task, the design and performance criteria were based on reference 4 and a review of Space Shuttle proposal efforts. In the assessment of the reactions of selected manufacturing defects relative to nonentry environments, certain other criteria became apparent.

Significant amounts of the following occurrences have been established as being critical to orbiter performance:

Pre-entry

Decreased ablator strengths;

Increase in elastic modulus and reduction in ultimate strain capability;

Loss of ablative material;

Initiation of ablator cracks;

Fill separation from cell walls;

Ablator billet delamination;

Material shrinkage.

Entry

Excessive backface temperature;

Loss of ablative material - outer face, char, other;

Surface roughening;

New, large internal voids;

Internal char cracks;

Loose cell surfaces;

Pyrolysis penetration.

Critical aspects of tested panels: The final analyses of the clues uncovered throughout and following the test sequence require careful comparisons against the standard panels. The environment at which the intended defect developed to a stage of possible criticality, and whether or not the prelaunch condition of these defective panels would have displayed the same deviations without the full environmental history, was not determined in this program.

Response to environments

High humidity - No violations of the criteria were apparent after this exposure. Reduced hardness values could be indicative of weakened ablator fill.

Ascent acoustics - No degradation occurred.

Uniaxial flexure - Testing in a wet state unfortunately was inconclusive with respect to defect panels. Panels investigating primary bond and honeycomb breaks (with no history of humidity exposure) strained successfully to 0.33%.

Thermal vacuum cycling - Although very few developing defects appeared in this test sequence, it is believed that this total environment history had a significant influence on events which followed. The environment thoroughly separated the ablator fill from its honeycomb in Panel 30, thereby pointing out the criticality of the B-staging heat level for the core wet-coating operation. In addition, Panel 23, representing low density deviations, displayed some shrunken core fill.

Since this was the end of the investigations concerning ablator to subpanel disbonds, broken honeycomb ribbons, and broken honeycomb node joints, it is surmised that, within the magnitude of these defects simulated, no criticality was evident.

Reentry heating - Undercut core errors proved here to be significant, as previously described, with considerable losses of outer material (Panels 35 and 36). Also, the questionable condition of Panel 30 deteriorated further in this exposure, with considerable unevenness developing on the surface.

Plotting of the thermocouple reading (max) vs position in the ablator thickness created two groupings of data, as summarized in figure 44. The right-hand group (Panels 19, 22, 23, 28, 29, 33 and 45) is of considerable interest since 5 of the panels were in Wave I, 4 of these filled Box 1 of the vacuum chamber during the Wave I exposure, and the only panel of Wave II to fall into the right-hand group was Panel 22 (investigation defect = overcure). Recalling the thermal control difficulties encountered during the Wave I thermal vacuum exposure (see table 9), it is surmised that any degree of elevated temperature for a period of time is equivalent to post-curing, and can lead to higher peak interior ablator temperatures during entry heating.

Descent acoustics - This test, following the reentry heating pulse, effected several significant changes in the samples. Once again, observations had to be restricted to external examinations whereby the material losses, surface roughening and stability of the outer layer of char were assayed.

Exceptionally fragile attachment of outer char caps point to the defects of undercure (Panel 21), wet basic material (Panel 26) and long B-staging of wet coat. However, even two of the control panels also displayed this phenomena.

Adverse surface roughening was predominant only in the defect previously discovered--the condition deteriorated farther in the acoustics environment. Significant cell spallations occurred for the undercured, hot B-staged and undercut core specimens. It perhaps was a matter of time before Panels 26 and 29 would have joined this group. The worse inner cell char losses were observed on the undercured and undercut core panels.

Sectional specimen examination - A negative statement could be made for every panel with respect to some aspect of the cross-section examinations--either more char formation than the standard's average, a large void just below the outer material cap, uneven outer surface, or more than the usual number of cracks dispersed through the section. The panels which were judged to be in a critical condition, relative to the appearance of the standard material sections, were Panels 21, 22, 23, 29 and 30, due mainly to a significant number of internal char cracks and/or considerable pyrolysis penetration.

Four-point flexure deductions - The virgin material of Panels 21, 24, 25, 26, 29, 33 and 34 displayed increases in elastic moduli in either the weak, strong, or both directions (see figure 50). This property deviation highlights the following defects:

Undercure	S (strong)(typ)
High density	W/S
Wet basic ingredients	W/S
Long B-staging of core wet coat	W/S
Horizontal cracks in the ablator fill	W/S

Yield strength data indicates that the following panels suffered declines: 21, 23, 27 and 30 (all in the weak direction) as indicated in figure 51. These represented:

Undercure;

Low density;

Undermixed;

Hot B-staging of core wet coat.

Ultimate strengths, as compared in figure 52, show degradations in Panels 21, 23, 30 and 35, indicative of:

Undercure;

Low density;

Hot B-staging;

Undercut core.

Primary indications of possible criticality focus therefore on:

Undercured ablator;

Off-density composites;

Undermixing;

Undercut core;

Improper B-staging of the core wet coat;

Horizontal cracks in the ablator;

Wet basic ingredients.

These apparently will have an effect on any flexural strength requirements up to the time of entry.

Designation of critical defects

Table 20 summarizes all the adverse comments made with respect to the intentional defect, the symtoms noted, and the environment(s) at which they were noted. If one were to be guided by the trends noted in the four point flexure tests, every defect could be suspect when compared to the standard results. The nature of this type of testing, however, would require many more samples than were used in this study, and we must consider other parameters.

The defects which must be avoided therefore center on ablator undercuring and overcuring, ablator low density, improper B-staging of the honeycomb core's wet coat, and undercut core topped off with ablator material to achieve a desired height of ablator. These defects have, in this study, displayed combinations of excessive backface temperature, internal char fracturing, surface deterioration, and material losses. The critical period begins at entry and continues to the safe return of the vehicle.

ADVANCED INSPECTION METHODS (TASK V)

Production of ablative heat shield panels involves not only the establishment of fabrication technology to formulate materials and assemble panels but also the development of controls and inspection methods to assure production uniformity and resultant performance reliability. Elastomeric ablator materials present a unique challenge to inspection technology because they can be fabricated with a wide variation in physical properties using the same basic formulations and fabrication processes. Physical property variations, in turn, can significantly affect the performance of the ablator in a flight environment and its response to nondestructive evaluation methods.

Engineering specifications for ablator materials must define required physical properties and tolerances on each property and/or fabrication parameter in accordance with end item performance requirements. In short, critical defects criteria (property and/or process variation) must be identified to permit detection with a demonstrated confidence level while avoiding control and inspection of nonrelevant parameters. Identification of critical defects and critical inspection parameters is accomplished by a concurrent iteration process during the materials development program.

General elastomeric ablator material anomalies have been established in previous work. Likewise, a general understanding of inspection approaches and the reaction of nondestructive evaluation methods to material anomalies has been established. The major objectives of the Task V program were to investigate advanced methods for inspecting and characterizing ablative heat shields and to develop improved methods for locating and identifying defects. Major efforts have been directed toward:

Reducing costs of inspection while maintaining maximum inspection confidence.

Verifying critical processing parameter conformance while minimizing in-process inspection.

Our approach has been directed primarily toward nondestructive evaluation techniques.

Discussion of the Problem and Approach

Previous work has shown that elastomeric ablators are "forgiving" materials whose performance is unaffected by relatively large changes in physical properties. Specific areas of concern are limited to:

Bond strength of the ablator to support subpanel;

Bond strength of ablator to honeycomb core;

Disbonds, cracks and delaminations; and,

Inhomogeneities in the ablator.

Change of the ablator mixture from MG-36 material to SS-41 material required some basic characterization to determine response to nondestructive evaluation methods. Change from the single facesheet to the honeycomb panel substrate also resulted in additional characterization. Basic concern areas did not change. The overall evaluation approach is shown in table 21.

Specimen Fabrication

NDT standard density/thickness variation panels. - Specimens for comparison and evaluation of nondestructive inspection techniques were fabricated early in the program such that the same specimen could be used for evaluation of various techniques. Twenty-four density/thickness variation samples were fabricated with density variations from 15 to 17.5 lb/ft^3 (240 to 280 kg/m^3) and thicknesses from 1/2 to 2 in. (1.3 to 5.1 cm). Specific description is shown in table 22.

NDT standard unbond reference panels. - Four standard unbond reference panels were fabricated with intentional unbonds. These were:

High pressure cure unbond panel;

Nominal pressure cure unbond panel;

Low pressure cure unbond panel;

Destructive unbond panel.

Each of the three pressure-cure variation panels were fabricated with intentional unbonds between the substructure facesheet and the ablative honeycomb structure in size ranges from 1/4-in. (0.64 cm) diameter to 2-1/2-in. (6.4 cm) diameter as shown in figure 53. The unbonds were created by placing a disc of pre-cured adhesive at the interface to maintain acoustic properties in the unbond area in a condition representative of an initial lack of bond or a secondary unbond. Figure 54 is a plan view of the destructive unbond panel. These unbonds were made by inserting a spatula at the desired interface to simulate a secondary unbond condition of the type created by handling and/or secondary environmental exposure conditions.

Unbonds were located as described in figures 54 and 55 as follows:

Unbond "A" - Bond Material and Facesheet #2 interface;

Unbond "B" - Facesheet #1 and Adhesive Film interface;

Unbond "C" - Facesheet #2 and Adhesive Film interface;

Defect "D" - Core #1 crushed and removed.

X-Radiographic Evaluation

X-radiographic evaluation is an effective tool for monitor of cracks, voids, density variations and mixture variations in elastomeric ablators. Use of x-radiographic techniques in production is limited primarily by inspection costs. Emphasis of the x-radiographic evaluation task was therefore directed toward automated inspection at maximum sensitivity. Initial work was directed at radiometric attenuation methods for indirect determination of ablator density.

X-ray energy absorption. - X-ray and gamma ray gaging is used routinely in industry to monitor the thickness of materials. Such gaging is based on the principle that a material will attenuate transmitted radiation according to the relationship:

$$I = I_o e^{-\mu x}$$

where: I is the intensity of transmitted radiation; I_o is the

intensity of incident radiation; μ is the linear attenuation coefficient; x is the material thickness.

and:

$$\mu = \frac{\mu_o}{\rho}$$

where: μ_o is the mass attenuation coefficient; and ρ is the density.

If the material density is held constant, μ_o and μ are constant at a constant energy value and the thickness x may be determined indirectly by determining the energy absorbed, i.e.,

$$x = - \frac{\ell n \left(\frac{I}{I_o}\right)}{\mu}$$

Conversely, if the thickness x is held constant, then

$$\mu = \frac{\mu_o}{\rho} = - \frac{\ell n \left(\frac{I}{I_o}\right)}{x}$$

$$\rho = \frac{\mu_o \, x}{\ell n \left(\frac{I}{I_o}\right)}$$

An experimental setup (figs. 56 and 57) was assembled to measure x-ray absorption characteristics of SS-41 ablator panels at various densities. Since the SS-41 ablator is a mixture of several materials, the equivalent amounts of each component of the mixture were also characterized to evaluate the effect of slight variation in mixture on the measured density. Measurements were made using a Baltograph 5/50 kV, 20 mA, 1 mm Be window x-ray source for the 0 to 50 kV energy range and a Norelco Model MG50, double focus tube, 3 mm Be window x-ray source for the 50 to 75 kV energy range. A "Radocon" Model 575 with a Model 612 proportional counter probe (Victoreen Instruments) was used as a detector. All exposures were made at 5 mA and at a 30 sec (equilibrium flux) counting cycle. An 18.0 in. (45.6 cm) source to detector distance was used for all measurements. The setup and x-ray energy output were monitored before and after each

experimental run. Temperature and barometric pressure corrections were made for all runs. A typical energy output run is shown in figure 58. The 24 Series A reference specimens were run to establish energy absorption versus density and thickness. Relative absorption of the 1/2-in. (1.3 cm)-thick specimens is shown in figure 59. This figure illustrates the increase in energy attenuation with increasing density. It also shows that the material is free from characteristic absorption peaks over the energy range monitored. At the low energy end of the spectrum, characteristic absorption peaks may not be indicated by this work due to the low incident flux and measured transmitted flux. The upper portion of the spectrum is, however, of primary interest due to the film image sensitivity realized at 65 to 75 kV exposures.

Components of the SS-41 mixture were run in concentrations equal to that required to formulate a 2-in. (5.1 cm) thick panel. These runs were repeated at twice and three times the basic mixture concentrations to evaluate the effect of mixture variation on absorption. Figure 60 shows the relative absorption of mixture components. The glass microspheres and resin are the most attenuative of the components and cause the greatest change in attenuation with slight variations in concentration. A 10% (by weight) change in the glass microsphere content could result in a 2.5 lb/ft^3 (40 kg/m^3) error in radiometric density measurement on a panel. Since a 10% change in the mixture would be considerably beyond normal mix tolerances, radiometric gaging may be considered as a viable nondestructive material density evaluation technique when used in combination with process control.

Calculation of linear and mass attenuation coefficients for panels of increasing thickness shows a considerable variation from actual values. At 65 kV, absorption coefficients varied from $\mu = 1.44$ & $\mu_o = 5.61$ for 0.5-in. (1.3 cm) thick panels, to $\mu = 1.77$ & $\mu_o = 3.06$ for two-in. (5.1 cm)-thick panels at a nominal 16.0 lb/cu ft (256 kg/m^3) density. (See table 23.) The classical absorption calculations have been derived for incompressible materials. Elastomeric ablator mixtures are compressible and attenuate x-ray energy primarily by internal scatter. Classical calculations do not closely apply. Experimental generation of absorption versus density data must be determined for each production thickness.

The conclusions and recommendations are as follows:

X-radiometric (or gamma) gaging is feasible for automatic monitoring of SS-41 panel density;

For a production operation, an increase in counting time would be recommended to improve measurement precision;

Process control of ablative mixture and panel thickness measurement must be performed to minimize errors in the x-ray readout.

A schematic concept for an automatic panel gaging setup is shown in figure 61.

X-ray evaluation for soundness. - Demonstration of the ability of x-radiography to ascertain ablator panel soundness was accomplished by fabrication and use of ablator step wedges and penetrameters for monitoring x-ray sensitivity. The step wedge was machined from a billet of 15 lb/ft^3 (240 kg/m^3) material and was stepped in 1/8-in. (0.32 cm) increments from two-in.-thickness down to a 1/2-in.-thickness (fig. 62). The step wedge was X-rayed along with the panel to provide an internal reference for comparison of variations within the panel and for monitoring of the contrast sensitivity of the finished radiograph.

The overall radiographic resolution was monitored by means of a penetrameter. A penetrameter was machined from a billet of 15 lb/ft^3 (240 kg/m^3) SS-41 material to a final thickness of 0.040-in. (0.102 cm) [for use on a 2-in. (5.1 cm) material]. Three holes were then drilled in the material having diameters equal to 1%, 2% and 4% of the panel thickness (ref. 6). Figure 63 illustrates a SS-41 penetrameter for use with 2-in.-thick panels. The penetrameter was mounted in a conventional 35 mm photographic slide frame to improve handling characteristics. A penetrameter was radiographed with each panel to provide an internal measure of the radiographic sensitivity. Visibility of the penetrameter corresponds respectively to 1%, 2% and 4% sensitivity.

The step wedge and penetrameter were used to establish an optimum X-ray technique for evaluation of all program panels.

In-motion radiography. - One of the major problems in X-raying any honeycomb bearing material is the parallax effect. Parallax is the result of using a point x-ray source which produces a

conical beam of energy. As the beam spreads, it does not penetrate along the axis of the honeycomb cell, thus the resultant x-ray image of a honeycomb cell is out of registration from top to bottom (see fig. 64 and 65). As the thickness of the honeycomb increases, the parallax probelm becomes more severe. In-motion radiographic techniques have been used successfully to minimize the parallax in examining structural honeycomb materials and should be applicable to ablative panels. The in-motion technique involves use of a collimating slit limiting the x-ray beam to the center parallel rays. The part and film are then moved smoothly and uniformly through the collimated beam to expose the film (fig. 66). By varying the slit width and the travel speed, the parallax and exposure may be controlled. The path of part travel may also be varied to accommodate exposure of curved parts with minimum parallax.

Ablator panels were taken to the Lockheed Georgia Company, Charleston, South Carolina, for evaluation on a production in-motion radiographic system. This system is an integral part of Lockheed's routine x-radiographic examination of honeycomb panels. The equipment is described as follows:

Dana Overhead Suspension System Model ELD;

150/300 Constant Potential x-ray Unit with 150 kV, beryllium window double focus 0.7 mm and 1.5 mm tube head, motor driven shutter-diaphragm;
Machlett Image Intensifier with adapter for closed circuit "Plumbicon" TV System;

Closed circuit Plubmicon TV System;

Video Tape Recorder.

Further reduction of inspection cost may be realized by judicious selection of the x-ray image recording medium. Data is readily available for cost analysis of recording materials. The relative results for x-radiography were evaluated for:

1) X-ray film - Kodak Type M, which is competitively priced with other industrial x-ray films of equivalent sensitivity.

2) X-ray sensitive paper - Kodak Industrex, which is competitively priced with industrial x-ray film, but enables rapid, low cost development.

3) Light sensitive recording paper - Visicorder, Type 2202 which is low in cost and requires only ultraviolet light development as described by Holloway, et al (ref 7).

4) Polaroid Type 52 - Photographic film which enables rapid development.

5) Direct fluoroscopic/television readout which enables filmless readout of the x-ray image (see figs. 67 and 68).

In-motion radiographs were made on the twenty-four (24) density reference panels and on two panels (2x9x12-in.) (5.1x22.8x 30.4 cm) having a radius of curvature of 15 in. (38 cm) and 25 in. (64 cm). Parameters for exposure using Kodak Type M film, Polaroid Type 52 film and Kodak Industrex paper are shown in table 24. The 2-in. (5.1 cm) 2T penetrameter could be resolved with the Kodak Type M film, but could not be resolved by either the Polaroid film or the Industrex paper. Extimated penetrameter sensitivies are 10% for Polaroid film and 30% for the Industrex paper. Figures 69, 70 and 71 show comparison of presentation with x-ray recording media. No results were obtained with the Visicorder paper becuase extreme exposure times would be required.

The direct fluoroscopic/television readout provides a convenient technique for evaluation of gross defects with an estimated sensitivity of 30 to 40%. Such gross evaluation might be provided rapidly and economically and may meet required defect sensitivity criteria. If the image can be obtained in a television format, automatic readout for voids and gross density variations could be readily effected. The television image could be fed to an image quantizer for analysis of density variations. A gate could be set in the quantizer unit to trigger an alarm when out of tolerance conditions are sensed. Since the panel is in-motion during x-ray evaluation, a complete readout could be obtained without additional panel manipulation. A typical presentation from a densitometer readout is shown in figure 72.

Video image processing. - X-radiographs of the 24 thickness/density reference panels were processed with a video system which enables analysis of varying image densities in the radiograph and redisplay of the image in a false color isodensity format. For the reference panels, the video controls were set using the low density and high density panels as the image density extremes. Variations within the midrange densities were

then enhanced and redisplayed in color. Panels 1 through 6 resulted in an optical (γ) density range from 1.75 to 1.96γ; panels 7 through 12 had densities from 2.0 to 2.5γ; panels 13 through 18 had densities from 2.3 to 2.8γ; and 19 through 24 had densities from 2.6 to 3.2. Panel 2 was selected for further analysis.

The total optical density range for the panel 2 radiograph was 1.78 to 2.2γ or a 0.42 total variation. The corresponding video densitometer readout range was 800 to 1900 millivolts or a total variation of 1100 mV. A 10% "gate" value was established at 110 mV corresponding to an optical density sensitivity of 0.04γ. Figure 73 is a white light photograph of the Panel 2 X-radiograph as normally viewed. Figure 74 is a video presentation of the Panel 2 radiograph illustrating the contrast enhancement obtained by going into the video format. Specific points on the image can be measured by the video densitometer by manipulation of the densitometer gate as indicated by the "cross-hair" presentation as shown in figure 75.

Using the "cross-hair" (point) densitometer selector, an area on the Panel 2 radiograph was selected for further contrast enhancement in the false color readout mode (fig. 76). Figure 77 illustrates the detailed variations obtainable by operation in the false color mode. Slight variations in density are of little consequence in ablator performance and thus present a "noise" problem for automatic image analysis. The same area was then evaluated by a derivative mode enhancement which normalizes slight density variations and amplifies the edges of areas where a greater density change is viewed. Figure 78 illustrates image analysis in the derivative enhancement mode.

Significant results of the video image processing analysis are:

- A contrast enhancement can be realized by simply going into the video format. A similar enhancement would be expected from a direct x-ray television input to the video analysis system thereby making it possible to improve the overall sensitivity from the 30% value obtained in the Lockheed in-motion radiography work using direct television readout.

- The derivative enhancement mode offers a potential for "noise" filtering of slight density changes thereby improving the capability for automatic gating and readout.

- The image magnification and point densitometer capabilities offer a convenient "on line" engineering analysis tool for specific panel evaluation.

In short, automatic readout of x-radiographs of ablator material is feasible, using the video processing technique.

Indentation Hardness Evaluation

In previous work with MG-36 ablator hardness (table 25) was shown to be sensitive to density variations, contamination, incorrect catalyst content, cure time and temperature and to moisture content. In short, Shore A: Durometer hardness was demonstrated to be a significant process verification tool which is sensitive to several process parameters. A limitation of the Shore A method is the gross penetration into the panel surface. A Shore D durometer was therefore modified to reduce the indentation into the panel surface and thereby more directly measure elastic material response. The modification involved changing the indenter foot to a flat disk configuration having a diameter of 0.12 in. (.29 cm) as shown in figure 79 and weakening the indenter load spring. The resultant range was selected such that a nominal cure SS-41 panel would have a hardness reading of approximately 80.0 units. Both Shore A and Shore D: modified hardness measurements were made on the Series A - Density/Thickness reference panels with results as shown in table 22. From this data the effect of density and thickness on indentation hardness are readily apparent. Also noted is the greater consistency of data with the Shore D: modified unit and the greater effect of panel thickness on the value obtained. We may therefore conclude that modification of a standard hardness unit to match material properties can be of significant value in panel acceptance. The hardness measurement can be automated to effect panel acceptance a minimum cost.

Panel Flexure

Presence and integrity of the ablator to honeycomb bond is a concern parameter. Our approach was to proof load the panel to a nominal strain value to demonstrate bond integrity. Several panel loading concepts were considered including a three point flexure loading, wrapping the panel around a mandrel with the aid of a series of rollers to minimize point loading, and vacuum bag loading over a curved mandrel. The vacuum bag concept was tested to determine applicability and sensitivity.

Sections of two panels which had no honeycomb to ablator wet coat were vacuum bag stress over a 400-in. (1010 cm)-radius mandrel at 9 in. (228 mm) mercury vacuum (see fig. 80). This method puts a calculated strain of 1/2% at the honeycomb/ablator interface. No evidence of ablator to honeycomb core separation could be visually observed. The flexure technique is therefore not considered to be a viable acceptance tool. Process control appears to be the best approach at this time for assurance of ablator/honeycomb bond integrity.

Summary of Panel Acceptance

Using the basic techniques described, an automated ablator panel acceptance cycle is both feasible and practical on a production basis. A typical acceptance cycle might include:

- Process control of mixture, honeycomb preparation, honeycomb packing, etc.
- Programmed panel machining and thickness verification.
- Automatic hardness testing for cure and density conformance.
- Automatic x-radiometric gaging for density conformance.
- Automatic x-ray evaluation and readout for panel soundness.

Sonic/Ultrasonic Evaluation

After ablator panel acceptance is complete, the next major inspection consideration is in verifying the presence and strength of the ablator-to-subpanel bond. Sonic/ultrasonic techniques have been used successfully for bond acceptance in critical hardware and was a logical choice for ablator to subpanel evaluation. The Series B-unbond reference panels were used as models for technique evaluation. Two instruments were evaluated for use in unbond detection, i.e.:

1) Sonic Resonator, Model 101C, North American.

2) Sondicator, Automation Industries.

Initial work was directed to detection of unbonds from the ablator side. The sonic resonator had been capable of detecting similar unbonds in a similar structure with a thinner ablator and was therefore considered to be a viable choice. No detection sensitivity was realized on initial evaluation. A vacuum cup transducer coupling device was evaluated in an attempt to improve the transducer coupling. The results were again negative and this technique was discarded.

Evaluation from the subpanel side was made with the sonic resonator using no acoustic couplant. Only a weak response from the larger unbonds was obtained. When glycerine was added as an acoustic couplant, the sensitivity was greatly improved and all unbonds and crushed core were detected in the NDT Destructive unbond panel. One-in.-diameter and larger unbonds were detected in the NDT Standard unbond panels with the exception of the one-in. diameter unbond in the high pressure panel. It was also noted that the one-in. diameter unbond in the low pressure panel gave a stronger response than it did in the nominal pressure panel. A destructive check was unable to determine conclusively if the bond material had actually adhered to the precured adhesive or if the degree of tightness was responsible for the change in responses.

The sondicator was then evaluated on the four unbond panels. Results when inspected from the facesheet side (the only side possible) were positive for all unbonds and crushed core in the destructive unbond panel but were negative for the three pressure panels. The roughness of the panel surfaces is thought to be the major problem. It should be noted that no coupling is used for this technique.

At this point in the program, detection of bond presence did not appear to be a great probelm when the sonic resonator was used within the limits of the detection sensitivities noted. Later evaluation of its use on the Task IV panels indicated that more development and evaluation might be in order. Although the technique was successful in monitoring the Task IV panels, acceptance tolerances were such that the evaluation was somewhat subjective.

Variation in instrument response are believed to be due to the nature of and the absorption of the bonding adhesive into the ablator panel (see fig. 3) and to thickness variations in the bond. In short, the technique appears to be applicable but

extensive characterization to specific panel bonding materials and parameters would be required before production application could be considered.

Holography

Holographic interferometry has shown promise for detection of unbonds in elastomeric ablators as demonstrated in previous MMA work with SLA-561. Figure 81 is a photograph of a double exposure hologram taken on a 1-in. (2.54 cm)-thick piece of SLA-561 bonded to an aluminum alloy facesheet with an intentional unbond located in the center of the panel. The exposure was made by vacuum stressing the panel at a 2-in. (51 mm) mercury pressure differential. The overall unbond is indicated by the concentration of fringes within the honeycomb core pattern matrix. The vacuum stress holographic technique depends on expansion of entrapped gases at the unbond interface to initiate a local change in surface contour. The technique is used routinely by G.C. Optronics, Inc. (Plymouth, Michigan) for evaluation of tires.

Two of the Series B unbond reference panels (high pressure and low pressure) were subjected to holographic evaluation by the vacuum stress technique. Increments of P = 2 in. (51 mm) Hg, 4 in. (102 mm) Hg and 8 in. (203 mm) Hg were applied between exposures. No indications of the programmed unbonds were detected on any of the four panel surfaces. A representative photograph showing the honeycomb pattern obtained is shown in figure 82. Insensitivity of the technique on SS-41 material is attributed to its greater stiffness and porosity. The holographic technique is not recommended for further evaluation.

Vacuum Cup Resonance

A vacuum cup resonance technique was evaluated for sensitivity to panel unbonds. The NDT Standard unbond panels were acoustically coupled to a variable frequency shaker table and vibrated at nominal panel resonance frequencies. An accelerometer was used to evaluate local surface response in known bonded areas and in known unbond areas. Unbond areas could be detected but difficulties in reproducing results were experienced. Reproducibility problems are attributed to the refinement of the test method. The technique shows promise but results of this quick look evaluation are inconclusive.

Vacuum Cup - Proof Loading

Evaluation of bond strength of the ablator to the subpanel was made using a vacuum-cup-proof loading technique, (fig. 83). This involved coupling the loading head of a standard tensile test machine to the ablator side of an unbond reference panel by means of a vacuum cup and loading the ablator in tension [at a constant 0.02 in./min (0.05 cm/min) rate] to a predetermined proof load level. The local deflection of the ablator was measured by an extensometer incorporated into load train. Values obtained for the NDT Standard Unbond panels are shown in figs. 84, 85, and 86. The large scatter in data is attributed to local elastic variations at the vacuum cup/ablator surface. Further consideration of the technique should be given when unbond acceptance criteria are established.

Conclusions and Recommendations (Task V)

Previous application of elastomeric ablator materials have been limited to low production rates. Advanced inspection methods for space shuttle ablators have been addressed in terms of applicability in a production operation mode at minimum recurring cost. Positive production inspection methods have been identified for basic ablator panel assurance.

No nondestructive inspection technique was found to assure integrity of the honeycomb to ablator bond. This paramater may be positively controlled by normal materials and process monitor. As automated fabrication techniques are established, such process controls may be incorporated at minimum cost and thereby answer a concern area for reliable ablator application.

No totally conclusive technique was identified for low cost assurance of the subpanel to ablator bond. The Sonic Resonator technique was used successfully to characterize the Standard Unbond panels and Task IV test panels but is not amenable to low cost production since it requires an acoustic couplant and extensive panel scanning to obtain results. Further work to develop alternate methods such as the proof load concept should be performed on actual production materials and shapes to assess applicability. If the alternate methods prove unsuitable for specific material and geometry combinations, a spot check (process monitor) by the Sonic Resonator technique is recommended as the most feasible inspection option.

The forgiving nature of elastromeric ablator materials makes their inspection and assurance less demanding than required for conventional aerospace hardware. A review of critical defects identified during this program limits specific concern areas to:

Panel density and cure;

Honeycomb wet coat application and cure; and

Honeycomb core undercut.

It is significant to note that bonding of the ablator panel to the subpanel was not identified as a critical concern.

The performance of the bond is attributed to the nature of the bond material, the absorption of the bonding material into the ablative panel which positively influences the bonding process, and careful process control during bonding operations. On the basis of this success, no requirement for nondestructive assurance of the adhesive bond joint is anticipated. Normal materials and process control are deemed sufficient for assurance of bond integrity. This position should be reviewed for complex geometries where fit-up difficulties normally cause processing problems. In a production operation mode, fit-up problems would be minimized and normal process control is anticipated to be sufficient.

On the basis of overall program results, the outlined Quality Assurance and inspection plan shown in figure 87 is recommended for "low cost", low risk elastomeric ablator panel production.

PROGRAM CONCLUSIONS

A number of fabrication-induced defects were found to be critical to performance of the ablator composite. Many more, however, were found to be of a non-sensitive nature when compared to baseline material criteria. A procedure for adequately inspecting assembly line production is feasible, based on a combination of state-of-the-art and advanced methods. Finally, this study indicates that costs can be reduced on ablator production when directed with concentration on key variances and relaxation on the appearance of non-critical flaws and/or operations.

Identification of Determined Critical Defects

The variations in manufacturing of ablator panels which were found to be of paramount concern were as follows:

Undercure (at 150°F (66°C) instead of 250°F (121°C))

Overcure (at 350°F (177°C) instead of 250°F (121°C))

Low Density (15 pcf (240 kg/m^3) instead of 16 pcf (256 kg/m^3))

Filler to reinforcement bonding (overtime and overtemperature)

Undercut core (0.1 and 0.2 in. (0.25 and 0.51 cm))

Large internal voids (sufficient to create 20% reduction in density)

Undercure. - This variation is critical in that it produces ablators which have low flexural strengths well before reentry heating. In addition, after the heating pulse of entry undercured material experiences loose cell surfaces, material losses, and a considerable number of internal char cracks.

Overcure. - Material which has been cured at too high a temperature during fabrication tends to develop a higher net thermal conductivity through the thickness, resulting in higher backface temperature values during reentry. Much internal char cracking also develops.

Low density. - Low density composites display low flexure strength and additional consolidation of the fill material in the honeycomb cells during the thermal vacuum exposure. This produces

a sunken appearance in each cell at the surface. Pyrolysis reaction during reentry is considerably greater than the standard. This, accompanied by extensive internal char breakup, renders this defect as critical.

Filler to reinforcement bonding. - The procedures involving the priming of the ablator's honeycomb reinforcement were found to be important in several aspects. An excess amount, properly B-staged, will still wipe down to the bottom of the cell under the piston action of the filler material installation. This increases net conductivity at the main attachment plane. Even more graphic is the effect of an over-temperature in the B-staging process. A thermal vacuum exposure completely frees the fill material while reentry and acoustics subsequently will cause material losses, surface roughening and deep pyrolysis.

Undercut core.- Entry heating initiates the loss of considerable amounts of the ablator surface due to the absence of reinforcement all the way to the outer surface of the ablator. The material lifts off in large pieces. Similar reactions are very possible for crushed core, damaged core, etc.

Large internal voids. - Early in the program it was observed that large voids are detrimental when they reduce the net density. Results are then as described under Low Density. The occurrance of voids such as these are improbable during fabrication, however. Normal, small voids have not proven to be a problem.

Status of Non-Critical Defects

Variations which proved, within the limits considered in this study, to be non-influencial on material performance were as follows:

High density

Wet basic materials

Inhomogeneity

Undermixing

Internal horizontal cracks

Broken reinforcement nodes

Broken reinforcement ribbons (6.45 cm^2)

Panel Disbond spots up to 2 $in.^2$ (6.45 cm^2) (max. studied)

Small internal voids

Formulation

Foreign inclusions (contamination)

Surface voids

It had been anticipated that the cure characteristics of mixtures containing defects such as wet basic materials, undermixing, etc. would modify to the point of criticality. This was not the case, however.

Adverse thermal and mechanical reactions within panels containing intentional defects tend to be dampened out by the compensating mechanisms characteristic of most of the ablator composites.

Finally, although the external appearances of some of the ablator panels with these defects may not aesthetically pass scrutiny, they are, to the extent investigated in this study, safe.

Applicability of Advanced Inspection Methods

Inspection methods investigated during this program included those techniques which are conventionally applied, advanced technology methods, and production scaling methods for lowest cost inspection. Efforts were concentrated on nondestructive inspection techniques. These included:

Visual

X-ray

Neutron radiography

Sonics/ultrasonics

Thermal

Microwave

Holography

Durometer Hardness

Process Control

All of the techniques were applicable to specific elements of ablator assurance, but are not necessarily required to assure ablator integrity to established design tolerances. Capabilities of the inspection techniques were evaluated as follows.

Visual inspection. - This was necessary for overall ablator appearance, soundness, etc., but was most useful for determination of undercut honeycomb core in a machined ablator.

X-ray techniques. - These methods were divided into x-ray gaging methods for rapid nondestructive determination of ablator panel density and x-radiographic inspection for soundness.

X-ray gaging: When the parameters were determined for nondestructive measurement of ablator density, a production sensitivity of $\pm$ ½ lb/ft^3 ($\pm$ 8 kg/m^3) density tolerance was determined to be feasible. An automatic readout system is feasible.

X-radiography: This technique was shown to be a sensitive technique for evaluation of ablator voids, foreign inclusions, density variations, homogeneity variations and soundness of honeycomb core. Three problems in application of the technique are, basically: a greater sensitivity than is required, parallax problems, and inspection cost. In-motion radiographic techniques were demonstrated to be adequate for minimizing parallax problems and were combined with direct television readout techniques to reduce cost and inspection sensitivity. Feasibility of an automatic video readout from the television image was determined.

Neutron radiography. - Feasibility and sensitivity of neutron radiography to ablator mix and packing anomalies was demonstrated. The cost and difficulties in using the technique routinely are not justified to meet the established soundness tolerances.

Sonic Resonator. - This technique was demonstrated to be sensitive to ablator to subpanel unbonds greater than 1-in. (2.54 cm)-diameter. The technique could be used on a sampling basis, but would be difficult and costly for production. Alternate bond

inspection techniques were evaluated for detection of small (1-in. (2.54 cm) diameter)-unbounds, but were not investigated for larger bond tolerances. In general, these techniques were not as sensitive as the sonic resonator.

Infrared scanning. - Thermal techniques were shown to be sensitive to gross unbond and ablator void anomalies. No production inspection application would be indicated, but the technique would be a candidate heat shield evaluation after a shuttle flight, i.e., on structure cool-down.

Microwave techniques. - These were demonstrated to be sensitive to ablator density, cure, thickness, moisture content and mix stoiciometry. The inherent sensitivity of the technique to many material and physical parameters make it unattractive for panel inspection, but a possibly useful technique for in-line process control.

Holographic interferometry. - Holography was demonstrated to be sensitive to be sensitive to ablator-to-subpanel unbonds for one (SLA-561) ablator material, but was insensitive for the SS-41 material. The technique appears to be material dependent (stiffness and porosity) and is not considered for production application at this time.

Durometer hardness. - These readings were shown to be sensitive to cure, density, and moisture content anomalies and may be rapidly performed. A modified Shore D durometer was shown to be sensitive to material anomalies and did not indent the ablator material. An automated technique is feasible for production application.

Process control. - A review of the critical defects identified reveals a need for raw materials and ablator fabrication process control to assure cure, density and honeycomb wet-coat tolerances. Such control may be accomplished by routine documentation and test sample evaluation and may be reduced and/or supplemented by production process automation techniques. Additional check points include:

Density - by radiometric gaging

Soundness - by durometer (Shore "D" modified) hardness

Bonding - by sonic resonator sampling

General

This study reinforces the belief that less rejections and reworking of production-line ablators are feasible. This, coupled with our finding of ablator performance insensitivity to a great number of flaws, should significantly reduce and/or simplify the myriad of fabrication and inspection steps currently required.

One final observation must be made on this study. How extensive were the effects of variances in the reproduction of day-to-day operations, (such as fabrication procedures, operator techniques, environment conditions, etc.) on the anomalies reported is impossible to ascertain.

RECOMMENDATIONS

The recommendations presented in this chapter concentrate on the possible future applications of the observations presented in this report. The concepts resulting represent a significant step toward low cost ablator production and must be further pursued if ablative TPS are to be competitive for Space Shuttle use.

Defects Evaluations

There is an immediate need for a study which would integrate the findings of this effort to determine their impact on unit costs.

The manufacturing process of ablators such as those used as baseline composites in this study should be modified with respect to unit procedures and specification requirements. This modification should begin to introduce the aspects of automation, since it is believed that the entire process will eventually establish along these lines.

In any future study, the baseline study composite should be changed to provide a more consistent standard against which cost saving investigations can be measured. This would include changes in formulation and/or the use of a seal coating to prevent excessive weight gains by the ablator due to moisture. Similar formulation changes are required to enhance the material's strain capability.

A comprehensive "new process vs. effect" test program should be conducted to substantiate the new approach to ablator fabrication. The program should contain a greater number of defect samples and larger panels than those used in the current study.

The absolute limit of ablator-to-subpanel disbonds should be established. The findings could lead to a form of peripheral bonding, strips, etc.

Any further effort should be subject to those mission environments which impose the most damage, i.e., panel flexure, thermal vacuum, entry heating, and descent acoustics.

The degree of roughness permitted for aerodynamic stability and control after entry still requires further definition to evaluate changes in ablator surfaces.

Postulated Inspection Requirements

On the basis of critical defects identified, it is apparent that minimal inspection is required to produce a reliable ablator panel. Critical items are discussed below.

Materials and process control is important but not critical in terms of material performance. Strict observations of ingredients and processes are required during fabrication to assure overall performance. Proper mixing and proper wet coat of honeycomb core are mandatory. Mixture ratios, times, and sequences could be readily automated such that calibration of materials measurements and mixing equipment could be performed on a periodic basis and conformance assured by occasional audit. Wet-coat application may also be automated to reduce risk and may be verified by usual inspection.

Problems encountered due to undercut core type defects could possibly be eliminated by fabricating the ablator panels with a head and machining inward on both main surfaces of the panel. Visual inspection may be used. Processing parameters may be adjusted such that only one side is machined. Visual inspection may also be used for verification.

At this point, panel thickness control is required before automated density gaging can be applied. Thickness may then be determined with a deep throat micrometer or with an automated electromagnetic scanning device.

Panel density can be rapidly ascertained by automatic radiometric gaging.

Cure variations must be monitored. The accomplishment of proper cure may be automatically determined by indentation hardness techniques. A modified Shore D unit provides nondestructive evaluation of panel cure, but readings must be located such that the indenter does not impact the honeycomb core. Automated techniques may be developed for this task.

X-radiography for soundness would provide an increased confidence level at minimum cost using an automated system approach. As processing confidence is gained, a statistical sampling may be used to further reduce cost.

Within the bound studied in this program, ablator-to-subpanel bonding was not ascertained to be an area for particular concern. It appears that the ablator bonding is somewhat process-insensitive due to the nature of the current process and ease of preparing the ablator surface for bonding. However, a minimal sampling of bonding processes is required to maintain a high confidence level.

High sensitivity X-radiography and in-line evaluation of the ablator-to-subpanel bonding are techniques which are well within the state-of-the-art but appear to be unnecessary tasks to provide assurance required to produce "critical defect-free" panels.

Additional materials qualification is necessary to establish maximum unbond tolerances and thereby finalize the optimum inspection approach.

Areas for Future Ablator Study

From an assurance technology viewpoint, inspection parameters are reasonably well established for the elastomeric ablator systems. Some attention could be addressed to establishing maximum unbond tolerances for the ablator-to-subpanel bonding and thereby firm up parameters for inspection. Likewise, additional attention could be addressed to establishing automated techniques for verifying adequacy of wet-coat applications. These tasks could be performed reasonably on a candidate ablator system and the results would be expected to have good transferability to most elastomeric ablator systems.

The specific ablator mix and fabrication process sequence can make a significant difference in the amount of inspection/verification required and on the end product reliability confidence level. For a low volume production involving many hand operations, a number of in-process check and verification points are required to maintain high confidence in performance. For a high-volume, automated production operation, process control and process uniformity may be assured by in-line monitor and recording devices to maintain performance confidence at minimum inspection costs. We have assumed a high volume production operation and have suggested automated nondestructive evaluation concepts for a candidate ablator material. Application to a specified ablator material would involve:

A review of specific processing parameters and tolerances.

A production plan for processing steps, including automation and flow paramters.

A prototype, pilot plant evaluation to establish and scale firm production requirement.

Design, build and qualification of the production process.

Two attachment concepts for ablator to spacecraft structure have been investigated during this program i.e., (1) an integral bonded facesheet and, (2) a secondary bonded subpanel. The attachement method makes a significant difference in the difficulty, and, hence, the cost of inspection. As such, a "design for inspectability" criteria is of great importance for high volume usage of ablators. In this study, the subpanel concept is much easier to inspect than the integral facesheet concept.

When a specific design concept is finalized, additional materials characterization peculiar to the design will be required. Production process development will then involve normal process analyses, process planning, pilot plant evaluation, production plant design, facilities, and qualification.

For purposes of estimating high volume production costs, an automated production analysis could be performed on a candidate material and attachement design concept using material "defect criticality" tolerances established during this program. Such an analysis would be useful for analysis of overall space shuttle heat shield cost tradeoffs for the complete Shuttle program.

Martin Marietta Corporation
Denver, Colorado 80201
July 24, 1973

REFERENCES

1. Love, Eugene S., *Advanced Technology and the Space Shuttle*, Tenth Von Karman Lecture, Astronautics and Aeronautics, February 1973.

2. Thompson, Raymond L., Rummel, Ward D., and Driver, Walter E., *Study of Critical Defects in Ablative Heat Shield Systems for the Space Shuttle*, (Tasks I, II, III), NASA CR-2010, April 1972.

3. Chandler, Huel H., *Low Cost Ablative Heat Shields for Space Shuttles*, NASA CR-111800, October 1970.

4. *Structural Design Criteria Applications to the Space Shuttle*, NASA SP 8057, January 1971.

5. *Terrestrial Environment (Climatic) Criteria Guidelines for Use in Space Vehicle Development*, NASA TMX 64589, 1971, Revised 10 May 1971.

6. Military Standard Inspection, Radiographic, Mil. Std. 453.

7. Holloway, J. A., Henderson, T. R., and Kamm, H. W., *Radiography Using Direct Print Recording Oscillograph Papers, Materials Evaluation*, Vol. XXIX, No. 3, March, 1973.

8. Jones, Robert A. and Hunt, James L., *Effects of Cavities, Protuberances, and Reaction-Control Jets on Heat Transfer to the Apollo Command Module*, NASA TM X-1063, 1965.

9. Hunt, James L. and Jones, Robert A. *Effects of Several Ramp-Fairing, Umbilical, and Pad Configurations on the Aerodynamic Heating to the Apollo Command Module at Mach 8*, NASA TM X-1640 1968.

10. Pyle, Jon and Montoya, Lawrence C., *Effects of Roughness of Simulated Ablative Material on Low-Speed Performance Characteristics of a Lifting-Body Vehicle*, NASA TM X-1810, 1969.

APPENDIX

COMPILATION OF DEFECTS*

Ablative Material Defects

The most important properties of the ablative material are its insulation characteristics, char stability, and resistance to surface erosion. In addition, the material provides added stiffness against bending and vibration or flutter-induced loads. The following defects have been identified as affecting these properties.

Cracks. - Cracks are defined as vertical discontinuities that can be contained with the filler of a given cell or run continuously across many adjacent cells.

Cause: Since the ablator material provides much of the basic stiffness for the reference design and for the large panels being considered for the Space Shuttle, 2 by 4-ft (0.67x1.22 m). cracking caused by unsupported handling becomes a very real possibility. Other causes would be residual stresses, cold soak strain, and thermal stresses during reentry.

Effect: Localized surface cracks that run out to the cell walls could lead to char loss if coupled with poor strength in the filler-to-core bond. Cracks running across cells could seriously reduce overall panel stiffness and, under flight-induced buffeting and vibration loads, the panel would be susceptible to crack propagation leading to excessive loading of the attachments and possible panel loss.

Delaminations. - Delaminations are defined as discontinuities approximately parallel to the ablative panel surface. They would normally be constrained by the cell walls and not be susceptible to propagation.

Cause: By our definition, delaminations occur in a plane normal to the applied pressure direction during filling and cure. Inhomogeneities in the filler can become stratified or layered under pressure and, at elevated temperatures, result in localized residual stresses after cure. These residual stresses are a possible source of delamination. However, a more likely source would be tension stresses developed during reentry tending to pull the char layer apart.

---

*From reference 2

Effect: If these delaminations are present or develop during reentry, they will affect char strength and could result in char loss.

Voids. - Voids are defined as material discontinuities with ablative material not in contact across the discontinuity. Voids in honeycomb-filled ablative materials normally are found near the face sheet or in areas where core splices have been made. Their size, number and orientations are generally random (see fig. 88.)

Cause: Voids are caused by lack of sufficient ablative material within a cell, entrapment of gases during fabrication, and obstructions in the cell passage. An example of an obstruction is surplus resin used for core splicing or core bond coating.

Effect: Voids can affect thermal performance in the following ways. Voids of Type I (large bubbles) are most detrimental when they occur near the surface and become exposed through surface recession. The increases in thickness required to maintain structure design temperatures has been shown to be approximately equal to the void dimension in the direction of heat flow. Voids of Type II (high-porosity) in effect reduce material density and could cause increased surface recession and roughness. Depending on degree, this could affect surface heating and ultimately increase structure temperatures. Voids of Type III (partially filled cells) are of special concern because they result in completely vacant cells below the obstruction. Although the effect on structure temperature is unknown, it could be catastrophic depending on the number and size of these voids.

Unbonds from honeycomb core. - Unbonds from the honeycomb core are defined as discontinuities at the interface between the honeycomb cell wall and the ablative filler. The unbonds can occur along one or more cell walls.

Cause: In many ablative-filled honeycomb structures, a bond between the filler and the core is achieved by pretreating the core often with an adhesive coating. Failure to perform this operation or failure to perform it properly can cause poor or weak bonds. Other cuases of unbonds would be thermal expansion of the ablator out of the cells, and thermal shrinkage during cold soak.

Effect: Bond failure could result in loss of filler during vacuum cold soak and loss of char during reentry. In addition, a crack or unbond along one side of a cell wall will prevent the transmission of strain to the adjacent cell, thus affecting panel strength and stiffness.

Density. - Density is a very important material characteristic because of its effect on insulation and ablation properties. Density variations from cell to cell and panel to panel can be produced during fabrication.

Cause: Density gradients result when pressure applied to the filler material at the top of the cell is not uniformly transmitted to the bottom of the cell. The major cuases of density variations from cell to cell are the localized use of impact force and its rather random application by fabrication personnel. Other less significant causes are the variation in filler density caused by such raw material variations as microsphere size and poor mixing of the material. The density gradient normal to the surface is a direct result of force transfer to the cell walls, reference 3.

Effect: Density variations cause complications and uncertainties in defining reliable analytical models for performance predictions. Aerodynamic performance could be affected by a density variation from one cell to another because the density variations could produce low-density areas at the surface. During reentry this could produce nonuniform surface recession and would affect aerodynamic smoothness, possibly causing downstream flow separation.

Filler integrity. - The major functions of the fillers in the ablative material are to provide added strength to the elastomeric matrix and reduce the composite density. The following defects can affect these properties.

Broken fibers: One way that fibers reinforce the char layer is by bridging the low-density pyrolysis zone. For these fibers to be effective, their length must be greater than the pyrolysis zone width. Since silica fibers are extremely small and brittle, they are susceptible to breakage.

Cause: During processing these fibers can become broken and and disintegrated because of their low physical strength.

Effect: Broken fibers may not be of adequate length to bridge the pyrolysis zone and thus will reduce the material's ability to retain its char. In addition, the strength of the char to resist skin friction shear forces may be reduced.

Broken microspheres: Microspheres are used as a low-density filler in many ablative materials and, because they have low strength, they can be broken quite easily.

Cause: A certain percentage of microspheres are broken when received from the manufacturer. Many more can be broken during mixing (the percentage depending on the shearing action of the mixer and mixing time) and packing of the ablative filler into the core.

Effect: Variations in the percent of broken microspheres from one batch to another could significantly affect such material properties as density and conductivity.

State-of-cure. - The state-of-cure or crosslinking in elastomeric ablative materials is known to be affected by state variables of temperature, pressure, and cure time.

Cause: Variations in temperature can result from a lack of oven control. Cure pressure can be affected by leaks in the vacuum bag, variations in pump operation, and variations in atmospheric pressure, Cure time can be affected by variations in warmup time for different sized parts, failure of oven controls, or neglect by operator.

Effect: Cure temperature and pressure variations can affect the thermal and physical properties of the ablative material. These variations may result in cracks and panel warpage affecting such things as char retention, bond strength, ultimate strain capability, and loading on the attachments.

Inhomogeneity. - Inhomogeneity is an undesirable characteristic in many engineering materials because of its adverse effect on properties. Inhomogeneities alter the molecular structures and give rise to stress concentrations. The following inhomogeneities have been identified for the ablative material considered in this study.

Fiber bundles: Fibers are normally included in an ablative material to provide a measure of reinforcement of both the char surface and the pyrolysis zone. For this reinforcement to be uniform and fully effective, fiber dispersion must be uniform.

Cause: Several factors have been identified as possibly causing nonuniformity in fiber dispersion. A predominant cause is thought to be the lack of shearing action during mixing. Another cause that has been identified is the collection of fibers on the sides of the mixing bowls. This presents two problems. First, when fibers separate from the walls, they do not redisperse. Secondly, some fibers are lost and the actual percentage in the material is reduced.

Effect: The effect of fiber bundles or poor dispersion is to reduce their effectiveness in reinforcing the char and the char retention strength in the pyrolysis zone.

Microsphere agglomeration: Microsphere agglomerations are defined as groups of microspheres that are bound together by mechanical forces.

Cause: The basic causes of these agglomerations are absorbed moisture and the pressures occurring during storage that, after sufficient time, tend to compact the microspheres.

Effect: The effects on ablative material properties are obvious since each agglomerate represents a domain of essentially foreign material with different properties. In addition, surface voids can be caused by agglomerates at or near the surface. This would directly affect insulative properties and surface smoothness.

Resin ratio variations: The basic function of the resin system is to bind together the other constituents. Nonuniform distribution of the resin will produce resin-rich and resin-starved areas, thus producing variations in material strength, thermal expansion, and other properties.

Cause: Resin variations are caused by microsphere agglomerates, inadequate ablative material mixing, and from the resin coating applied to the core.

Effect: Resin-rich areas would have a much greater coefficient of expansion and produce high local stresses on temperature change. These stresses could open cracks during cold soak, cause shear failure of the filler bond with the core, and load the face sheet at the core bond in tension. Significant effects can also be expected in strain capability, elastic modulus, and conductivity.

Formulation variations. - Small variations in constituent percentages will likely have little or no effect on material properties, with perhaps the exception of the catalyst percentage.

Cause: The causes of formulation variations would most likely be errors in measurements, although, as cited earlier, fibers can become lost due to their tendency to collect on surfaces.

Effect: Changes in the catalyst percentage can affect the onset of cure, degree of cure, and the amount of reaction products remaining in the cured material. In all cases, detrimental effects on mechanical properties can be expected. The percentage of fibers can be expected to have some effect on char strength and retention.

Foreign matter. - Foreign matter is any unwanted matter that enters into the material by accident.

Inhibitors: Inhibitors are characterized by their neutralization of the catalyst, thus retarding or completely stopping cure.

Cause: These inhibitors can be introduced in many innocent ways, such as a faulty seal in a mixer allowing oil or grease to fall into the material batch.

Effect: Total cure prevention will depend in most cases on the percentage of inhibitors included. However, some variation in mechanical properties can be expected if inhibitors are included.

Inerts: Poor process control could result in introduction of inert materials. The most typical of these would be metals and wood that are commonly used as manufacturing aids. Particle sizes may vary considerably from microscopic to a size easily detected by radiographic inspections. In addition, salt compounds of the alkali metals such as sodium chloride and potassium chloride have been found in ablative materials.

Cause: These inerts can be introduced in several ways, including poor quality control, contaminated raw materials, and by equipment wear.

Effect: The microscopic particles that would likely result from wear of equipment are not of concern because they should not significantly affect any of the material properties or performance requirements. Although alkali metals will have little effect on performance properties, they could add to the problems of compatibility of the ablator with RF transmission during reentry.

Moisture content. - A significant characteristic of low-density materials is their affinity for absorbing moisture.

Cause: Two possible causes of moisture in the material are moisture contained in the raw materials, particularly the microspheres, and moisture absorbed by the ablative panel from the environment.

Effect: Moisture contained in the microspheres can cause the spheres to burst during vacuum cure and thus affect density. Moisture absorbed by the finished ablative panel can freeze in the launch and orbit environments and thus cause unwanted cracking and promote spallation during reentry.

Honeycomb Core Defects

The function of the honeycomb core in the ablative material is to attach the ablative layer to the fiberglass face sheet; reinforce and attach the char layer to the virgin ablative layer; and control cracking in the char layer. The following defects associated with the honeycomb have been defined on the basis of potentially interfering with these three functions (the various honeycomb core defects are shown in figures 89 and 90.

Crushed core. - Crushed core is defined as wrinkled core ribbons both internally and near the ablative panel surface.

Cause: This defect is caused by column loading of the core. It is expected to occur primarily as a result of impacting the ablative filler during the packing process. When the layer of ablative filler is driven completely into the honeycomb core and the top of the core is exposed during the impacting process, crushing of the core can be expected.

Effect: Crushed core results in a loss of its integrity and, therefore, a loss in its effectiveness to reinforce the char layer.

Distorted core. - This defect occurs when the cell shape is deformed from its original configuration. An example is where the cells have been distorted from a hexagon shape to a sine wave shape, or where the surface has been pushed sideways and tips the cell walls from the vertical.

Cause: Core distortions can be caused by abnormally high packing pressures or by lateral forces imposed by a vacuum bag.

Effect: Distorted core may imply that there are residual stresses in the ablator layer imposed between the distorted core and the ablative filler material. This could result in cracking when the surface is heated during reentry and possibly result in some char loss.

Broken core ribbons. - When the cell walls are torn either vertically or horizontally, the defect is defined as broken core ribbons. They can vary from a partial break in one cell wall to breaks extending over many cells.

Cause: These breaks or tears can be caused by excessive packing pressure, overflexing of the honeycomb, or lateral forces imposed by the vacuum bag.

Effect: Broken core ribbons can result in a weakened attachment of the ablative layer to the fiberglass face sheet, reduction in the reinforcement of the char layer, or excessively wide surface cracks in the region of the broken ribbons. The weakened attachment and wide cracks may cause failure either during cold soak or reentry.

Broken node bonds. - When the ribbon-to-ribbon bond has been separated making the cell walls discontinuous, the defect is described as a broken node bond. This defect is similar to vertically broken core ribbons.

Cause: These breaks can be caused by excessive packing pressure or overflexing of the honeycomb.

Effect: These breaks can result in excessively wide surface cracks either during cold soak or during reentry.

Undercut core. - This defect refers to a variation in core thickness so the core does not extend all the way to the outer surface of the ablative layer. Fabricating panels oversize and machining them to final thickness would alleviate the problem.

Cause: The defect would be caused by an undertolerance core and/or machining errors.

Effect: The most significant effect on end performance would be the lack of support in the filler at the panel surface. This could affect the char retention and the ability of the honeycomb to control surface cracks.

Defective core splices. - Splices that have excess resin or are not bonded are considered defective core splices. This is shown in figure 90.

Cause: Defective core splices can be caused by the application of an improper amount of resin at the bondline.

Effect: The result of an excessive amount of resin is to block adjacent cells and thus interfere with cell filling and packing operations, in addition to causing a local anomaly in the ablator layer. A deficient amount of resin will produce a poorly bonded or unbonded core splice that may result in an excessively wide crack when the panel is subjected to cold temperatures or heated during reentry.

Face Sheet or Subpanel Defects

It is assumed that the Shuttle ablative panels will be directly attached to the metal structure. Although this will provide some support against pressure loads, inertia and thermal loads will produce large bending loads tending to warp and lift the panel away from the metal structure. Large tension loads will be produced at the attachments. The primary function of the face sheets will be to provide adequate bearing and shear strength at the attachment loacations. The following defects have been identified as affecting these strength properties.

Delaminations. - Delaminations are physical separation of the two plies of cloth.

Cause: Delamination during fabrication can be caused by organic contaminates, resin-starved areas, and staged or cured resin areas.

Effect: The effects of delaminations on shear or bearing strength will depend on the relative location of the delamination with respect to the attachment points. A delamination at

the attachment hole would result in greatly reduced face sheet stiffness because of a lack of interlaminar shear strength between the plies. This could readily result in attachment failure and lead to the more catastrophic failure of panel loss.

Spliced face sheets. - Spliced face sheets would be an overlapping of two adjacent pieces of cloth to form a larger sheet.

Cause: The reason for overlapping is simply the unavailability of a manufactured piece of the desired size.

Effect: The splice could result in local unbonds or poor bonds of the core because of the step introduced along its boundaries. The effect on performance would be to reduce the ablative material bond strength.

Configuration Defects

This refers to variations in panel dimensions, general conditions of edges, and surfaces. The following defects associated with panel configuration are identified.

Thickness. - This is defined as the ablative layer dimension required to limit the temperature of the structure to a specified design value.

Effect: Thickness is a most important dimension to be controlled because of its effect on both structure temperature and vehicle weight. In addition to establishing manufacturing tolerances, when determining thickness acceptance criteria, we should consider the question of designing to a minimum or designing to a constant thickness.

Width and length. - These dimensions control overall panel size.

Cause: Width and length dimensions can vary because of the difficulties in machining ablative materials and operator errors.

Effect: Overall panel dimensions must be maintained to assure mechanical mating with adjacent panels and to control gaps and joint sizes between panels. Of course, this problem can be minimized by the use of compatible sealer materials to fill these gaps and reduce heat leaks to the structure.

Attachments. - Poor hole alignment and interface match will impose added loads at these attachment points and interfaces.

Hole alignment: This is defined as the location of attachment holes in the ablative panel with attachment anchor studs on the structure.

Cause: Manufacturing out-of-tolerances.

Effect: Improper mating with the attachment stud can cause prestraining of the entire panel. This would not normally be a problem if design tolerances are maintained. Also floating attachment points can be used to minimize mechanical and thermally induced strains.

Interface mismatch: This defines the distance between ablative panel face sheets and the support structure at the attachment.

Cause: Interface mismatch can be caused by warped panels and out-of-plane attachment locations.

Effect: Strains produced by forcing an interface match can result in high built-in bondline strains that could produce cracks during orbit and reentry.

Edge conditions. - This refers to such defects at the panel edges as unfilled cells, and chipped, worn, and uneven edges and corners.

Cause: Since the specified panels do not contain edge members or reinforcement coatings, they are susceptible to damage during machining, handling, transportation, and installation.

Effect: Poor edges will result in heat leaks to the structure.

Surface smoothness. - The surface of a flight vehicle should be as smooth as possible to eliminate perturbations of the aerodynamic performance characteristics and heating. The following defects associated with surface smoothness have been identified.

Waviness: Waviness is defined as a random curvature of the surface.

Cause: This could be caused by contouring the ablator outer surface to the substructure. It could also result during reentry due to thermal strains causing bowing of the ablative panels.

Effect: Waviness in supersonic flow will produce antisymmetrical pressure distributions around the crests and troughs of the wall and increase the drag force.

Mismatch of edges: This refers to a step in the outer surface from one panel to the next.

Cause: Mismatched edges would result from a change in panel thickness or displacement of the attachment surface.

Effect: Two types of steps can occur -- a rise and drop. In both cases, an attached shock could be produced in supersonic flow, increasing local heating by an order of magnitude, 8 and 9.

Roughness: Roughness refers to a lack of surface smoothness or evenness.

Cause: Rough surfaces can be caused by accidental chipping, gouging, and tool marking during machining and transportation. Also, uneven expansion and recession between the ablator and core or from cell to cell can occur during reentry heating.

Effect: Roughness can affect the boundary layer and produce turbulence, separation, and vorticity that affect both heat transfer and flight performance, reference 10.

APPENDIX B

FABRICATION OF SS-41 ABLATOR HEAT SHIELD PANELS

Tasks IV and V used a modified version of the NASA-Langley ablator MG-36, i.e., SS-41. Details of the modified design using SS-41 are illustrated in figure 3 and presented in this Appendix.

Ablator Packing Method

The current honeycomb core packing process was developed on a recent IRAD program at Martin Marietta's Denver division as a result of experiments made to determine the packability of low density ablators. Results indicated that any pressure or vibration loads on the ablative material caused it to compact badly. The compacted material then became difficult to load into the honeycomb core since it formed tight plugs on entering the cells. This resistance was found to be great enough to cause core damage before the cells were filled.

Preliminary experiments were then made pressing the honeycomb core into partially and fully packed ablative material. Little difference was found as the ablator quickly packed into a dense block ahead of the core. The major improvement in packing occurred when the core was vibrated, causing vertical shock waves to be transmitted through the cell walls. When the core and material were sufficiently vibrated, the former easily penetrated the ablative material.

To minimize the density gradient through the ablator thickness the material was vibrated into both sides of the core. The proportion of material in each side was varied to determine the optimum packing ratio. At the optimum ratio, the front and back surfaces of the panels had a similar density and the center portion was slightly lower. The maximum density gradient was less than 1 lb/ft^3 and averaged ½-lb or approximately 3%. (Previous packing methods had produced density gradients as high as three pounds per cubic foot through the ablator and lateral gradients as high as one pound per cubic foot.) Typical density variations through the ablator panel are shown in figure 91.

APPENDIX B

The lateral density gradients were controlled to approximately ¼ lb/ft^3 (4 kg/m^3) (1½ %) by using a dense pack loading technique. In this method, the ablative material was compacted in screed frames, eliminating any significant density variation across the panel surface. Each screed contained the proper proportion of material for one side of the core. As the vibration packing method causes practically no lateral movement of the ablative material, the distribution remained uniform.

Overall ablator density was controlled by the vibration frequency and magnitude plus the ram pressure. These parameters were precisely controlled by direct gage readings and pressure settings. With consistent raw materials, the ablator density variation was found to be within one percent. The screeds provided an accurate means of checking the ablative material bulk density, as they were weighed with their volumetric charge before being used. The vibration packing method was found to be equally efficient on large and small panels. Both Hexcel 3/8 HRP and Martin Marietta core were used with equal ease of packing.

Raw Material Control

To minimize fabrication time and costs, very little processing of raw materials was done on the SS-41 raw materials. The phenolic microballoons were dried under vacuum in a V-blender to remove moisture. Nylon powder, IG101 glass spheres, and the phenolic microballoons were sieved through 30-mesh to remove large matter and to break up agglomerated lumps.

Density variation of the raw materials was found to be significant. Two batches of IG101 glass spheres varied in bulk density from 12.25 to 14.64 lb/ft^3 (196 to 235 kg/m^3). The glass also settled in transit, causing a density gradient within each container.

Use of the dense glass spheres resulted in an increase of approximately one-half pound per cubic foot in the final mix density. As the vibration packing method fills honeycomb core volumetrically, the higher density caused rejection of several ablative panels. It was at this time that screed weighing was instituted as a bulk density check. An attempt was made to compensate for the high material density by packing at a lower pressure, but the possibility of voids caused by inadequate filling was increased. Material from the heavier batch was rejected, and all other raw material containers were shaken to mix the material.

APPENDIX B

Particle size of the phenolic and glass spheres moderately affected the SS-41 bulk density. The larger spheres were found to be much less dense than the smaller ones. A typical sieve analysis is shown in table 26. As shown, the density variation was not great enough to discard any of the major fractions except the -200 mesh (74 micron) glass. The -200 mesh material, therefore, should be discarded or processed to reduce the bulk density.

Broken spheres were found to be a major cause of high density, as the fragments nest with one another and with unbroken spheres. The broken spheres are easily removed along with other high density material by washing in methyl-ethyl-ketone, as they settle to the bottom of the fluid. The density of washed IG101 glass microspheres was 9.7 pcf (155 kg/m^3). This was a reduction of over 2 pcf (32 kg/m^3) from untreated material. Phenolic microballoons decreased 1.5 pcf (24 kg/m^3) after washing. Washing is therefore a possible treatment for density reduction if the raw materials have high bulk density.

The SS-41 ablative material for the panels was mixed in 3200 gram batches in a 15 gallon (57 liter) Hobart mixer. Each batch was sufficient for one panel, including a ½-in. (1.3 cm) head. The SS-41 formulation is presented in table 27. A fabrication check list was used to assure traceability of raw materials, document the bulk density and quantity of each ingredient, record loading technique and panel cure parameters, and record final panel physical data. As each panel contained a single batch of the ablative mix, there was no carryover of material from one panel to another.

Special care was taken in the mixing operation to assure that the resin and catalyst were thoroughly blended prior to their addition to the mixing vessel. This was done to assure that no uncatalyzed resin could enter the ablative material, causing uncured inclusions in the final panels. An excess of the resin mix was prepared so the proper amount could be weighed into the mixer bowl for each batch.

Twenty percent of the phenolic microballoons were added to the resin at slow speed and mixed for three minutes. All of the glass microballoons and the nylon powder were then added and mixed for three minutes. The final mix time was 45 min, with scraping after 10 min. A bulk density of the mixed ablator was then taken and recorded on the fabrication check list.

The mixed ablative material was then packed in screed frames containing the proper volume for filling the core. After loading, the frames were weighed to confirm that the proportion was correct for each side to be packed. As the volume of each frame was known, the bulk density of the prepacked material was easily calculated. This density together with the known density of the honeycomb core provided an accurate prediction of the final panel density.

Before being packed with ablative material, the core was wet-coated, spraying with Monsanto SC1009 phenolic resin. The coated core was then heated for 45 min. at 150°F (339°K) to B-stage the resin. In the B-stage the resin acts as an efficient primer for bonding the ablative material to the core. The weight and density of the core was recorded before and after coating.

In the packing operation, the prepared honeycomb core was placed upon the ablative material in the screed. A fixture and spacers were then placed around the screed so the height equalled the height of the core being filled. The assembly was then placed in the vibrator press and aligned with the upper platen. Pressure was applied to the core and the vibrator motor was started. The pressure was maintained until the core penetrated the ablative material, which was indicated by the platen becoming level with the top of the fixture.

The assembly containing the partially-filled core was then inverted over the second screed containing the remainder of the ablative material. Alignment of the two screeds was made by sliding the outer frame down, engaging both screeds at the same time. Pressure and vibration were again applied to the core to force it into the second charge. After the desired pressure was obtained, the vibrator motor was run for one minute. Pressure was maintained for an additional four minutes.

After completion of the press cycle, the assembly was inverted over a curing frame. The alignment frame was then pressed downward engaging the curing frame for the transfer operation. The assembly was returned to the press and the filled core was pressed from the screed assembly into the cure frame without damage to the core. After removal of the screed, spacer, and alignment frame, the cure frame was pushed down, exposing the head.

The assembly was then placed on a vacuum bagging plate and prepared for molding. A vacuum of 23-24 in. (584-610 mm) Hg was applied and maintained during the cure and cooldown. The cure was 16 hrs at 250°F (394°K). Ablator machining consisted of surface grinding the panels to proper thickness and trimming the edges with a diamond saw.

Honeycomb Subpanels

The subpanesl consisted of 0.014-in. (0.36 mm) glass phenolic face sheets bonded to ¼-in. (0.6 cm) cell honeycomb core, 0.613-in. (1.55% cm)-thick. The face sheets were three ply laminates of 91 LD on Style 120 glass fabric, molded at 50 psi (35 N/cm^2) in an autoclave. Face sheet bonding surfaces were grit blasted and covered with HT 424 adhesive film. The face sheets were made slightly oversize to allow for final trimming.

Honeycomb core was cut with an excess of ½-in. (1.3 cm) on each side. The outer edge of the honeycomb was then filled with epoxy to strengthen the outer edge of the finished subpanel. The filled core was then sandwiched between the two prepared face sheets. Tooling blocks were placed around the panel to prevent crushing of the honeycomb edges during cure. A vacuum bag was used to apply 24-in. (610 mm) of Hg pressure and the part was cured for 30 minutes at 340°F (444°K). The subpanels were cut to size with a diamond saw.

TPS Panel Assembly

In the intermediate panel studies of Task IV, Part 1, the SS-41 ablative panels were bonded to subpanels with a RTV adhesive. At first, the panels produced were bonded with an RTV which had been used extensively as an adhesive bond for similar low density ablators. During the tests of the ablative panels in biaxial flexure, the bond failed on several test panels. The panels were rebonded using an RTV adhesive (and new bonding process) with higher peel and tensile strength which had been developed under Martin Marietta effort.

A bonding fixture was used to firmly position the ablative panel on the subpanel during the adhesive cure operation. The assembly was placed on a tooling plate and a vacuum bag installed. The part was cured at 23-24 in. (584-610 mm) of Hg for 4 hrs at 200°F (366°K) and cooled under pressure.

APPENDIX B

Ablator SS-41F

An attempt was made in the early part of Task IV to manufacture a version of SS-41 without honeycomb. Reinforcement was to be provided by the addition of E-glass fibers (table 27-2). Several panels were molded in this manner using vacuum bag techniques. The resulting high density and delaminations observed caused the material to be dropped from consideration.

APPENDIX C

METHOD OF INSTALLING FABRICATION DEFECTS (TASK IV)

This appendix summarizes the variations in fabrication processes enacted in order to obtain the 12 defect under consideration in the Task IV experimental study. Similar details on the earlier defect installations (Task III) are contained in reference 2.

Undercure

The cure oven for the ablator billet was set at 150°F (339°K) instead of 250°F (394°K) for the specified time period, Panel 21.

Overcure

The curing temperature used 350°F (450°K) instead of 250°F (394°K), Panel 22.

Low density

The fill mixture was 13.7 pcf (219 kg/m^3) instead of the customary 14.1 pcf (226 kg/m^3) due to the low density phenolic microballoons used 7.1 pcf (114 kg/m^3) and a low honeycomb packing ram pressure (28 psi, 19 N/cm^2), Panel 23.

High density

The fill mixture was 15.0 pcf (240 kg/m^3) (compared to 14.1, 226) because of the high density phonolic microballoons used (8.7 pcf, 139 kg/m^3). This, along with a high ram packing pressure (93 psi, 64 N/cm^2) produced the billet for Panel 24.

Moist Ingredients

Two quantities of phenolic microballoons were soaked in a humidity chamber until they registered 5 and 10% weight pickup respectively, Panels 25 and 26. The prescribed loads for the batch mixtures were weighed from these, essentially starving the final composites by these percentages of microballoons.

APPENDIX C

Inhomogeneity

These panels had undermixed fills, hopefully containing unblended components. Panel 27's fill was mixed only 1/3 of the prescribed time and Panel 28's for 2/3 of the required period.

Overtime Fill-To-Core Bond Primer Preparation

The B-staging of the phenolic primer applied to the ablator's honeycomb core cell walls was allowed to proceed for twice the normal time period, Panel 29.

Overheated Fill-To-Core Bond Primer Preparation

The B-staging in this case was for the proper time period, but at a higher temperature, 250°F (394°K) instead of 150°F (339°K), Panel 30.

Horizontal Crack Layer in Ablator Fill

The standard proportions of the two screed loadings were used. Lampblack was then dusted on one portion in order to eventually create a horizontal discontinuity in the final packing. The cured billets, with their plane of discontinuity showing around the edges, were machined in accordance with the two crack plane locations stipulated (Panels 33 and 34).

Undercut Core

The ablator honeycomb components for Panels 35 and 36 were deliberately foreshortened in heights. Final billet machining to the proper height placed unreinforced material at the outer surfaces.

Billet to Subpanel Delaminations

Discs of precast bond material, sprayed with a Teflon release film and as thick as the anticipated bond line, were located in specified patterns on the subpanels for Panels 37 and 38. Normal assembly followed, with successful delamination spotes in the bond line.

Broken Nodes and Ribbons

A spatula blade was used to create broken nodes and ribbons in the reinforcement honeycomb prior to the packing of the ablator filling. Panels 39, 40, 41 and 42 were involved.

APPENDIX D

REDUCTION OF FOUR POINT FLEXURE DATA

Four-point flexure data were obtained on 133 beams of ablator billet, representing many of the intentional defects and control panels in Task IV (see fig. 92). A typical recording of the load vs centerline deflection is presented in figure 93. The yield point was defined as the point at which the loading slope dropped off and ultimate load was represented by beam failure. The slope of the curve up to the yield point was used in modulus derivation. All the pertinent data and calculations are summarized in tables 12 to 15; formulae are presented in this appendix.

Yield and Ultimate Strength Formula

The standard beam formula was used; symbols are defined in figure 92:

$$\sigma = \frac{Mc}{I} = \frac{9}{8}\frac{PL}{bh^2}$$

Flexural Modulus

The standard beam formula relating the modulus E to the slope of the deflection/load curve is, for four point loading:

$$\frac{\gamma}{p} = \frac{117}{512}\frac{L^3}{Ebh^3}$$

This produced the values for E found in table 14.

It was postulated in a recent comparison of various published divergent values for RSI flexural modulus that the effect of the low shear modulus of transversely isotropic materials such as RSI was disregarded in data reduction of three-point beam flexure tests. Reanalyzing the data, it was concluded that a significant contribution to the deformation of a flexure specimen occurs due to low shear modulus (G), 30 to 90% of the total, depending on the length-to-depth ratio of the beam.

APPENDIX D

A solution, modified for a four-point beam of our dimensions, modifies the deflection/load expression as follows:

$$\frac{\gamma}{p} = \frac{117}{512}\,\frac{L^3}{Ebh^3}\qquad 1.0 + \frac{12.8}{13.0}\,\frac{E}{G}\,\frac{h^2}{L^2}$$

Influence of G

The two unknowns in this expression were accommodated by testing similar beams of two different heights and solving two simultaneous equations for E, See figure 94.

A summary of flexural moduli calculated in this manner is reported in table 15. Apparently, the E/G ratio (flexure/shear ratio) for SS-41 must be sufficiently large to neglect the influence term, since the average values for E increased just slightly.

TABLE 1.- POTENTIAL CRITICAL DEFECTS

Potential critical defect \ Critical properties	Thermal	Ablative layer mechanical	Char layer integrity	Surface erosion resistance	Chemical composition and stability	Ablative layer bond to subpanel	Dimensional	Subpanel mechanical
Ablative material								
Cracks		●	●					
Delaminations		●	●					
Voids	●		●					
Unbonded to honeycomb	●	●	●					
Density	●		●	●				
Constituent integrity	●	●	●	●				
State of cure		●	●	●	●			
Homogeniety	●	●	●	●				
Formulation	●	●	●	●	●			
Foreign matter								
Inhibitors		●	●	●	●			
Inert to resin			●		●			
Moisture content			●		●			
Honeycomb								
Crushed			●					
Broken ribbons		●	●					
Distorted cells		●	●					
Broken node bonds		●						
Splices	●	●						
Undercut			●					
Unbonded to substructure		●				●		
Panel substructure								
Resin content, mold cycle								●
Panel configuration								
Thickness	●						●	
Width and length	●		●				●	●
Edge conditions	●		●				●	
Attachment alignment		●	●			●	●	●
Contour	●						●	

TABLE 2.- NOMINAL CONDITIONS USED IN PLASMA ARC SPLASH TESTS

Point	$\dot{q}_{cw}$		Time	Q_{cw}		H_s		P_{STG}	
	Btu/Ft^2-sec	MW/m^2	Sec.	Btu/Ft^2	MJ/m^2	Btu/lb	MJ/kg	atm	kN/m^2
1	23	0.28	1200	27 600	313	3800	8.84	.0056	0.572
2	55	0.62	900	49 500	562	6400	14.90	.0088	0.891

TABLE 3.- SUMMARY OF FABRICATION TO ENTRY STUDY, TASK III

Defect	Critical?		Comments
	No	Yes	
Density	x		Gradients - Dense outer ⇒ greater mass loss ζ = 15 PCF ⇒ (240 Kg/m^3) 40°F Overshoot (295°K)
Unbond H/C		Excess Resin Larger Net K	Substrate Temperature Δ Overshoots > 75°F (314°K)
Voids		$\zeta <$ 14 PCF (244 Kg/m^3) Δ Overshoots > 75°F(314°K)	
Formulation	x		
Cure Variation	x		

TABLE 4.- RESULTS OF DESCENT ACOUSTIC ENVIRONMENT TESTS OF MG-36 PANEL 2

Exposure cycle	Overall** dB level	Duration (sec)	Comments
1	150	120	Some char lost in the area of crushed core
2	152	120	No observable change
3	154	120	Some char loss in "damaged areas"***
4	154	240	Additional char loss in areas of: Crushed core Undercut core Soft cure

Notes: ** The input acoustic environment had a similar spectral distribution at each exposure level.

*** Several areas in the char had been damaged during pretest handling, and during bonding of the 18" x 18" acoustic test assembly.

TABLE 5.- TPS PANEL PHYSICAL MEASUREMENTS

Panel number	Composition	Density				Hardness (Shore A)	
		As-fabricated		After all tests		As-fabricated	After all tests
		pcf	kg/m^3	pcf	kg/m^3		
3	SS-41	15.98	256	Dummy panel		---	---
4	SS-41	16.42	263	16.58	264	48-50	55
5	SS-41	16.49	264	16.69	267	50	45-50
6	SS-41	16.41	263	16.60	266	45-55	45
7	SS-41	16.49	264	16.64	267	45-55	35-40
8	SS-41	16.45	264	16.23	260	48-50	52
9	SS-41	16.24	261	16.20	259	45-55	50
10	SS-41	16.15	259	16.30	261	45-55	50
11	SS-41	16.45	264	16.76	269	45-55	55-60
12	SS-41	16.30	261	16.83	270	45-55	60
13	SS-41	16.72	268	17.11	274	45-55	55
14	SS-41F	17.33	278	17.63	283	40-50	55
15	SS-41F	18.50	296	18.55	297	45-50	60
16	SS-41	16.13	258	16.13	258	50-55	50-55
17	SS-41	16.75	269	---	---	---	---
18	SS-41	16.09	257	16.09	257	50-55	50-55

TABLE 6.- ENVIRONMENTAL TEST MATRIX

Panel number	Humidity	Dehydration	Ascent acoustics	Biaxial flexure room temperature	Thermal and cold soak and vacuum	Cold soak and vacuum	Biaxial flexure cold soak	Descent acoustics	Four-point flexure
3	Trial Panel for Facility Checkout								
4	X	X	X	X	X			X	
5	X	X	X	X					X
6	X	X		X					X
7	X	X		X					X
8				X	X		X		X
9			X	X		X			
10				X		X	X		X
11			X	X	X			X	
12					X		X		X
13							X		X
14			X	X		X	X		X
15									X
16									X
18									X

TABLE 7.- BIAXIAL FLEXURE TEST RESULTS (AMBIENT TEMPERATURE)

Panel no.*	Previous exposure	Press/strain stiffness		Surface elastic elon-gation %	Observations		
		psi/in./in.	$N/cm^2/cm/cm$		Delami-nations	Cracks parallel to ribbon	Disbonds on (i) sides
10	A	1430	970	0.60			1
8	A	1540	1045	0.30			1
9	B	1360	925	0.45		x	2
11	B	1210	825	0.46			2
4	C	1210	825	0.40			
5	C	1290	880	0.50		x	
6	D	1250	850	0.38			
7	E	890	605	0.36			
16	B	785	535	0.50			2

* All panels were SS-41 except No. 16 (SLA-561)

Previous environments (up to biaxial flexure test)

A None
B Ascent acoustics
C 10 days humidity, dehydrated, ascent acoustic
D 10 days humidity, dehydrated
E 16 days humidity, dehydrated

TABLE 8.- SUMMARY OF DATA FOR HUMIDITY, ASCENT ACOUSTICS, AND UNIAXIAL FLEXURE

Panel	% gain in ablator weight during humidity exposure	Maximum % strain observed in uniaxial flexure test		Ascent acoustics overall level db
		Post-humidity	Post-vacuum	
19	7.4	.20	---	162.0
20	---	---	---	---
21	8.1	.40	---	162.5
22	7.4	.20	---	162.5
23	7.7	.25	---	162.5
24	7.3	.18	---	161.5
25	7.5	.20	---	163.0
26	7.8	.20	---	162.5
27	7.5	.45	---	163.0
28	7.8	.08	---	163.0
29	7.3	.30	---	162.5
30	7.4	.20	---	162.5
31	7.0	.10	---	163.0
32	---	.60	---	---
33	7.4	.25	---	162.5
34	7.7	.22	---	163.5
35	7.3	.12	---	163.5
36	7.6	.15	---	163.5
37	7.6	.12	.33	164.0
38	7.6	.20	.33	163.0
39	8.0	.08	.33	163.0
40	7.9	.08	.33	163.5
41	7.5	.15	.28	163.0
42	7.7	.08	.28	163.5
43	7.6	.08	.39	163.0
44	6.6	.08	---	163.5
45	---	---	---	---

TABLE 9.- SUMMARY OF TYPICAL TEMPERATURE EXTREMES IN VACUUM EXPOSURES

Time Point	Wave	Temperature, °F (°K) read on the thermocouples indicated																							
		1	2	3	4	5	6	7	8	9	10	11	12	13	14	15	16	17	18	19	20	21	22	23	24
End of main heat cycle, plus °F, (°K)	I	198 (365)	199 (366)	198 (365)	198 (365)	160 (344)	201 (367)	203 (368)	204 (367)	206 (370)	206 (370)	168 (370)	214 (374)	203 (368)	169 (349)	207 (370)	208 (371)	208 (371)	208 (371)	204 (369)	159 (344)	207 (370)	207 (370)	205 (369)	205 (369)
	II	208 (371)		204 (369)	204 (369)	195 (364)	209 (371)	208 (371)		209 (371)	209 (371)	206 (370)	218 (376)	217 (376)	200 (366)	218 (376)	218 (376)	214 (374)	212 (373)	205 (369)	191 (361)	208 (371)	208 (371)	208 (371)	207 (370)
	III	203 (368)	208 (371)	206 (370)	207 (370)	192 (362)	208 (371)	207 (370)	209 (371)	209 (371)	209 (371)	204 (369)	217 (376)	212 (373)	201 (367)	213 (374)	213 (374)	213 (374)	213 (374)	205 (369)	191 (361)	208 (371)	208 (371)	208 (371)	208 (371)
Third cold cycle, minus °F, (°K)	I	165 (347)	142 (334)	142 (334)	146 (336)	0 (255)	170 (350)	168 (349)	131 (328)	139 (332)	139 (332)	11 (261)	179 (355)	179 (355)	6 (259)	168 (349)	152 (340)	149 (338)	149 (338)	170 (350)	1 (256)	170 (350)	142 (334)	131 (328)	131 (328)
	II	189 (360)		140 (333)	134 (330)	152 (340)	189 (360)	225 (380)		134 (330)	130 (327)	130 (327)	208 (371)	207 (370)	145 (336)	179 (355)	182 (356)	195 (364)	196 (364)	200 (366)	135 (330)	195 (364)	165 (347)	165 (347)	177 (354)
	III	190 (361)	131 (328)	136 (331)	134 (330)	151 (339)	191 (361)	211 (372)	134 (330)	141 (334)	141 (334)	162 (345)	212 (373)	210 (372)	164 (346)		181 (356)	179 (355)	188 (360)	196 (364)	131 (328)	205 (369)	175 (352)	179 (355)	181 (356)

TABLE 10. - Entry Heating Summary

Panel	Defect	Previous History "Humidity to thermal vacuum" except:	Test observations														
			Appearance					Stream enthalpy		Run time (sec)	Maximum readings on thermocouples (center panel)					
			Pre-" test "Normal" except for:	Post-test							Outer surface		Mid-thickness		Back surface	
				Outer Surface "Firm" except for:	Inner surface			Btu/lb	MJ/kg		°F	°C	°F	°C	°F	°C
					Virgin	Brown	Dark Brown									
19	None					X		11 000	25.6	1100	1630	888	940	504	320	160
20	None	None				X	X	11 000	25.6	1100	---	---	---	---	---	---
21	Undercure				X			9 045	21.1	1100	1325	718	440	227	140	60
22	Overcure					X		9 045	21.1	1100	1825	996	850	454	325	163
23	Low density		(e)	(e)		X	X	10 400	24.2	1100	1900	1038	920	493	280	138
24	High density			(f)	X			9 045	21.1	1100	1600	871	525	274	250	121
25	Wet basics				X			10 400	24.2	1100	1825	996	510	266	170	77
26	Wet basics				X			8 150	19.0	712	1415	768	350	177	130	54
27	Undermixed				X			10 400	24.2	1100	1490	810	615	324	---	---
28	Undermixed				X			6 045	14.1	1100	1640	893	790	421	300	149
29	Long B-stage			(a)			X	6 045	14.1	1100	1870	1021	765	407	190	88
30	Hot B-stage		(g)	(g) (b)		X		7 905	18.4	920	1740	949	440	227	265	129
31	None		(e)	(e)(f)		X		6 045	14.1	1100	1525	829	550	288	280	138
32	None	None		(f)	X			7 000	16.3	1100	1515	824	595	313	260	127
33	H. crack in fill					X		7 000	16.3	1100	1865	1018	875	468	315	157
34	H. crack in fill				X			8 150	19.0	1100	1670	910	590	310	205	96
35	Undercut core			(c)	X		X	8 150	19.0	1100	1525	829	455	235	250	121
36	Undercut core			(d)		X		8 760	20.4	1100	1525	829	525	274	---	---
45	None	None				X		8 760	20.4	1100	1665	907	835	446	400	204

Note:
(a) Top of core thickened;
(b) Fill shifts + 0.03 to - 0.13 (+0.08 to -0.33); in. (cm.)
(c) 50% of topping off as a 0.1 (0.25) skin;
(d) All of topping off as a 0.2 (0.51) skin;
(e) Some cells depressed;
(f) Aft edge bumped in Plasma Arc test:
(g) Core fill is loose

m = 0.05 lb/sec (0.0226 kg/s)
p = 15 Torr (1999.83 N/m^2)

TABLE 11.- SUMMARY OF DESCENT ACOUSTICS TESTING

Test observations				
	Post-test appearance			
		Spalled cells		120 sec
Panel	Surface "Firm" unless noted	Number of cells	Depth range, in. (cm)	Overall Level (dB)
19	(m)	5	0.3 (0.76)	151.0
20	(m)	8	0.3 to 0.6 (0.76 to 1.52)	150.0
21	(m)	30	0.1 to 0.5 (0.25 to 1.27)	150.5
22		1	0.2 (0.51)	150.5
23		0	-----	151.0
24		3	0.1 (0.25)	150.5
25		0	-----	150.0
26	(m)	9	0.1 (0.25)	150.5
27		6	0.2 (0.51)	151.0
28		1	0.4 (1.16)	150.0
29	(m)	0	-----	150.0
30	(n)	20	0.05 to 0.3 (0.13 to 0.76)	150.0
31		14	0.1 (0.25)	150.5
32		5	0.1 (0.25)	150.0
33		4	0.1 to 0.6 (0.25 to 1.52)	150.5
34		0	-----	150.5
35	(n) (p)	15	0.1 to 0.7 (0.25 to 1.78)	150.5
36	(n)	20	0.1 to 0.7 (0.25 to 1.78)	150.5
45		0	-----	151.5

(m) Hard outer skin easy to push down into cell;
(n) Crunchy at touch
(p) No further damage to skin, spalling occuring over pre-test exposed area

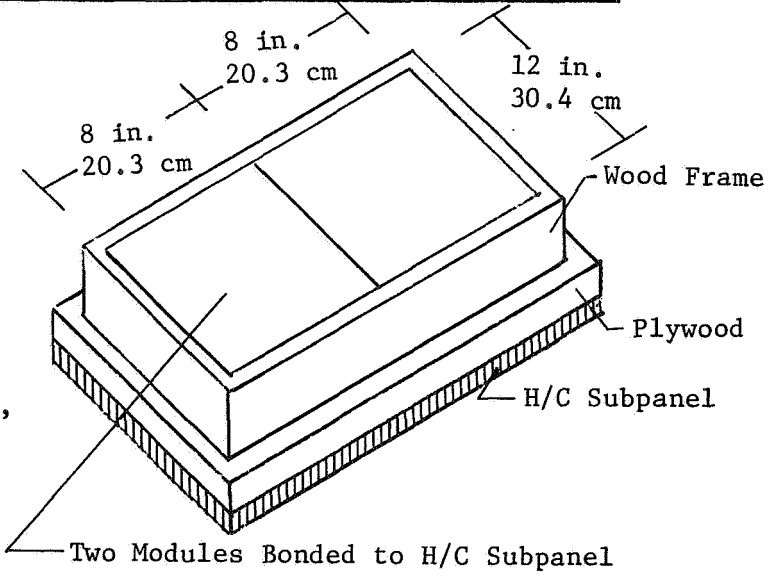

TABLE 12.- YIELD STRENGTH IN BEAM FLEXURE

Panel	Bending across grain				Bending along grain		
	h_2		h_1		h_2	h_1	
	F	G	D	E	C	A	B
19	82	87	134	126	134	131	103
	57	60	93	88	93	91	72
21	59	67	76	80	160	131	166
	41	47	53	56	111	91	115
22	172	---	153	125	---	203	220
	119	---	106	87	---	141	153
23	94	75	73	88	177	161	158
	65	52	51	61	123	112	110
24	129	145	141	136	230	240	222
	90	101	98	94	160	167	154
25	136	128	94	134	235	228	245
	94	89	65	93	163	158	170
26	72	86	114	109	164	148	151
	50	60	79	76	114	103	105
27	104	96	77	74	NA	182	166
	72	67	53	51		126	115
28	108	104	91	94	176	185	194
	75	72	63	65	122	128	135
29	108	97	120	160	253	245	248
	75	67	83	111	176	170	172
30	74	28			238	286	261
	51	19			165	199	181
31	87	104	---	105	198	233	236
	60	72	---	73	138	162	164
33	96	96	108	94	201	134	159
	67	67	75	65	140	93	110
34	169	169	171	143	276	197	200
	117	117	119	99	192	137	139
35	134	101	114	109	191	160	160
	93	70	79	76	133	111	111
36	121	---	97	108	177	128	162
	84	---	67	75	123	89	113
20	142	125	120	119	199	210	193
	99	87	83	83	138	146	134
32	71	71	73	60	124	139	136
	49	49	51	42	86	97	94
45	127	107	93	104	175	192	184
	88	74	65	72	122	133	128

(Typical)
lb/in.^{2} ← 222
N/cm^2 ← 154

i	h_i = height (approx)	
	in.	cm
1	1.25	3.175
2	0.75	1.905

D	E
---	212
---	147

all @ h_1

TABLE 13.- ULTIMATE STRENGTH IN BEAM FLEXURE

Panel	Bending across grain				Bending along grain		
	h_2		h_1		h_2	h_1	
	F	G	D	E	C	A	B
19	87	95	137	131	205	273	279
	60	66	95	91	142	190	194
21	82	95	91	97	266	308	337
	57	66	63	67	185	214	234
22	182	136	166	144	261	454	318
	126	94	115	100	181	315	221
23	122	109	113	121	228	267	277
	85	76	78	84	158	185	192
24	177	177	165	164	310	424	392
	123	123	115	114	215	294	272
25	155	151	97	148	274	263	304
	108	105	67	103	190	164	211
26	96	107	126	116	240	297	275
	67	74	88	81	167	137	191
27	118	113	92	103	NA	319	338
	82	78	64	72	NA	222	235
28	118	123	108	110	289	411	347
	82	85	75	76	201	285	241
29	143	139	144	191	341	297	365
	99	97	100	133	237	206	253
30	84	75			270	355	270
	58	52			188	247	188
31	124	136	314	111	264	285	302
	86	94	218	77	183	198	210
33	121	120	126	140	272	368	264
	84	83	88	97	189	256	183
34	182	201	202	177	310	383	348
	126	140	140	123	215	266	242
35	143	135	129	126	215	242	308
	99	94	90	88	149	168	214
36	149	112	122	125	240	309	313
	103	78	85	87	167	215	217
20	148	136	125	130	292	312	301
	103	94	87	90	203	217	209
32	108	108	104	94	318	289	294
	75	75	72	65	221	201	204
45	156	139	144	130	317	339	347
	108	97	100	90	220	235	241

(Typical)
lb/in.^{2} ← 392
N/cm^2 ← 272

i	h_i = height (approx)	
	in.	cm
1	1.25	3.175
2	0.75	1.905

D	E
195	229
135	159

all @ h_1

TABLE 14.- FLEXURAL MODULUS USING SIMPLE BEAM FORMULA

Panel	Bending across grain				Bending along grain				
	h_2		h_1		h_2	h_1			
	F	G	D	E	C	A	B		
19	2252 (1564)	2399 (1666)	2666 (1852)	2366 (1643)	4075 (2830)	5300 (3681)	4570 (3174)		
21	2736 (1900)	2522 (1752)	2635 (1830)	2796 (1942)	7820 (5432)	6642 (4613)	6965 (4838)		
22	4573 (3176)	3715 (2580)	3728 (2589)	3670 (2549)	5036 (3498)	8139 (5653)	8019 (5570)		
23	3049 (2118)	2935 (2039)	2842 (1974)	3076 (2150)	7010 (4869)	6250 (4341)	6267 (4353)		
24	4549 (3160)	4368 (3034)	4071 (2828)	4080 (2834)	9018 (6264)	8617 (5985)	8826 (6130)		
25	3942 (2738)	4176 (2901)	3695 (2566)	3850 (2674)	8957 (6221)	6360 (4417)	7080 (4918)	← psi ← N/cm^2	
26	3345 (2323)	3500 (2431)	3624 (2448)	3557 (2471)	7767 (5345)	6499 (4514)	6353 (4413)		
27	3614 (2510)	3348 (2325)	3175 (2205)	3111 (2161)	---	8399 (5834)	7259 (5042)		
28	3828 (2659)	3702 (2571)	3695 (2566)	3647 (2464)	9362 (6503)	9434 (6553)	9142 (6350)		
29	4774 (3316)	4352 (3023)	4452 (3092)	4293 (2982)	10485 (7283)	9920 (6890)	8862 (6155)		
30	1442 (1002)	1431 (994)	---	---	5756 (3948)	5680 (3945)	4430 (3077)	4465 (3101)	4019 (2791)
31	3428 (2381)	3112 (2162)	4594 (3191)	2804 (1948)	7535 (5234)	7225 (5018)	7804 (5420)		
33	3845 (2671)	3495 (2428)	3696 (2569)	3688 (2562)	7862 (5461)	7388 (5132)	7085 (4921)		
34	4544 (3156)	4218 (2930)	4869 (3382)	4731 (3286)	8700 (6043)	8280 (5751)	8274 (5747)		
35	3193 (2218)	3810 (2646)	3695 (2566)	3704 (2573)	6390 (4438)	7262 (5044)	6980 (4848)		
36	3954 (2746)	2460 (1709)	3020 (2098)	3690 (2563)	7512 (5218)	7193 (4996)	7502 (5211)		
20	2938 (2041)	3242 (2252)	2636 (1831)	2347 (1630)	7350 (5105)	7757 (5388)	7348 (5104)		
32	3232 (2245)	3378 (2346)	3194 (2218)	3222 (2238)	7120 (4945)	7335 (5095)	7293 (5066)	} all @ h_1	
45	4238 (2944)	4085 (2837)	4087 (2839)	4077 (2832)	9483 (6587)	9021 (6266)	9480 (6585)		

i	h_i = beam height (approximately)	
	in	cm
1	1.25	3.175
2	0.75	1.905

TABLE 15.- FLEXURAL MODULUS USING DATA FROM TWO BEAMS

Panel	Bending across grain				Along grain	
	D vs. F	D vs. G	E vs. F	E vs. G	A vs. C	B vs. C
19	2070 (1438)	2260 (1570)	2190 (1521)	2410 (1674)	3600 (2500)	3830 (2660)
21	2790 (1938)	2460 (1709)	2700 (1875)	2390 (1660)	8660 (6015)	8380 (5807)
22	5240 (3640)	3700 (2570)	5320 (3695)	3720 (2584)	4170 (2896)	4180 (2903)
23	3040 (2112)	2860 (1986)	3040 (2112)	2850 (1980)	7540 (5237)	7520 (5223)
24	4890 (3396)	4550 (3160)	4880 (3340)	4540 (3153)	9320 (6473)	9170 (6369)
25	4110 (2855)	4490 (3119)	4010 (2785)	4370 (3035)	11600 (8057)	10470 (7272)
26	3220 (2237)	3430 (2382)	3250 (2257)	3470 (2410)	8720 (6057)	8880 (6168)
27	3980 (2764)	3510 (2438)	3960 (2751)	3500 (2431)	7503 (5211)	8159 (5667)
28	4000 (2778)	3850 (2674)	4000 (2778)	3850 (2674)	9310 (6466)	9460 (6571)
29	4970 (3452)	4300 (2987)	5090 (3535)	4400 (3056)	10850 (7536)	11670 (8106)
30	1440* (1000)	1280* (889)	--- ---	--- ---	5800 (4000)	6860 (4765)
31	3000 (2084)	2640 (1834)	3910 (2716)	3310 (2299)	7620 (5293)	7340 (5098)
33	3920 (2723)	3390 (2355)	3930 (2730)	3400 (2362)	8150 (5661)	8340 (5793)
34	4380 (3042)	3920 (2723)	4440 (3084)	3960 (2751)	8960 (6223)	8960 (6223)
35	2970 (2063)	3880 (2695)	2970 (2757)	3870 (2688)	6010 (4174)	6130 (4258)
36	4200 (2917)	2100 (1459)	4090 (2841)	2080 (1445)	7700 (5348)	7520 (5223)

h 1.25 in (3.175 cm)

h 0.75 in. (1.905 cm)

psi

N/cm^2

D vs. C	E vs. C
7510 (5216)	7510 (5216)

(No 0.75-in. (1.905 cm) test results for Panels 20, 32 or 45)

* EST.

TABLE 16.- SUMMARY OF PHYSICAL OBSERVATIONS WITH ENVIRONMENTAL EXPOSURE

Panel	Ablator density				Total assembly weight										Hardness values						Post thermal vacuum	
	as fabricated		Post thermal vacuum		As bonded		Post humidity		Post acoustics		Post flexure		Post thermal vacuum		Pre-bond		Post bond		Post humidity			
	pcf	kg/m^3	pcf	kg/m^3	lb	kg	lb	kg	lb	kg	lb	kg	lb	kg	Shore "A"	Shore "D" mod	Shore "A"	Shore "D" mod	Shore "A"	Shore "D" mod	Shore "A"	Shore "D" mod
19	16.1	257	16.0	256	9.56	4.340	10.06	4.567	10.02	4.547	9.98	4.529	9.42	4.279	44	90	34	75	21	53	44	80
20	16.5	265	16.4	262	9.66	4.385	---	---	---	---	---	---	9.65	4.382	34	83	37	78	--	--	36	81
21	16.0	256	15.7	251	9.49	4.307	10.04	4.558	10.01	4.544	9.94	4.511	9.36	4.250	26	71	40	83	26	60	47	89
22	15.7	251	15.7	251	9.35	4.245	9.84	4.469	9.83	4.461	9.77	4.437	9.27	4.210	41	88	53	91	35	71	52	91
23	15.2	244	15.9	255	9.02	4.096	9.51	4.319	9.48	4.303	9.44	4.284	8.93	4.055	30	78	44	87	27	60	50	87
24	16.9	270	16.8	269	9.76	4.431	10.28	4.667	10.24	4.651	10.21	4.634	9.65	4.380	46	91	49	89	35	73	52	92
25	16.1	257	16.1	257	9.45	4.290	9.96	4.522	9.93	4.508	9.88	4.487	9.32	4.233	47	90	43	88	31	74	53	87
26	16.1	257	16.1	257	9.36	4.248	9.89	4.488	9.84	4.467	9.77	4.436	9.25	4.201	35	86	43	86	30	72	47	89
27	15.6	250	15.5	249	9.27	4.207	9.76	4.433	9.77	4.435	9.76	4.432	9.13	4.147	35	84	38	81	26	64	50	86
28	16.2	260	16.1	257	9.45	4.290	9.98	4.533	9.96	4.523	9.92	4.504	9.35	4.244	38	86	44	86	32	73	56	90
29	16.6	266	16.6	266	9.61	4.364	10.13	4.598	10.07	4.572	10.04	4.556	9.47	4.299	31	80	43	85	31	71	53	87
30	16.6	266	16.4	262	9.46	4.293	9.97	4.527	9.92	4.503	9.89	4.488	9.34	4.240	30	78	47	86	25	60	40	74
31	15.7	251	15.2	244	9.37	4.256	9.86	4.475	9.83	4.463	9.79	4.445	9.23	4.189	--	85	37	79	24	63	41	80
32	15.8	253	15.8	253	9.38	4.260	---	---	---	---	---	---	9.37	4.256	38	87	44	88	31	--	40	88
33	16.0	256	16.0	256	9.26	4.202	9.76	4.429	9.73	4.418	9.68	4.394	9.11	4.138	44	87	43	85	29	69	53	86
34	17.0	272	16.9	270	9.85	4.470	10.41	4.726	10.37	4.708	10.33	4.689	9.77	4.436	52	90	51	90	31	69	55	92
35	15.9	255	15.8	253	9.44	4.285	9.93	4.507	9.87	4.482	9.84	4.468	9.30	4.222	43	85	44	87	28	67	50	93
36	15.9	255	15.9	255	9.48	4.305	10.00	4.539	9.95	4.518	9.91	4.499	9.36	4.248	44	87	42	83	29	69	53	93
37	15.7	251	15.7	251	9.30	4.222	9.80	4.450	9.75	4.427	9.69	4.400	9.18	4.170	27	74	33	78	34	70	50	89
38	15.5	249	15.6	250	9.27	4.208	9.76	4.433	9.72	4.414	9.67	4.390	9.16	4.159	45	91	50	91	30	73	51	91
39	16.3	261	16.3	261	9.53	4 327	10.08	4.577	10.05	4.564	10.02	4.547	9.47	4.301	28	78	45	89	31	72	52	91
40	15.4	262	16.4	262	9.58	4.350	10.13	4 599	10.09	4.579	10.04	4.557	9.52	4.320	27	79	41	88	31	71	50	90
41	16.0	256	16.1	257	9.54	4.330	10.06	4.566	10.01	4.546	9.99	4.534	9.45	4.290	42	89	42	89	31	70	52	91
42	16.0	256	16.1	257	9.43	4.281	9.96	4.521	9.92	4.502	9.87	4.483	9.35	4.244	41	90	40	89	33	73	49	91
43	16.5	265	16.6	266	9.79	4.445	10.33	4.690	10.29	4.674	10.28	4.658	9.71	4.407	52	89	51	90	31	70	53	91
44	15.5	249	15.6	250	9.09	4.126	9.65	4.382	9.61	4.361	9.56	4.341	9.07	4.120	--	90	37	81	26	63	41	84
45	16.7	268	16.8	269	9.92	4.505	---	---	---	---	---	---	9.92	4.502	48	90	32	79	--	--	52	87

TABLE 17. - SUMMARY OF CROSS SECTION OBSERVATIONS

Panel	Char penetration				Gap just below surface material			Overall view horizontal fissures (excluding 1st gap)			
	Fwd 6" (15cm)		Aft 6" (15 cm)								
	in.	cm	in.	cm	Small	Large	Note	None	Few	Mod.	Many
19	0.95	2.41	0.81	2.06		x		x			
20	0.93	2.36	0.82	2.08		x	a	x			
21	0.79	2.01	0.70	1.78	x						x
22	0.90	2.29	0.73	1.85	x						x
23	1.02	2.59	0.95	2.41	x						x
24	0.67	1.70	0.55	1.40	x					x	
25	0.82	2.08	0.71	1.80		x		x			
26d	0.50	1.27	0.40	1.02		x			x		
27	0.76	1.93	0.66	1.68	x					x	
28	0.83	2.11	0.72	1.83	x						x
29	0.91	2.31	0.80	2.03	x						x
30d	0.74	1.88	0.62	1.57	x			x			
31	0.70	1.78	0.53	1.35		x		x			
32	0.73	1.85	0.56	1.42		x			x		
33	0.98	2.49	0.77	1.96	x		b		x		
34	0.81	2.06	0.71	1.80	x					x	
35	0.56	1.42	0.38	0.97	x		c	x			
36	0.94	2.39	0.64	1.63			c	x			
45	0.89	2.26	0.73	1.85		x					x

Notes:
a Surface cap tilted in many cells
b Artificial crack widened considerably
c Outer layer had buckled off
d Shorter heat exposures, could extrapolate to 1100 seconds

TABLE 18. - SUMMARY OF DENSITY CHANGES IN PANELS

Time	Number of panels	Ablator density						
		Lowest		Highest		Average		
						Value		Percent change from as-fabricated
		pcf	kg/m^3	pcf	kg/m^3	pcf	kg/m^3	
As-fabricated	27	15.2	243	17.0	272	16.1	258	0
After humidity	24	16.4	263	18.5	296	17.3	277	+ 6.9
After vacuum	24	15.0	240	16.8	269	15.8	253	- 1.9
After separation	19	15.2	243	16.9	270	16.0	256	- 0.6

TABLE 19.- BASELINE STRENGTH VALUES FOR CONTROL MATERIALS

Exposure history	Property	Weak direction		Strong direction	
		lb/in.^{2}	kN/m^2	lb/in.^{2}	kN/m^2
From fabrication	Yield strength	103	710	178	1 227
To thermal	Ultimate strength	118	814	280	1 931
Vacuum	Flexural modulus	3610	2489	7480	51 573
	Yield strength	98	676	173	1 193
As-fabricated	Ultimate strength	127	876	312	2 151
	Flexural moduls	3000	2068	7500	51 711

TABLE 20.- SUMMARY OF CRITICAL COMMENTS ON DEFECTS

Environment stage	Flaw	Cure		Density		Wet basics		Undermix		B-staging		H. cracks		U/cut core	
		Under	Over	Low	High	5%	10%	1/3 t	2/3 t	Long	Hot	1/4 in. (0.6 cm)	1/2 in. (1.3 cm)	0.1 in. (0.25 cm)	0.2 in. (0.51 cm)
	Panel	21	22	23	24	25	26	27	28	29	30	33	34	35	36
Humidity															
Ascent acoustics															
Uniaxial Flexure															
Thermal vacuum				P7							P5				
Four point flexure		P1 P2		P1	P2	P2	P2	P1	P1	P2	P1	P2	P2	P1	P1
Reentry heating			E1								E3			E2 E3	E2 E3
Descent acoustics		E2 E6					E6			E6	E2 E3			E2 E3	E2 E3
Cross sectioning		E5	E5	E5 E7						E5	E7				

Pre-entry
- P1 Low strength
- P2 High modulus
- P5 Fill separation
- P7 Material shrinkage

Entry
- E1 High backface temperature
- E2 Material losses
- E3 Surface roughening
- E5 Internal char cracking
- E6 Loose cell surfaces
- E7 Deep pyrolysis

TABLE 21. - ADVANCED INSPECTION METHODS

Anomaly	Inspection method	
Inhomogenity in the ablator panel Cracks Voids Density variations Mixture variations	X-radiography	X-radiometric gaging Step wedge and penetrameter aids In-motion radiography x-ray television video image processing
Cure variations	Indentation hardness	
Bond strength ablator to honeycomb core	Panel flexure	
Disbonds, delaminations ablator to subpanel	Sonics/ultrasonics Holography Vacuum cup resonance	
Bond strength ablator to subpanel	Vacuum cup - proof loading	

TABLE 22.- SERIES A THICKNESS/DENSITY REFERENCE SPECIMENS
6 x 6 in. (15.30 x 15.30 cm) PANELS

Panel number	Thickness		Density		Average hardness values	
	in.	cm	pcf	kg/m^3	Shore "A"	Shore "D" modified
46	1/2	1.27	14.98	240	25	69
47		1.27	15.66	251	26	71
48		1.30	15.99	256	32	86
49		1.27	16.61	266	37	88
50		1.28	17.00	273	41	91
51		1.27	17.43	279	43	92
52	1	2.55	14.70	239	27	76
53		2.54	15.39	247	35	82
54		2.56	15.97	256	30	85
55		2.55	16.53	265	47	92
56		2.55	16.97	272	42	88
57		2.60	17.44	279	48	92
58	1 1/2	3.82	14.98	240	29	70
59		3.82	15.52	249	37	83
60		3.82	15.86	254	35	88
61		3.81	16.42	263	33	87
62		3.82	17.01	273	47	92
63		3.81	17.53	280	48	93
64	2	5.07	14.99	240	32	91
65		5.08	15.48	248	33	91
66		5.13	15.94	256	36	88
67		4.97	16.54	265	34	85
68		5.08	16.99	272	55	95
69		5.02	17.58	282	38	94

TABLE 23.- CALCULATED ABSORPTION COEFFICIENTS FOR SS-41 WITH INCREASING THICKNESS, 65 KV

Nominal Panel density		1/2" (1.27 cm)		1" (2.54 cm)		1½" (3.81 cm)		2" (5.08 cm)	
		μ	μ_o	μ	μ_o	μ	μ_o	μ	μ_o
lb/ft^3	g/cm^3								
15	.240	1.42	5.92	.97	4.05	.625	2.61	.75	3.12
15.5	.249	1.43	5.70	.98	3.96	.650	2.61	.76	3.12
16.0	.256	1.44	5.61	1.01	3.95	.645	2.51	.77	3.06
16.5	.264	1.55	5.85	1.015	3.88	.680	2.50	.82	3.10
17.0	.273	1.48	5.45	1.005	3.70	.680	2.50	.70	2.86
17.5	.279	1.57	5.65	1.001	3.70	.65	2.30	.795	2.83

TABLE 24.- SUMMARY OF IN-MOTION RADIOGRAPHY PARAMETERS FOR HONEYCOMB REINFORCED SS-41 ABLATOR

Study		In-motion films									Fluro-scopic/ tele-vision scans
Power		110 KV						50 KV			---
Intensifying screen		None						F 1			---
Film type		Kodak M ready-pak industrial x-ray			Poloroid 52			Kodak industrex 600 paper			---
Planform dimen-sions in. (cm)	Thick-ness in. (cm)	No. of panels	MA	No. of passes	No. of panels	MA	No. of passes	No. of panels	MA	No. of passes	No. of panels
6 x 6 (15.30 x 15.30) flat	0.5 (1.3)	6	11	3	1	11	3	6	7	1	1
	1.0 (2.5)	6	11	4	1	11	4	6	8	1	1
	1.5 (3.8)	6	11	5	1	11	5	6	10	1	1
	2.0 (5.1)	6	11	7	1	11	7	6	11	1	1
12 x 9 (30 x 23) curved	2.0 (5.1)	1 15"R (38cm) 1 25"R (64cm)	11	7	0	--	-	2	11	1	1
12 x 12 (30 x 30) flat	2.0 (5.1)	1	11	7	0	--	-	1	11	1	1
Fixed param-eters		Focal film distance = 8 1/2 ft (2.16 m) (maximum available) Traverse speed = .30 in./minute (76 cm/min) (movement erratic at slower speed) Diaphragm opening at the tube head = 1/8" (0.32 cm) (minimum available)									

TABLE 25.- SHORE "A" DUROMETER HARDNESS VS MATERIAL VARIATIONS FOR MG-36

Hardness sample	Description	Density, lb/ft^3	(kg/m^3)	Durometer average value (shore A)
	A. Average durometer value vs density of selected NDT samples			
6	Low density	11.8	(189.0)	35.8
5	Low density	14.2	(227.5)	64.4
7	Density control	15.2	(243.5)	44.4
6a	Density control	16.1	(258.0)	62.6
6b	Density control	16.6	(266.0)	64.4
5b	Density control	16.7	(267.5)	66.8
5a	High density	17.6	(282.0)	76.4
7a	High density	17.8	(285.0)	73.4
7b	High density	18.5	(296.5)	70.0
	B. Average durometer value vs grease contamination in selected NDT ablative samples			
5b	Control	16.7	(267.5)	66.8
16	One gram of grease contamination	17.0	(272.5)	70.8
17	Two gram of grease contamination	16.5	(264.5)	64.2
	C. Average durometer values vs percent catalyst in selected NDT ablative samples			
18	6% catalyst	18.8	(301.0)	66.4
7a	10% catalyst (control)	17.8	(285.0)	73.4
19	14% catalyst	17.3	(277.0)	77.6
	D. Average durometer value vs cure temperature of selected NDT ablative samples			
20	225°F (381K) cure	18.0	(288.5)	69.8
7a	250°F (395K) cure (control)	17.8	(285.0)	73.4
21	275°F (408K) cure	17.9	(287.0)	78.4
	E. Average durometer value vs cure time of selected NDT ablative samples			
22	12-hr cure	17.2	(275.5)	72.2
5b	16-hr cure (control)	16.7	(267.5)	66.8
23	20-hr cure	17.0	(272.5)	72.2
	F. Average durometer value vs vacuum for selected NDT ablative samples			
24	24 in. of Hg (81 kN/m^2) (control)	16.2	(259.5)	66.8
25	12 in. of Hg (40.5 kN/m^2	16.2	(259.5)	68.4
	G. Average durometer value vs moisture for selected NDT ablative sample			
24	Control	16.2	(259.5)	66.8
26	Moisture	17.0	(272.5)	69.4

TABLE 26.- SIEVE ANALYSIS OF IG101 GLASS MICROSPHERES

Mesh size	Percent by weight	Bulk density
+ 100	40.45	10.4
+ 150	9.43	10.6
+ 200	22.34	11.4
- 200	27.78	12.5

TABLE 27.- FORMULATION OF SS-41 AND SS-41F

Component	SS-41 parts by weight	SS-41F parts by weight
Resin, GE 655 part A	22.7	19.7
Curing agent, part B	2.3	2.0
Phenolic microspheres, BJO 0930	50.0	43.6
Glass microspheres, IG-101	15.0	13.0
Nylon powder, 66D	10.0	8.7
Fibers, E-glass-1/2 inch	---	13.0
	100.0	100.0

Note: SS-41 is packed into Honeycomb core for curing, while SS-41F is cured as a molding compound.

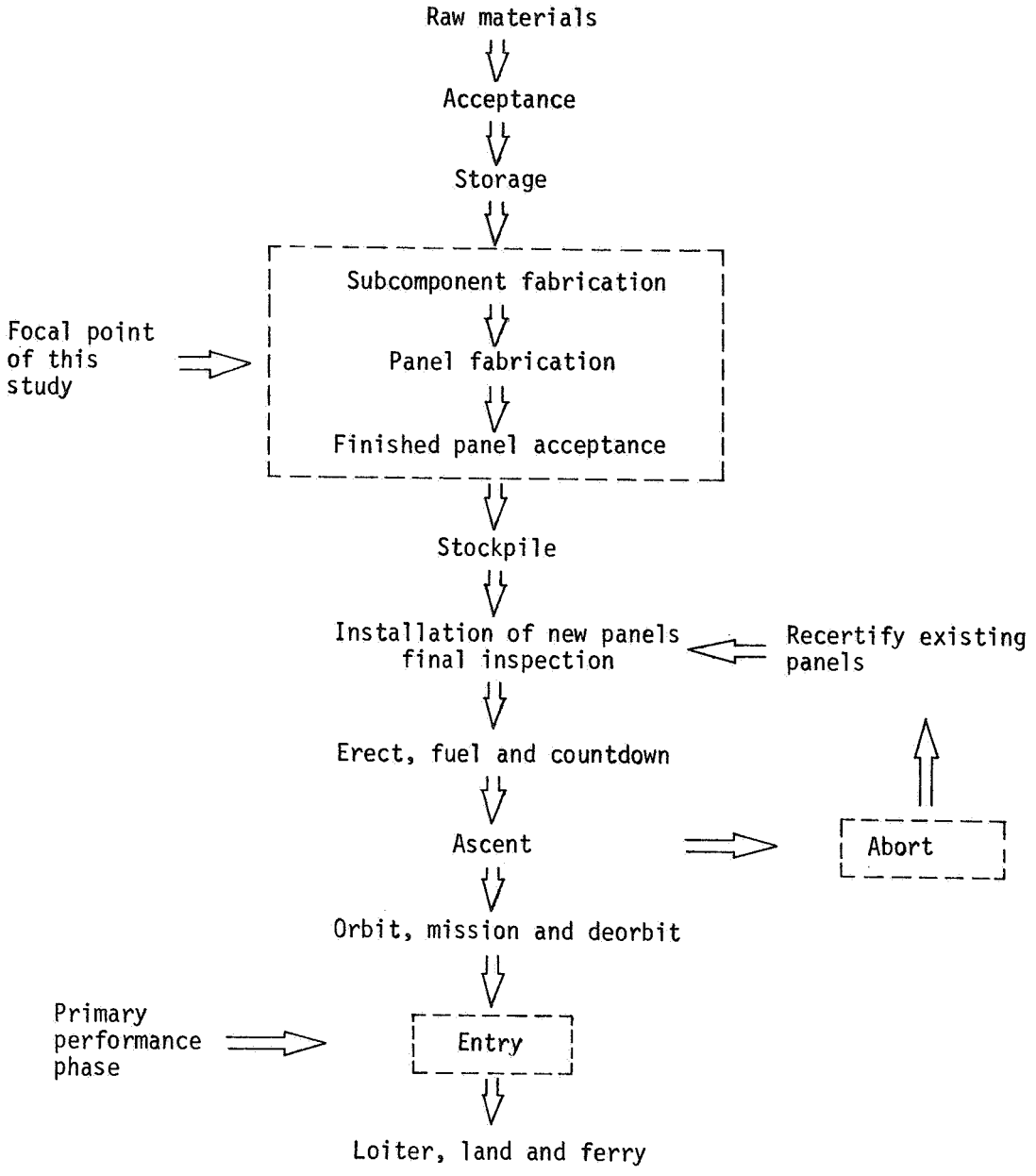

Figure 1.- Ablator Panel Life Sequence

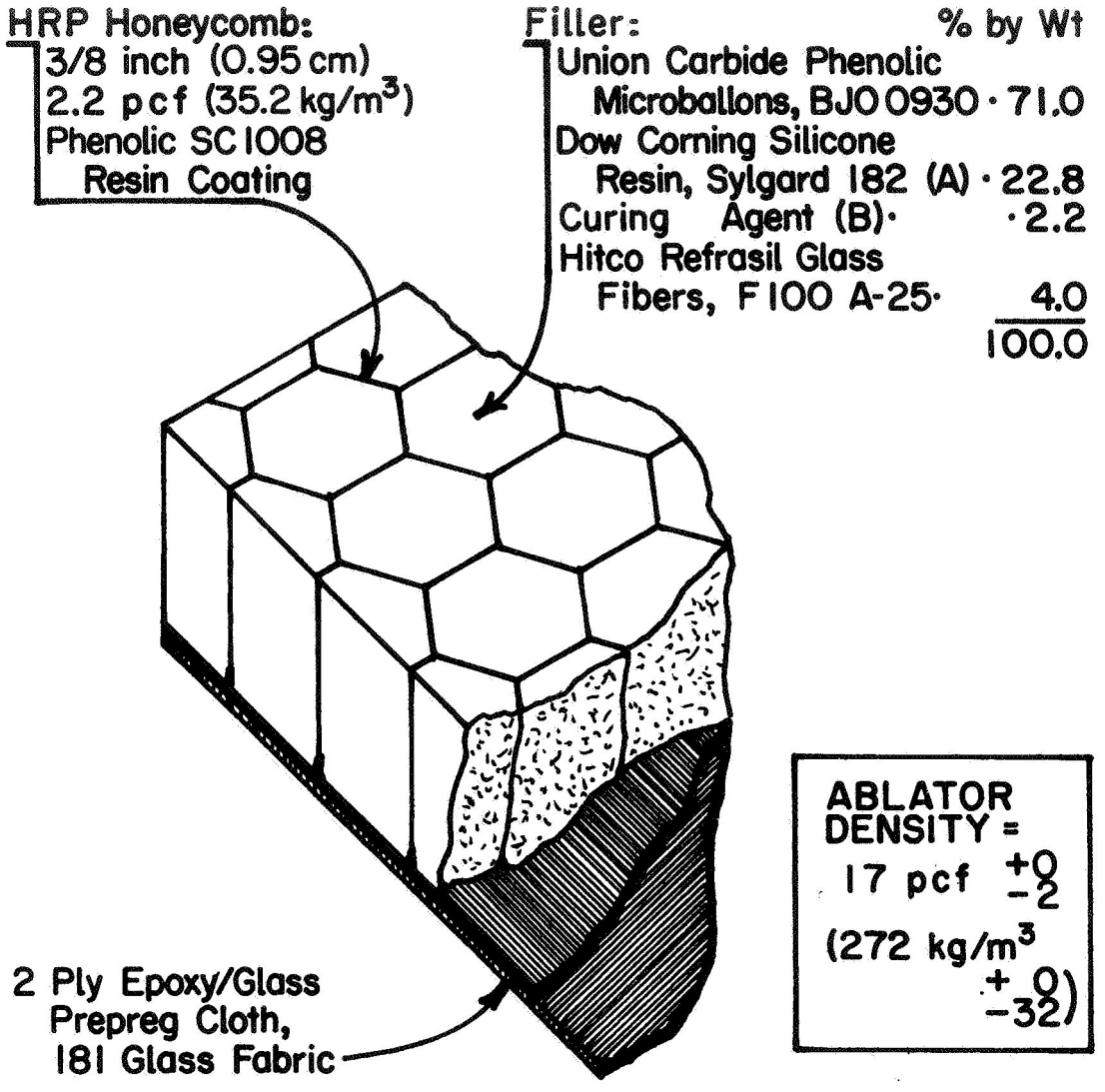

Figure 2.- Baseline Configuration for Study During Tasks I, II, and III, MG-36

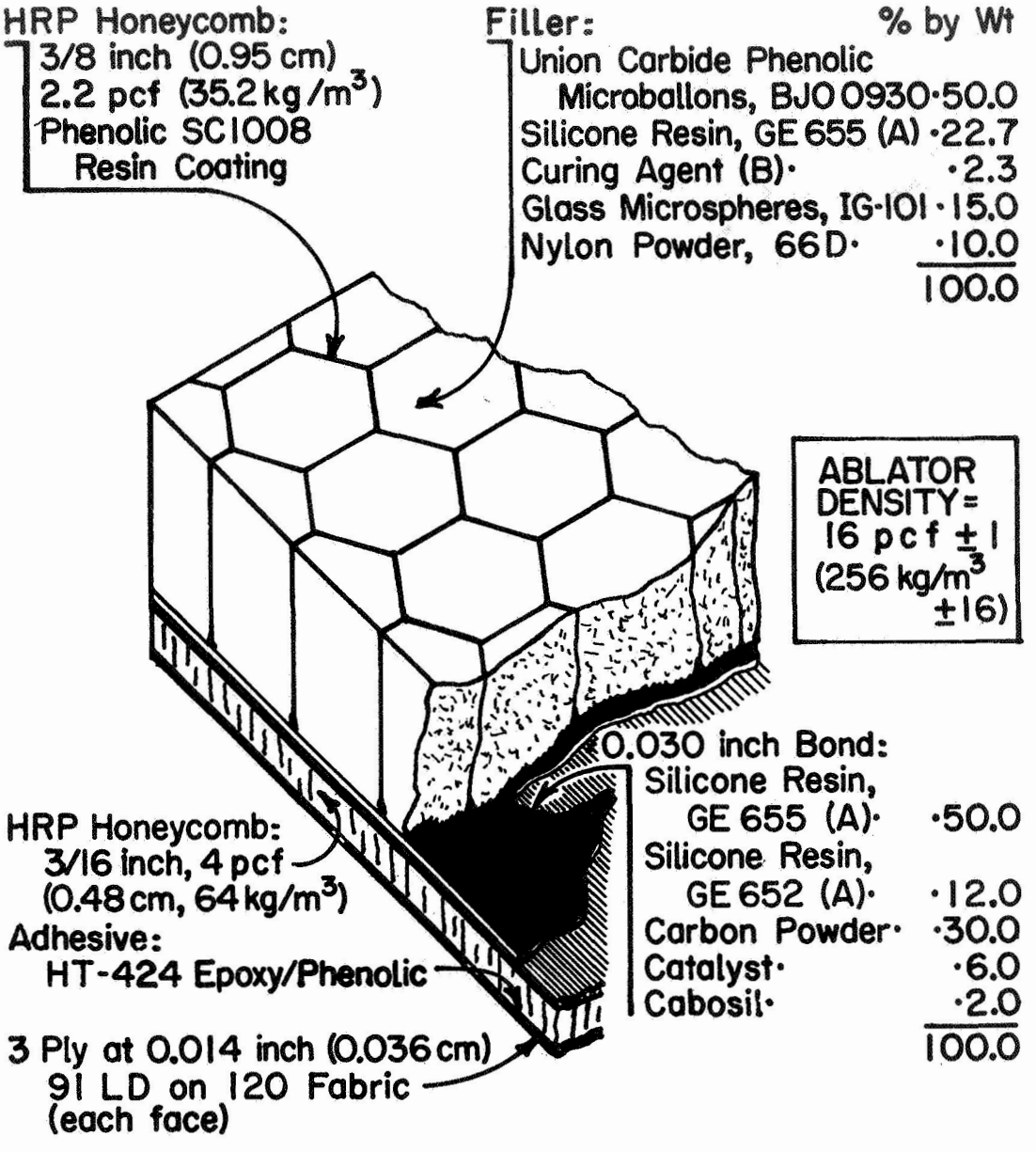

Figure 3.- Baseline Configuration for Study During Tasks IV and V, SS-41

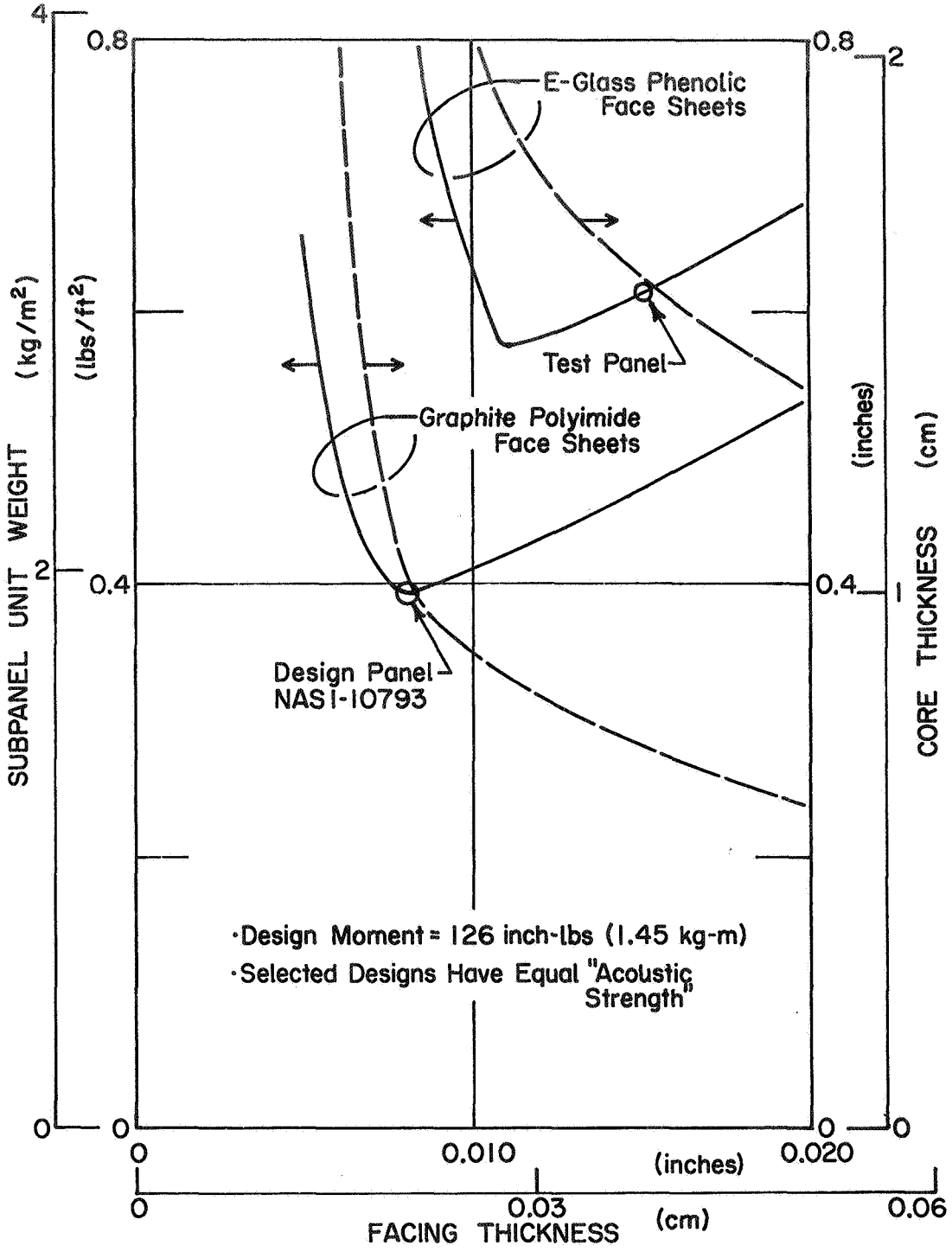

Figure 4.- Subpanel Design Curve

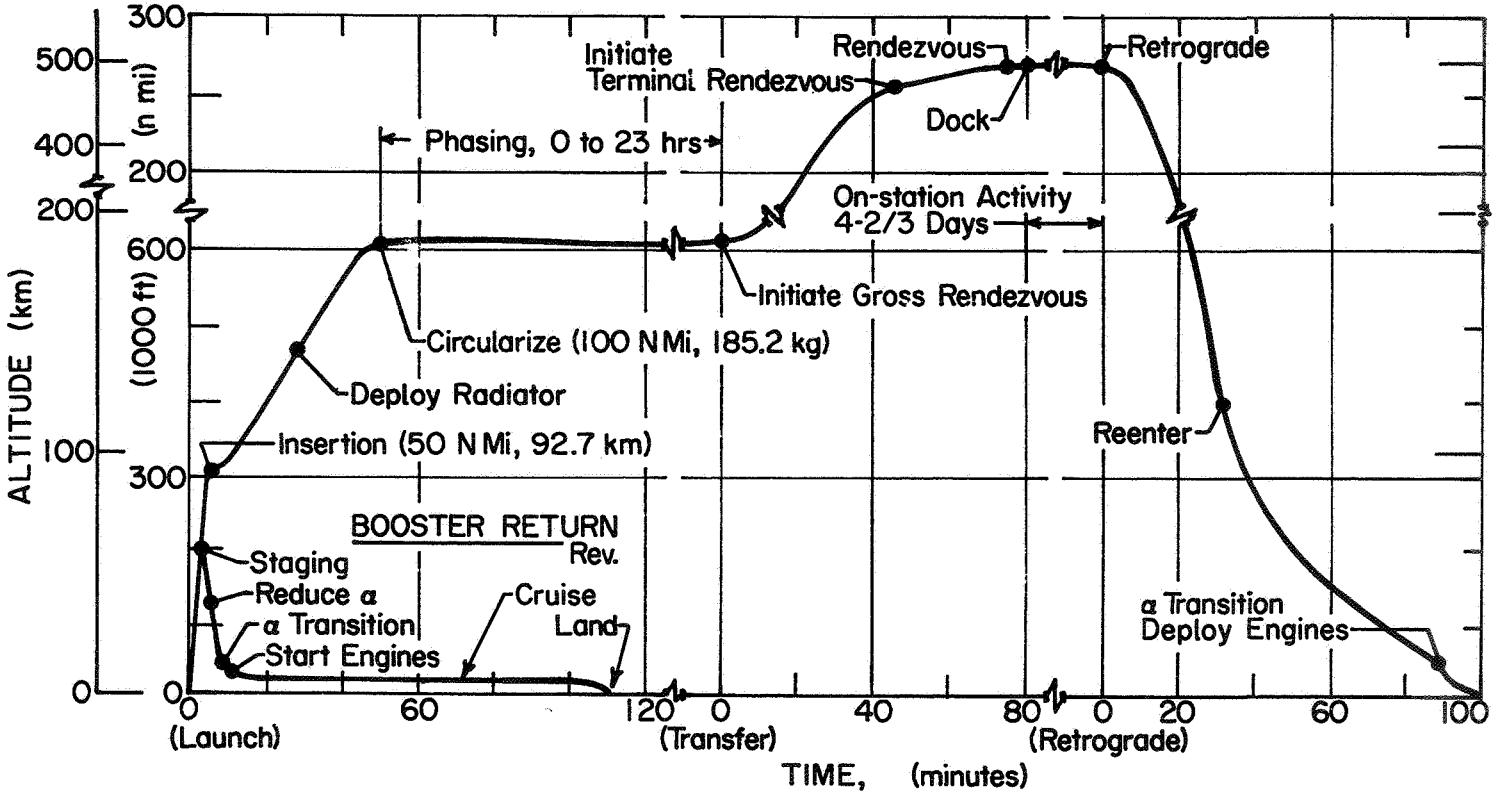

Figure 5.- Baseline Logistics Mission Profile, High Crossrange System

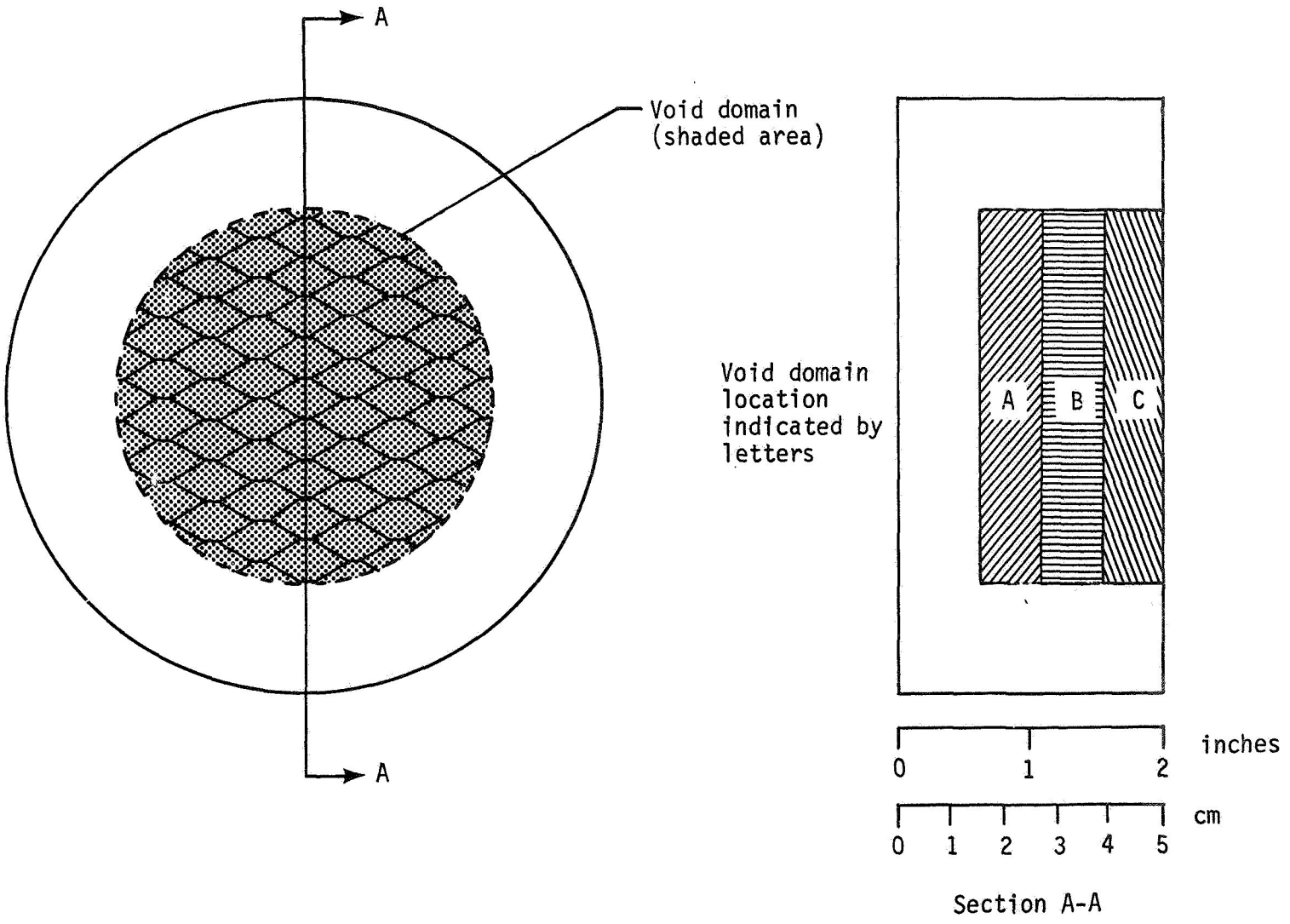

Figure 6.- Void Specimen Design

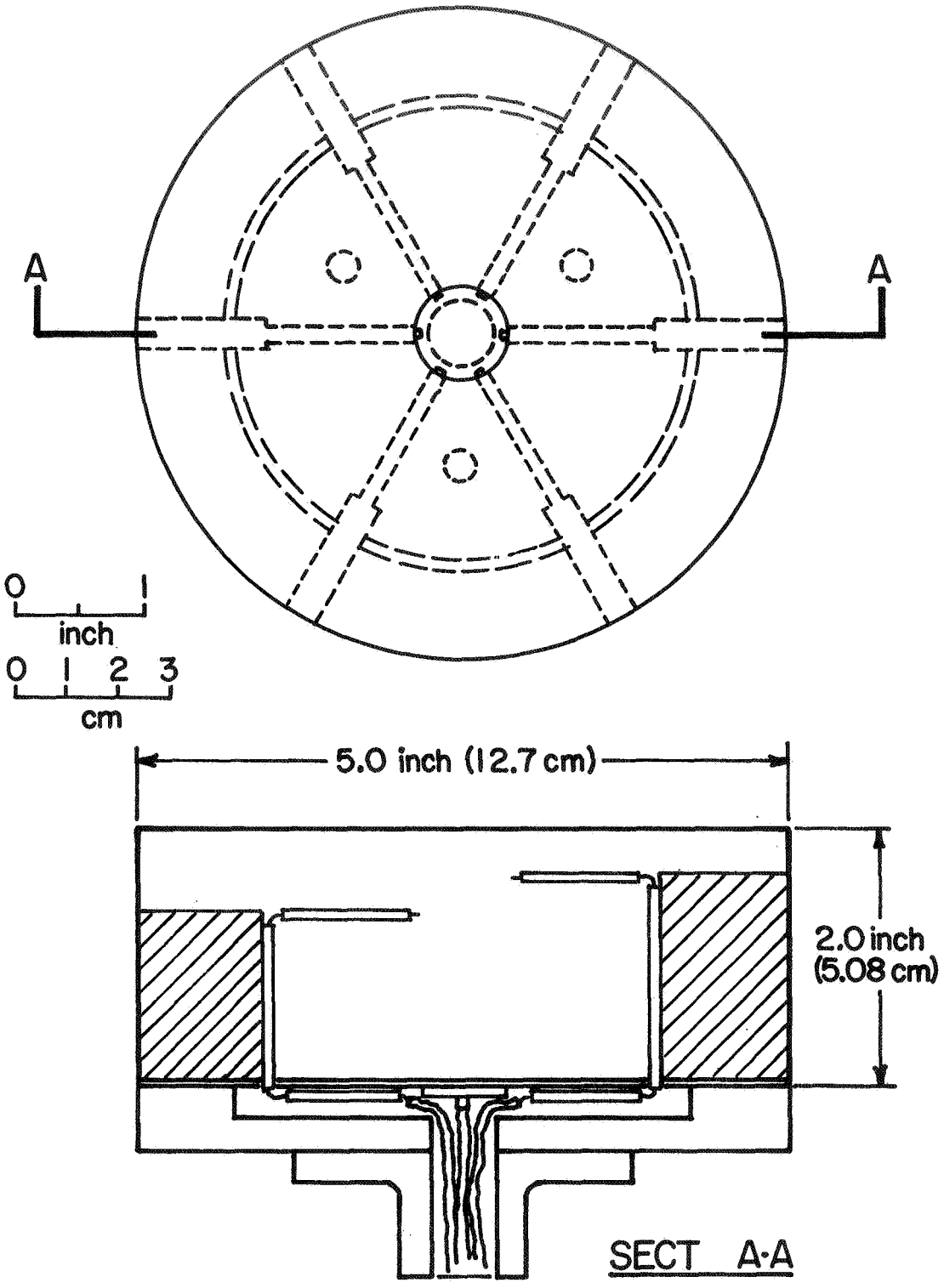

Figure 7.- Plasma Arc Test Specimen Design, Section A-A

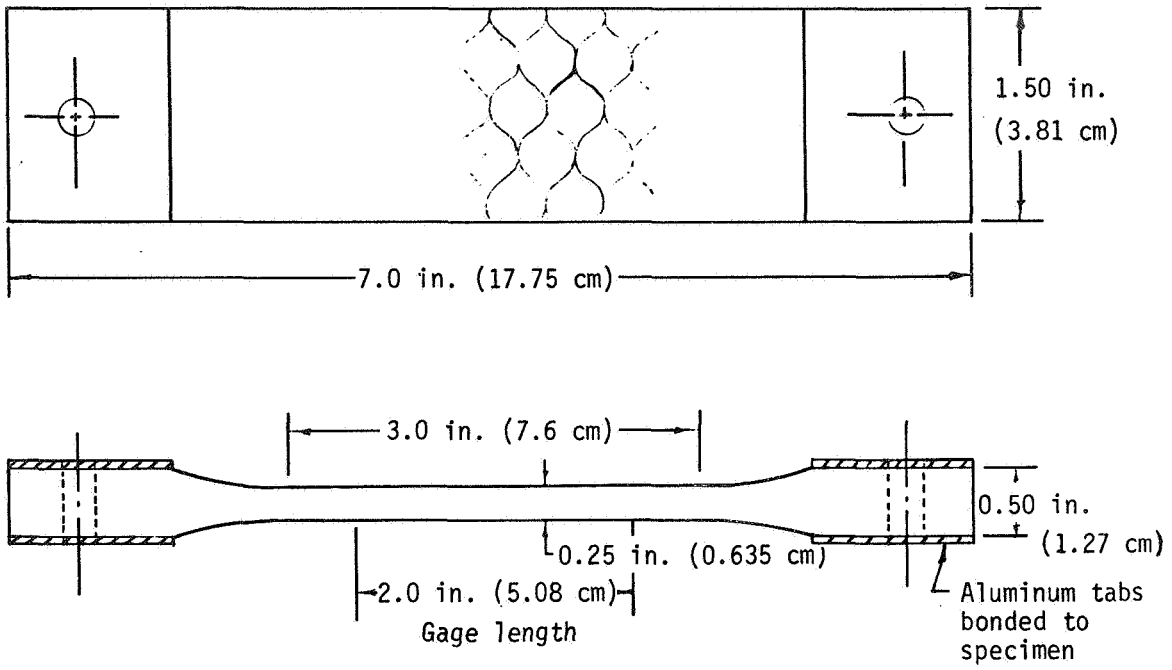

Figure 8.- Tensile Specimen, Ablator in Honeycomb

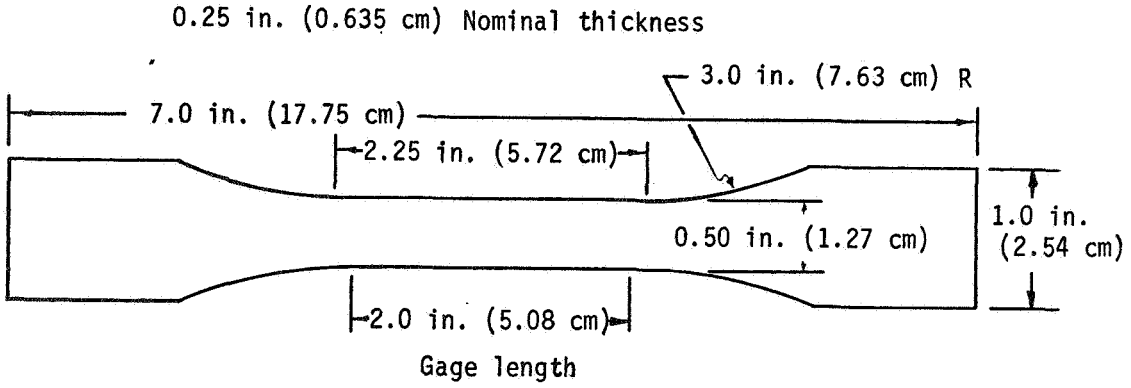

Fi Figure 9.- Tensile Specimen, Ablator

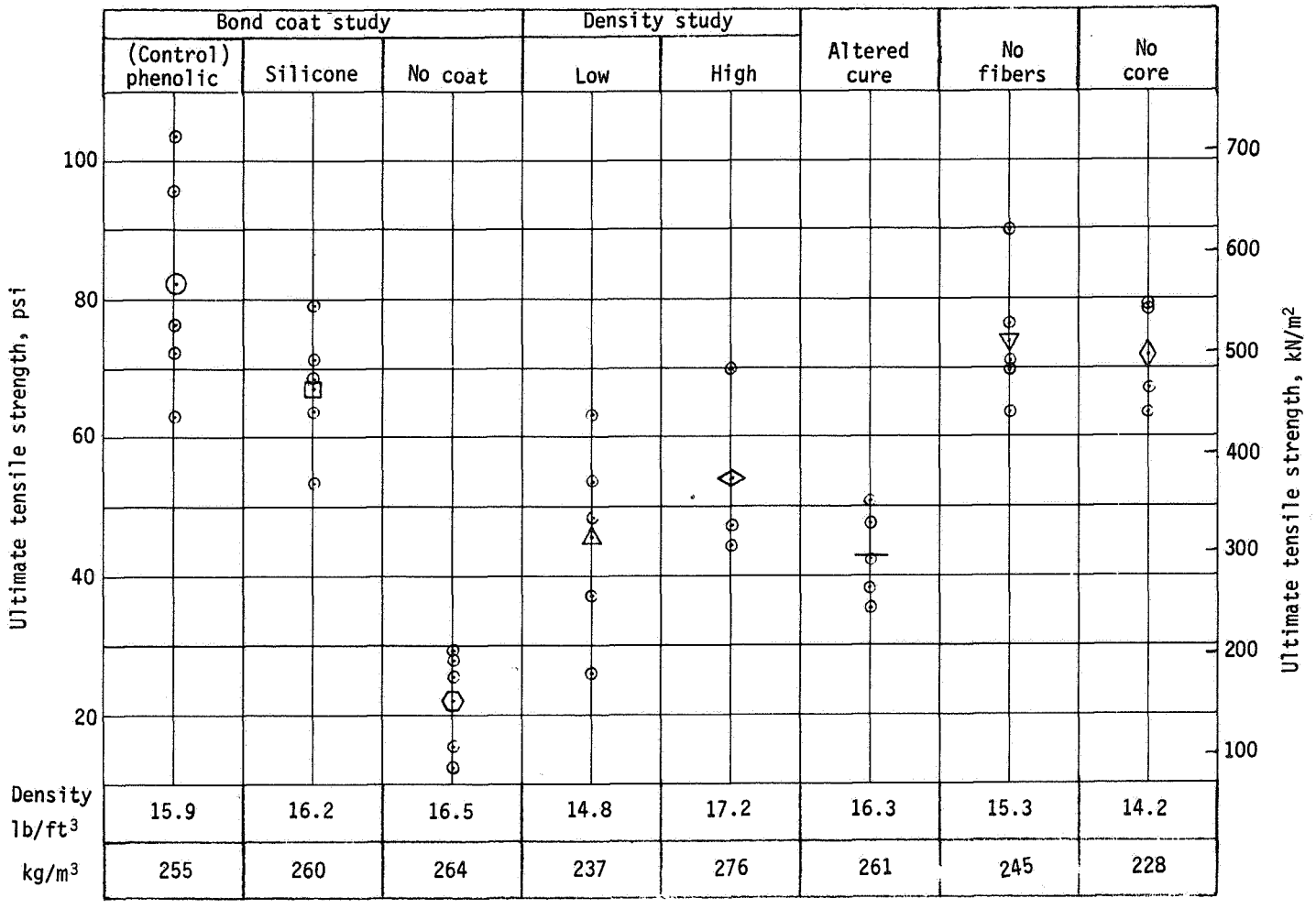

Figure 10.- Tensile Strength at Ambient Temperature

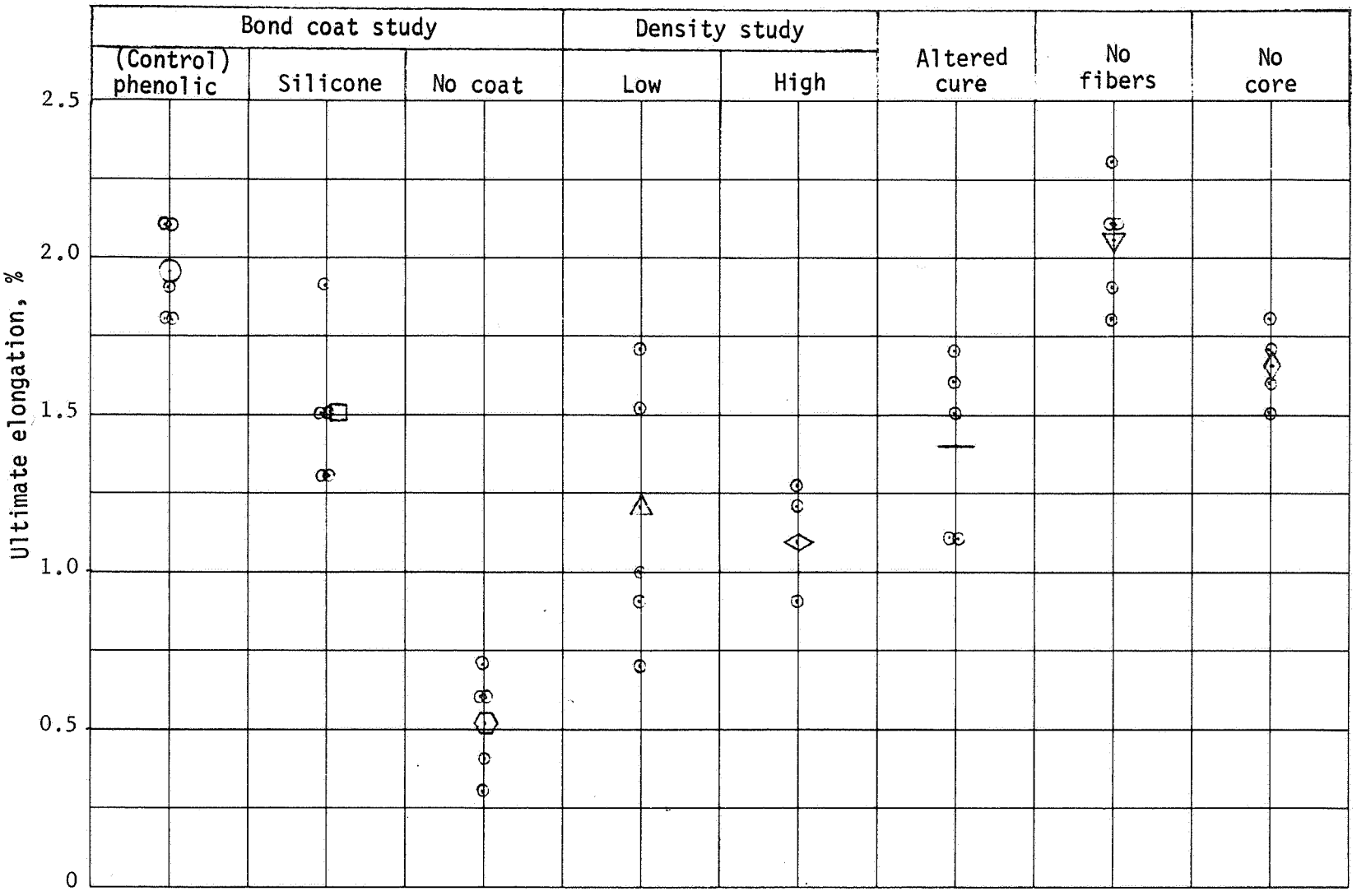

Figure 11.- Tensile Elongation at Ambient Temperature

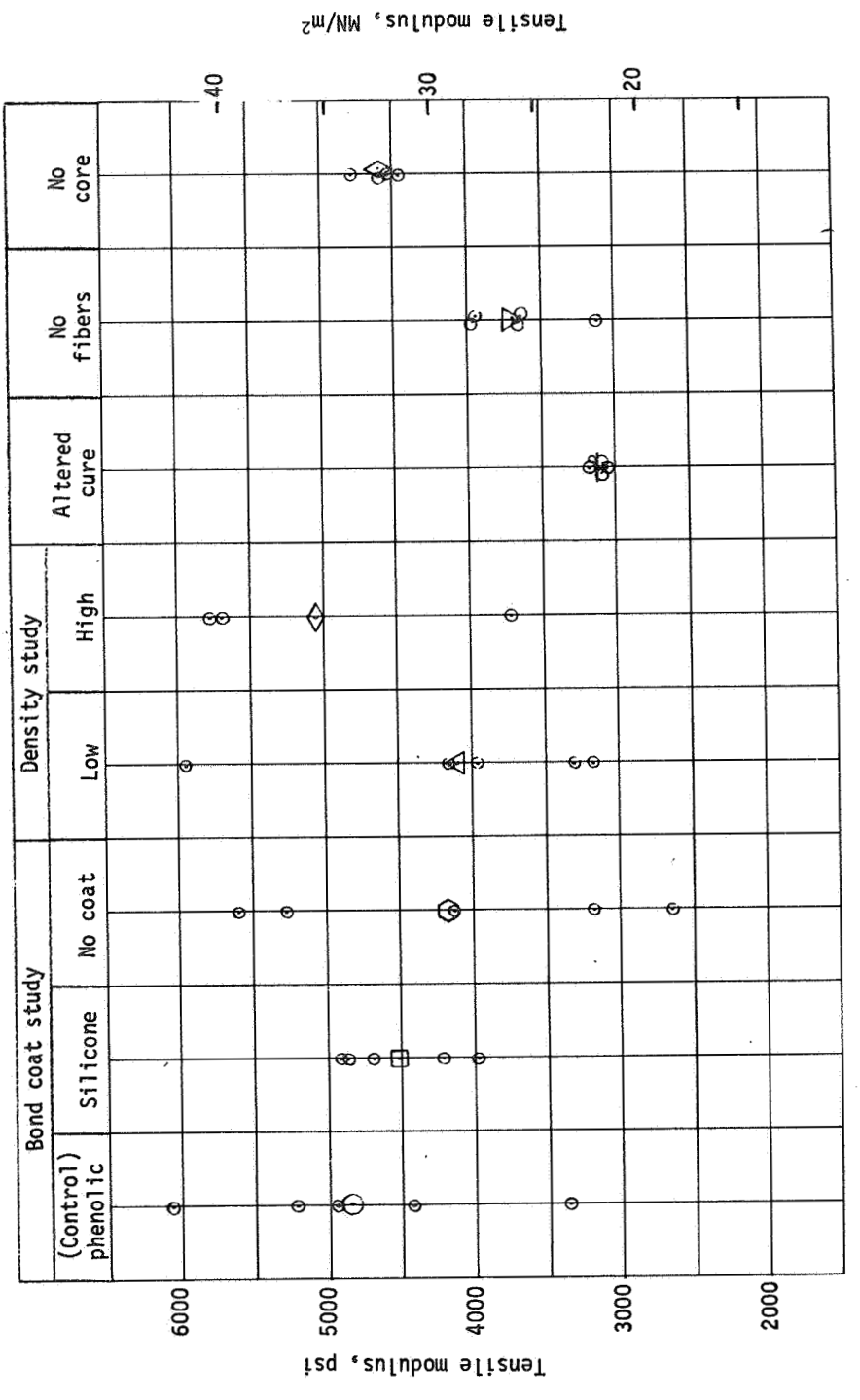

Figure 12.- Tensile Modulus at Ambient Temperature

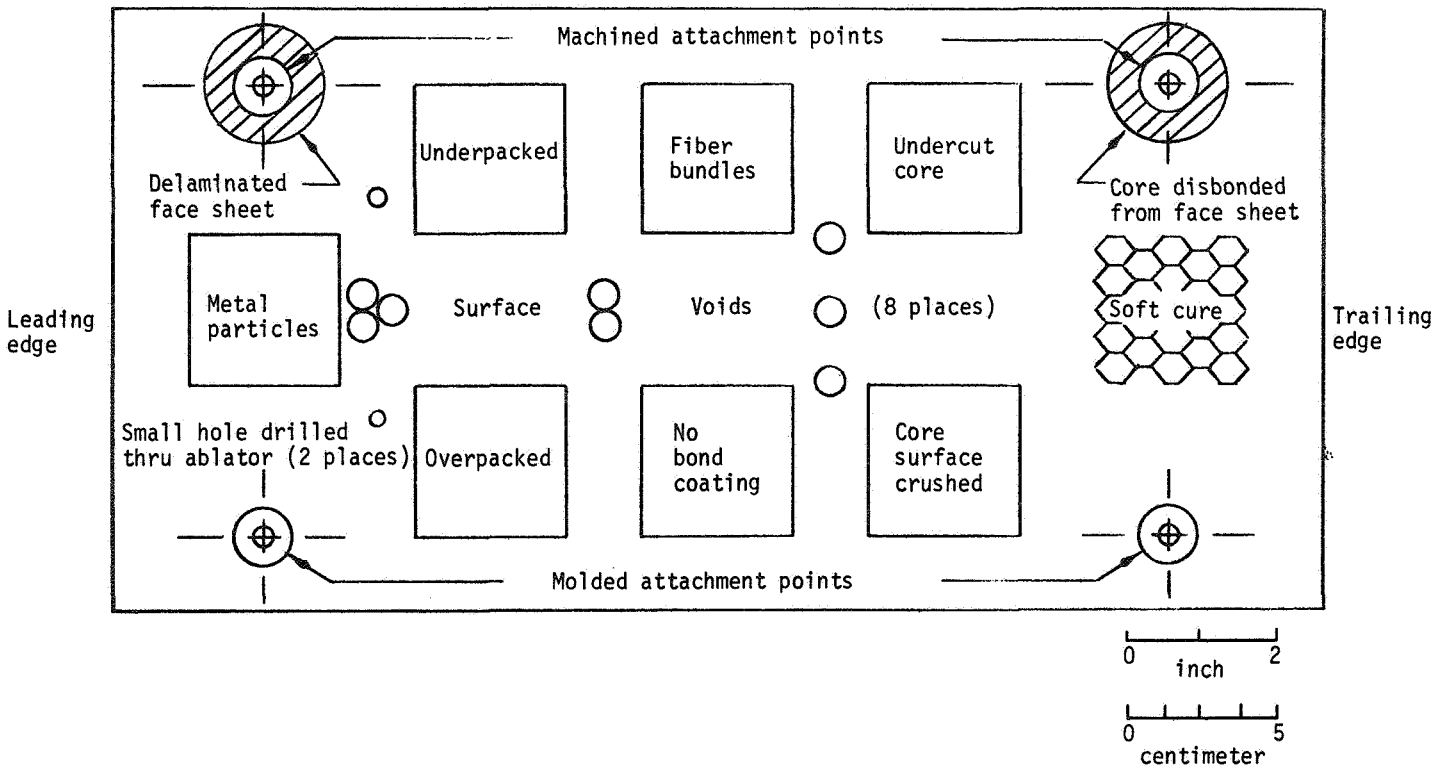

Figure 13.- Large Test Panel No. 2, Defect Locations

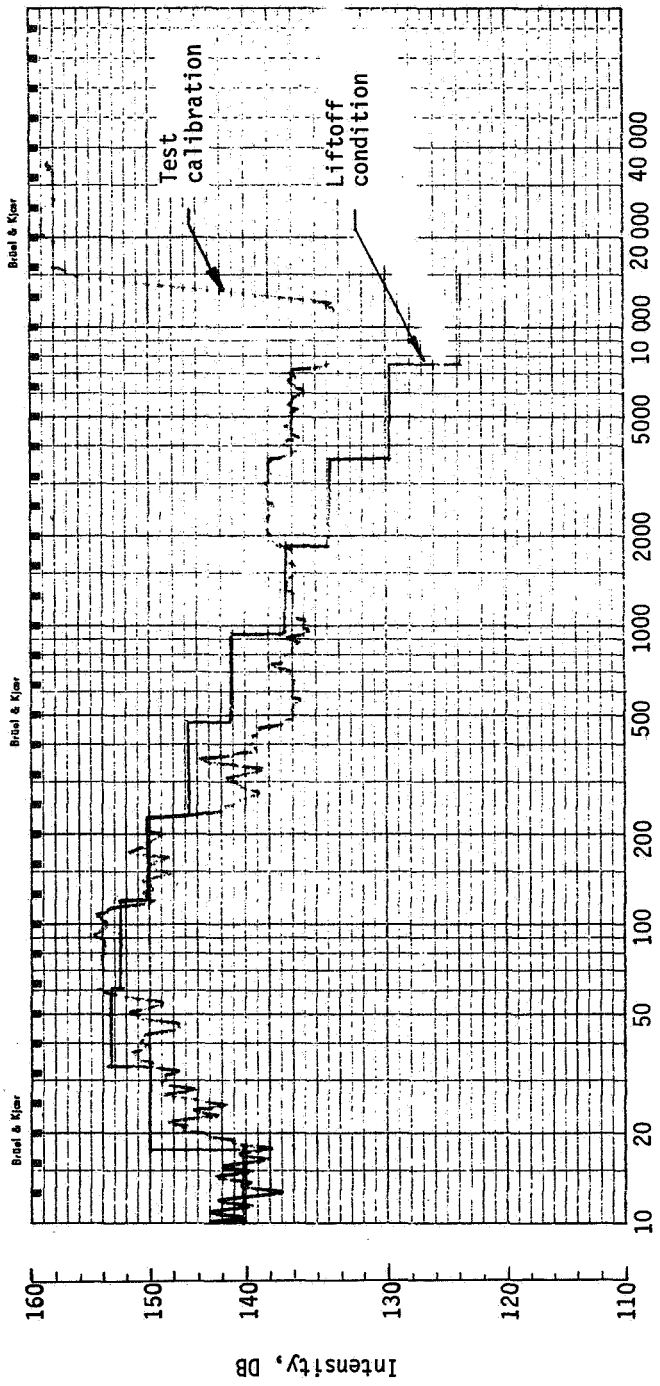

Figure 14.- Sound Spectrum Used in Acoustic Tests

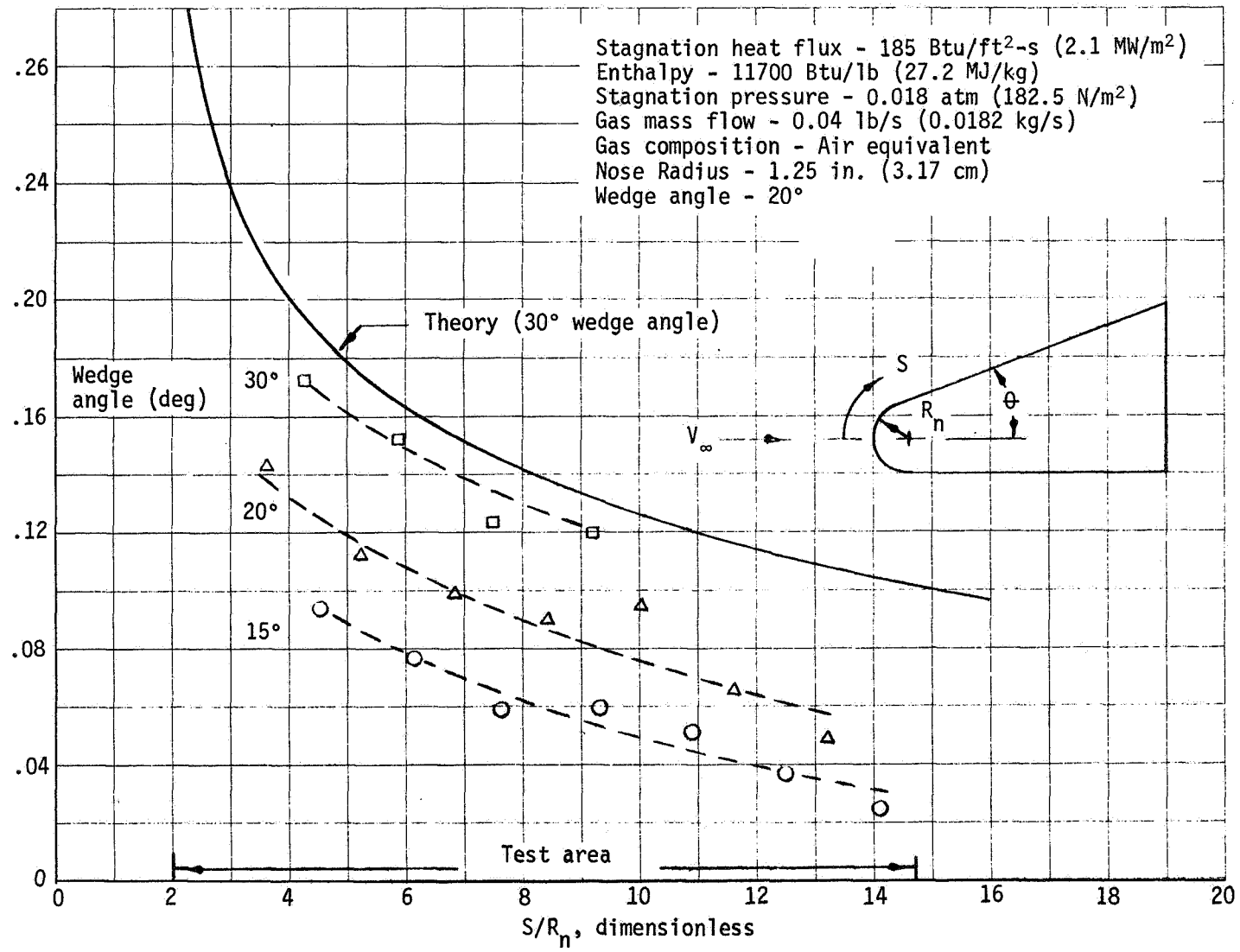

Figure 15.- Experimental Heating Distribution Over Cylinder-Wedge (Task III)

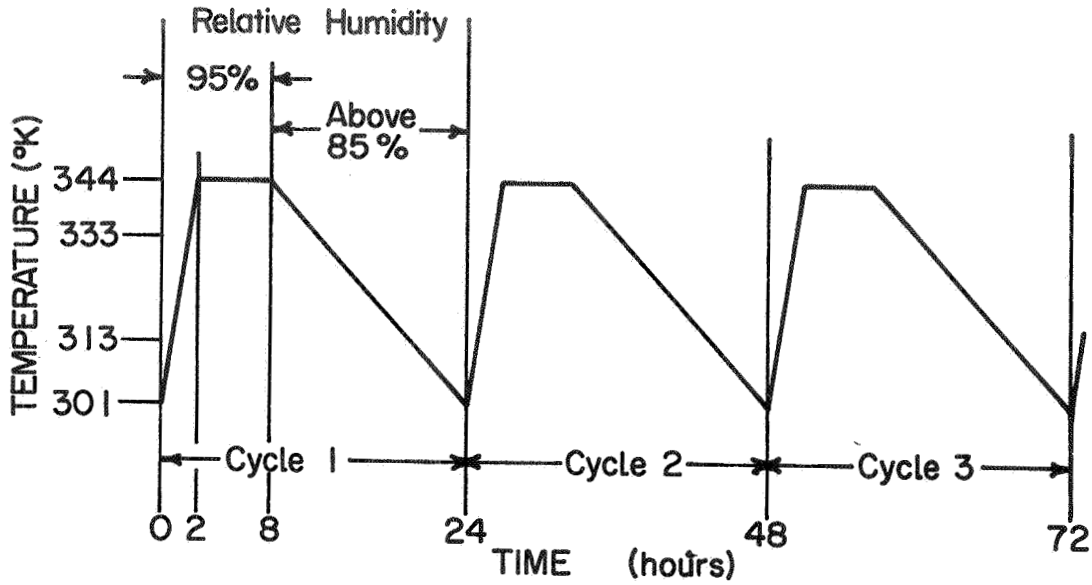

Figure 16.- Humidity Environment Number 1

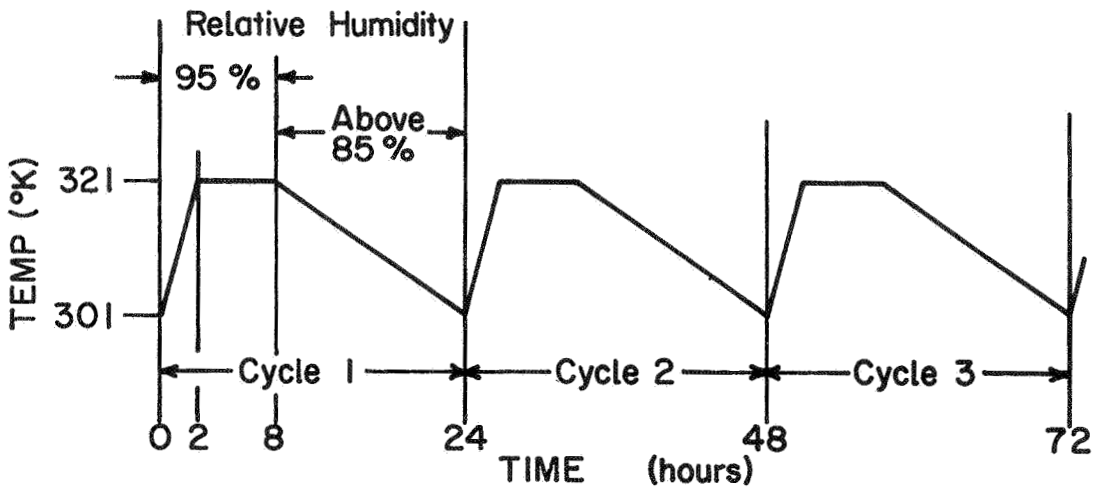

Figure 17.- Humidity Environment Number 2

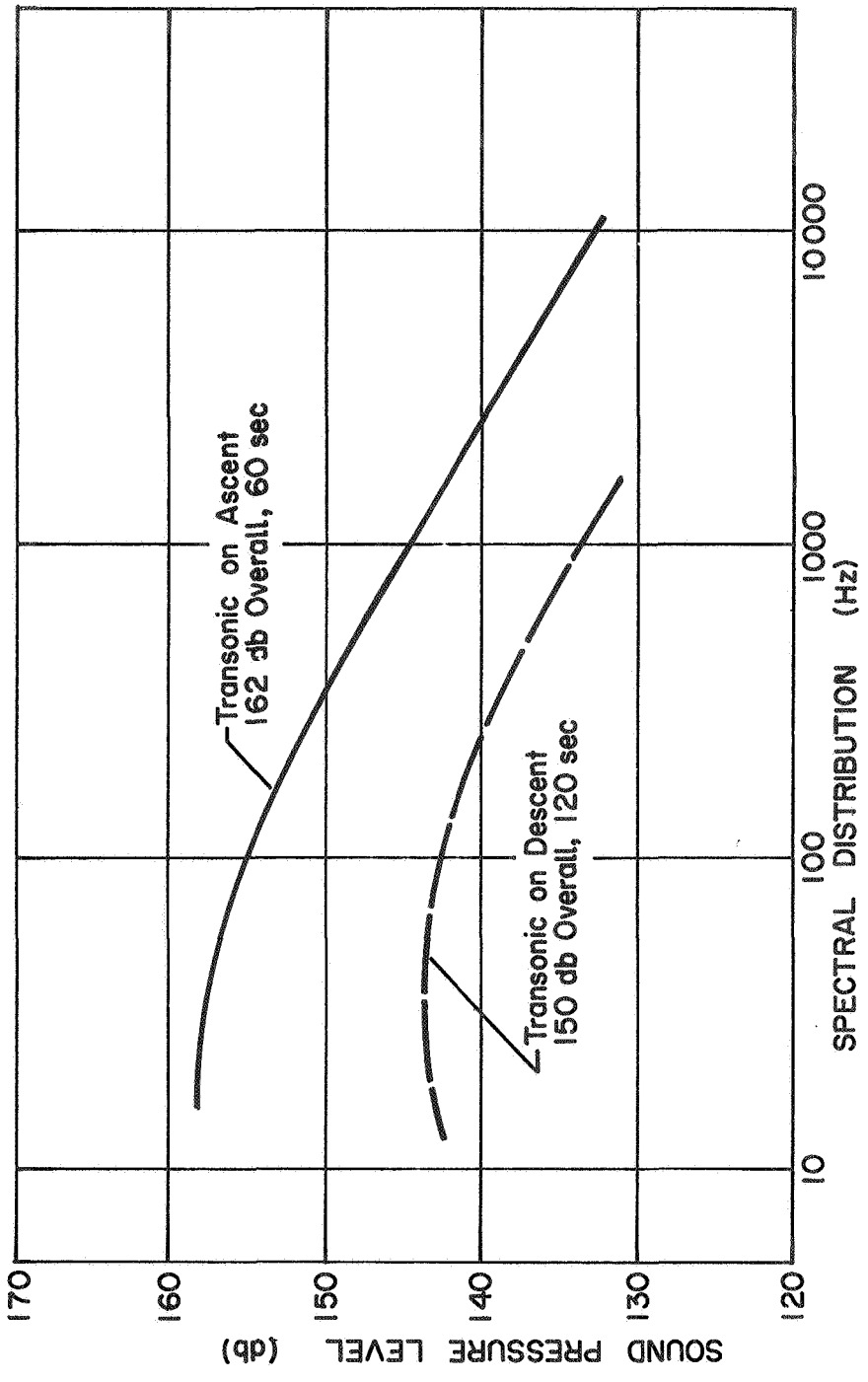

Figure 18.- Orbiter Forward Region Transonic Acoustic Environments

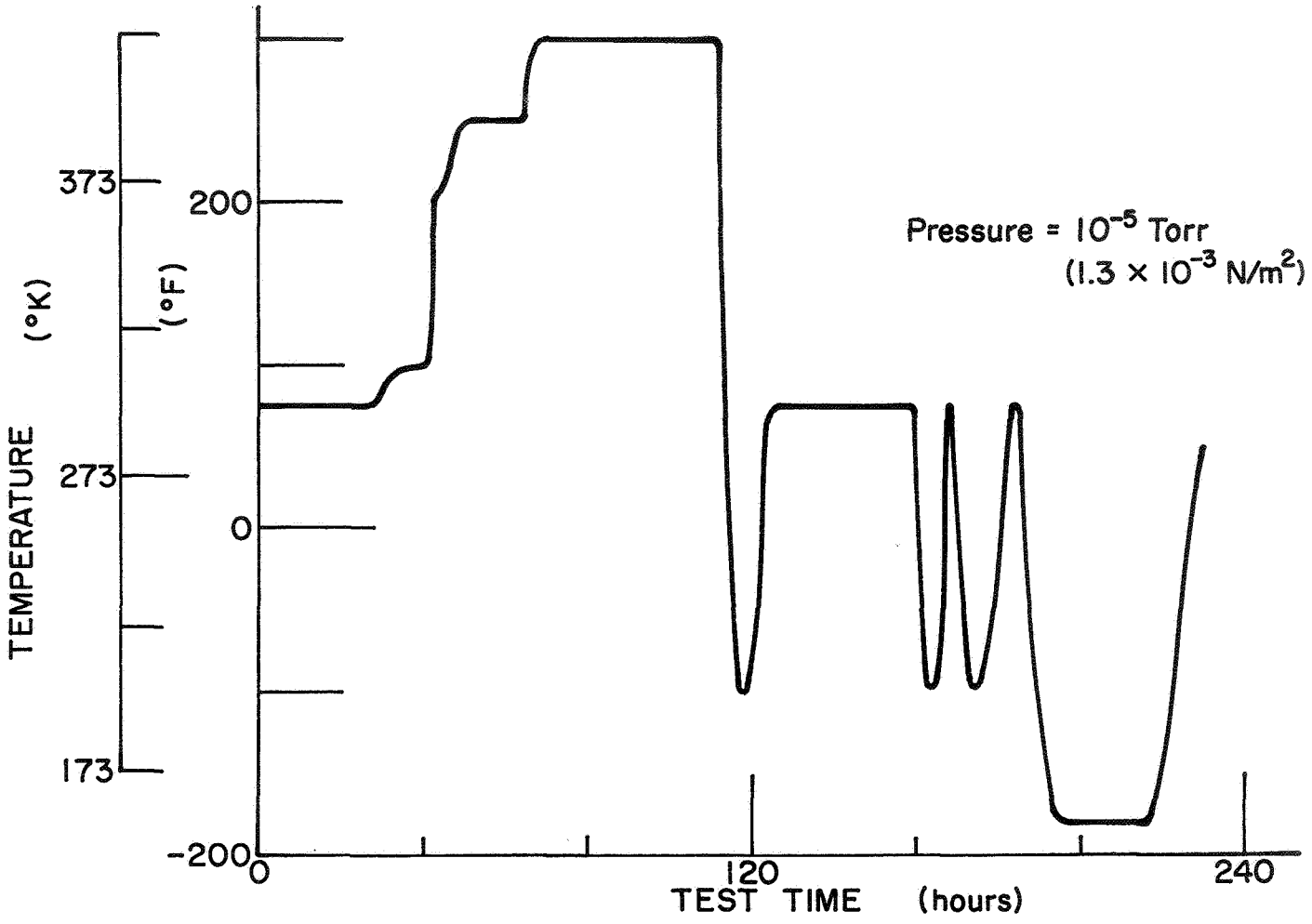

Figure 19.- Thermal Vacuum Exposure (Panels 4, 8, 11 and 12)

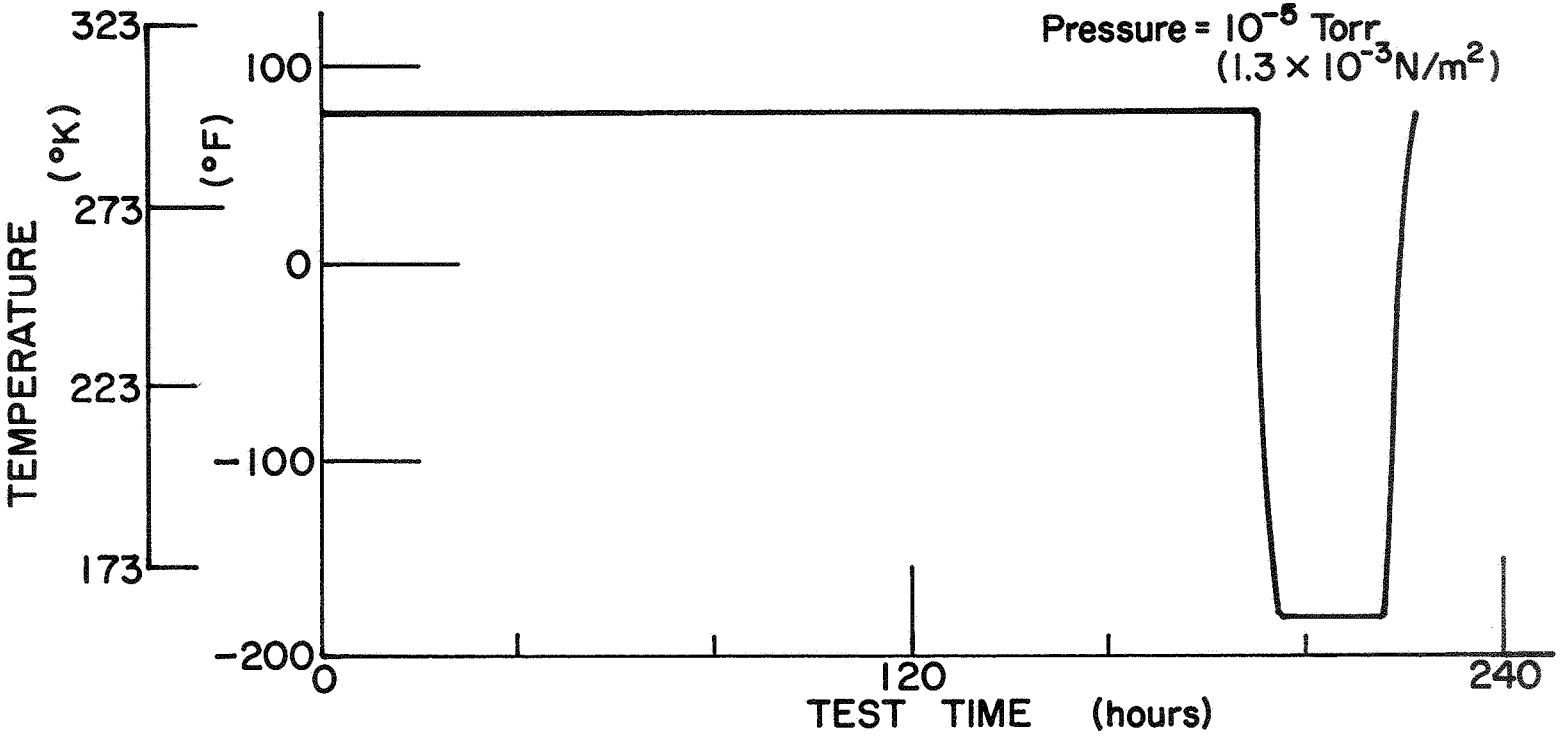

Figure 20.- Thermal Vacuum Exposure (Panels 9, 10, 14 and 16)

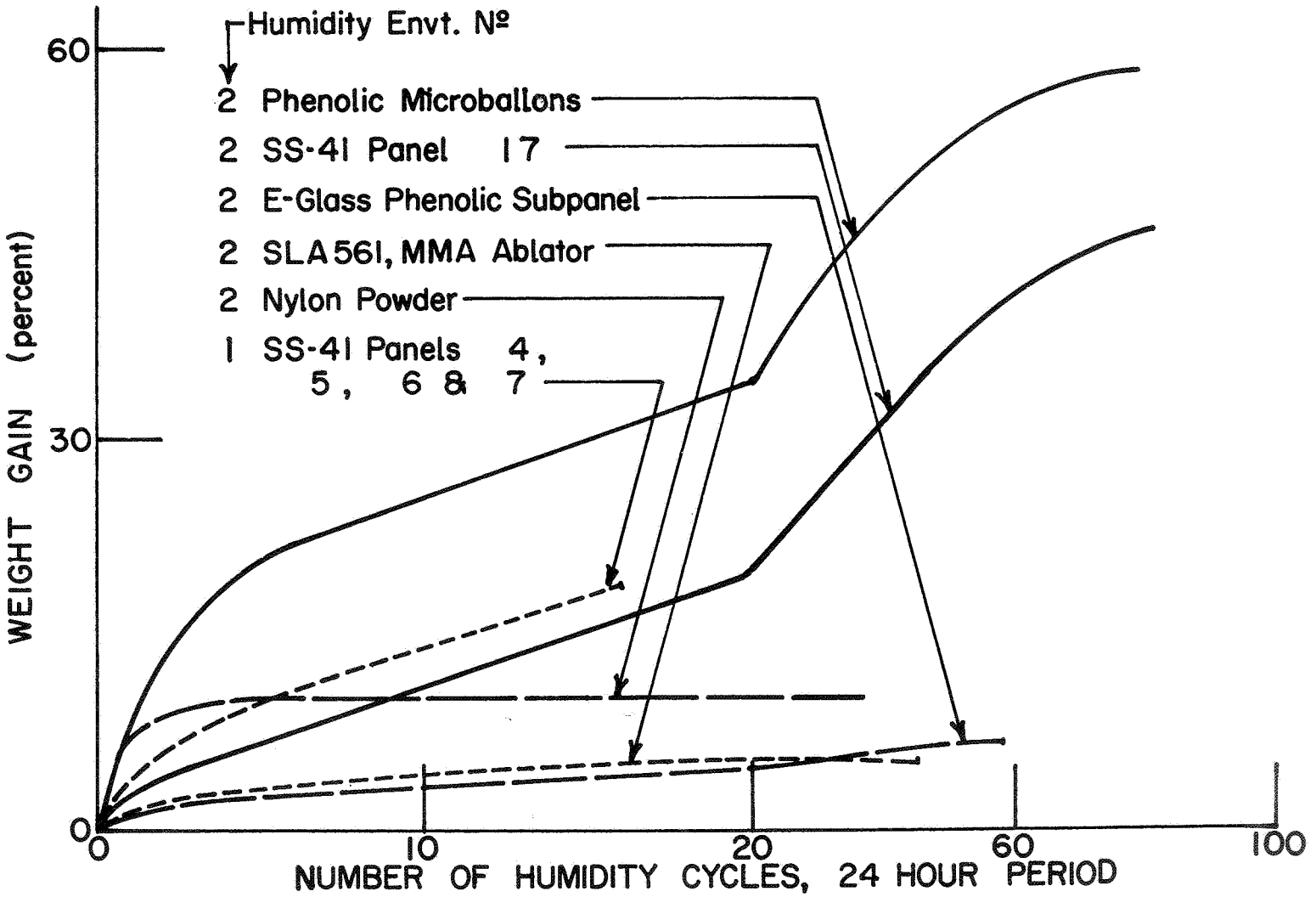

Figure 21.- Weight Gain in a High Humidity Cyclic Environment

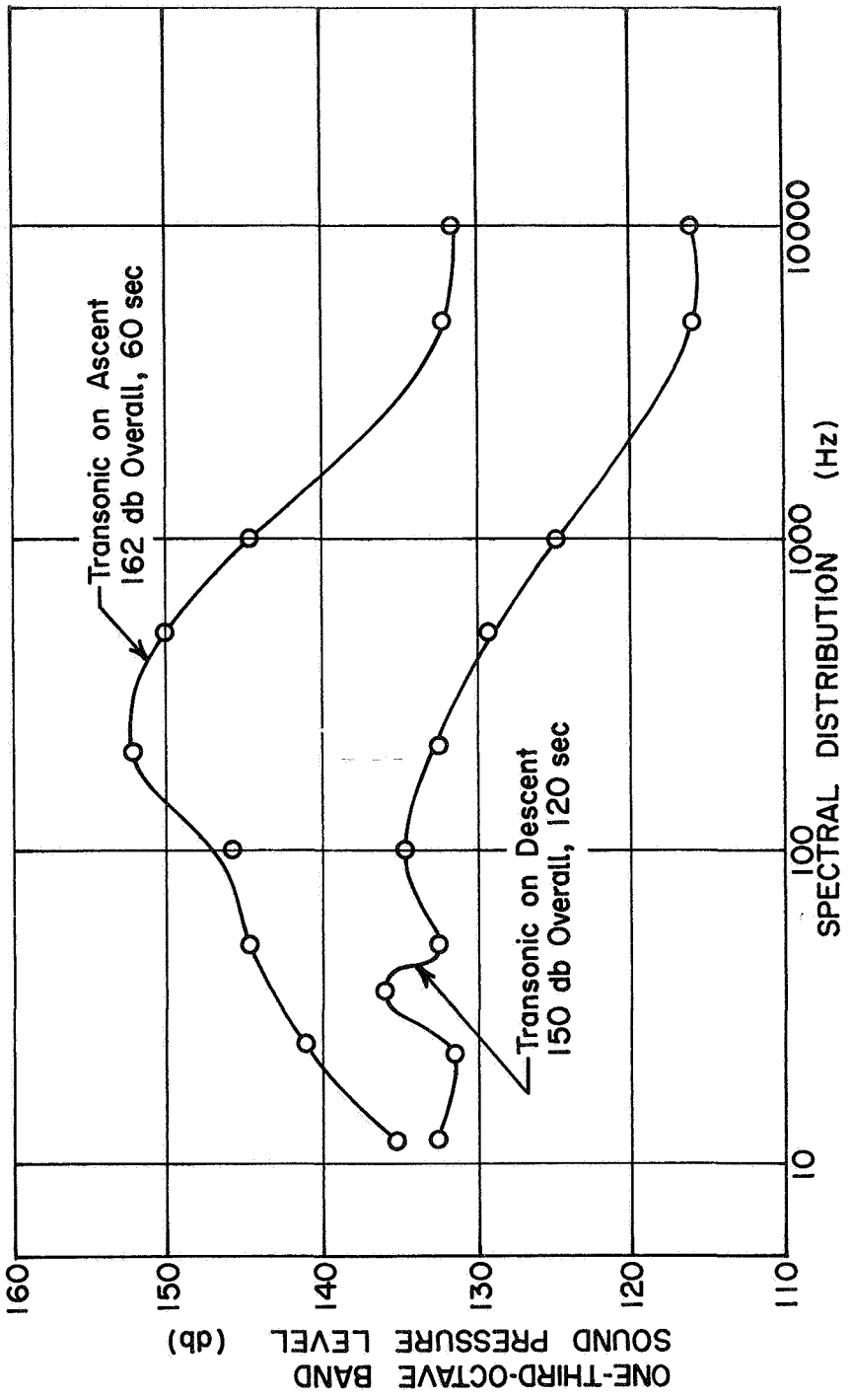

Figure 22.- Measured Transonic Acoustic Spectral Distributions

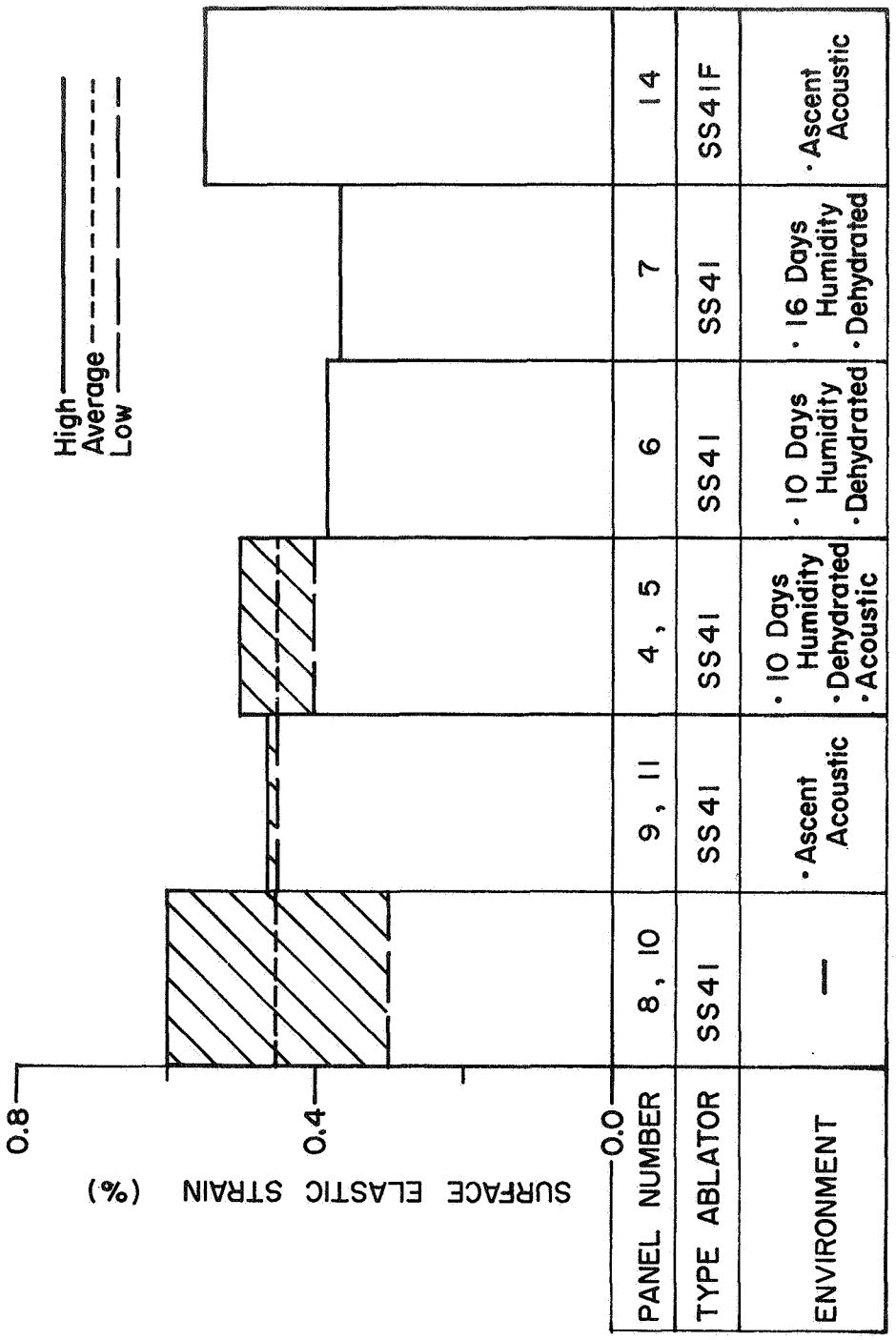

Figure 23.- Biaxial Loading, Surface Elastic Strain at Room Temperature

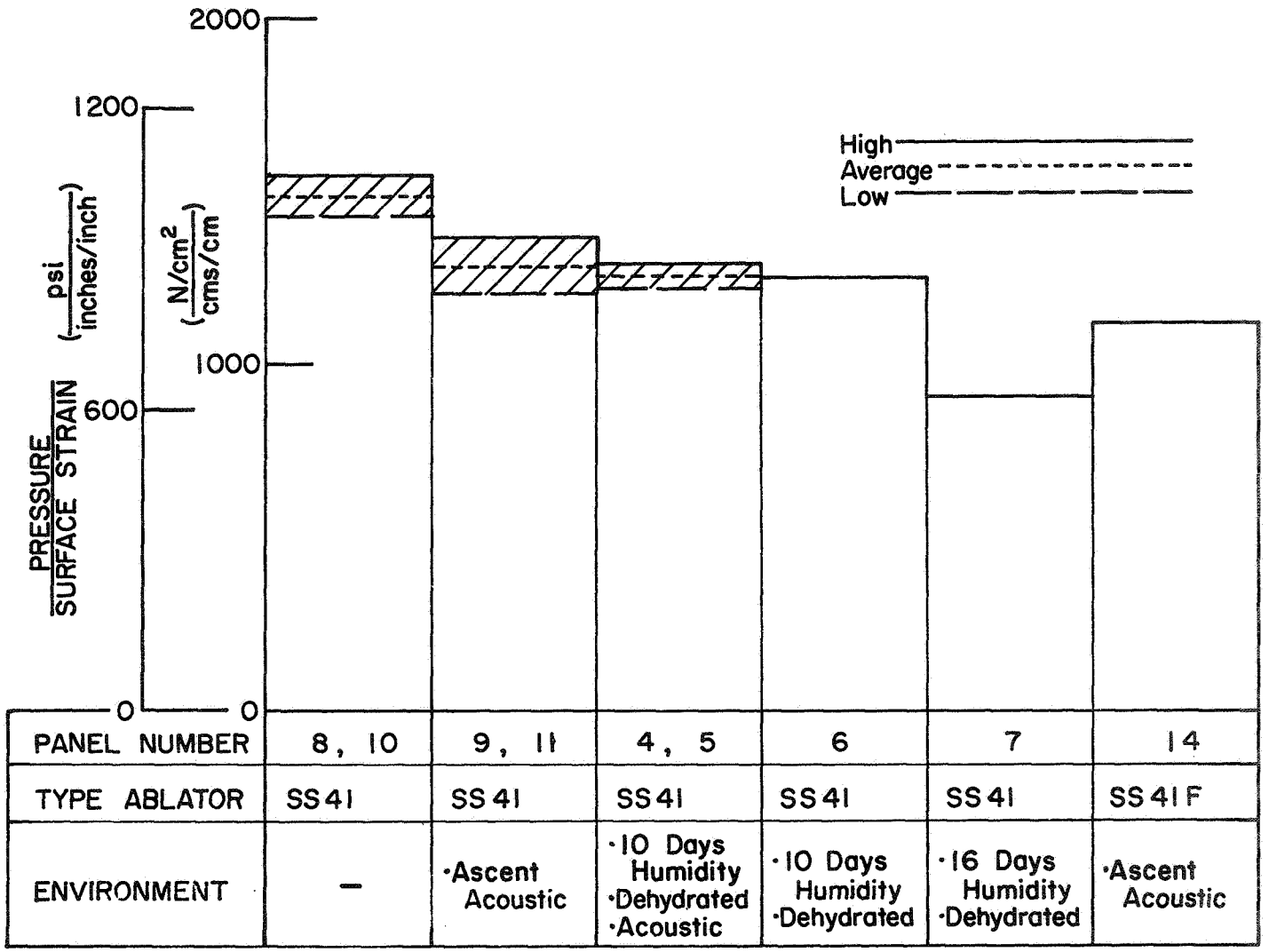

PANEL NUMBER	8, 10	9, 11	4, 5	6	7	14
TYPE ABLATOR	SS41	SS41	SS41	SS41	SS41	SS41F
ENVIRONMENT	–	•Ascent Acoustic	•10 Days Humidity •Dehydrated •Acoustic	•10 Days Humidity •Dehydrated	•16 Days Humidity •Dehydrated	•Ascent Acoustic

Figure 24.- Biaxial Loading, Panel Stiffness at Room Temperature

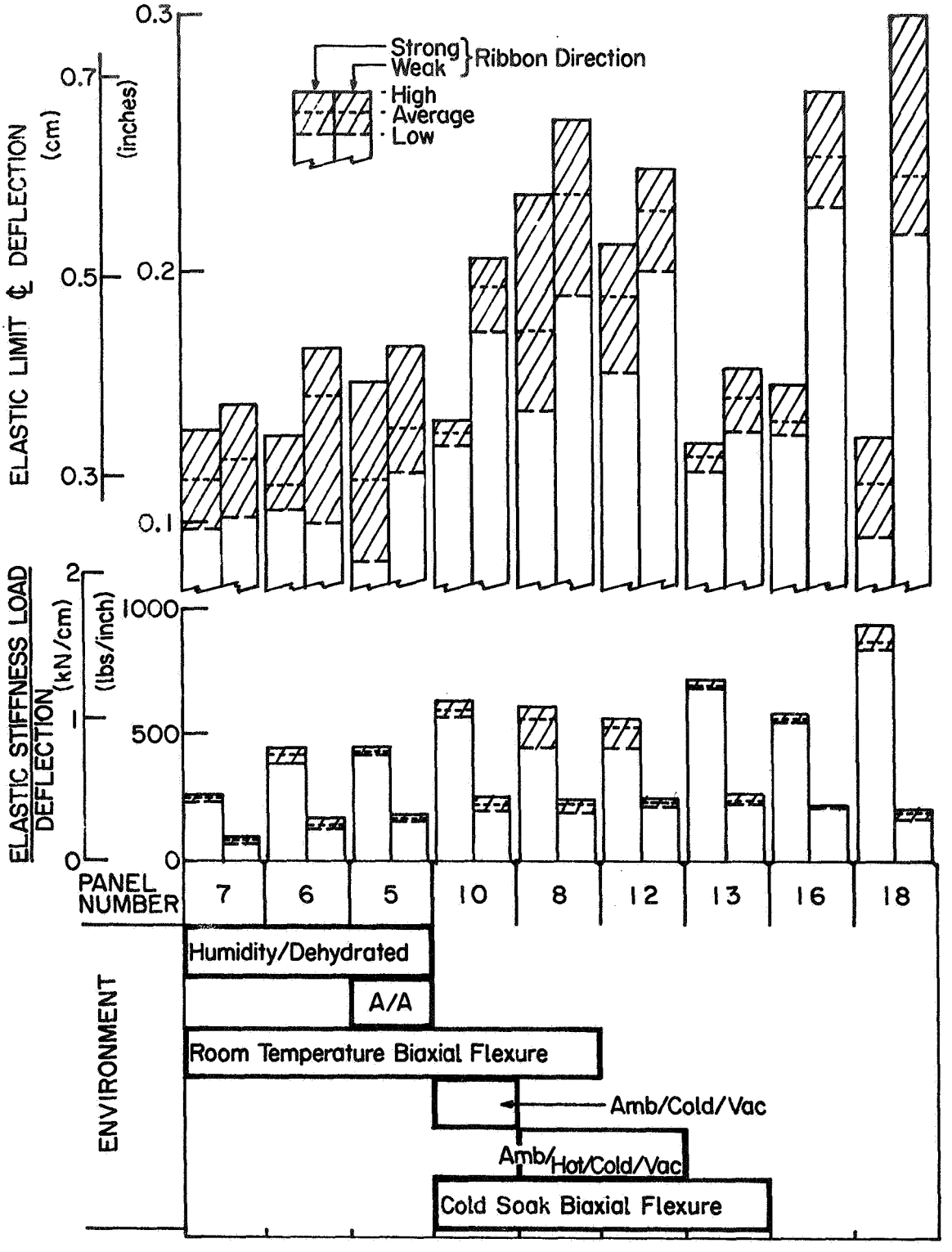

Figure 25.- Early Four-Point Flexure Results on SS-41

Defect = entire panel	Basic (perfect) condition	Variance	Notes	Panel no.
None			Panels 19, 20, 31, 32, 43, 44 and 45	
Undercure	@ 250°F (394°K)	@ 150°F (339°K)		21
Overcure		@ 350°F (450°K)		22
Low density	16 pcf ± 1 (256 kg/m^3±1.6)	15 pcf ±0.1(240 kg/m^3±1.6)		23
High density		17 pcf ±0.1(272 kg/m^3±1.6)		24
Filler Moisture	0%	5% in microballons	Weigh out moisturized microballons as if normal	25
		10% in microballons		26
Undermix	45 min	15 min		27
Undermix		30 min		28
H/C bond (B-stage wet coat)	45 min @ 150°F (339°K)	90 min @ 150°F (339°K)	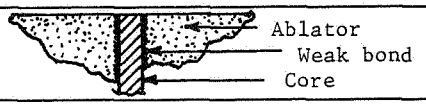	29
H/C bond (B-stage wet coat)		45 min @ 250°F (304°K)		30
Ablator discontinuity	None	d = 0.25 in. (0.64 cm)		33
Ablator discontinuity		d = 0.50 in. (1.27 cm)		34
Undercut core	None	d = 0.10 in. (0.25 cm)		35
Undercut core		d = 0.20 in. (0.51 cm)		36
Disbonds to subpanel	None	d = 1.0 in. (2.5 cm)	See Fig. 27 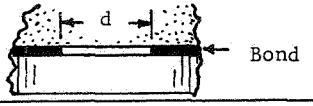	37
Disbonds to subpanel		d = 1.5 in. (3.8 cm)		38
Broken node bonds	None	Center of panel	See Fig. 27	39
Broken node bonds		Edge of panel		40
Broken ribbons	None	Center of panel	See Fig. 27	41
Broken ribbons		Edge of panel		42

Figure 26 - Defects Description (Task IV)

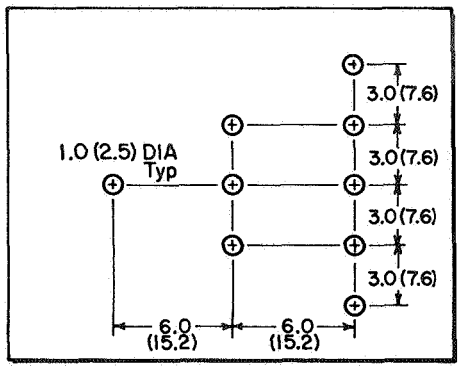

PANEL 37

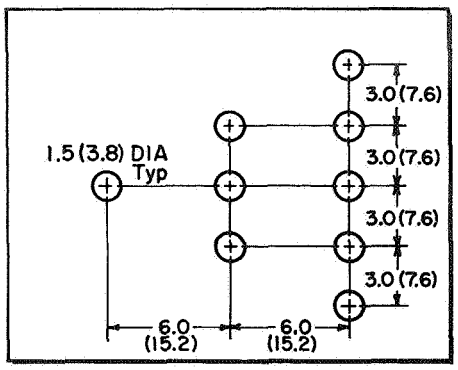

PANEL 38

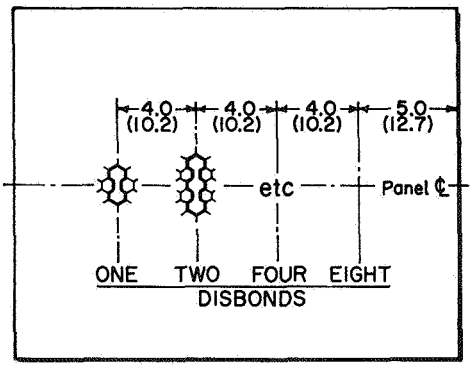

PANEL 39

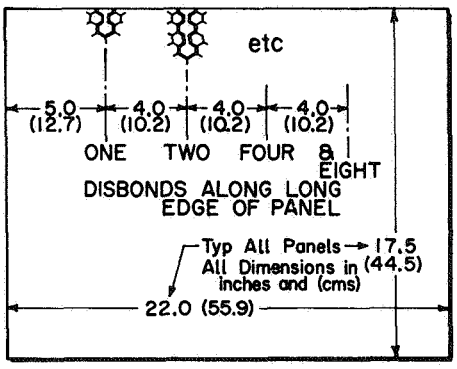

PANEL 40

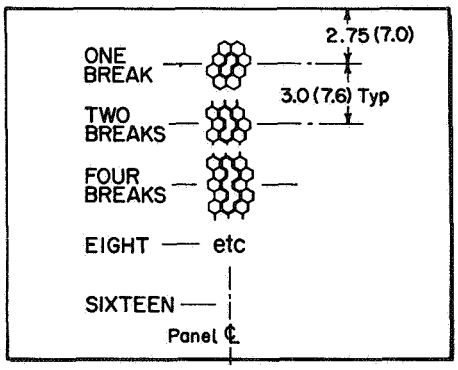

PANEL 41

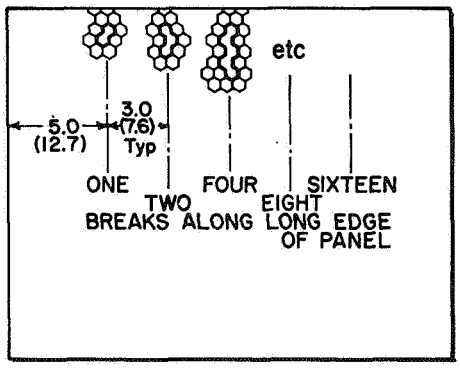

PANEL 42

Figure 27.- Details of Disbond and Damaged Honeycomb

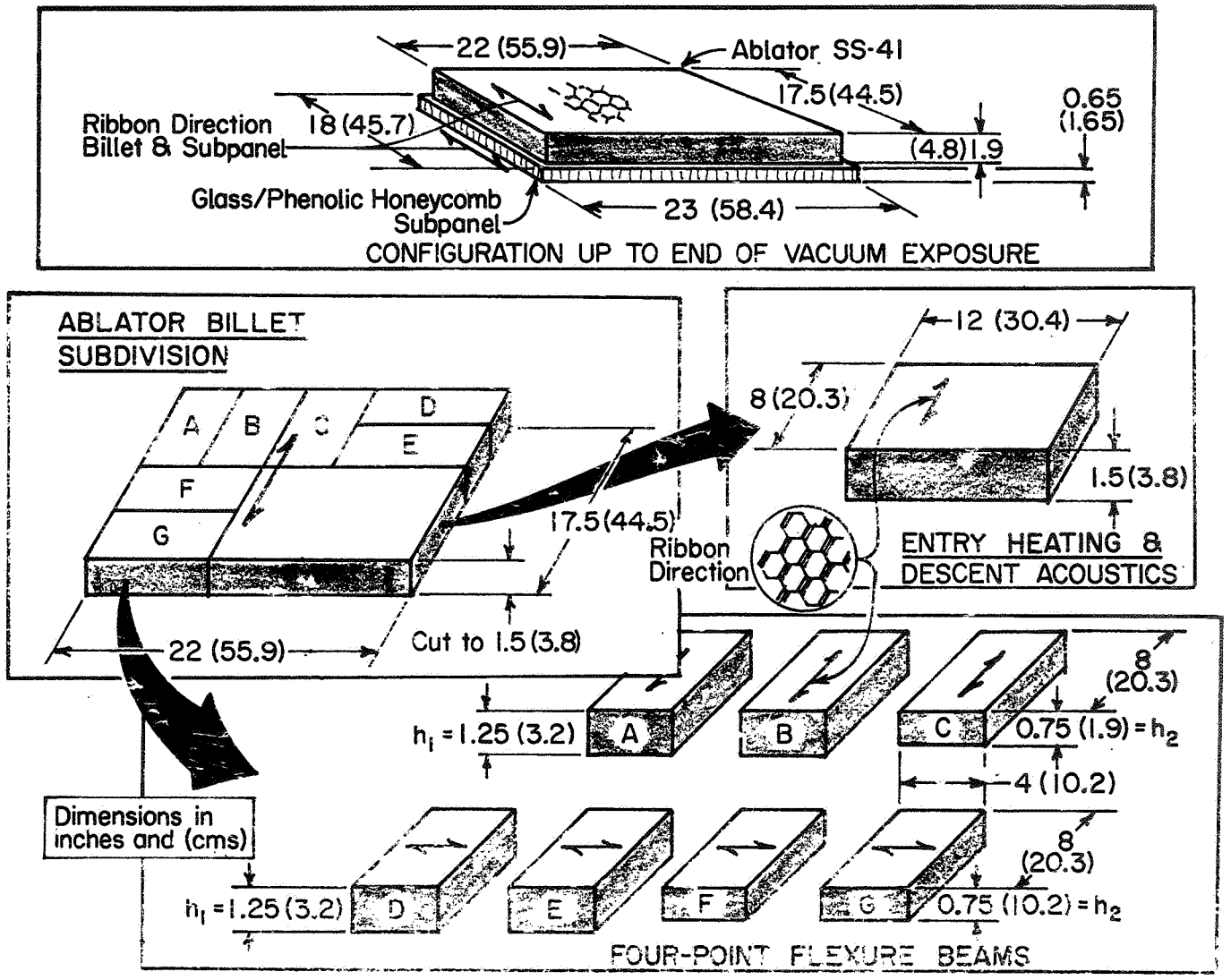

Figure 28.- Basic Panel and Subdivision.

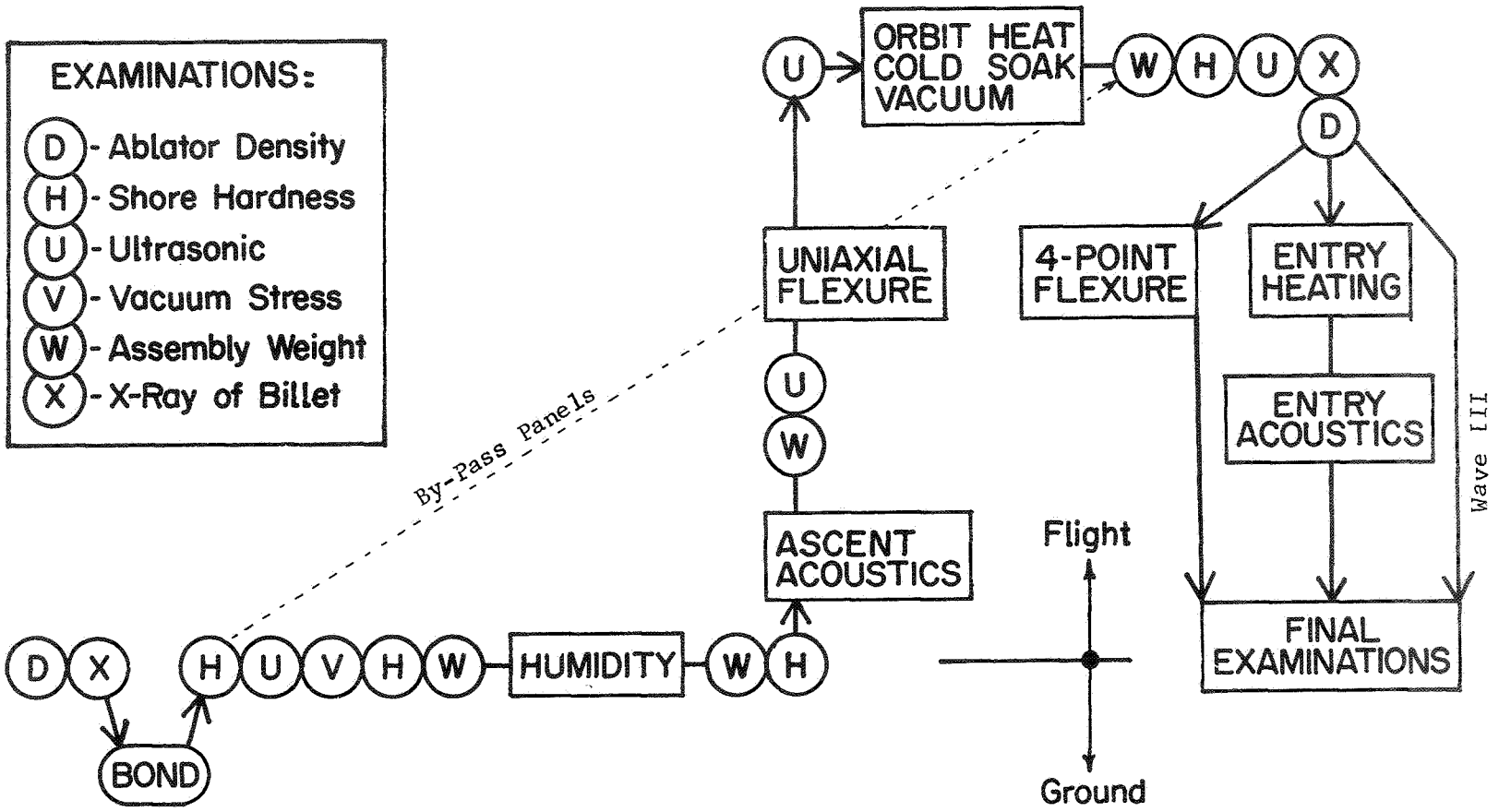

Figure 29.- Sequence of Environments and Examinations (Task IV)

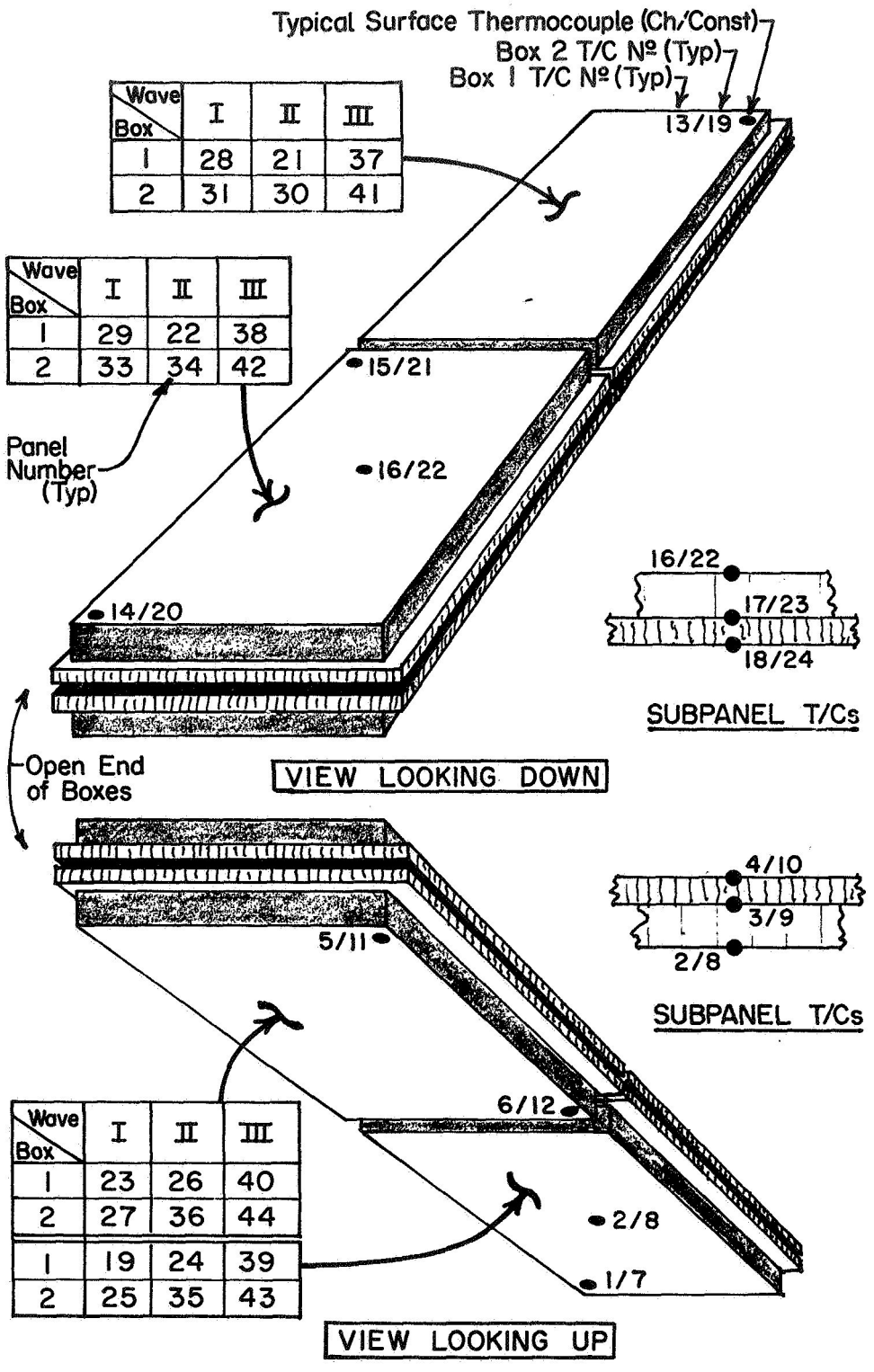

Wave / Box	I	II	III
1	28	21	37
2	31	30	41

Wave / Box	I	II	III
1	29	22	38
2	33	34	42

Wave / Box	I	II	III
1	23	26	40
2	27	36	44
1	19	24	39
2	25	35	43

Figure 30.- Thermal Vacuum Exposure, Panel Placement and Thermocouple Location

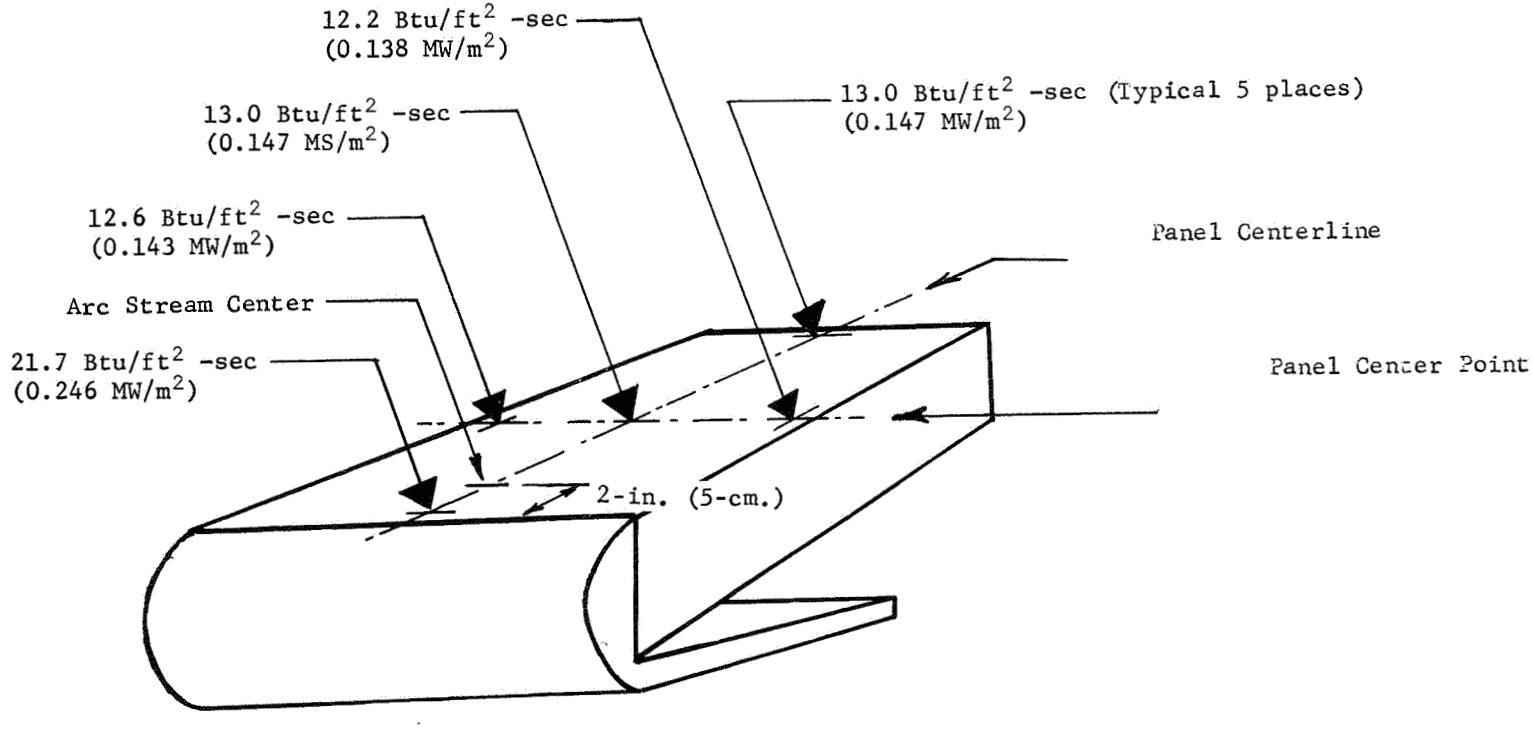

Figure 31.- Heat Distribution During Plasma Arc Wedge Exposure (Task IV)

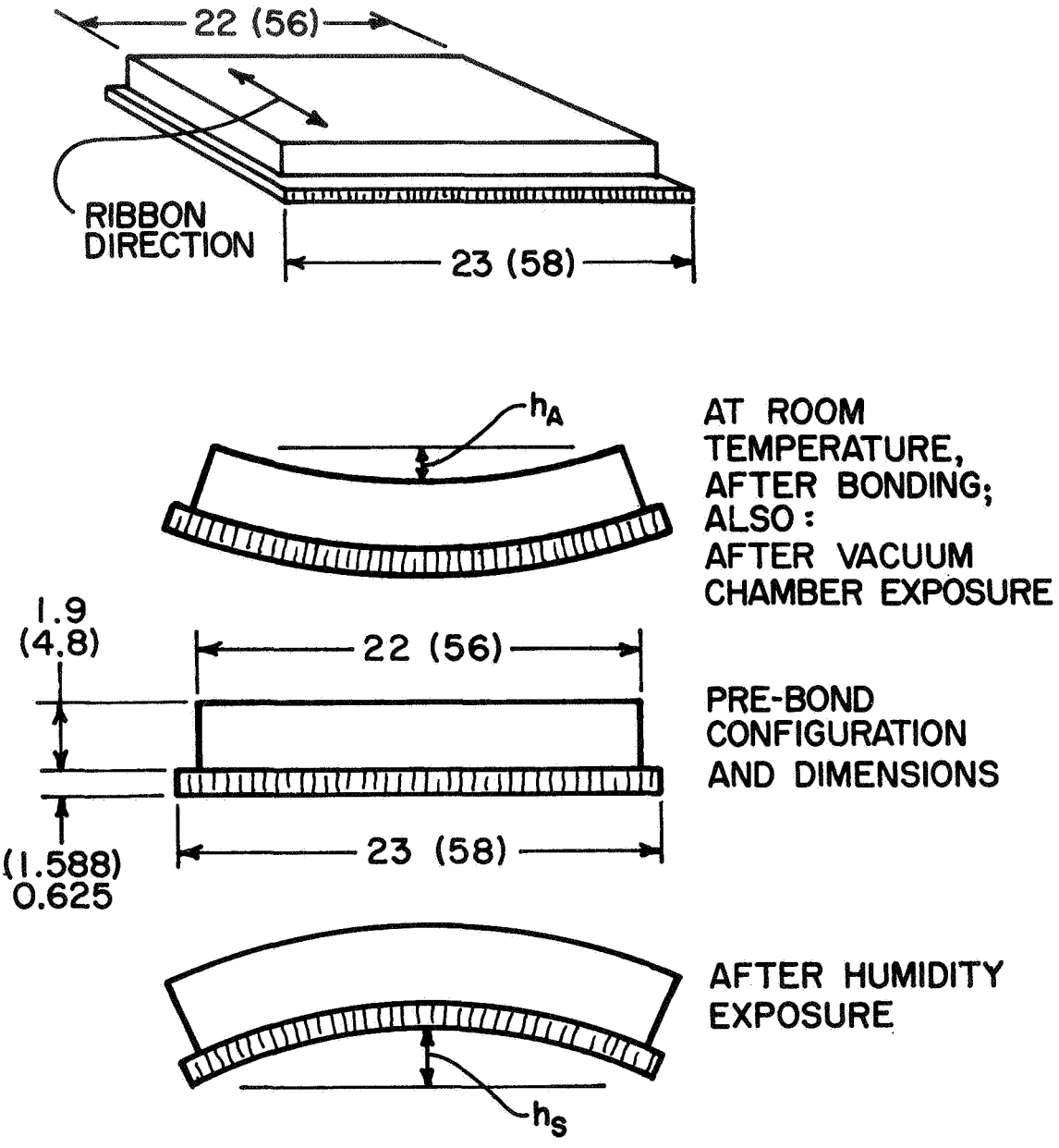

Figure 32.- Panel Curvature Trends

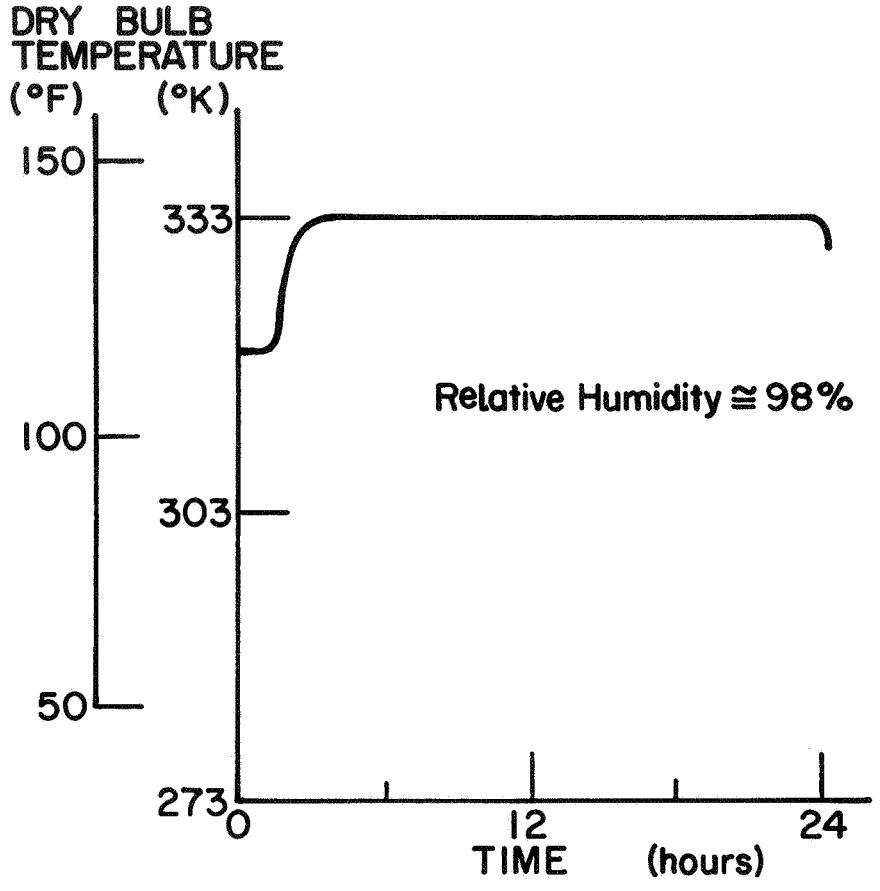

Figure 33.- Humidity Environment Number 3

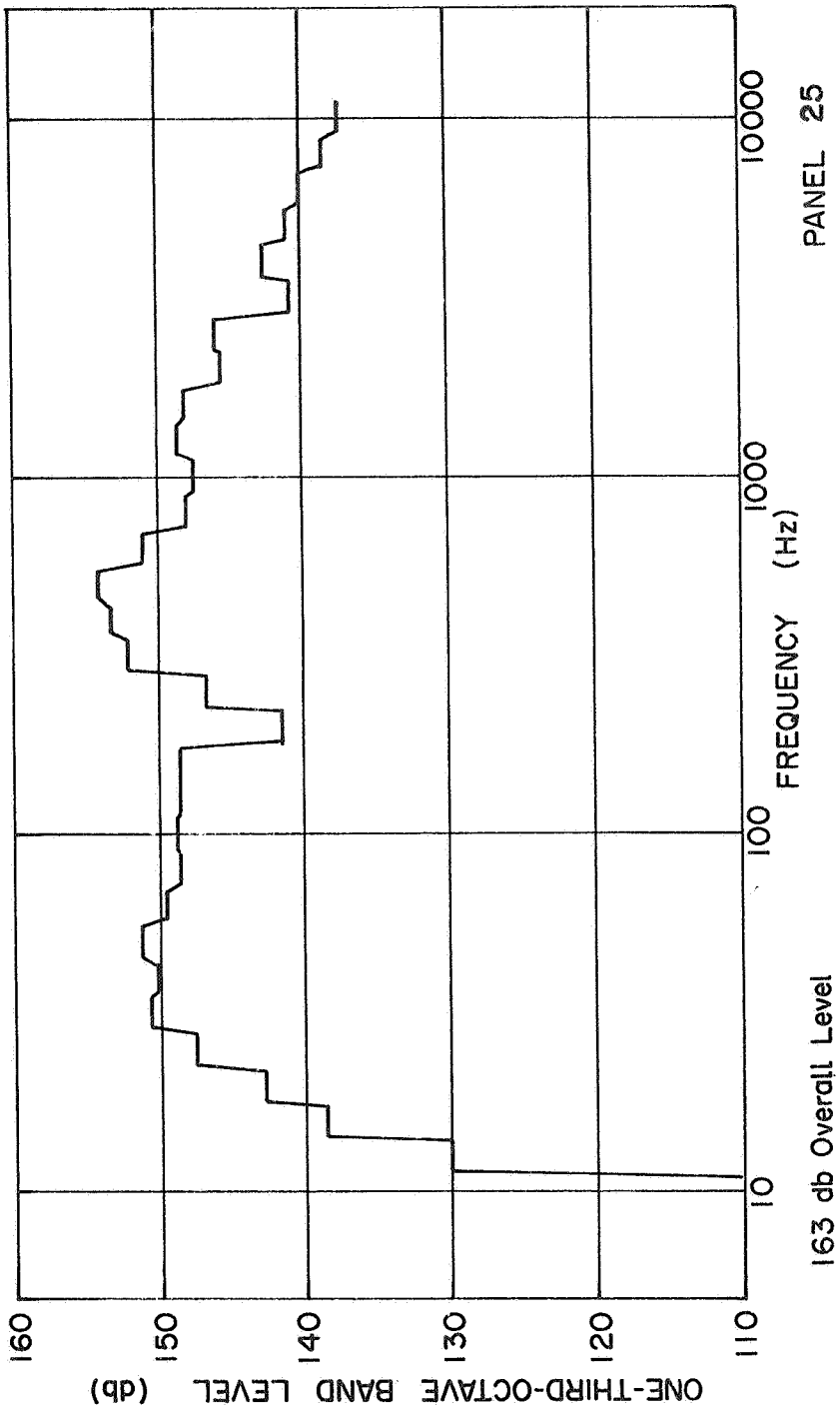

Figure 34.- Typical Ascent Acoustic Spectrum Distribution on Final Panels

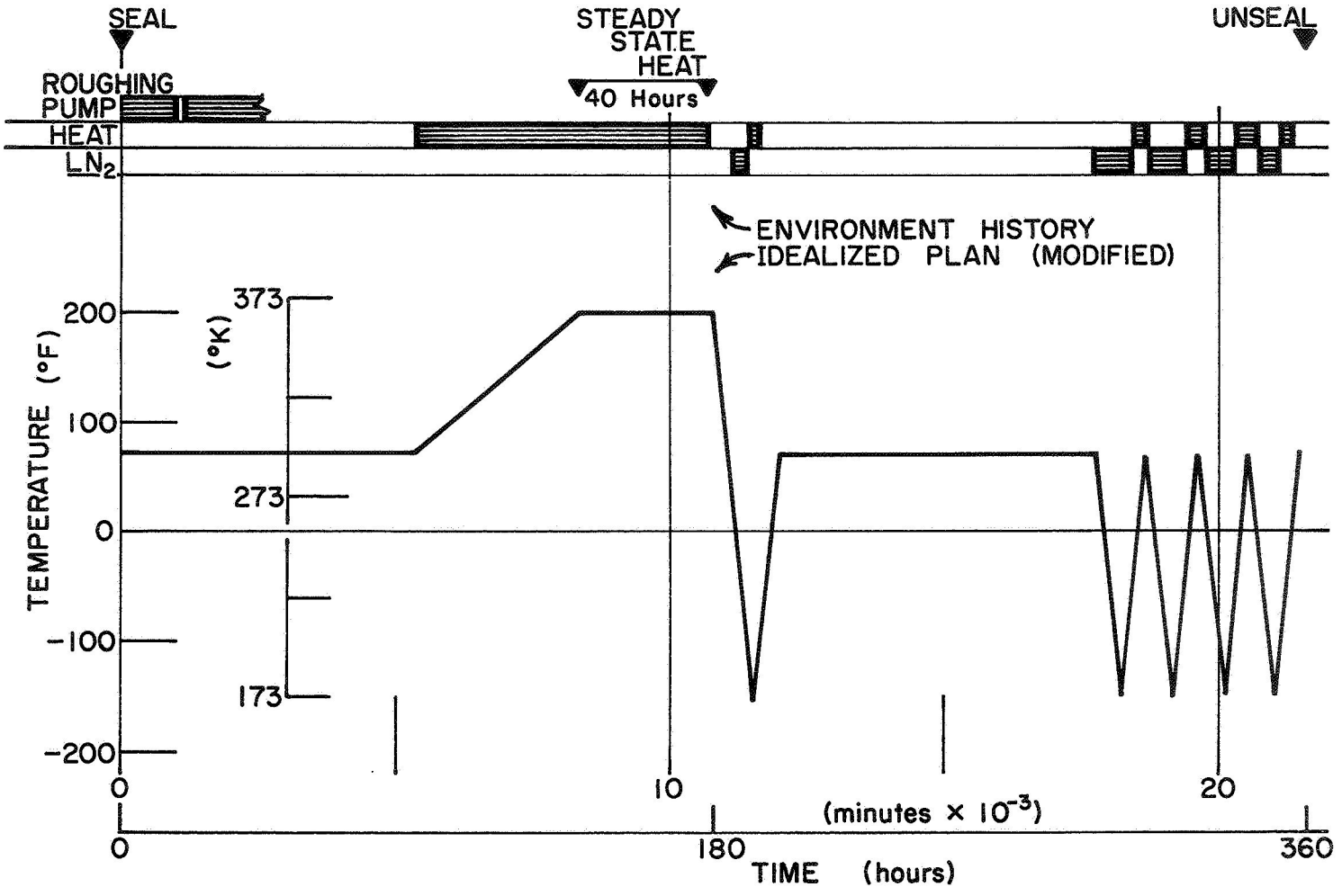

Figure 35.- Thermal Vacuum Sequence, Wave I

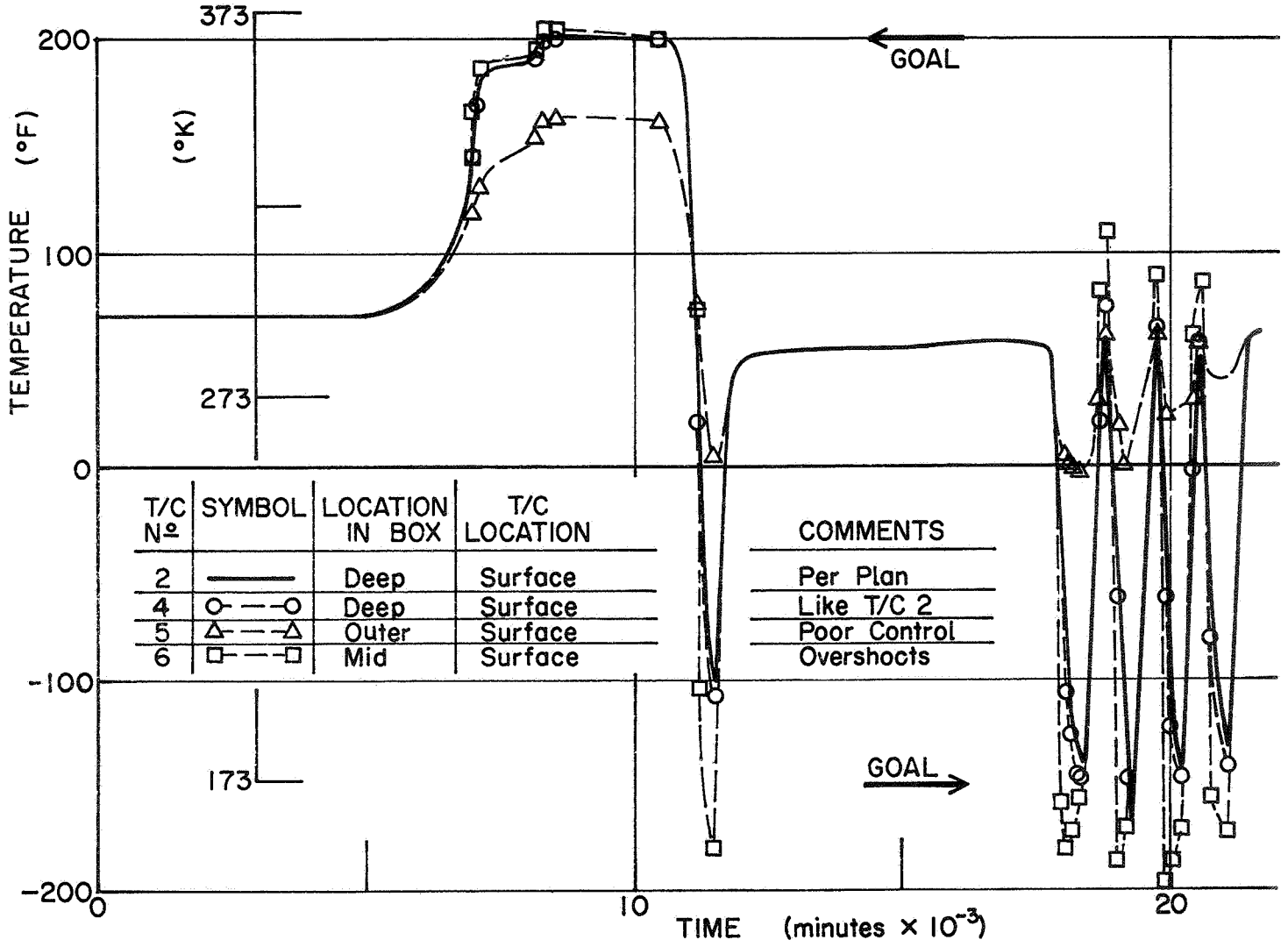

Figure 36.- Wave I Temperature Histories, Thermal Vacuum Exposure

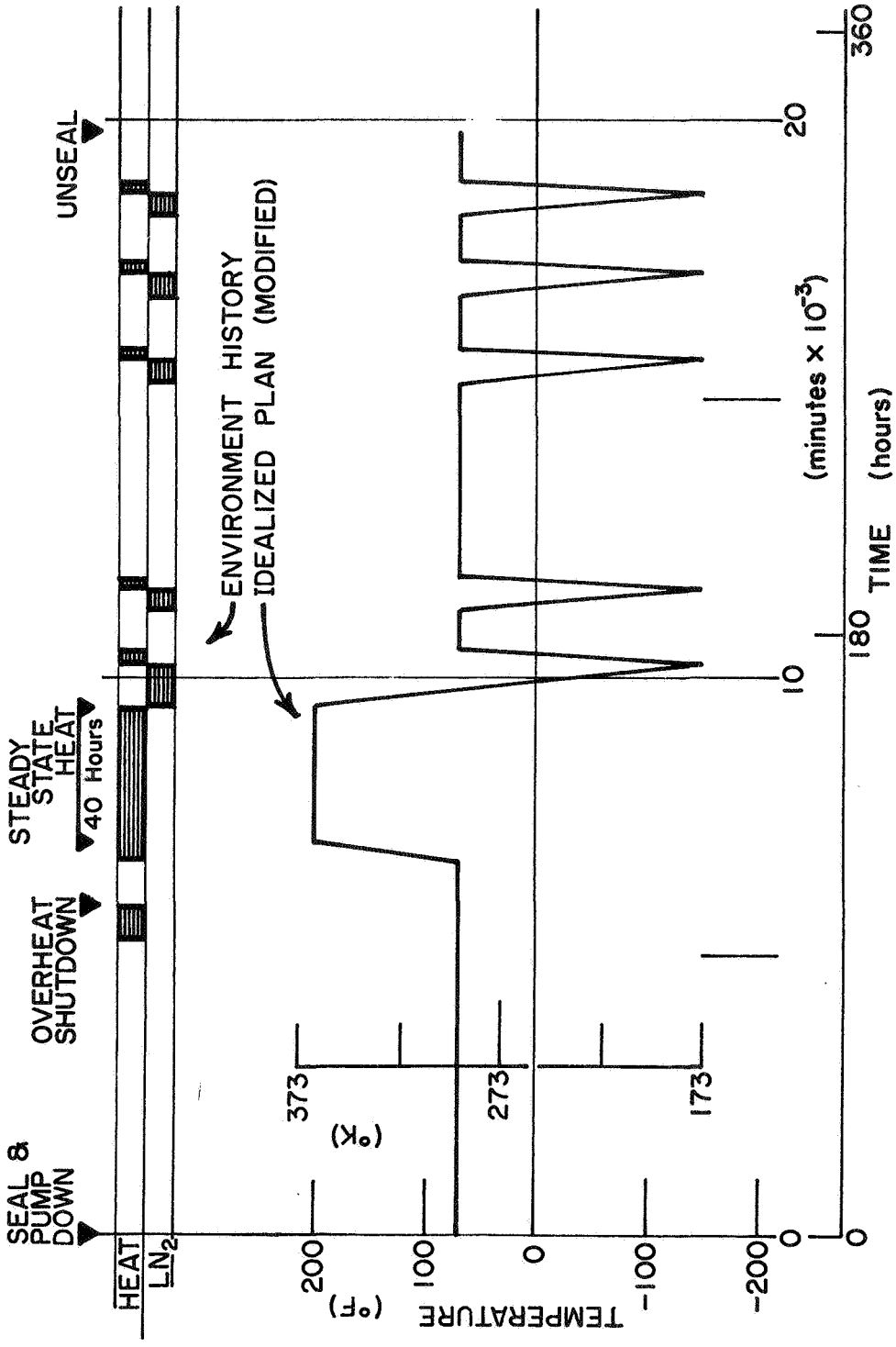

Figure 37.- Thermal Vacuum Sequence, Wave II

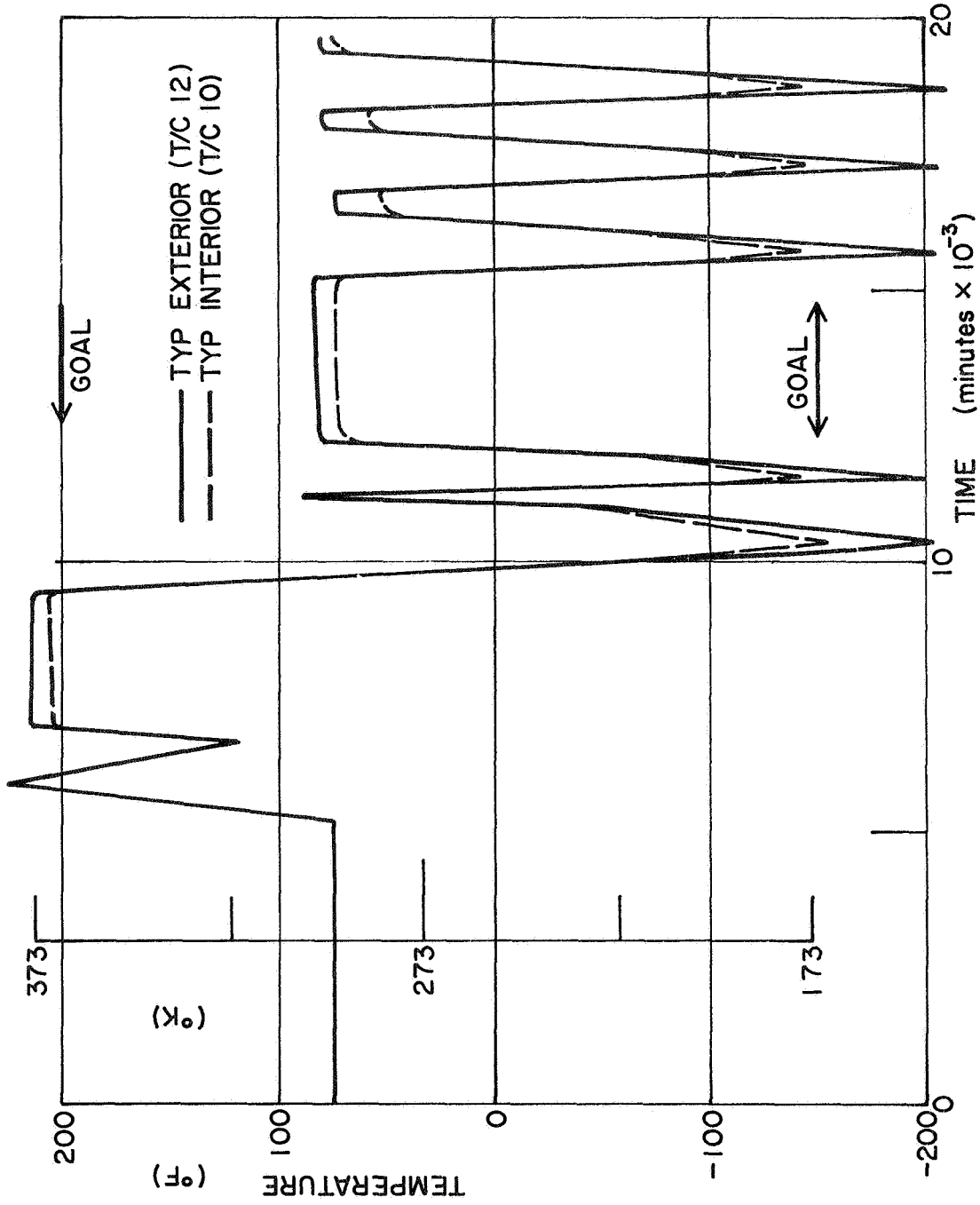

Figure 38.- Wave II Temperature Histories, Thermal Vacuum Exposure

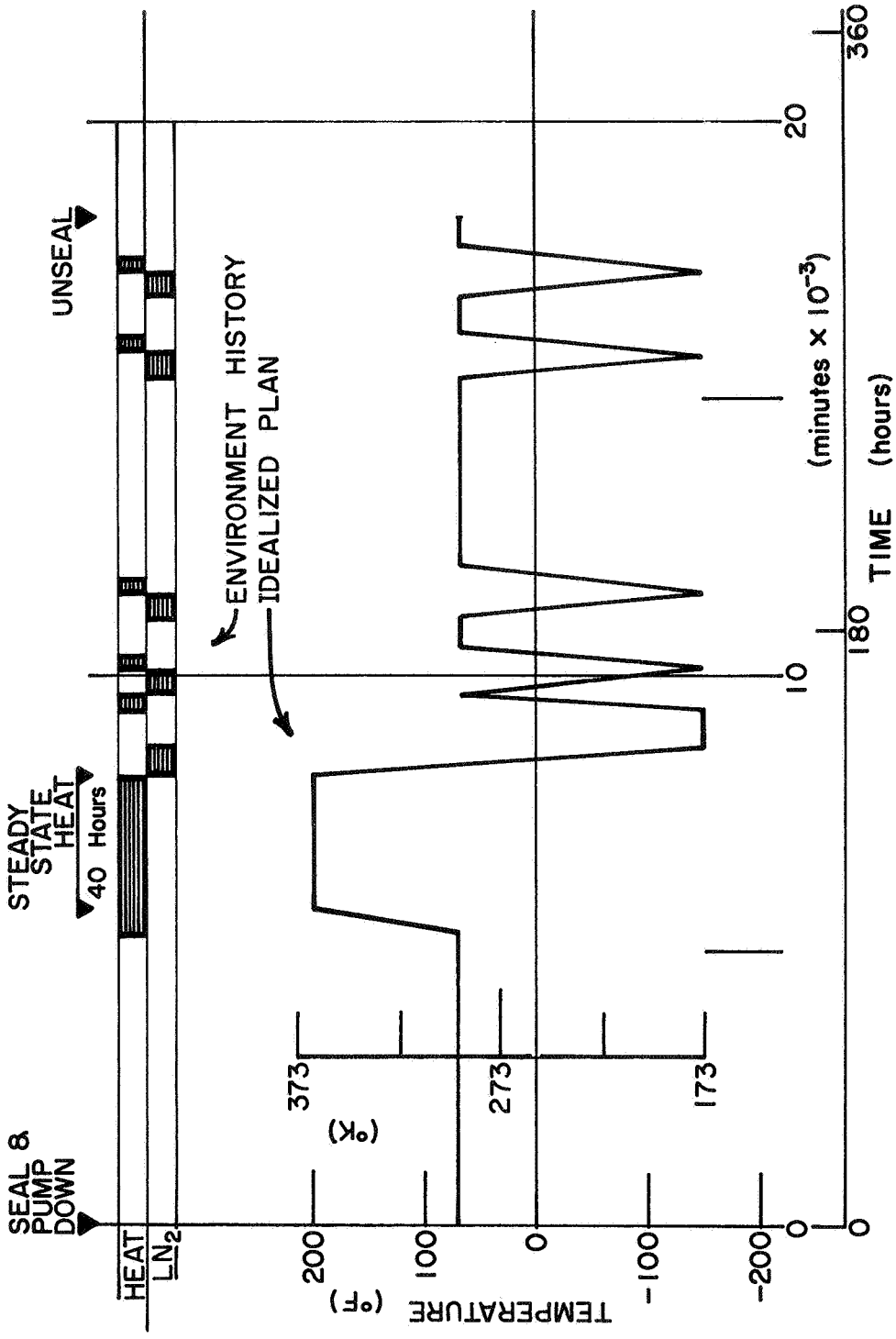

Figure 39.- Thermal Vacuum Sequence, Wave III

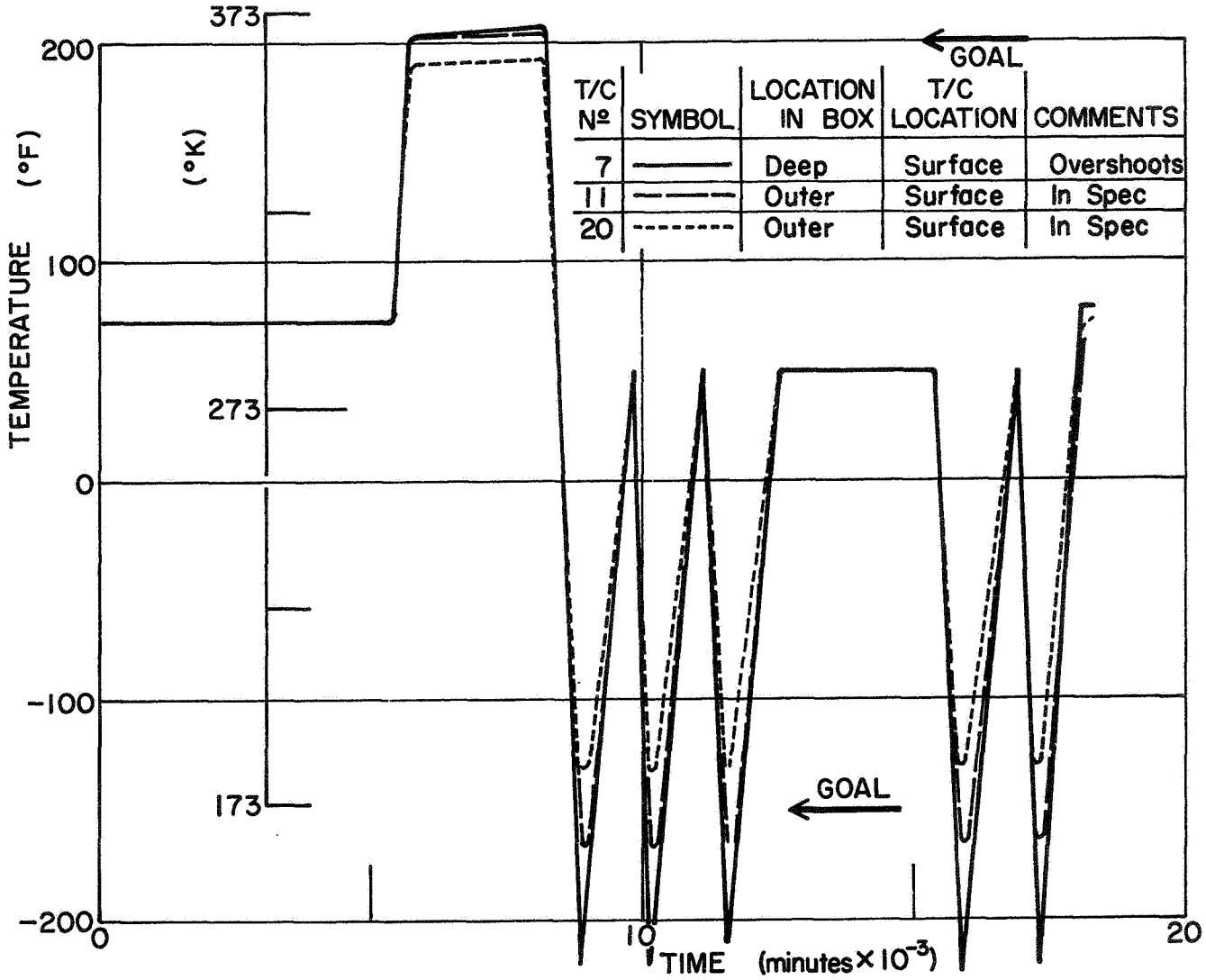

Figure 40.- Wave III Temperature Histories, Thermal Vacuum Exposures

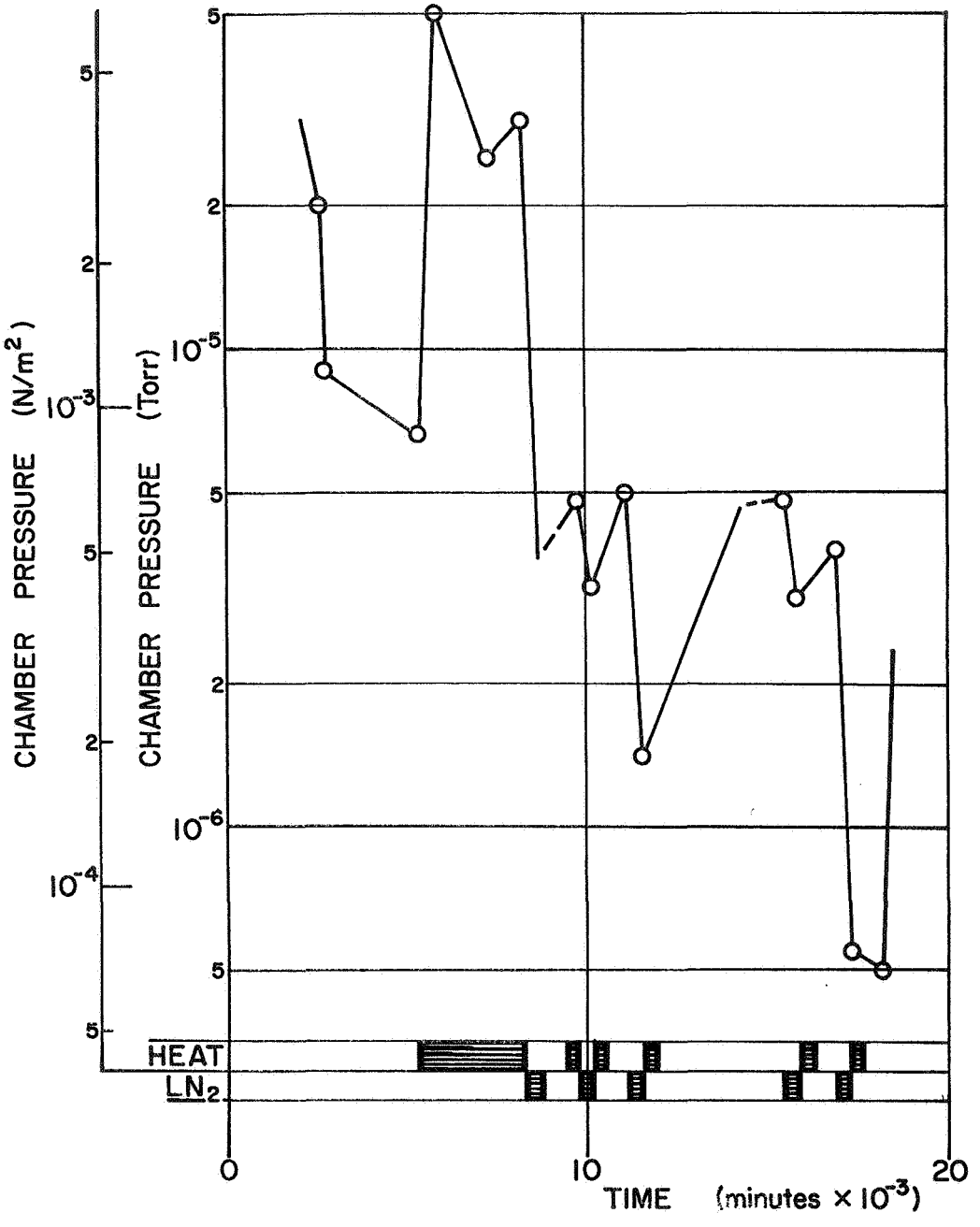

Figure 41.- Vacuum Chamber Pressure History, Wave III

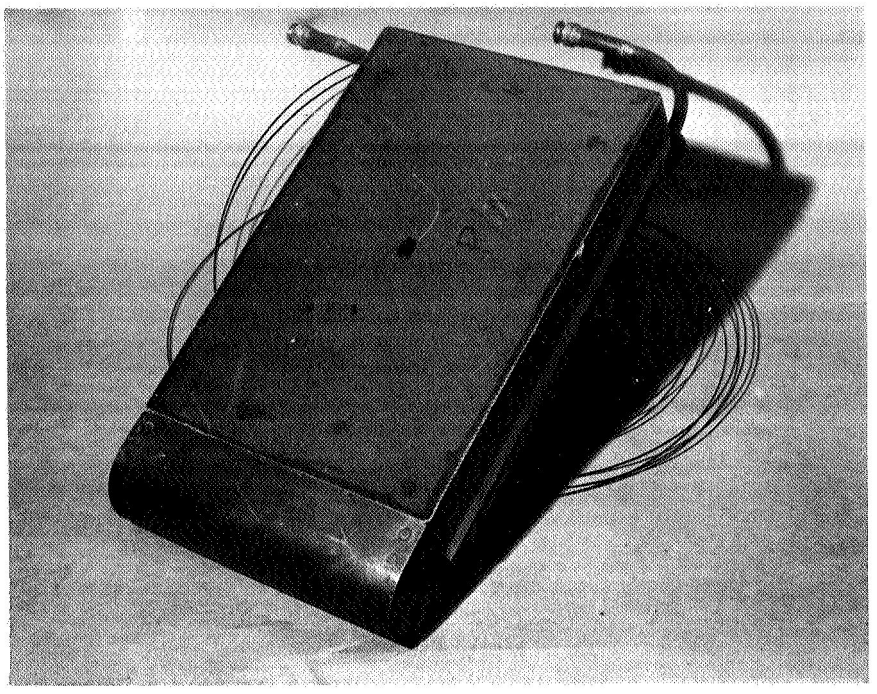

Figure 42.- Typical Entry Heating Panel in Plasma Arc Fixture (Pre-test)

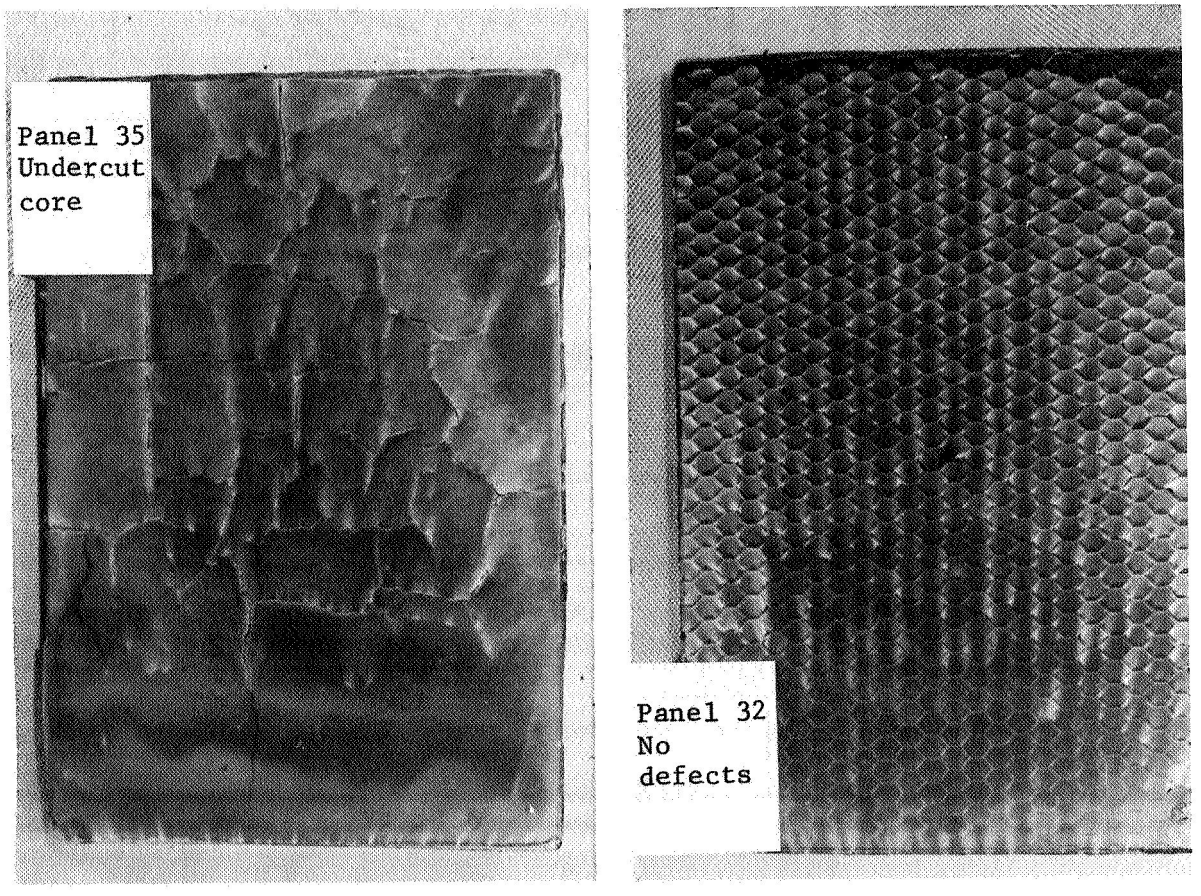

Figure 43.- Typical Post Entry Heating Appearance

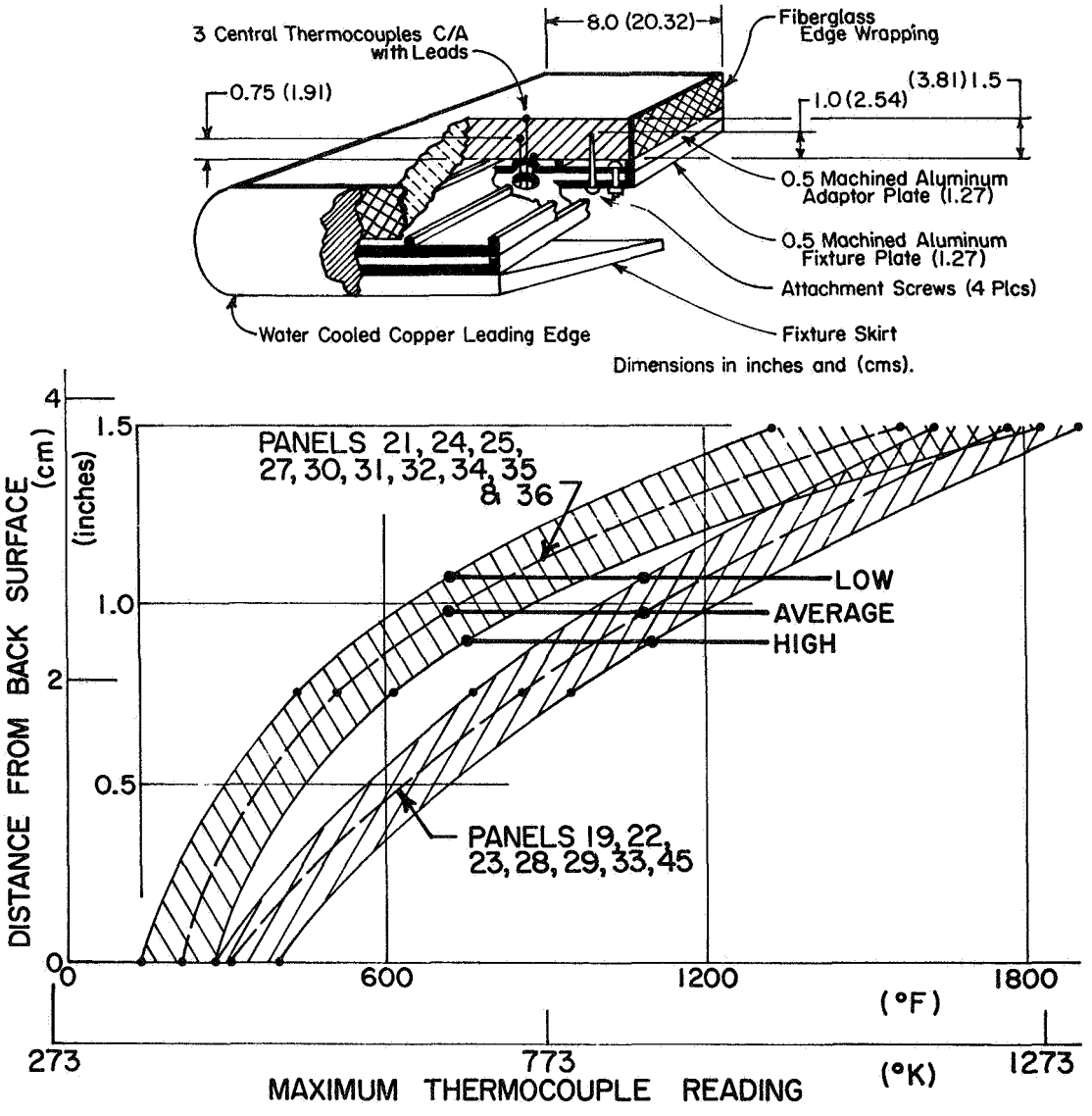

Figure 44.- Summary of Maximum Thermocouple Readings, Plasma Arc Exposures

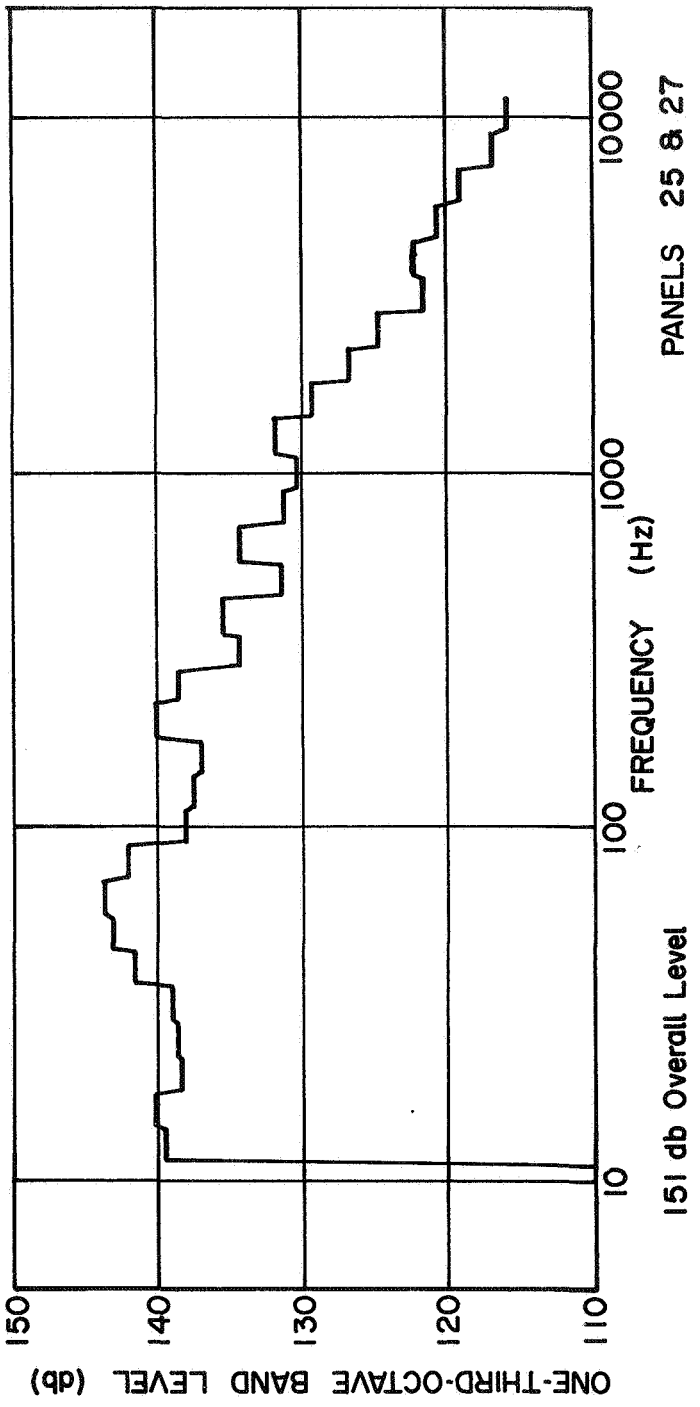

Figure 45.- Typical Descent Acoustic Spectrum Distribution on Final Panels

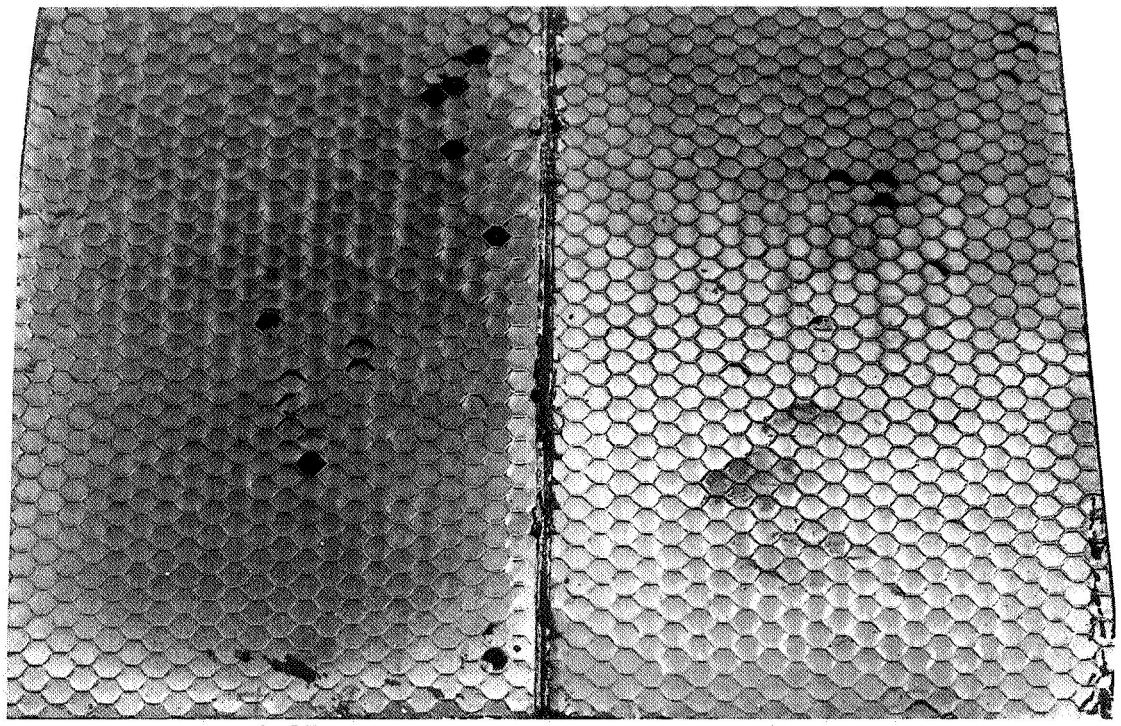

Panel 27
(Undermixed filler)

Panel 25
(Wet basic ingredients)

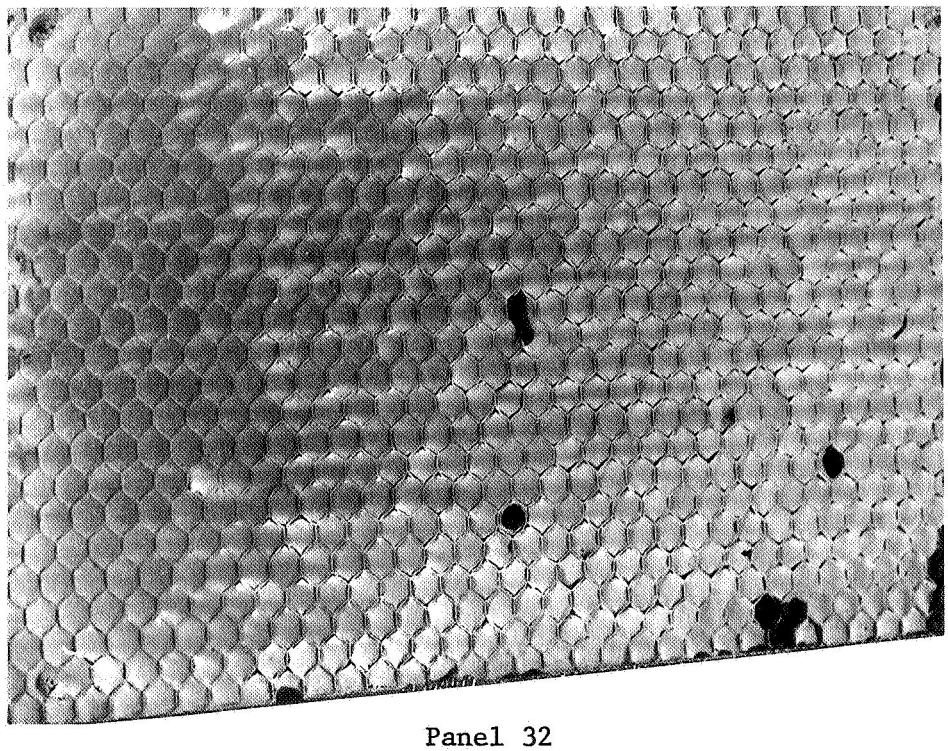

Panel 32
(No defects)

Figure 46.- Post-Acoustics (Good Appearance)

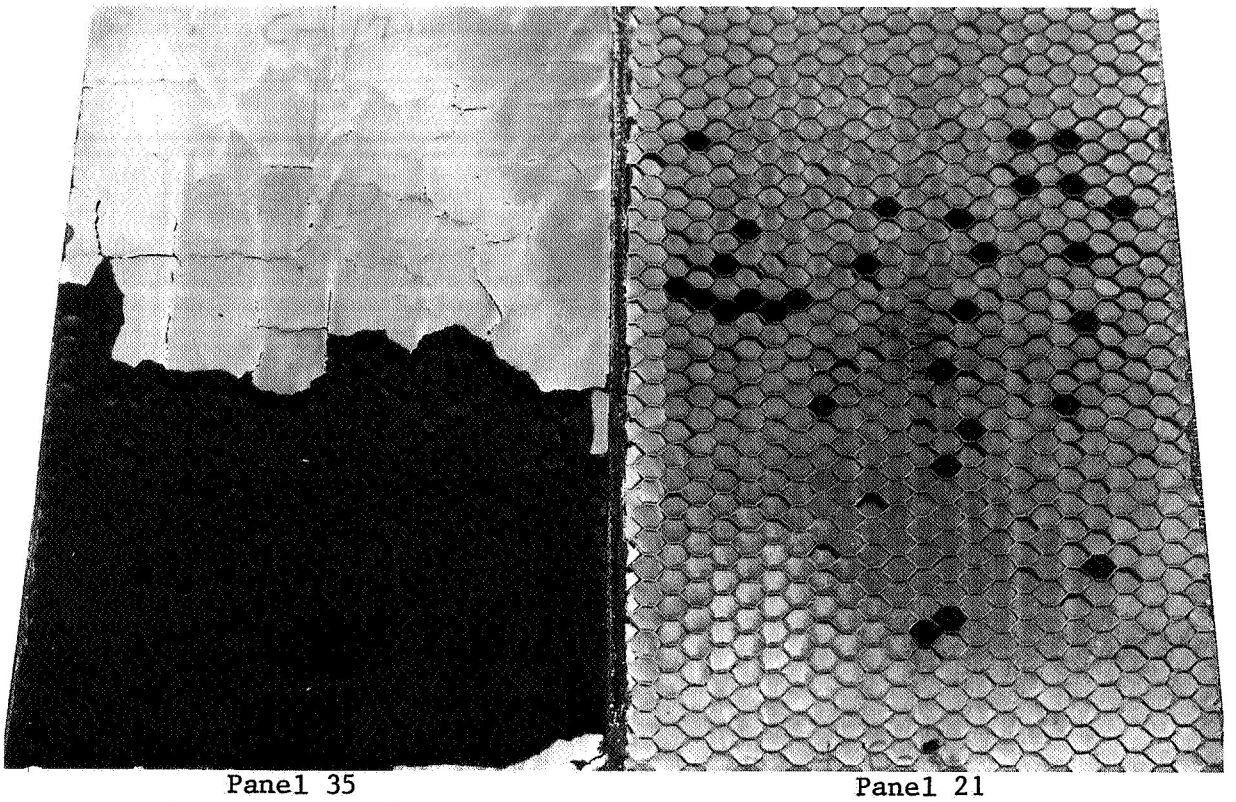

Panel 35
(Undercut core)

Panel 21
(Uncured)

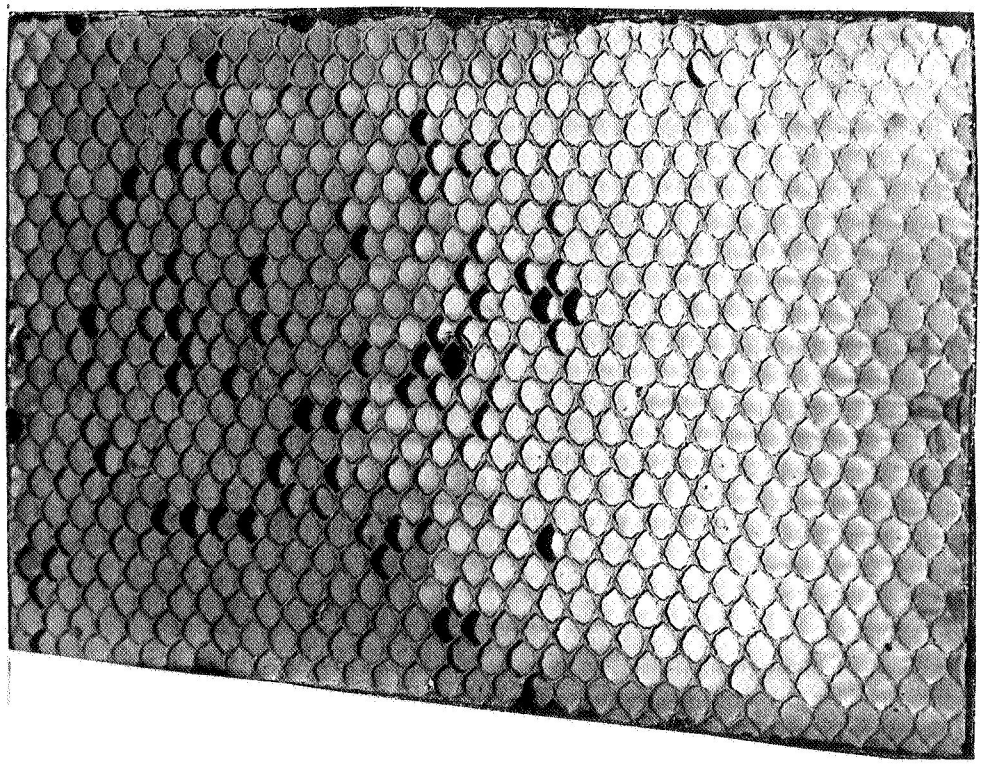

Figure 47. Post-Acoustics (Poor Appearance)

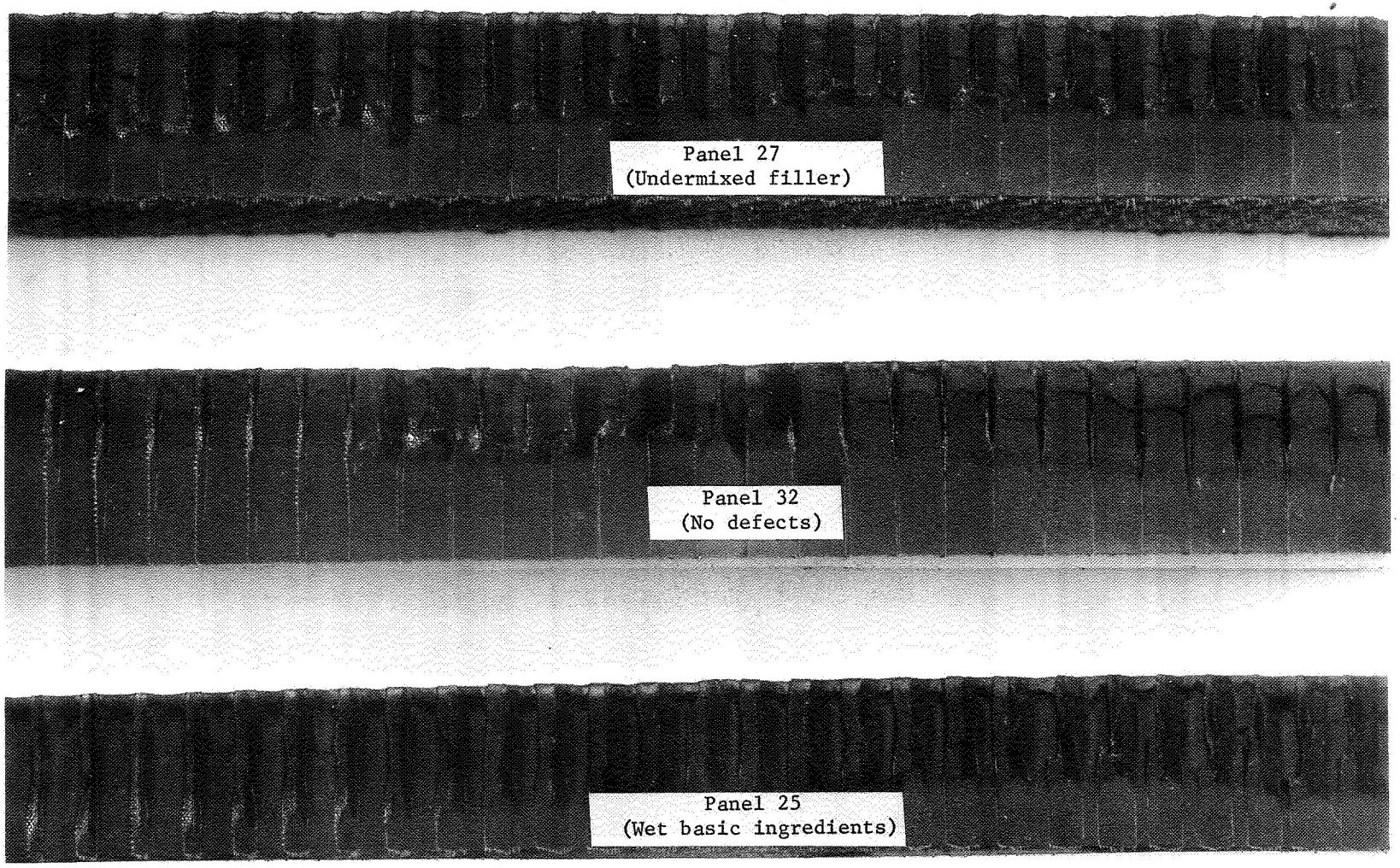

Figure 48.- TypicalSectioning (Good Appearance)

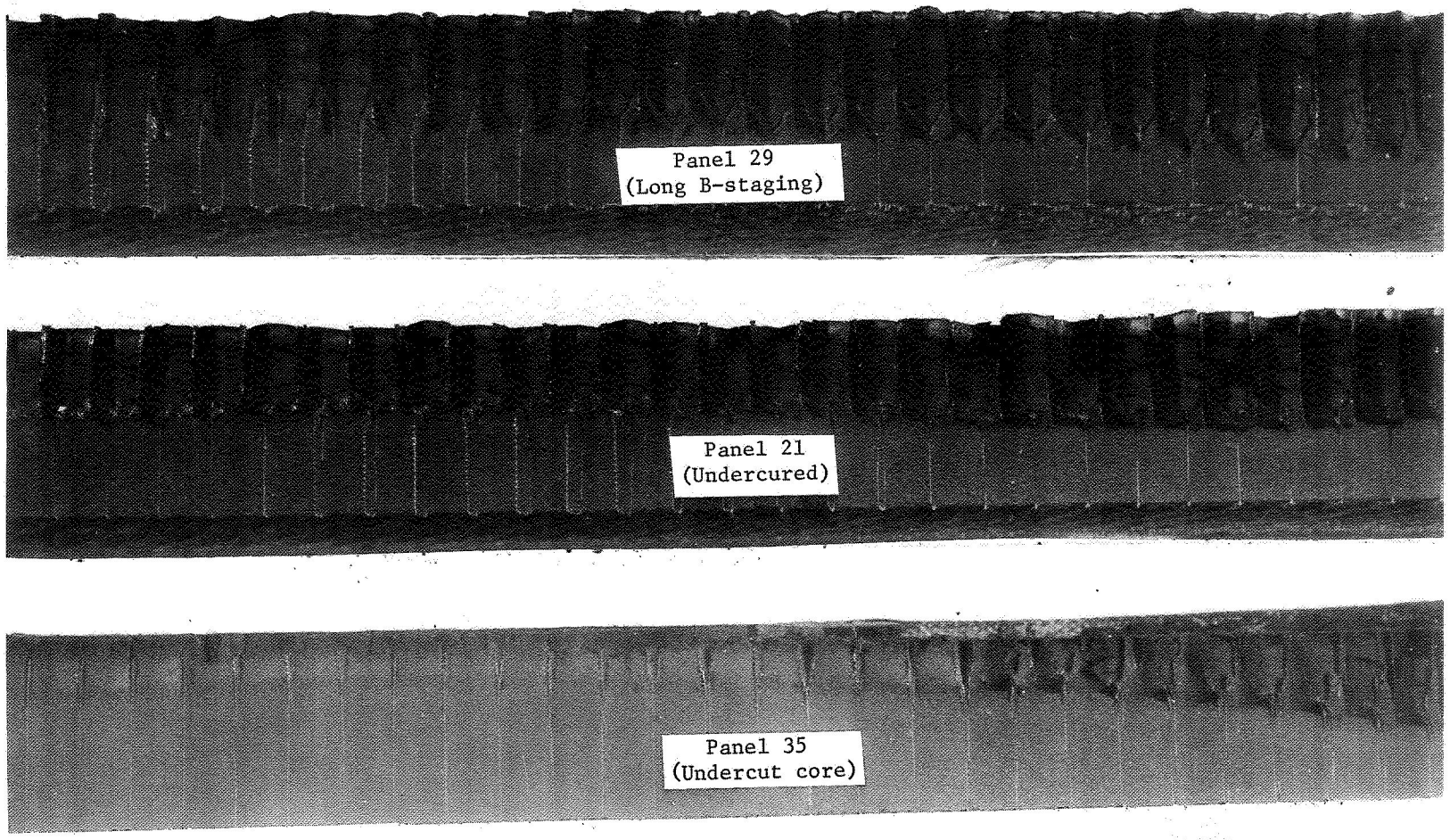

Figure 49.- Typical Sectioning (Poor Appearance)

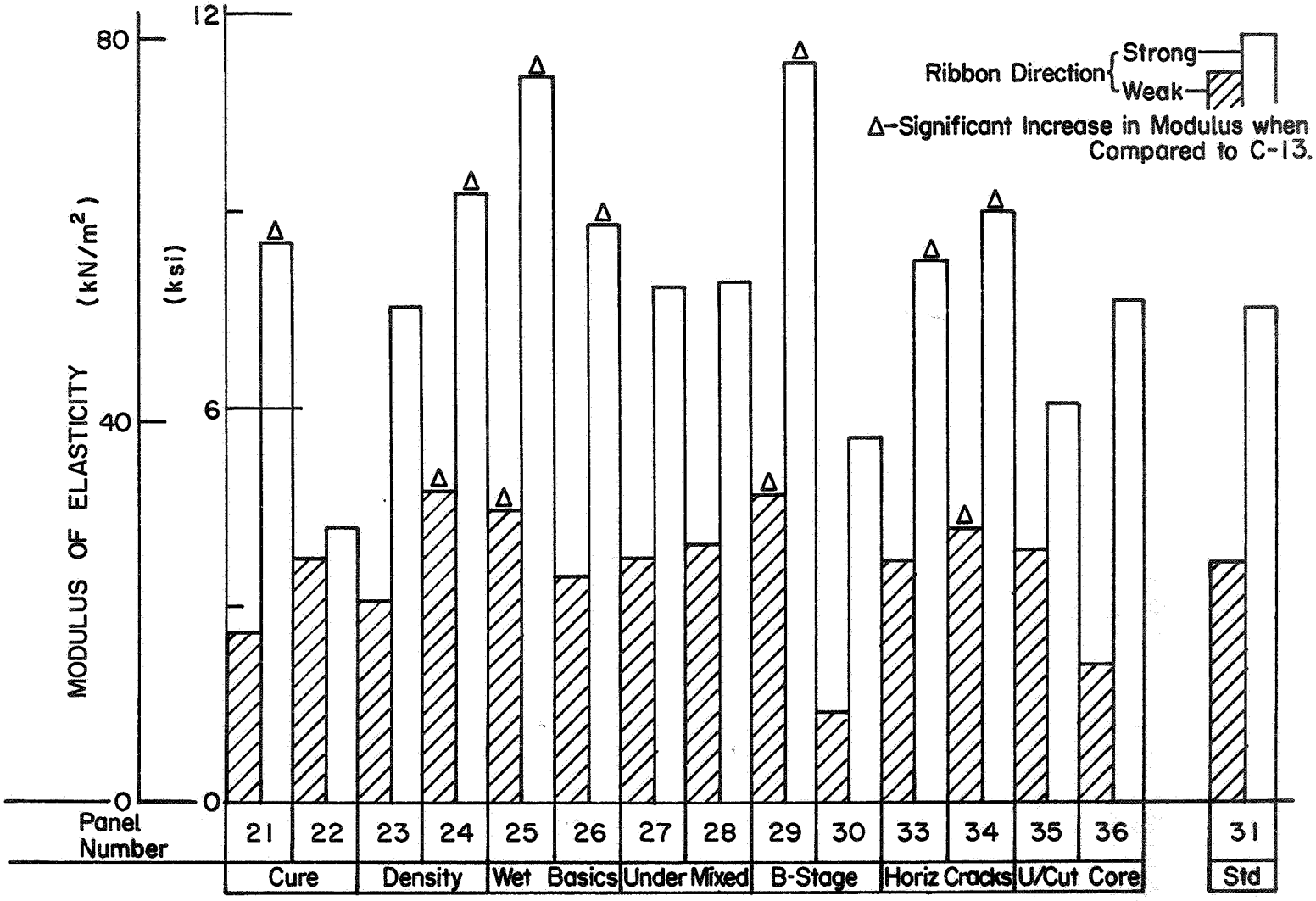

Figure 50.- Trends in Ablator Flexural Modulus for Defect Beams

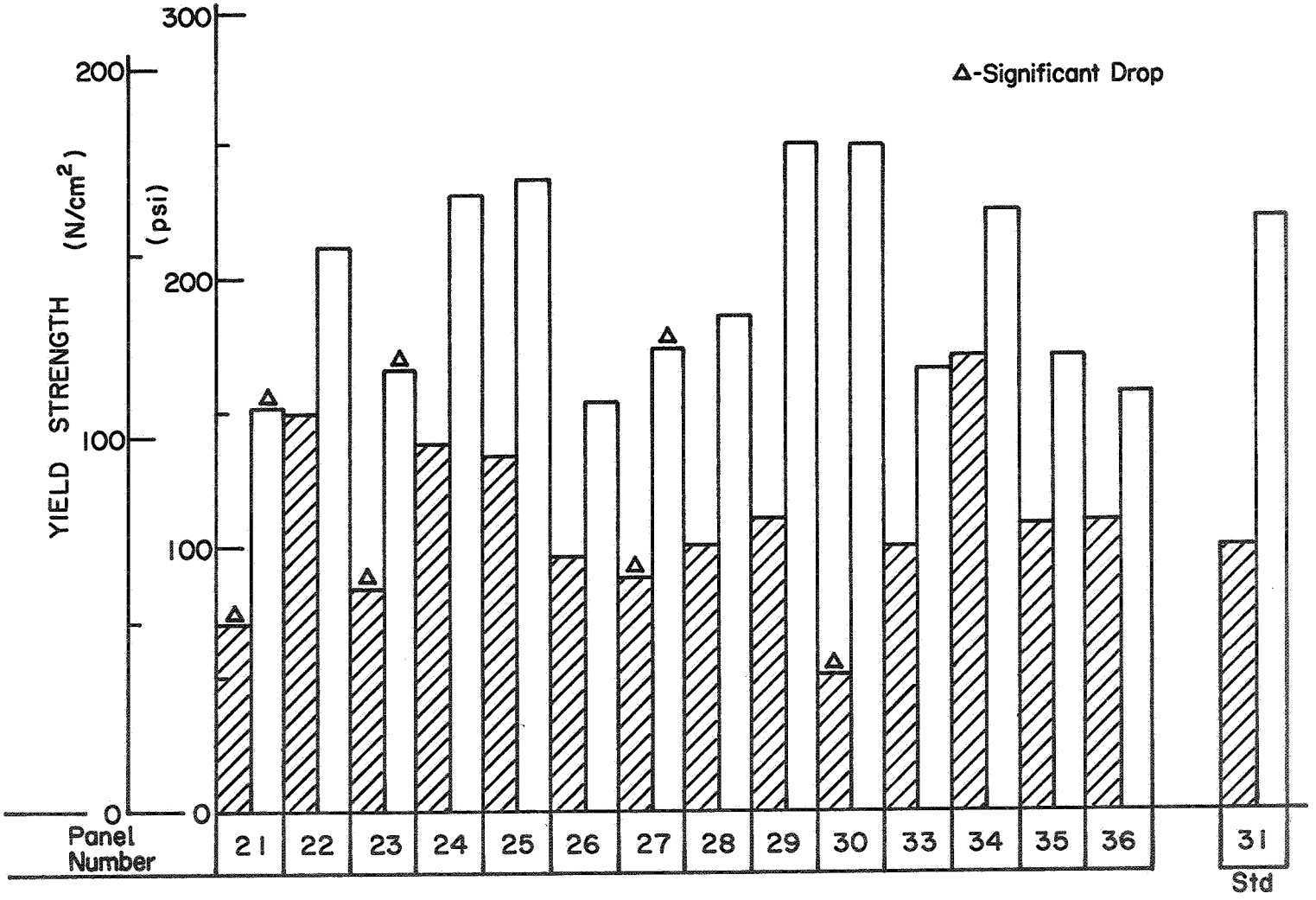

Figure 51.- Trends in Ablator Yield Strength for Defect Beams

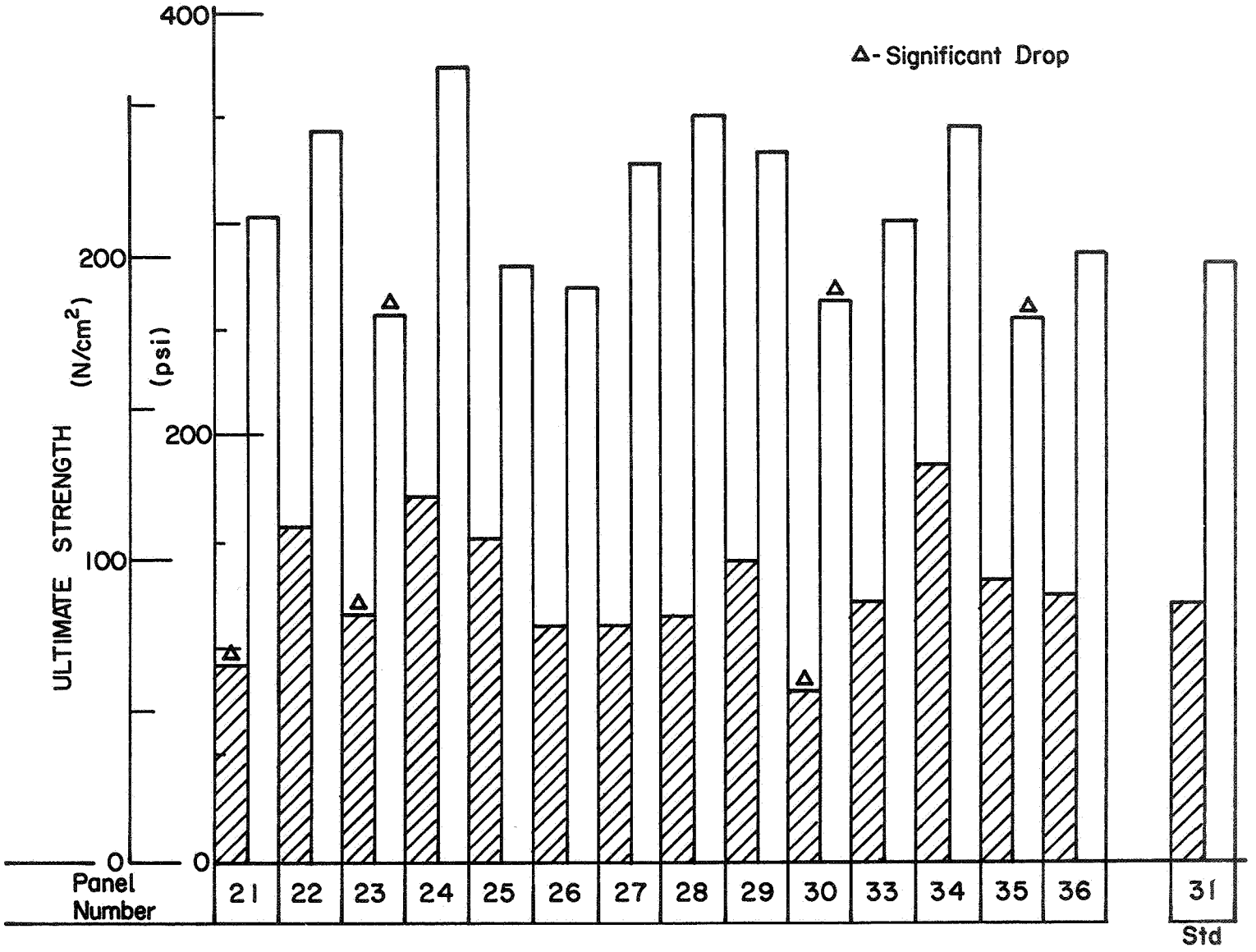

Figure 52.- Trends in Ablator Ultimate Strength for Defect Beams

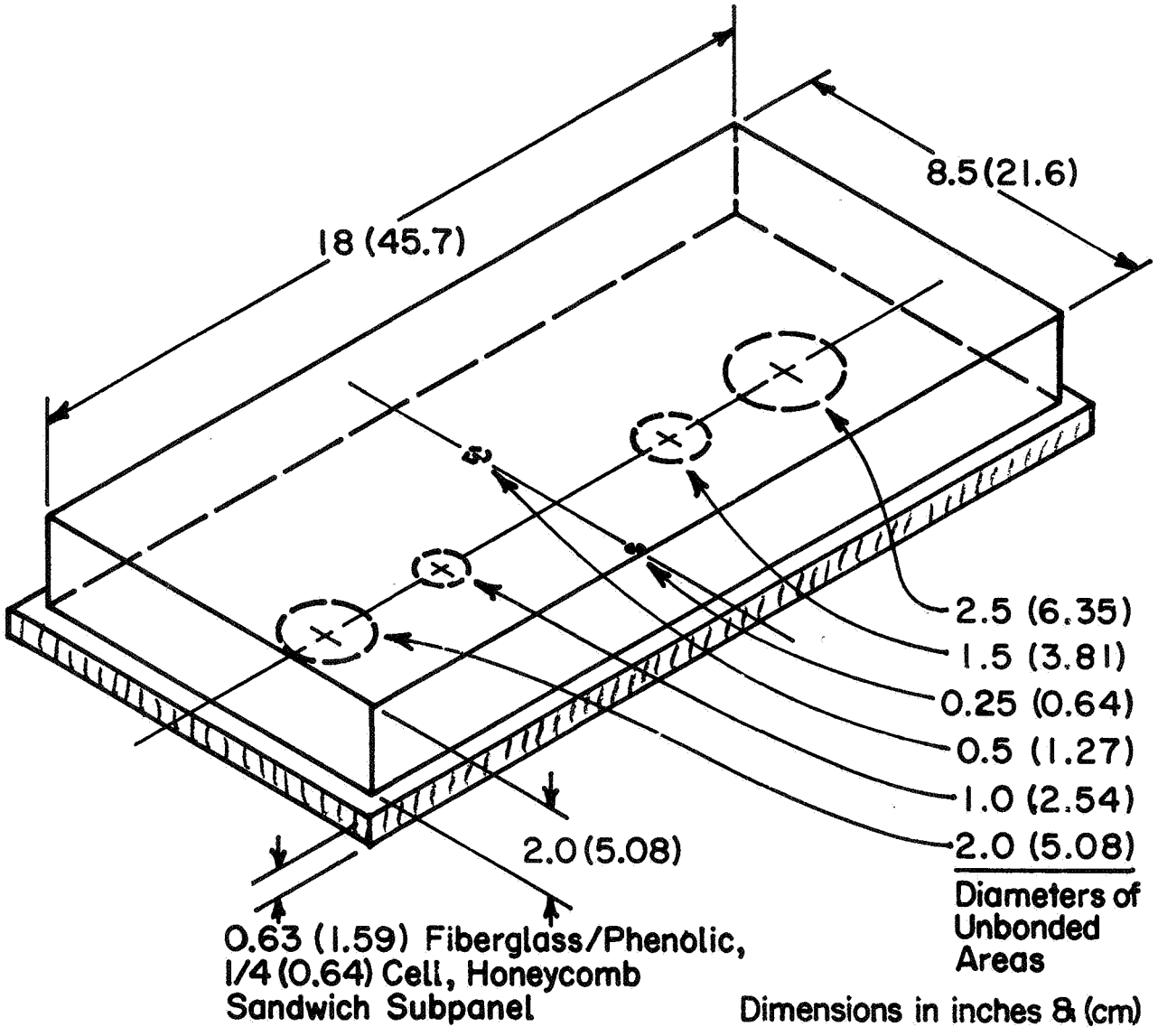

Figure 53.- Series B, NDT Standard Unbond Reference Panel

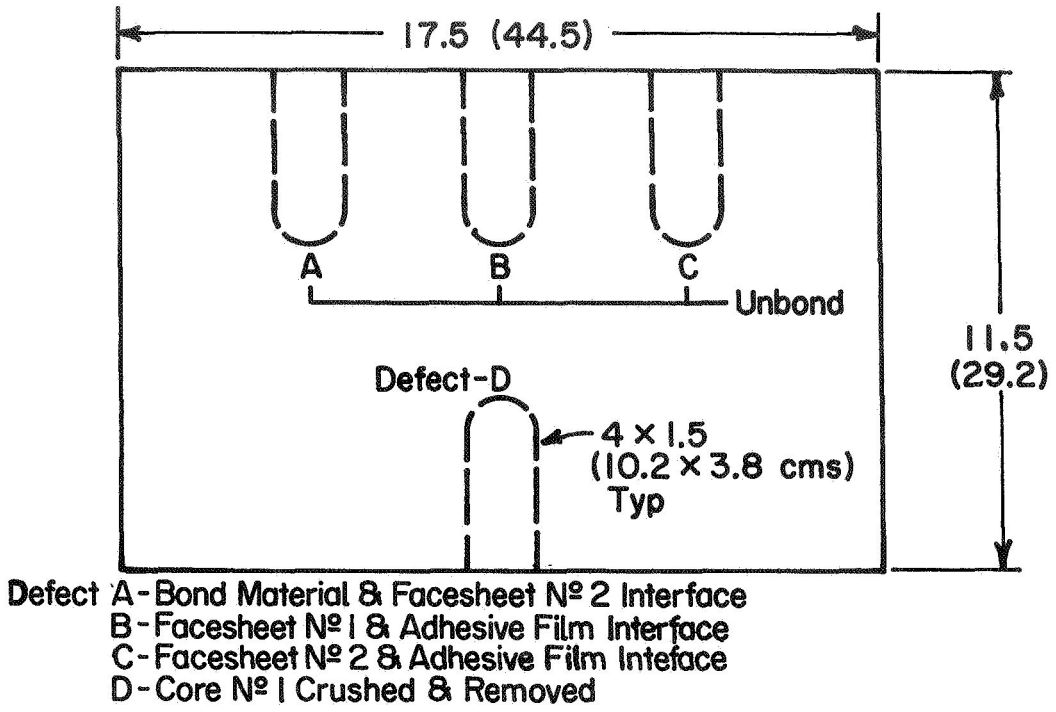

Figure 54.- NDT Destructive Unbond Panel

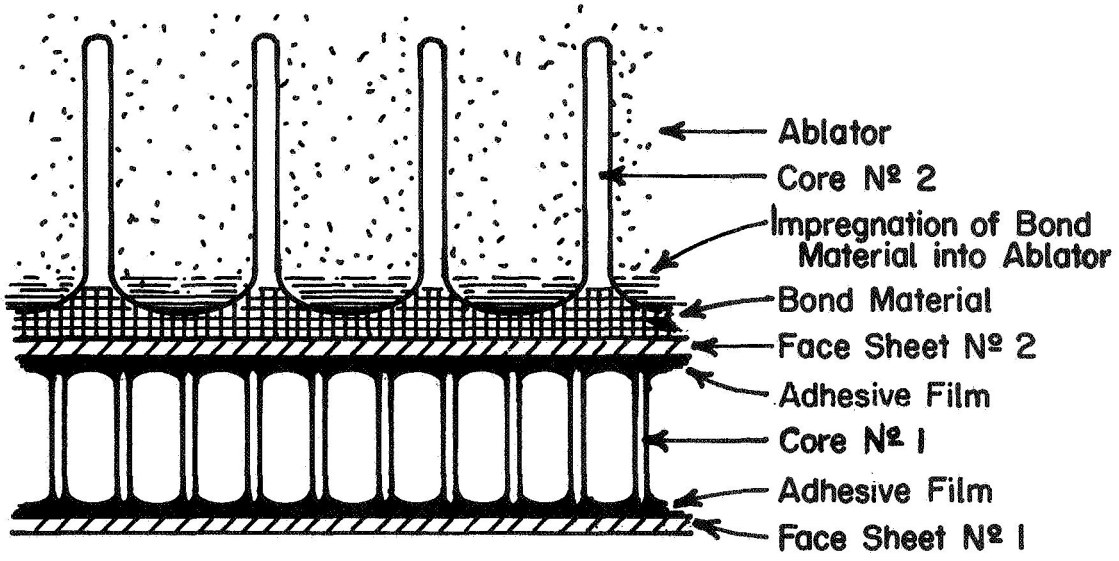

Figure 55.- Cross Section of Critical Defects Panel

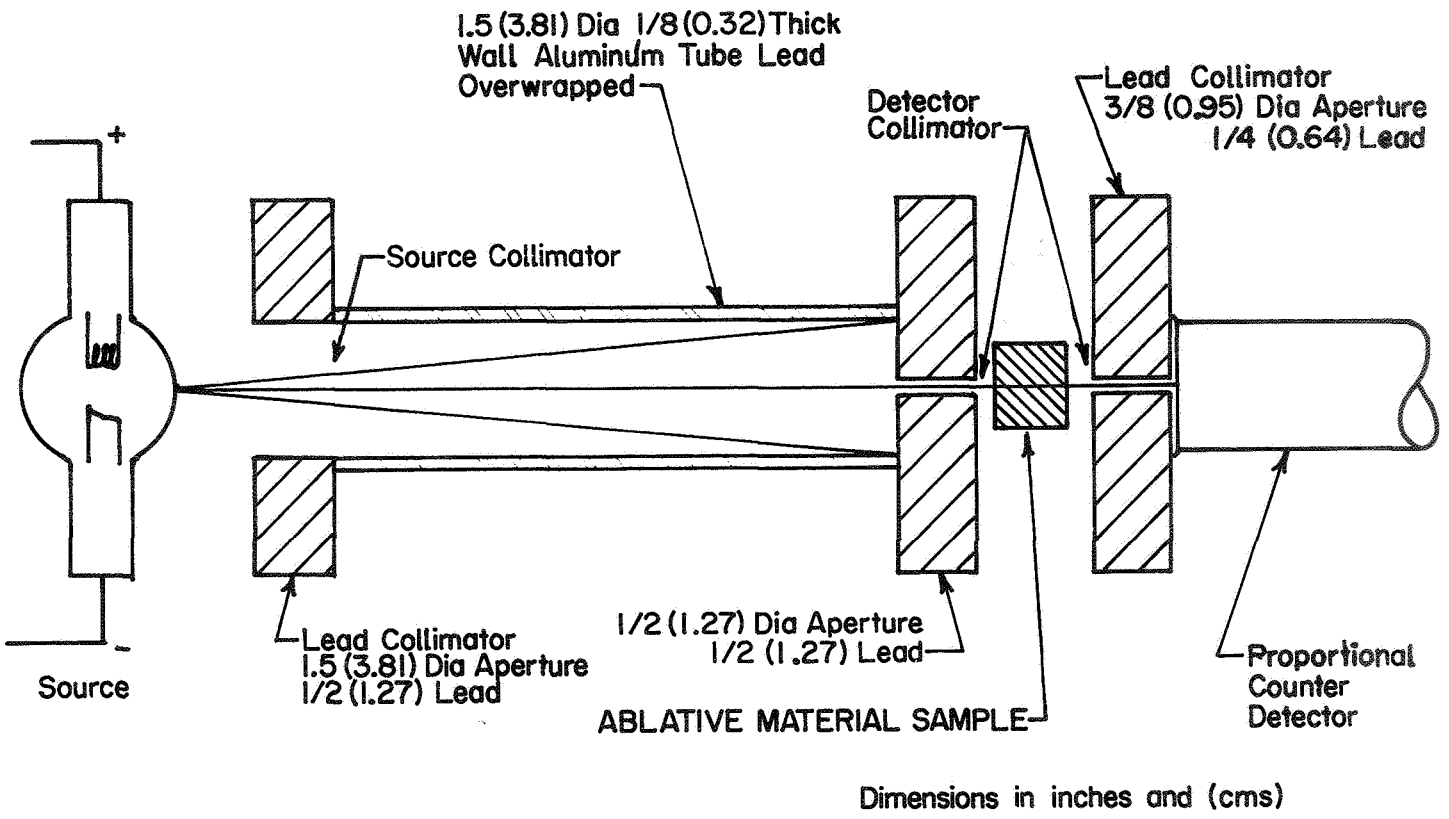

Figure 56.- Schematic View of the X-Ray Absorption Set Up (Narrow Beam)

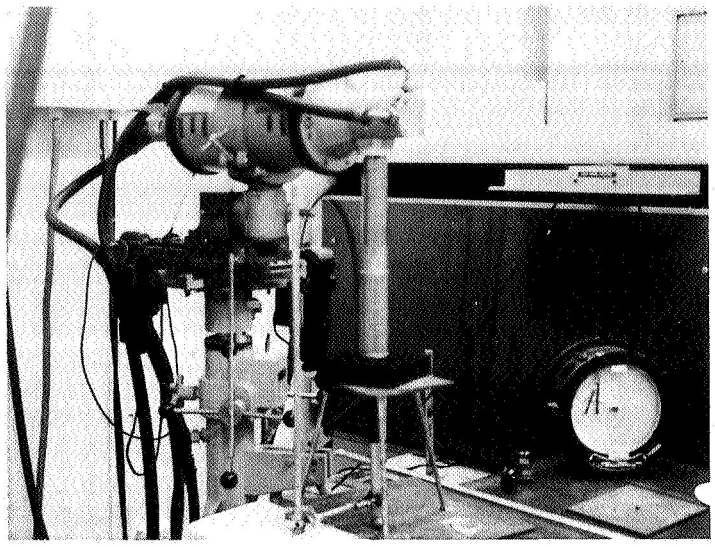

Figure 57.- Experimental Energy Absorption Set Up

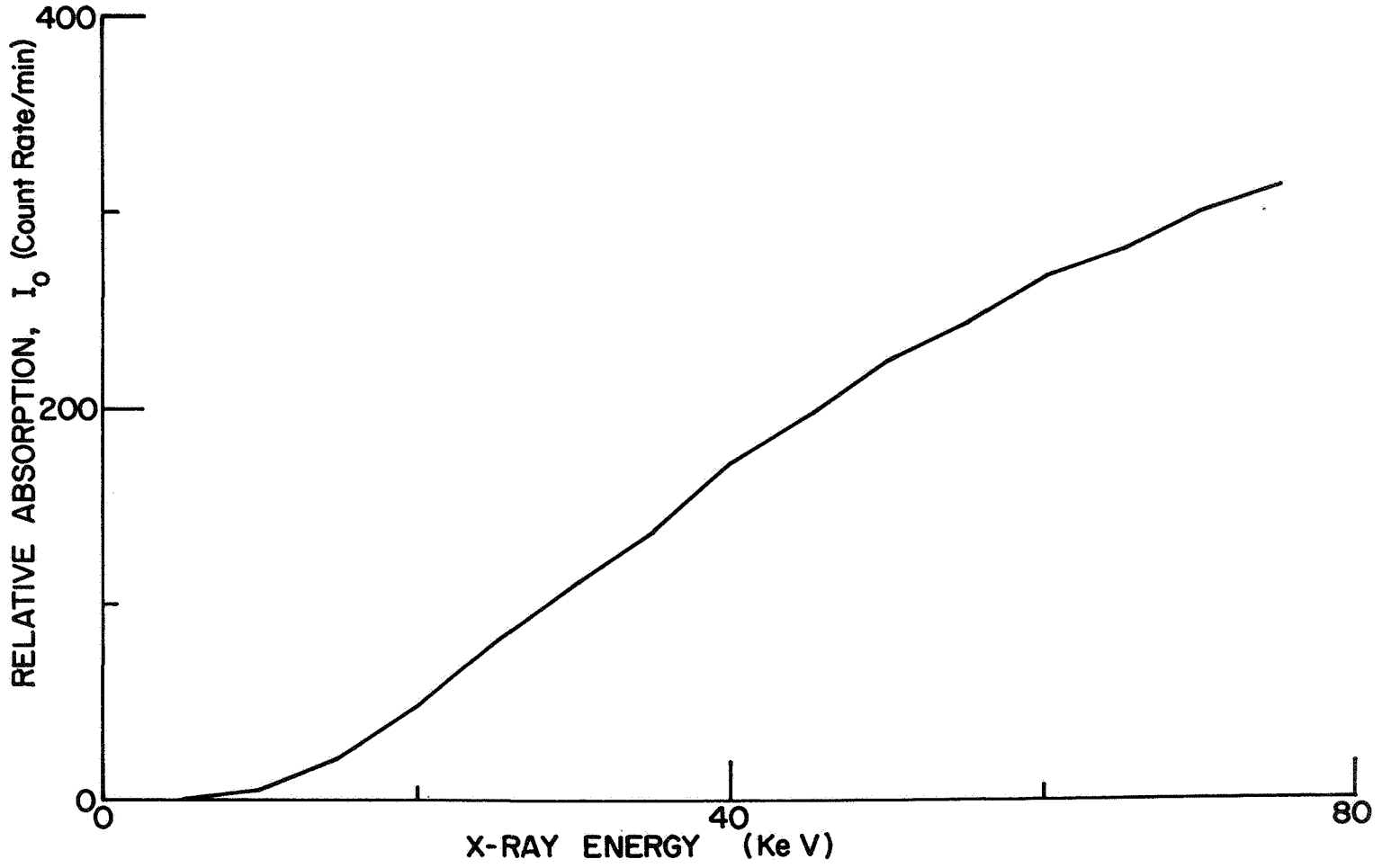

Figure 58.- Typical X-Ray Energy Output for the Experimental Absorption Set-up

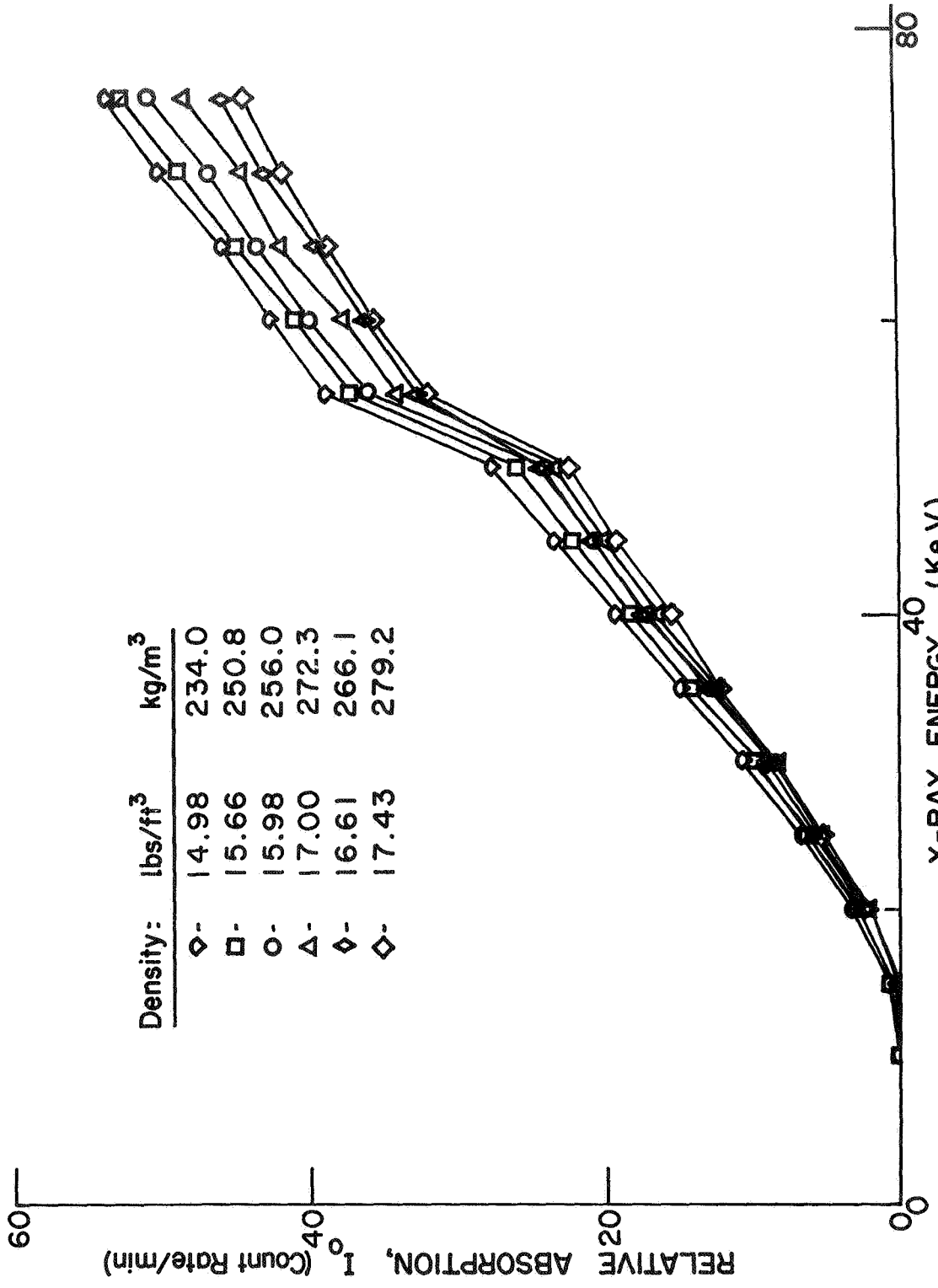

Figure 59.- Relative X-Ray Absorption for 1/2-in. (1.3 cm)-Thick Specimens

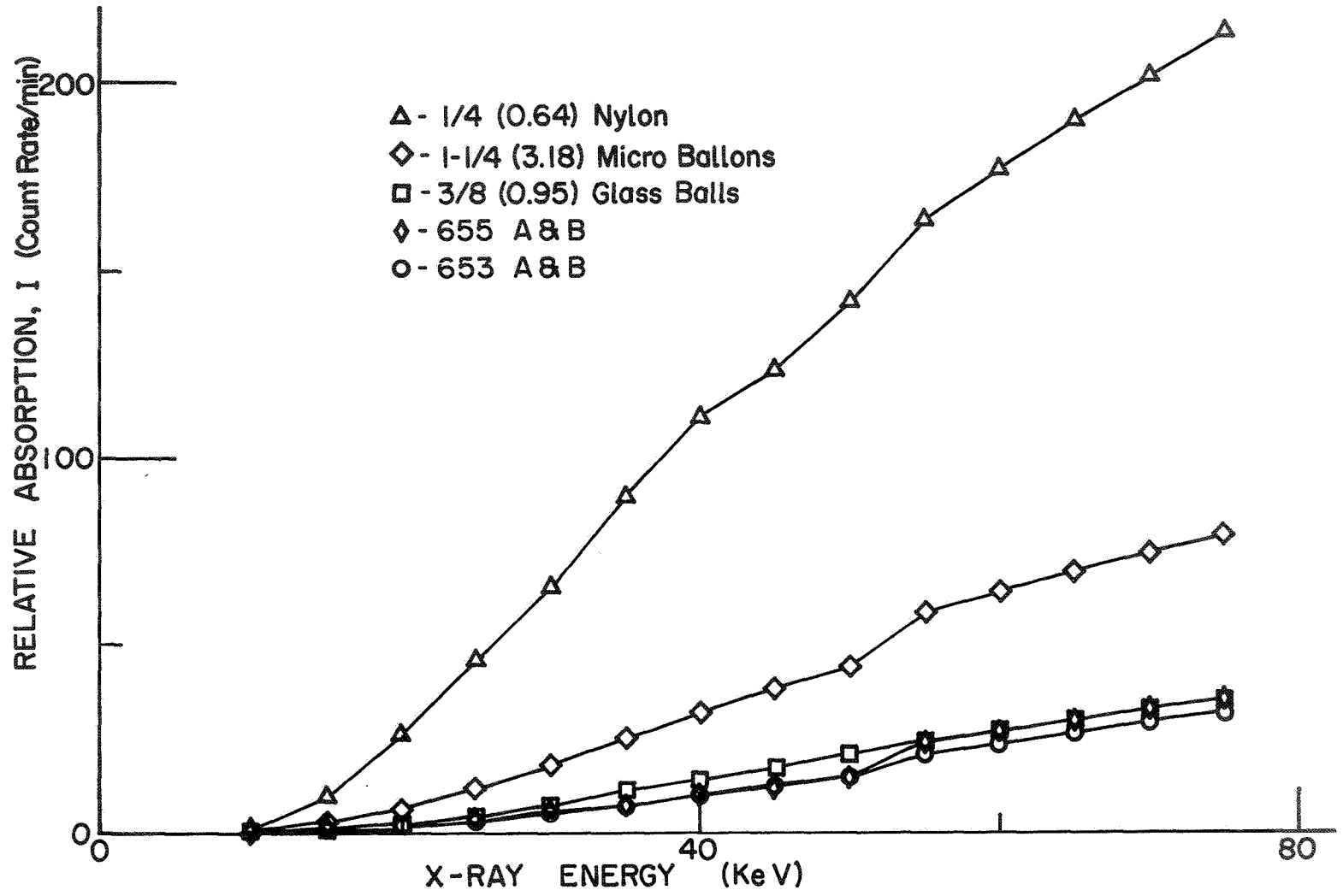

Figure 60.- Relative Absorption of the SS-41 Mixture Components at a Nominal Mix Ratio

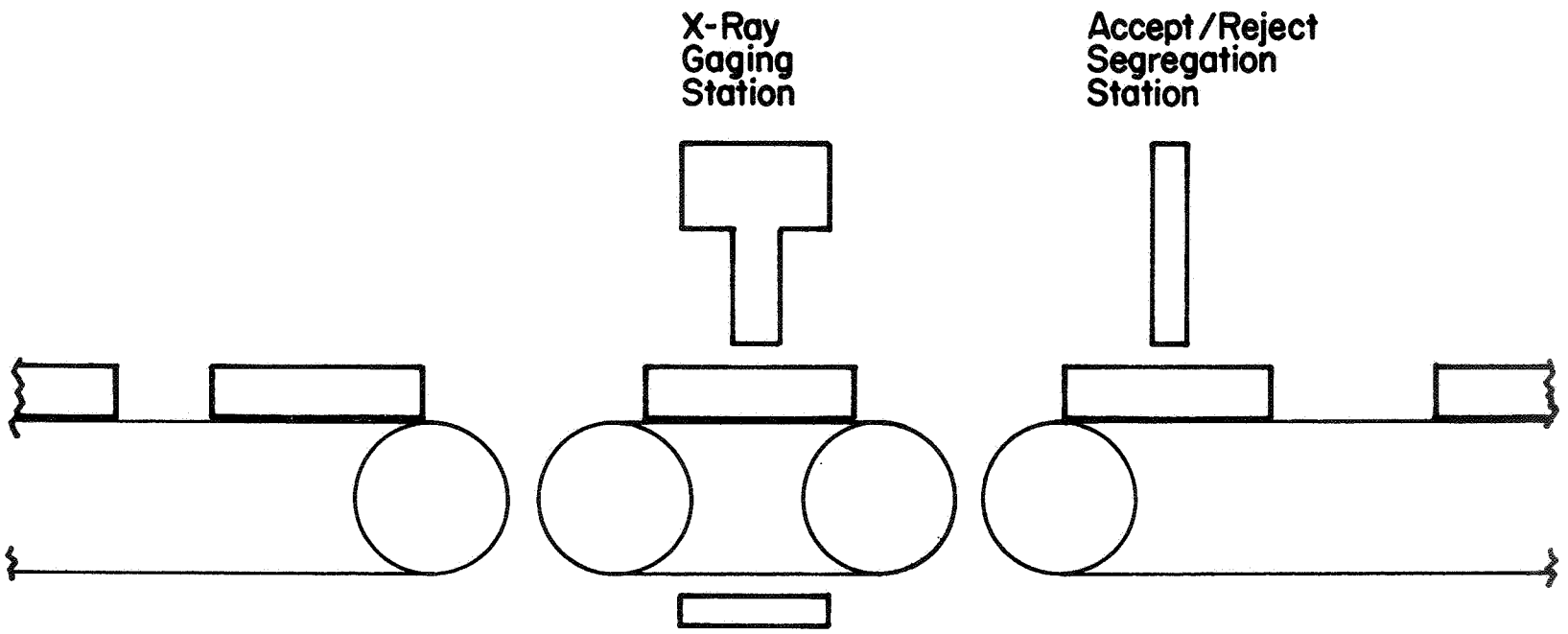

Figure 61.- Schematic View of an Automated X-Ray Gaging Set-up

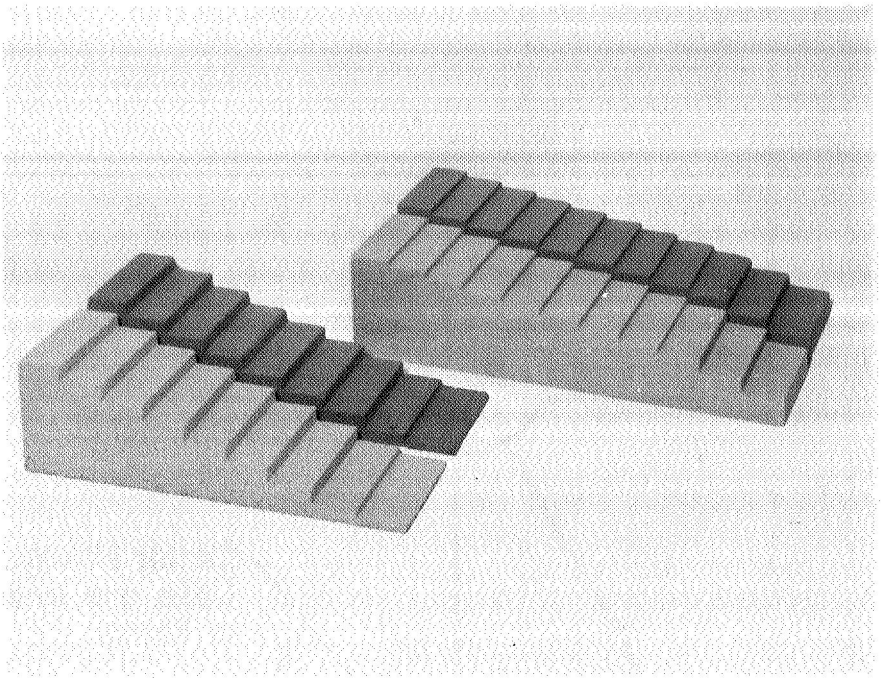

Figure 62.- Ablator Step Wedges for Monitor of Radiographic Contrast Sensitivity

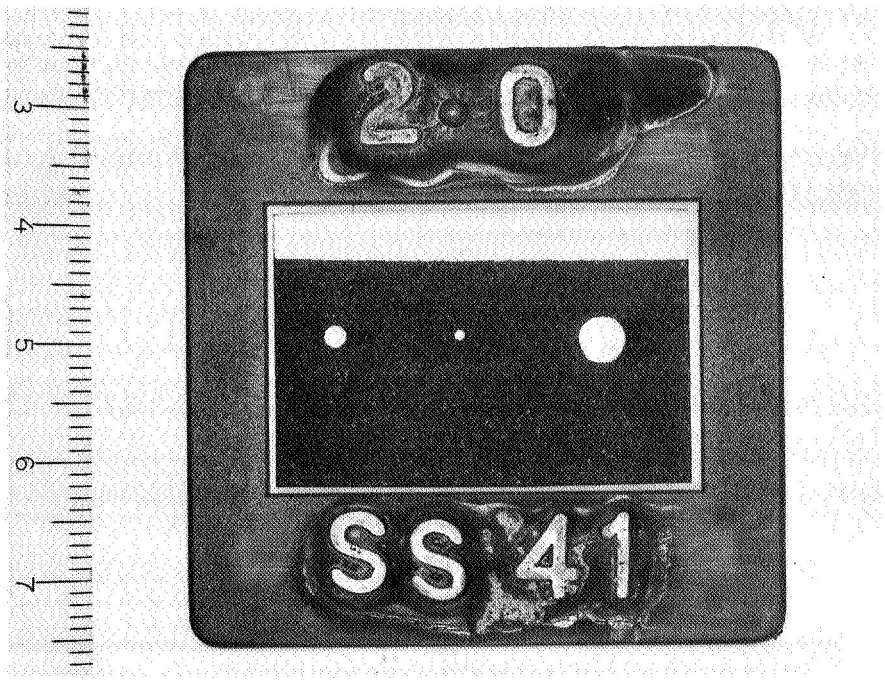

Figure 63.- SS-41 - Penetrameter for Monitor of Radiographic Resolution

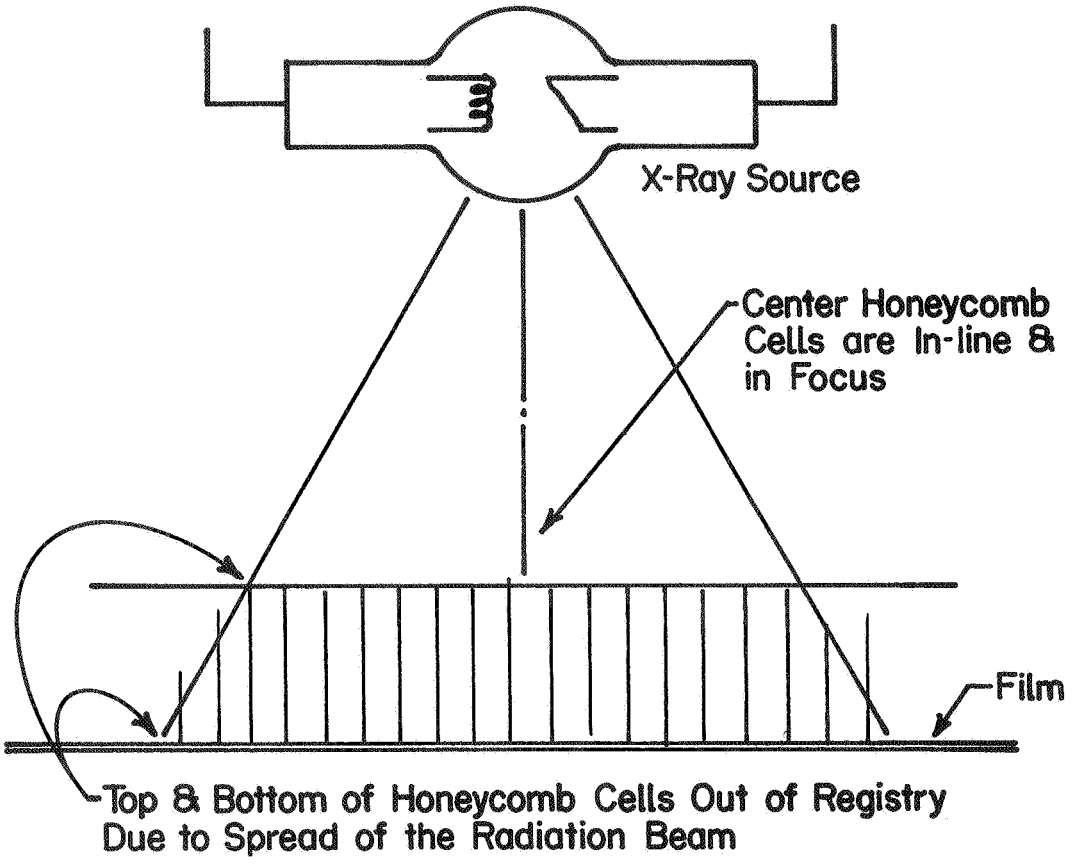

Figure 64.- Schematic View of an X-Radiographic Set-up Illustrating the Parallax Effect

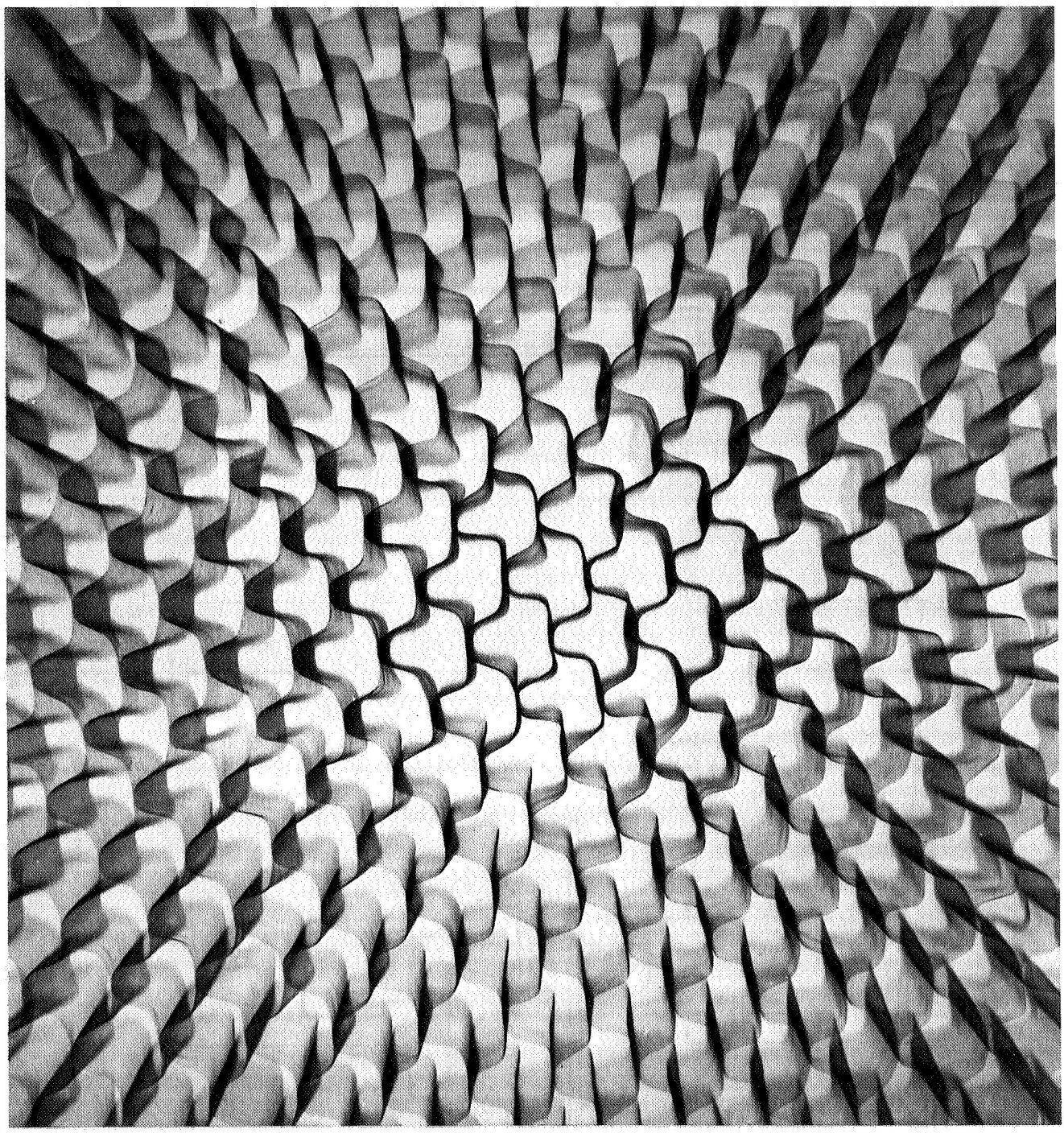

Figure 65.- X-Radiograph of an Ablator Panel Showing Extreme Parallax

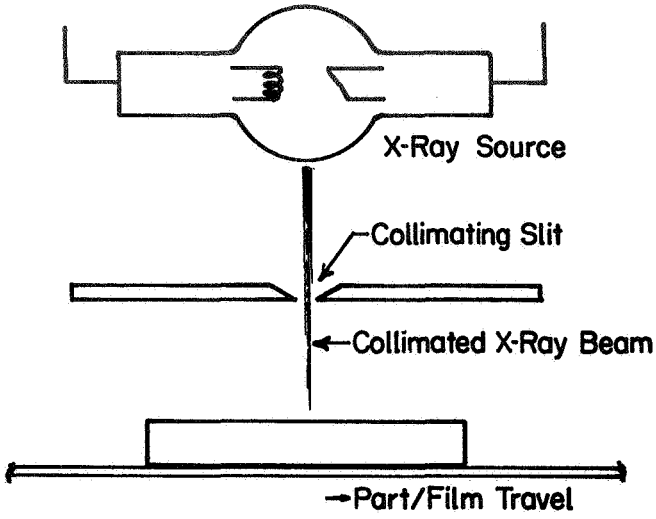

Figure 66.- Principle of the In-Motion Radiographic Technique

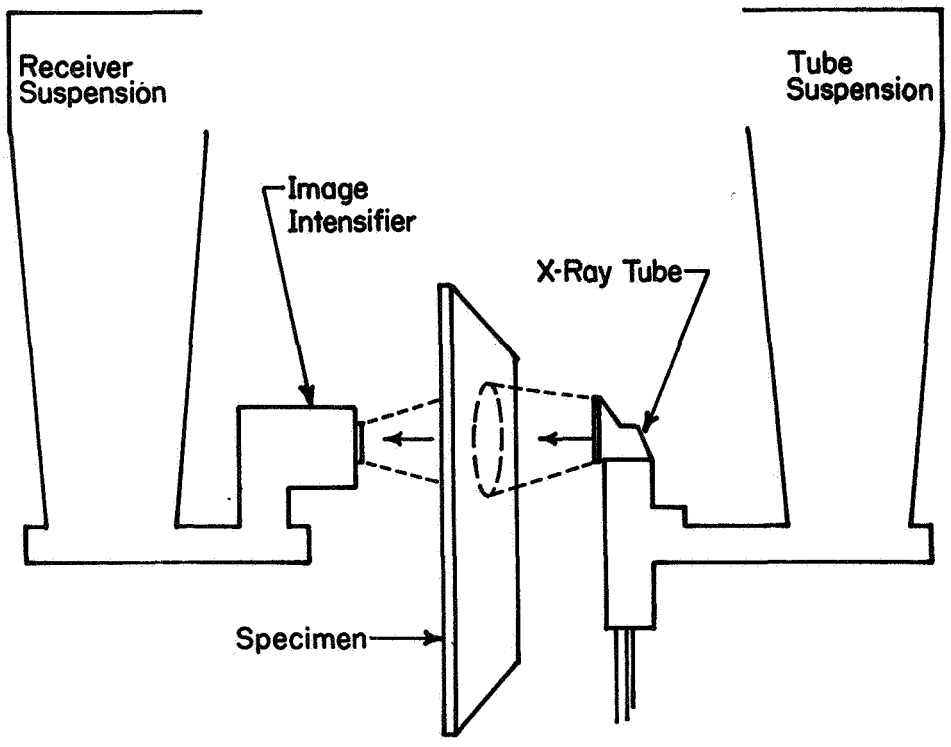

Figure 67.- Schematic View of a Direct X-Ray Viewing System

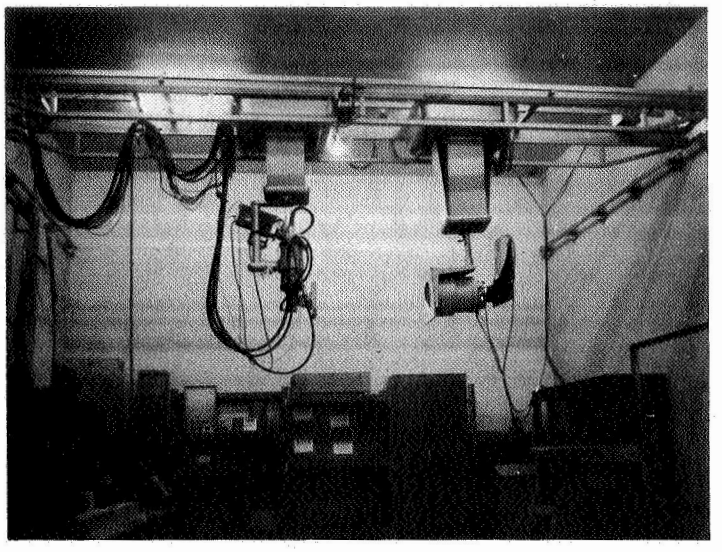

Figure 68.- The Lockheed In-Motion Radiography System

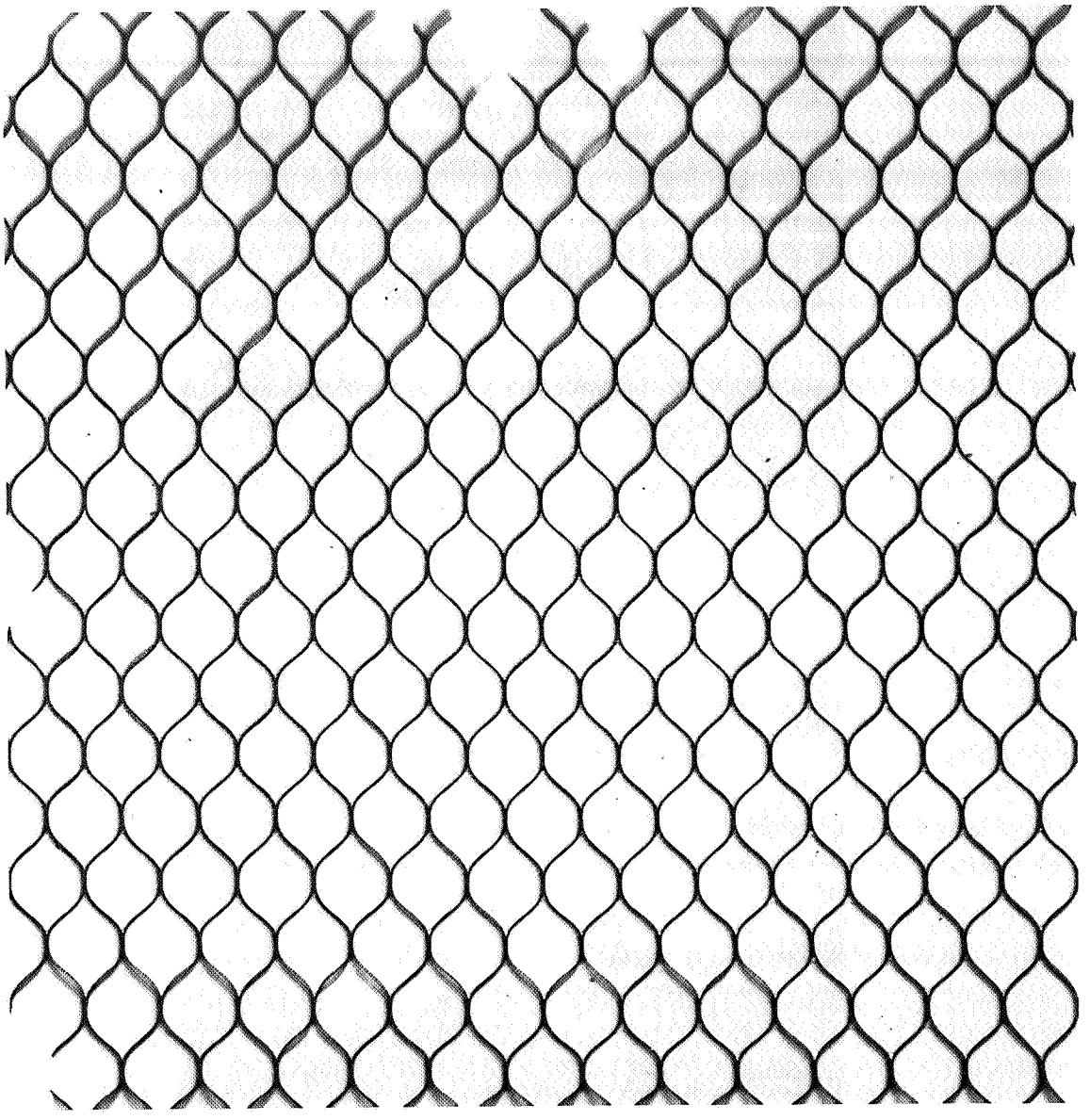

Figure 69.- In-Motion X-Radiograph of a 2 in. (5.1 cm)-Thick Panel, Type M Film

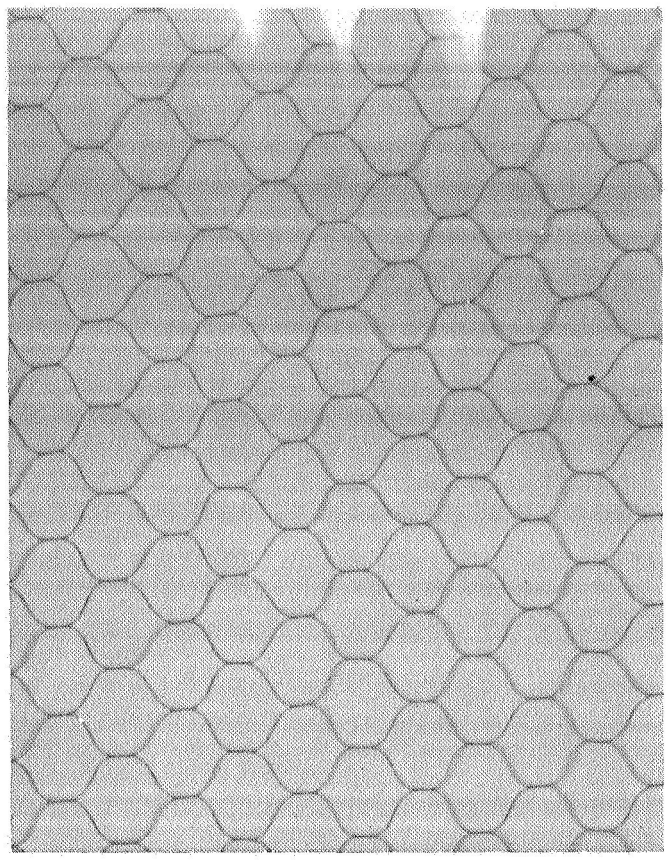

Figure 70.- In-Motion X-Radiograph of a 2 in. (5.1 cm)-Thick Panel, Poloroid Type 52 Film

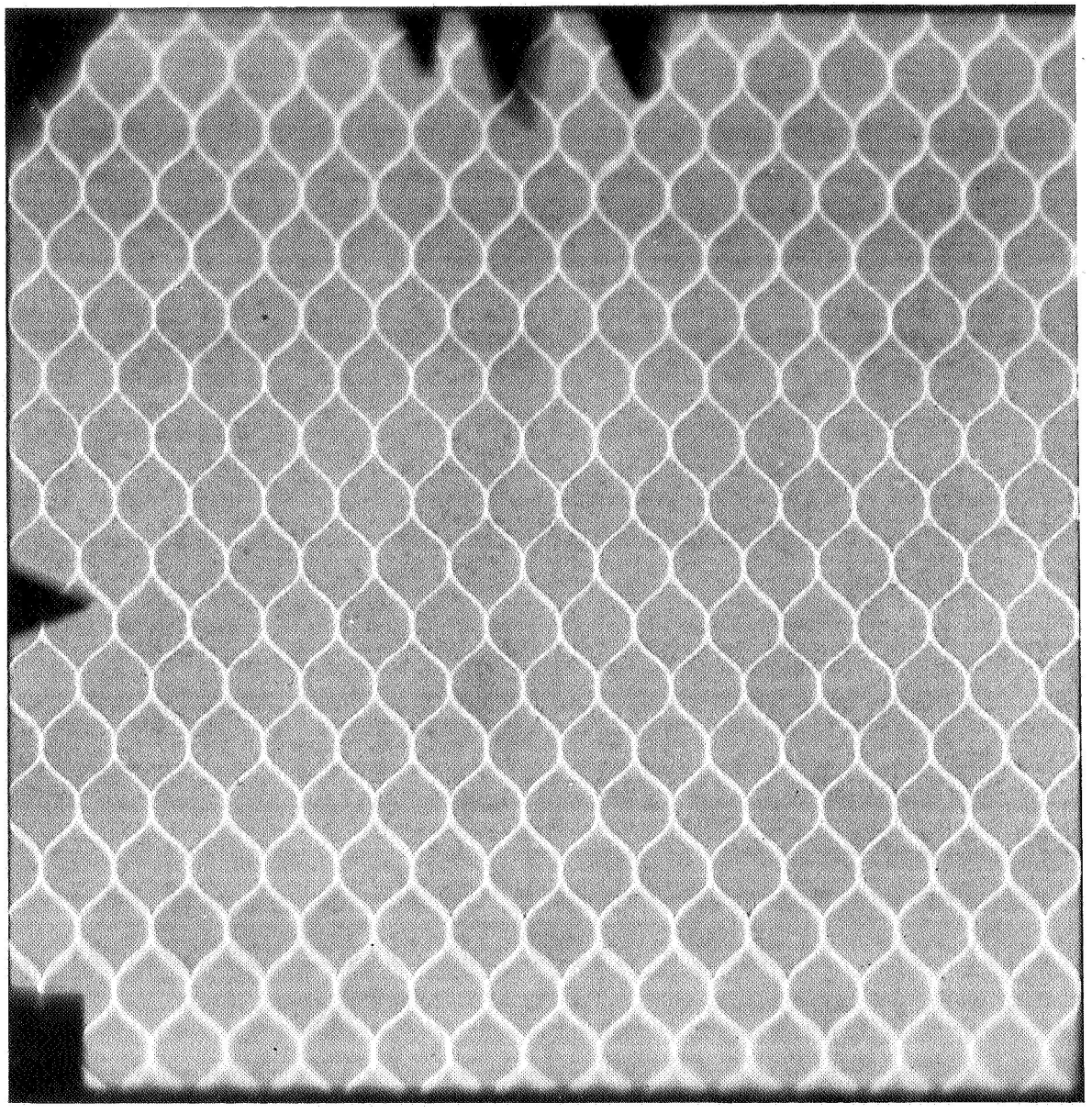

Figure 71.- In-Motion Radiograph of a 2 in. (5.1 cm)-Thick Panel, Kodak Industrex Paper

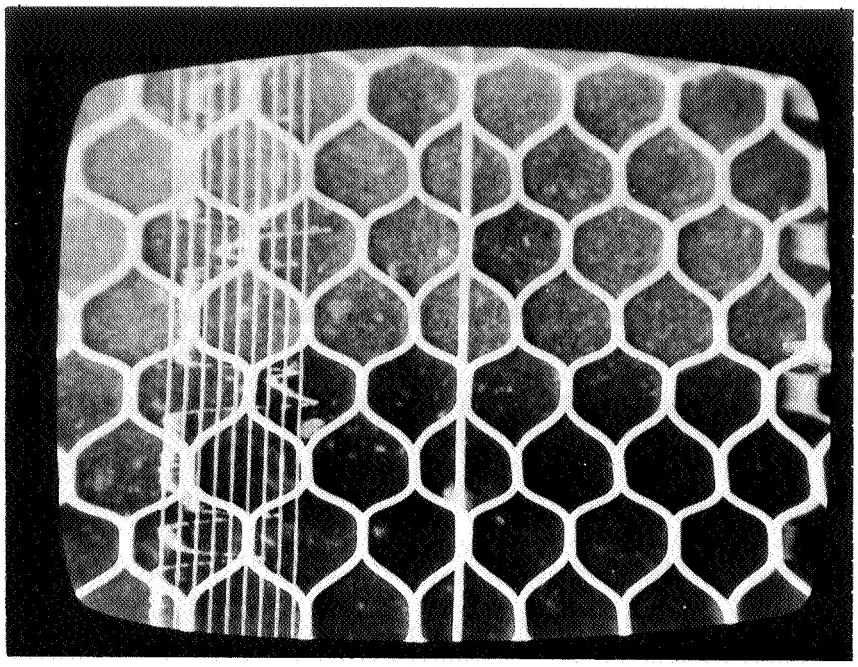

Figure 72.- Video Image Densitometer Readout

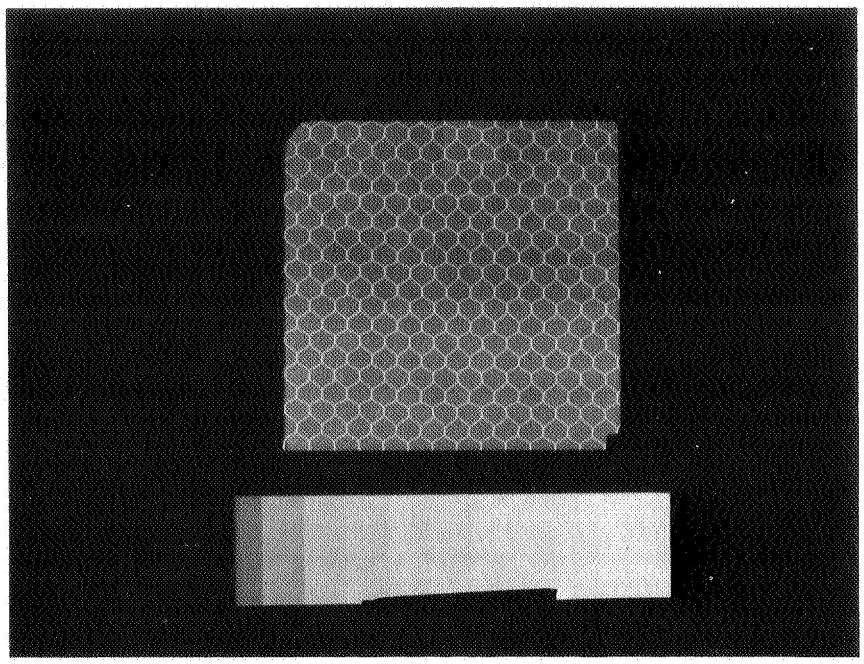

Figure 73.- White-Light Image of a Panel #2 Radiograph as Normally viewed

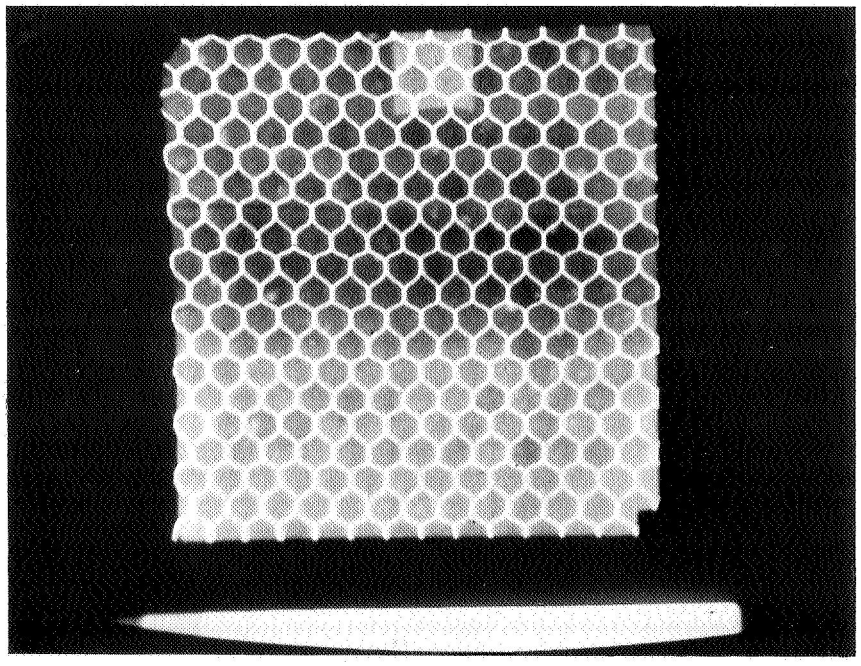

Figure 74.- Video Format for a Panel #2 Radiograph

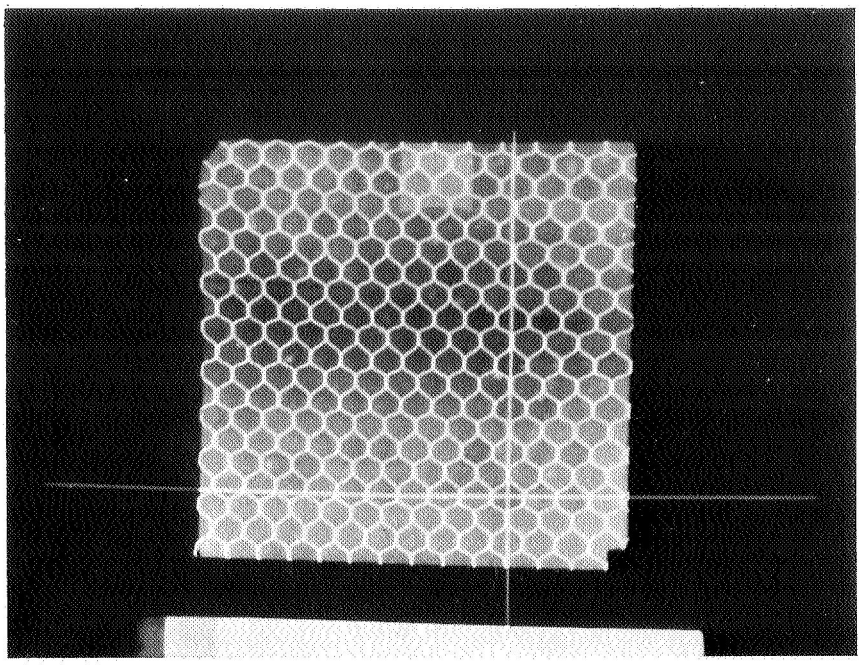

Figure 75.- Point Densitometer Readout for Image Analysis

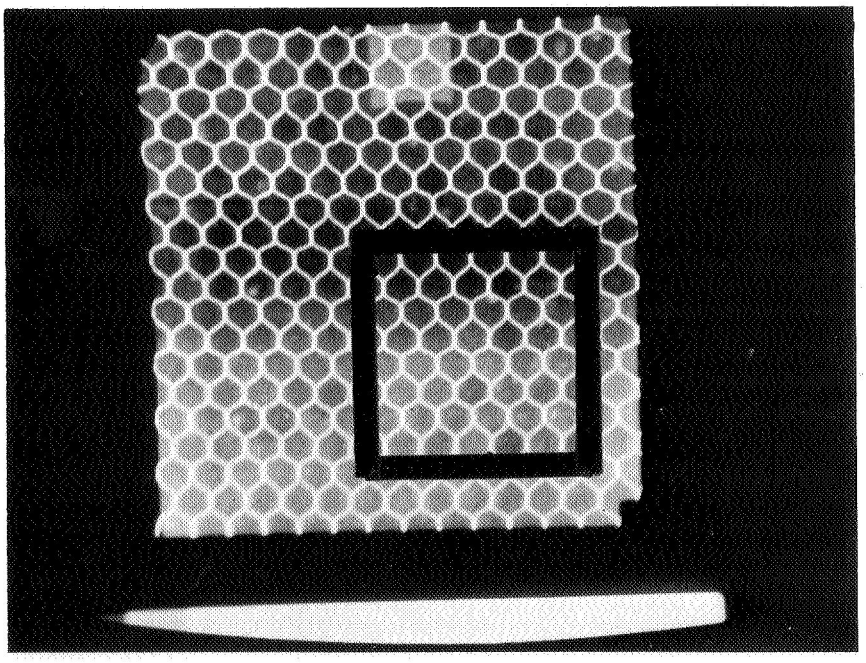

Figure 76.- Selected Area For False Color Enhancement

Figure 77.- False Color Enhancement Mode

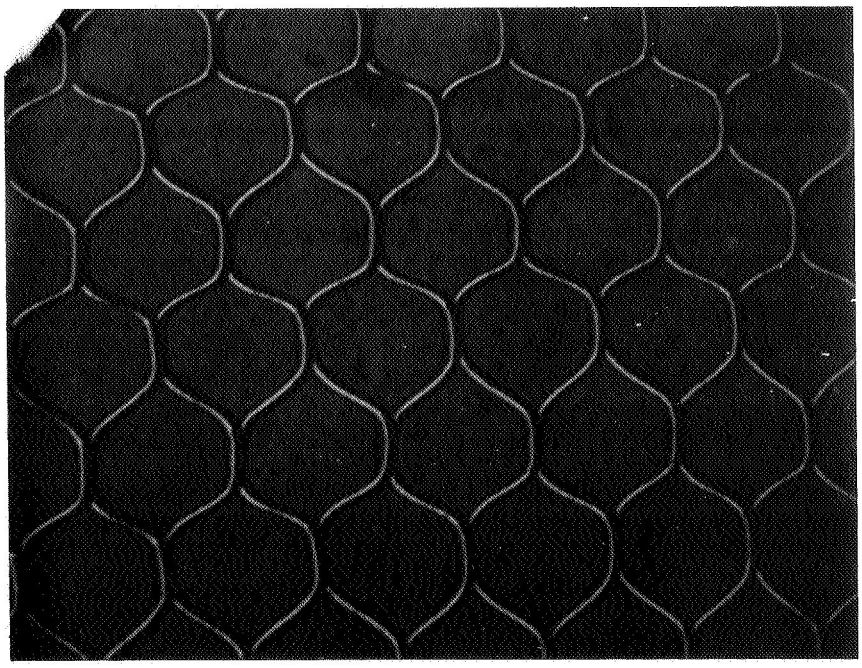

Figure 78.- Derivative Enhancement Mode

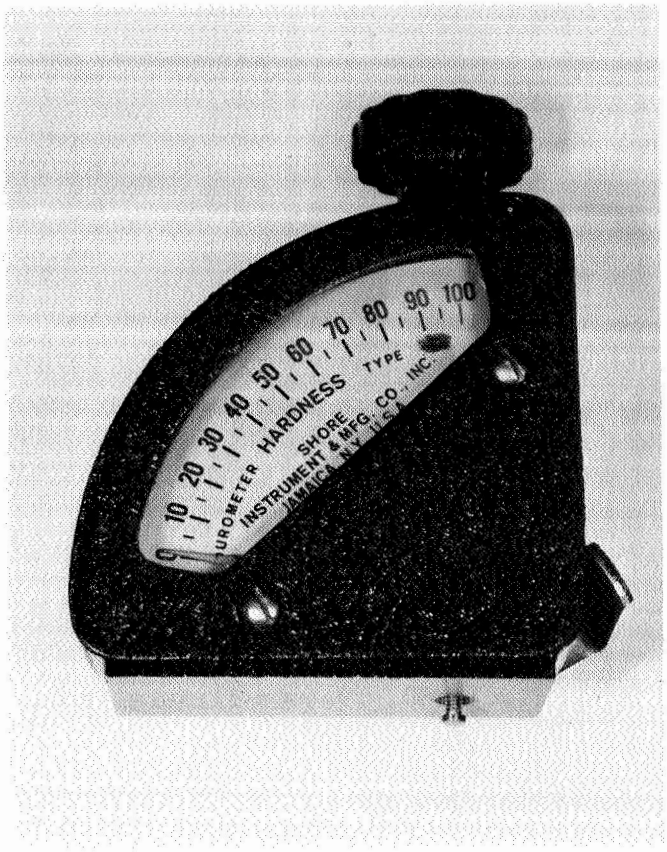

Figure 79.- Shore D Modified Indentation Hardness Unit

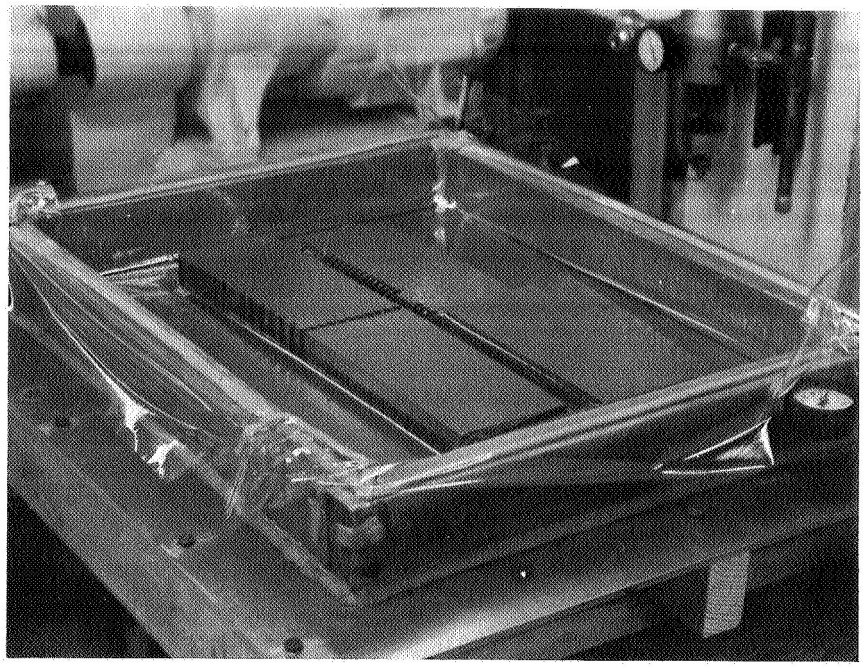

Figure 80.- Vacuum/Flexure Test

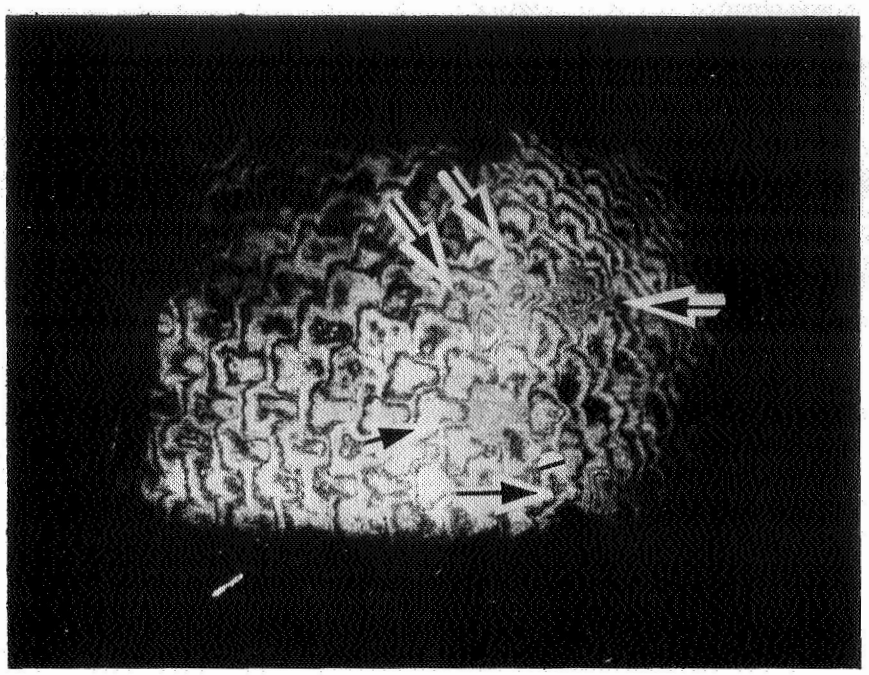

Figure 81.- Double Exposure Hologram Of An Elastomeric Ablator Showing Unbounds

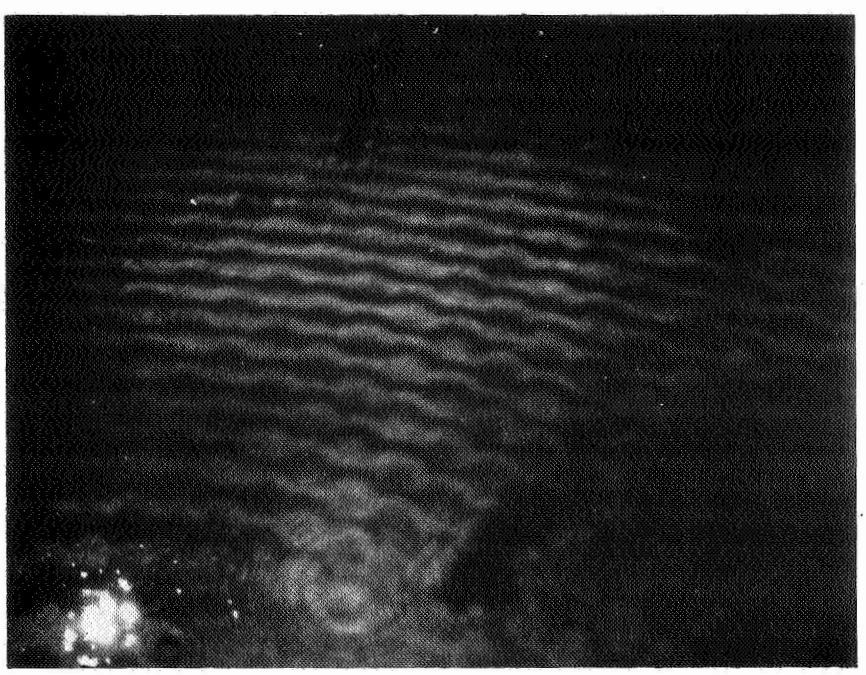

Figure 82.- Double Exposure Hologram Of An SS-41 Unbound Panel

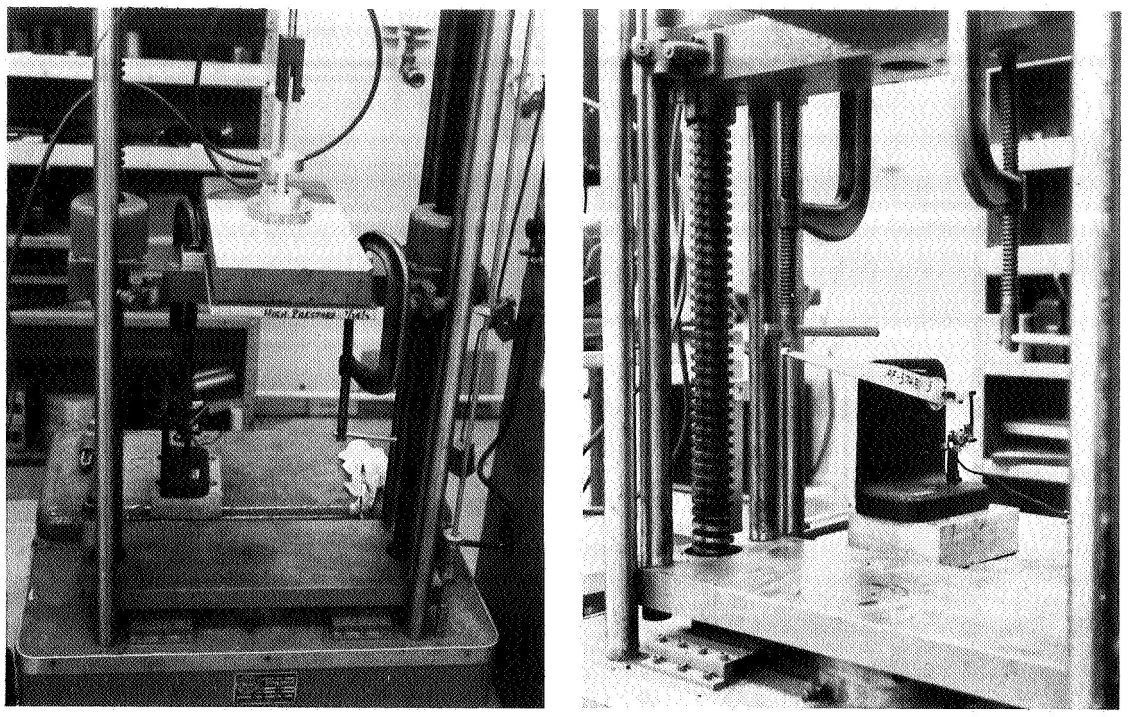

Figure 83.- Vacuum Cup Proof Load Test Set-Up And Extensometer Read-Out

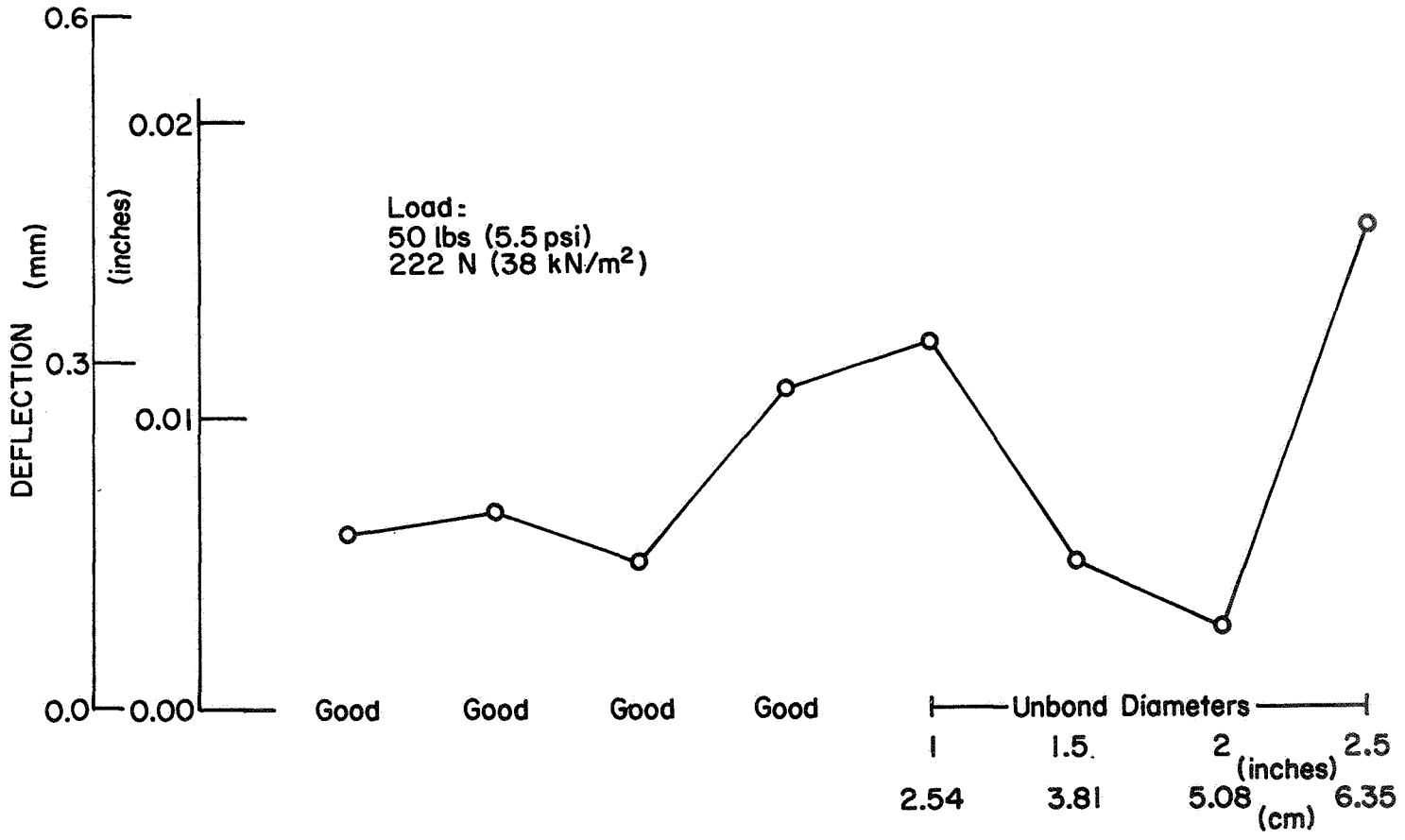

Figure 84.- Proof Load/Deflection Values for the NDT Standard Unbond High Pressure Panel

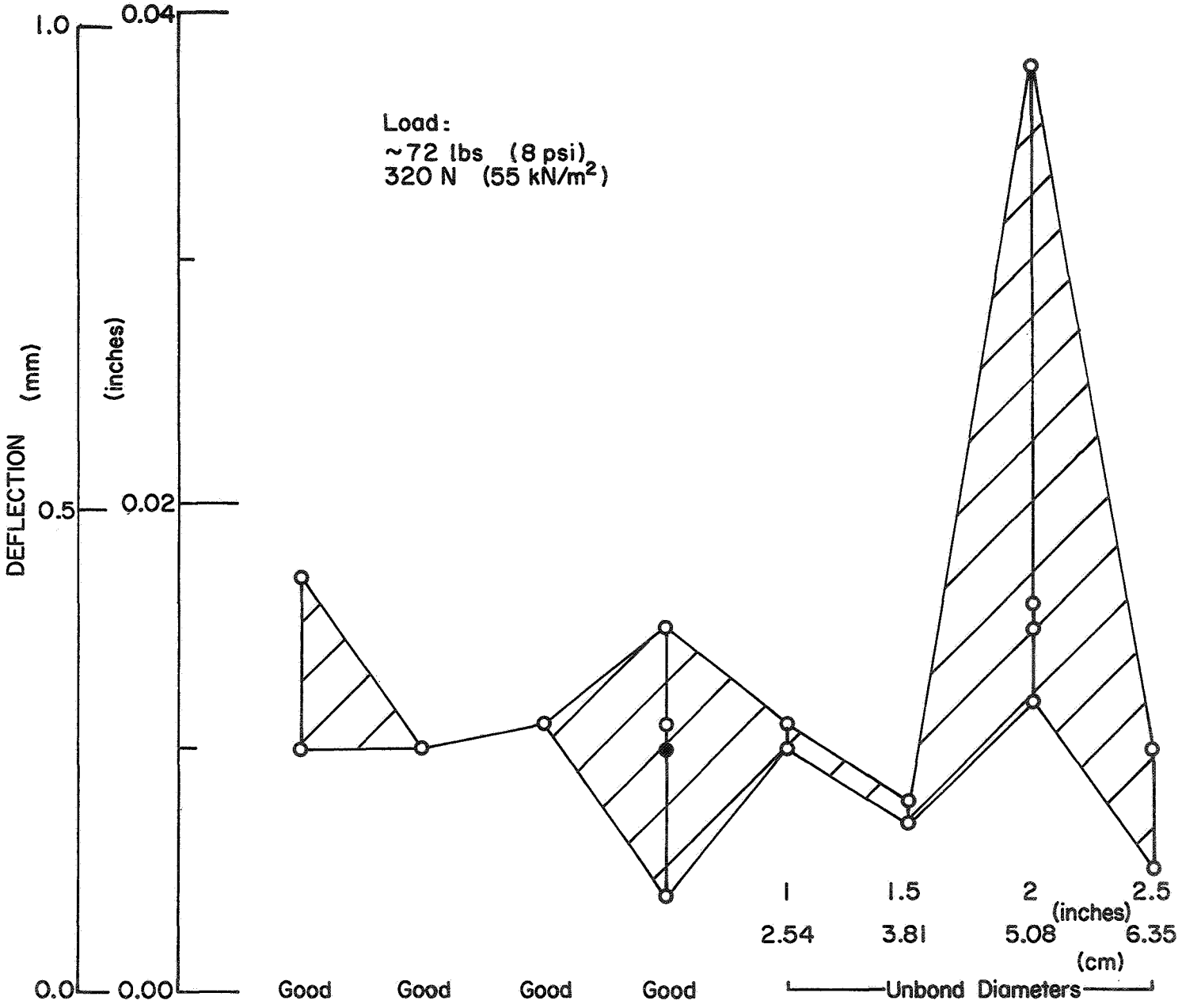

Figure 85.- Proof Load/Deflection Values for the NDT Standard Unbond Low Pressure Panel

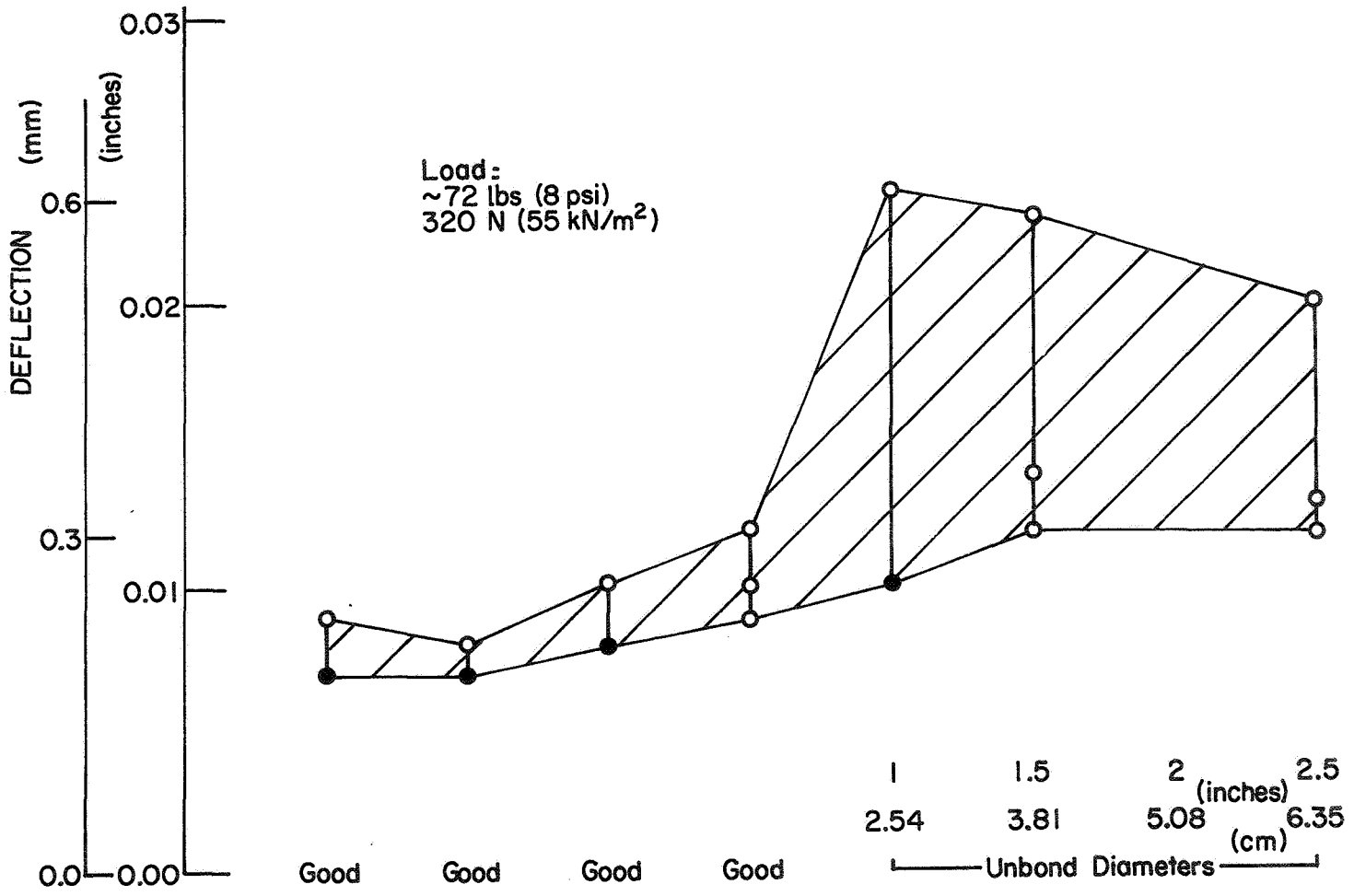

Figure 86.- Proof Load/Deflection Values for the NDT Standard Unbond Nominal Pressure Panel

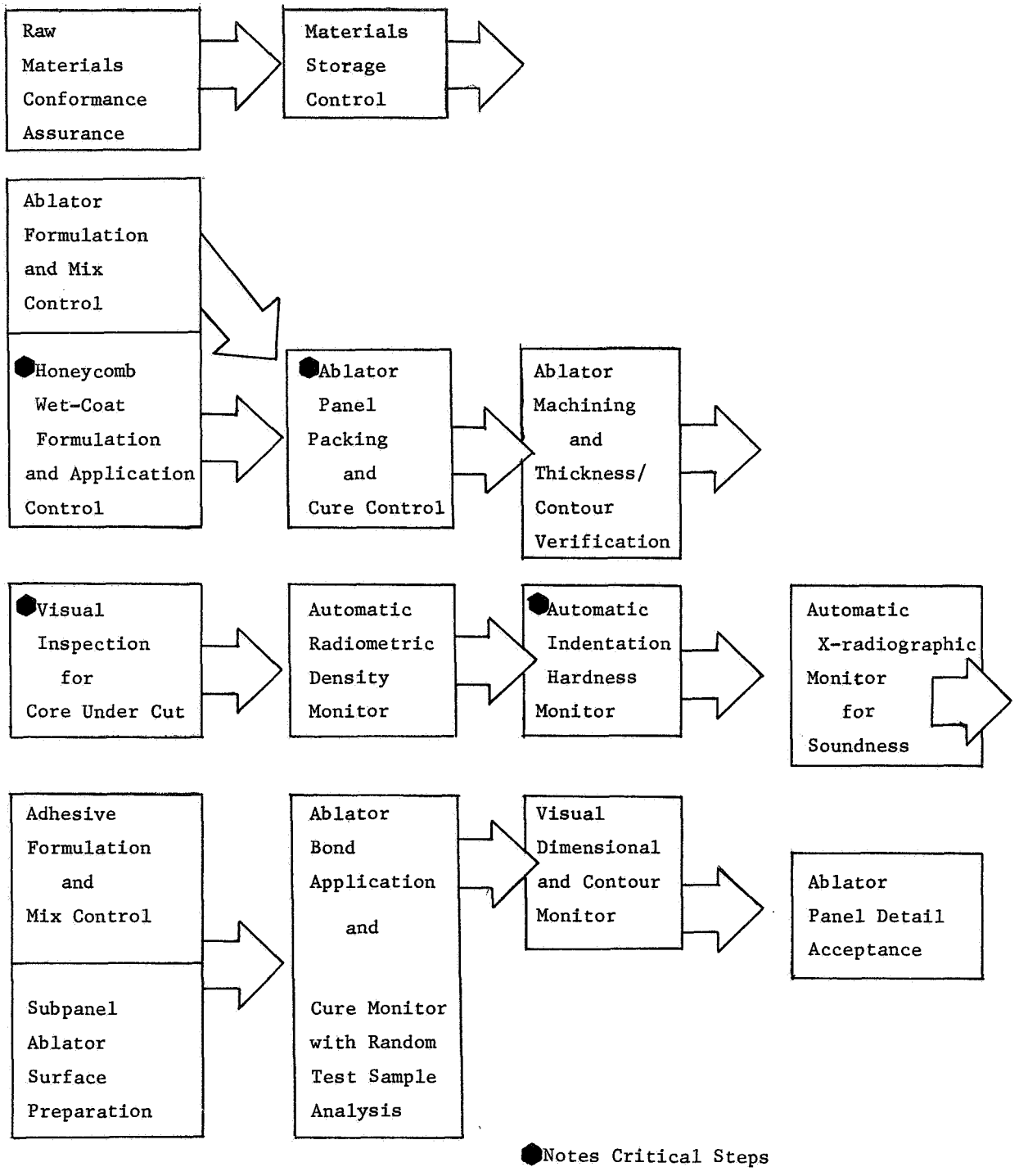

Figure 87.- Quality Assurance and Inspection Plan for "Low-Cost," Low-Risk Ablator Panel Production

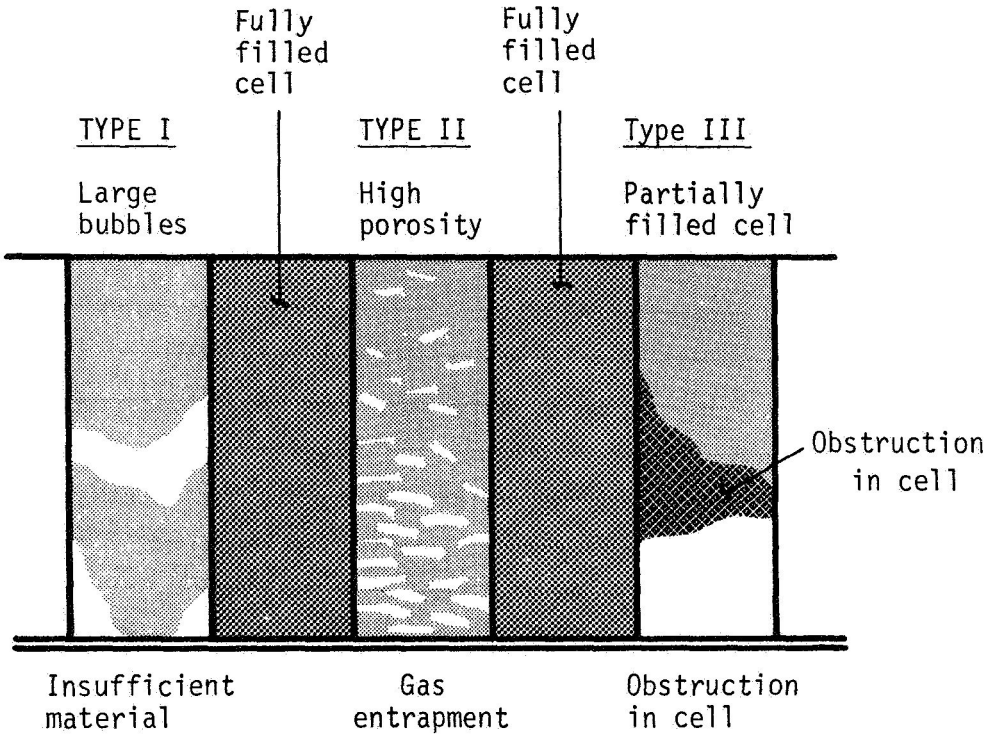

Figure 88.- Voids in Ablative Material

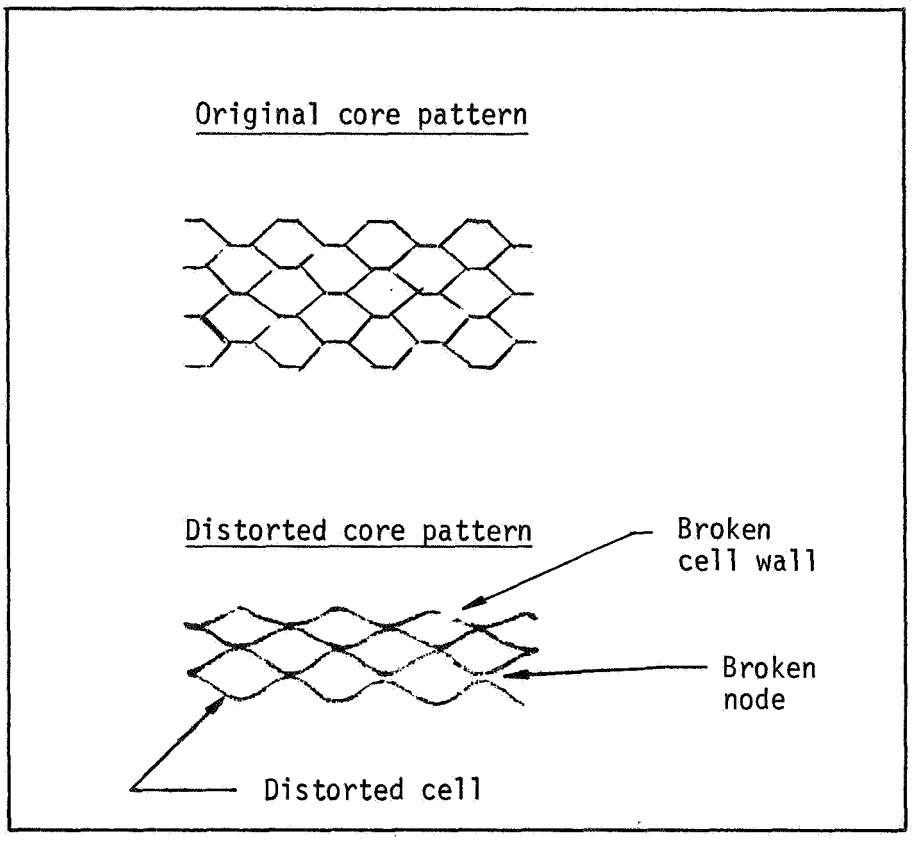

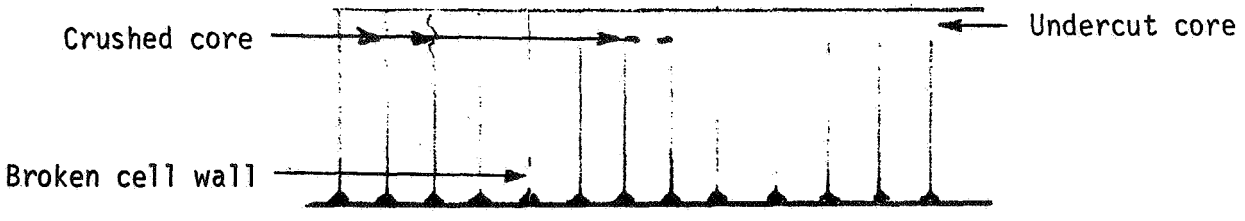

Figure 89.- Honeycomb Core Defects

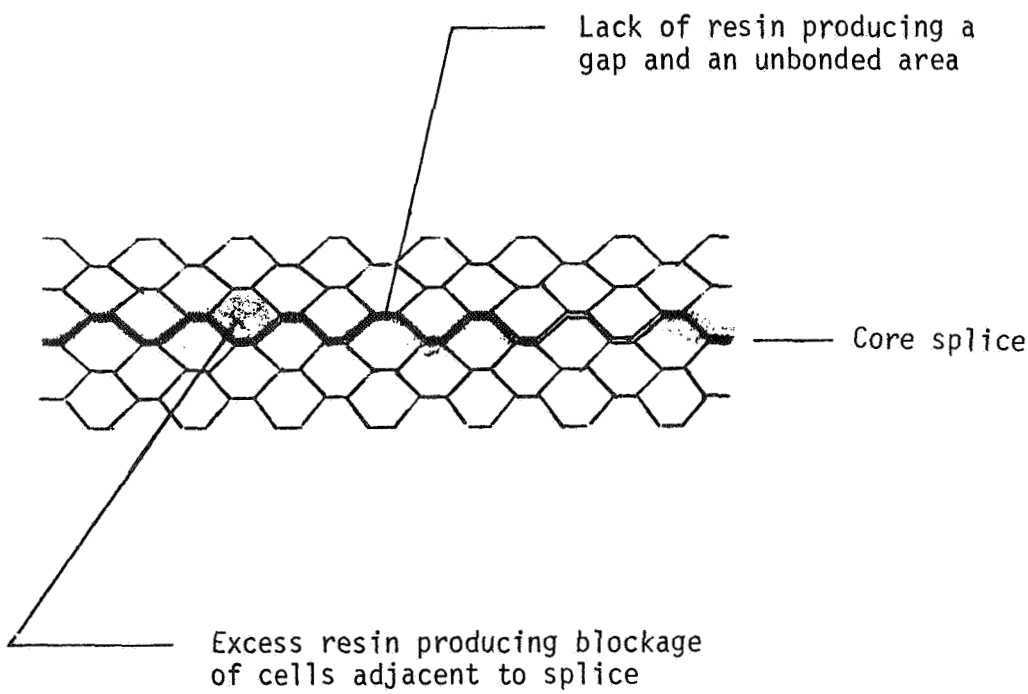

Figure 90.- Defective Core Splice

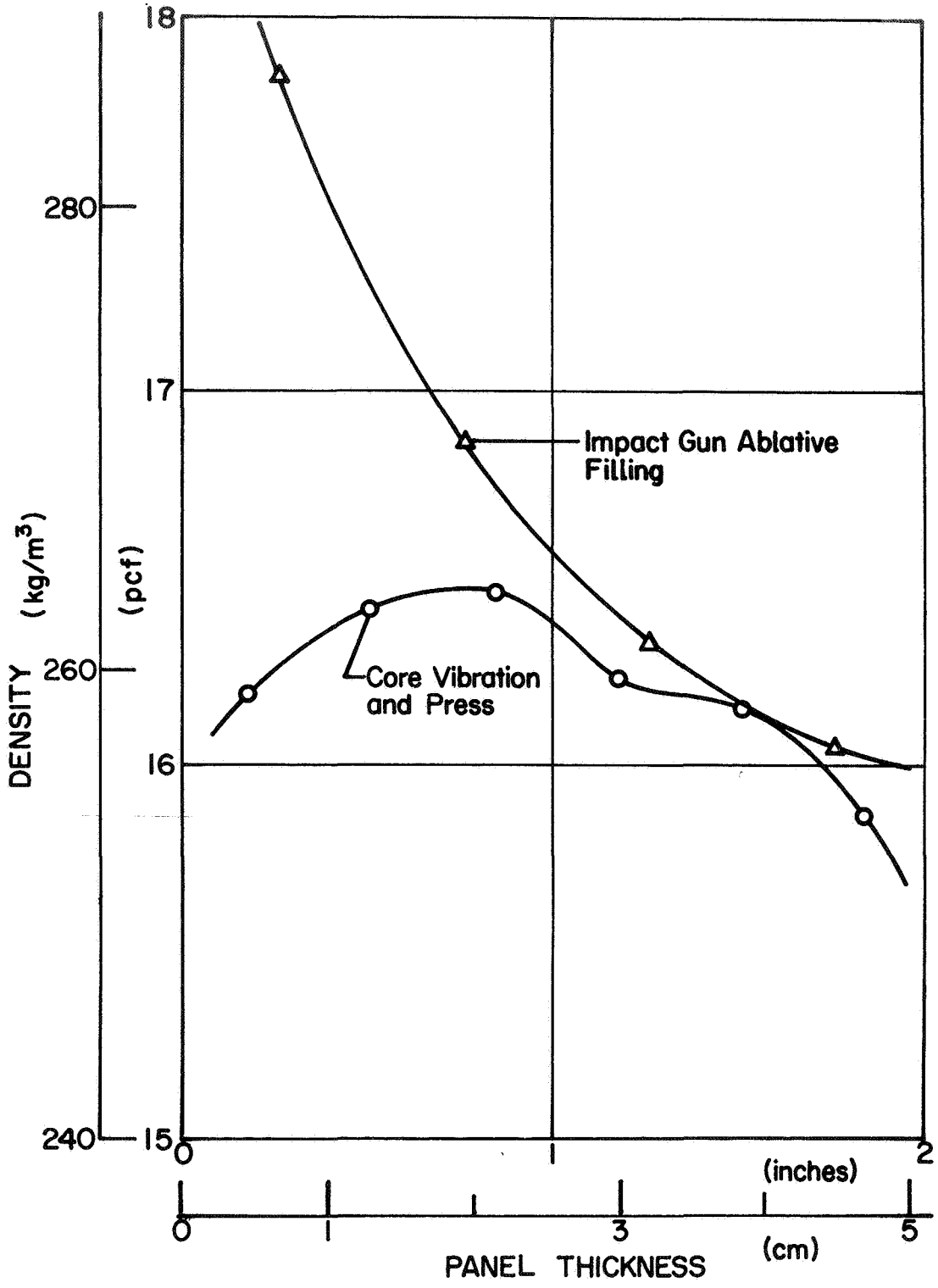

Figure 91.- Ablator Density Variations

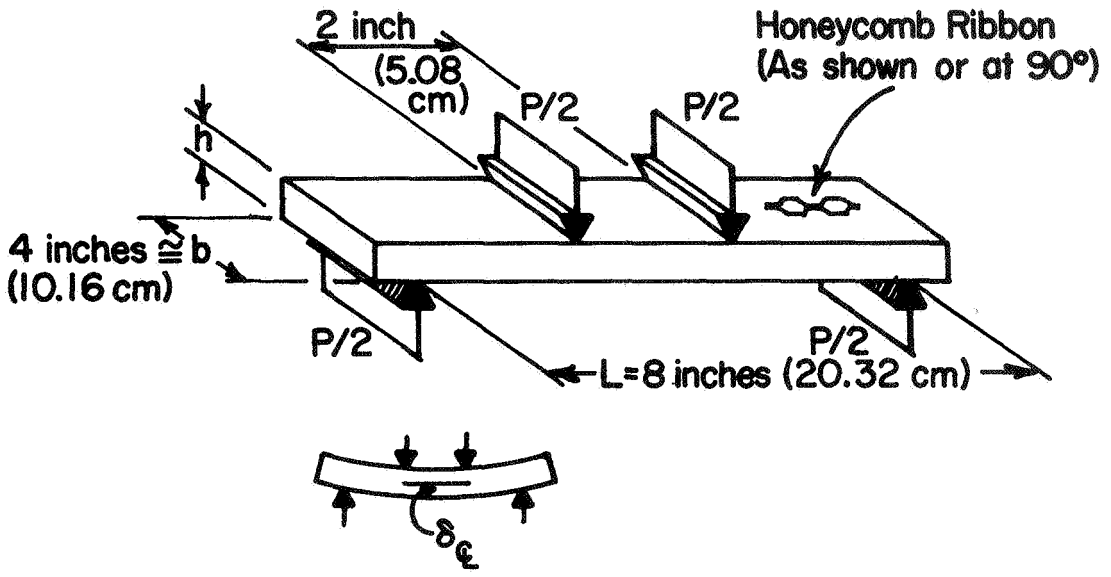

Figure 92.- Typical Beam Arrangement

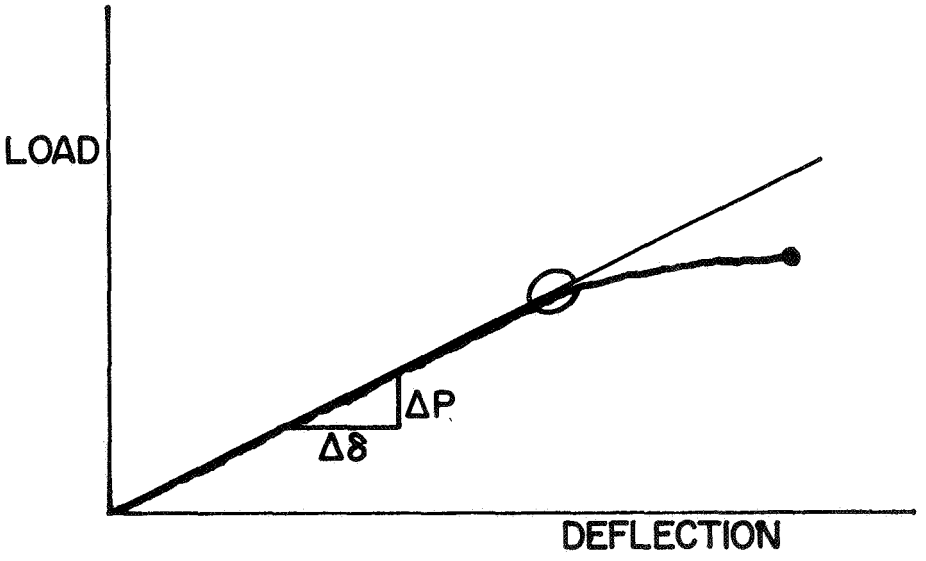

Figure 93.- Typical Load vs Deflection Curve

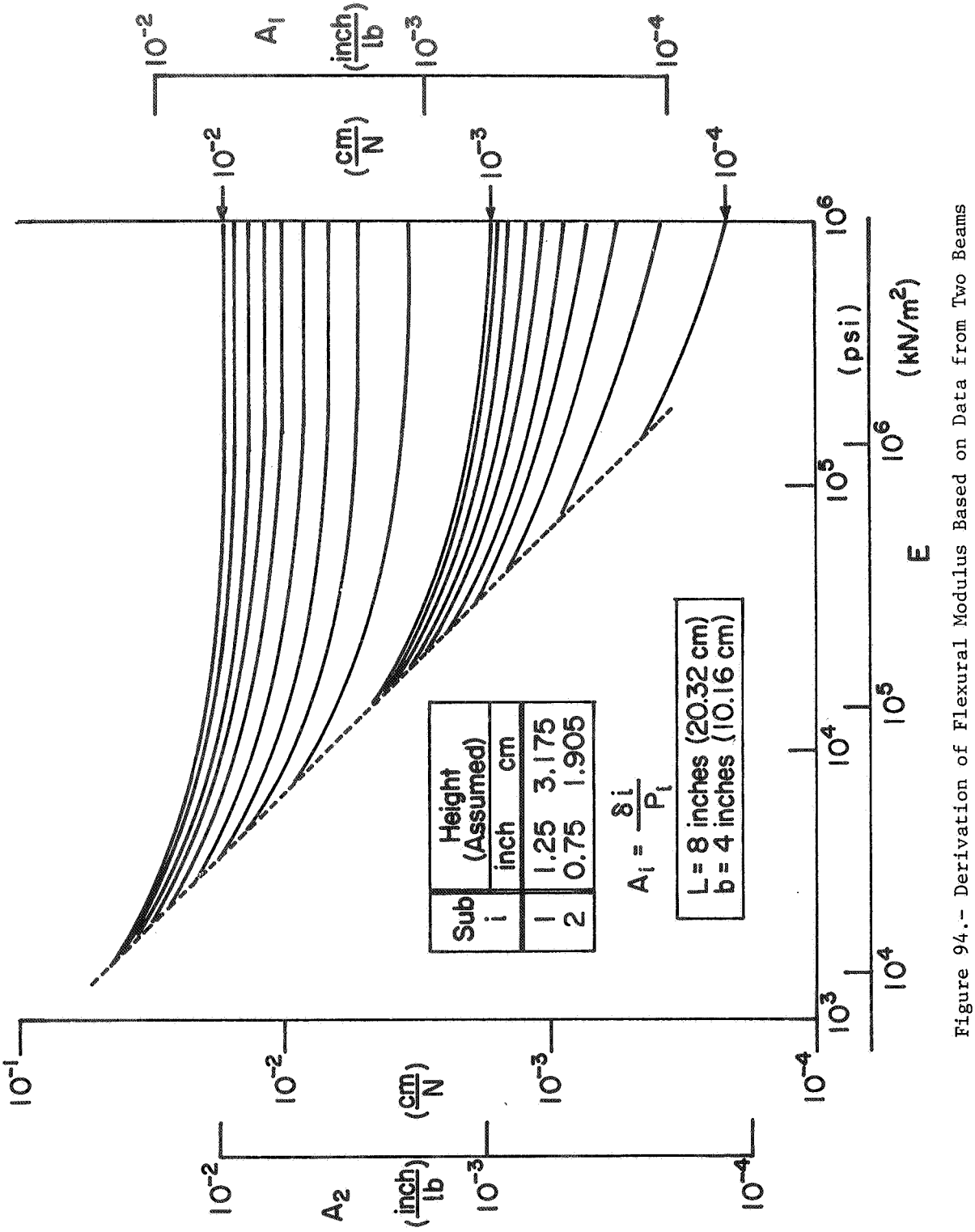

Figure 94.- Derivation of Flexural Modulus Based on Data from Two Beams

1. Report No.	2. Government Accession No.	3. Recipient's Catalog No.
NASA CR-2336		

4. Title and Subtitle	5. Report Date
Study of Critical Defects in Ablative Heat Shield Systems for the Space Shuttle	February 1974
	6. Performing Organization Code
7. Author(s)	8. Performing Organization Report No.
C. C. Miller and W. D. Rummel	MCR-73-184
	10. Work Unit No.
9. Performing Organization Name and Address	
Martin Marietta Aerospace Denver Division Denver, Colorado 80201	11. Contract or Grant No. NAS1-10289
	13. Type of Report and Period Covered Contractor Report
12. Sponsoring Agency Name and Address	
National Aeronautics and Space Administration Washington D. C., 20546	14. Sponsoring Agency Code

15. Supplementary Notes

This is a final report.

16. Abstract

Experimental results are presented for a program conducted to determine the effects of fabrication-induced defects on the performance of an ablative heat shield material. Exposures representing a variety of space shuttle orbiter mission environments--humidity, acoustics, hot vacuum and cold vacuum--culminating in entry heating and transonic acoustics, were simulated on large panels containing intentional defects. Non-destructive methods for detecting the defects, considering state-of-the-art and advanced techniques, were investigated. The baseline materials used were two honeycomb-reinforced low density, silicone ablators, MG-36 and SS-41. Principal manufacturing-induced defects displaying a critical potential included: off-curing of the ablator, extreme low density, undercut (or crushed) honeycomb reinforcements, and poor wet-coating of this honeycomb. A concurrent, comprehensive quality assurance effort establishes the mode of fabrication and inspection modifications which should be enacted in future ablator preparation.

17. Key Words (Suggested by Author(s))		18. Distribution Statement
Space Shuttle	Non-Destructive Evaluation	Unclassified--Unlimited
Heat Shield	Orbit Environments	
Ablators	Humidity	
Defects	Ultrasonic	
Acoustics	Holography	
	X-Radiographics	Cat. 33

19. Security Classif. (of this report)	20. Security Classif. (of this page)	21. No. of Pages	22. Price*
Unclassified	Unclassified	208	$5.50

* For sale by the National Technical Information Service, Springfield, Virginia 22151

"The aeronautical and space activities of the United States shall be conducted so as to contribute . . . to the expansion of human knowledge of phenomena in the atmosphere and space. The Administration shall provide for the widest practicable and appropriate dissemination of information concerning its activities and the results thereof."

—NATIONAL AERONAUTICS AND SPACE ACT OF 1958

NASA SCIENTIFIC AND TECHNICAL PUBLICATIONS

TECHNICAL REPORTS: Scientific and technical information considered important, complete, and a lasting contribution to existing knowledge.

TECHNICAL NOTES: Information less broad in scope but nevertheless of importance as a contribution to existing knowledge.

TECHNICAL MEMORANDUMS: Information receiving limited distribution because of preliminary data, security classification, or other reasons. Also includes conference proceedings with either limited or unlimited distribution.

CONTRACTOR REPORTS: Scientific and technical information generated under a NASA contract or grant and considered an important contribution to existing knowledge.

TECHNICAL TRANSLATIONS: Information published in a foreign language considered to merit NASA distribution in English.

SPECIAL PUBLICATIONS: Information derived from or of value to NASA activities. Publications include final reports of major projects, monographs, data compilations, handbooks, sourcebooks, and special bibliographies.

TECHNOLOGY UTILIZATION PUBLICATIONS: Information on technology used by NASA that may be of particular interest in commercial and other non-aerospace applications. Publications include Tech Briefs, Technology Utilization Reports and Technology Surveys.

Details on the availability of these publications may be obtained from:

SCIENTIFIC AND TECHNICAL INFORMATION OFFICE

NATIONAL AERONAUTICS AND SPACE ADMINISTRATION

Washington, D.C. 20546